Department of Mechanical Engineering

Chemical Machining of Advanced Ceramics

Ting Huey Tze

This thesis is presented as part of the requirements for the award of the Degree of Doctor of Philosophy of the Curtin University

April 2013

Declaration

To the best of my knowledge and belief this thesis contains no material previously published by any other person except where due acknowledgment has been made.

This thesis contains no material which has been accepted for the award of any other degree or diploma in any university.

Signature: …….

Date: 19 April 2013

To my beloved family

Abstract

Not until recently did we see an enormous surge of interest in the study of machining of advanced ceramics. This has resulted in significant advances lately in their development and usage. Machinable glass ceramics, boron nitride and silicon carbide are commonly used in the industry and their major features of attraction are their inherent properties. Previous studies on machining of these materials were mainly performed by other machining methods, such as electrode discharge machining, laser beam machining and abrasive jet machining. Although chemical machining is one of the oldest machining methods employed, the literature survey reveals a lack of knowledge in this particular aspect. Further understanding is required on the chemical machining characteristics of advanced ceramics as well as their performance and relationship between the variables and parameters involved in the process. Therefore, the aim of our study is to examine and establish the relationship between etching rate, surface roughness and dimensional accuracy with the relevant variables involved and at the same time to develop the predictive models for all outputs that we believe are beneficial to the manufacturing industries.

A comprehensive review was written and published recently in a Journal on the current advanced ceramics machining techniques [1]. The chemical machining process was successfully conducted in this study with a variety of selected etchants. Using the RSM methodology the first and second order models were developed to study the chemical machining process and relationship between the outputs (etching rate, surface roughness and dimensional accuracy) with the selected variables, namely, etching temperature, etching duration, etchant and etchant's concentration. A number of predictive models were developed followed by optimisation studies of chemical machining to obtain the best performance of chemical machining of advanced ceramics. Artificial neural network was also used as the analytical tool to evaluate the experimental data and validate the results generated by response surface

roughness, and both results were found to be in good agreement with each other. Artificial neural network was performed by software of NeuroSolution 5.

From the chemical etching studies both the etching temperature and etchant used have significant influence on the etch rate. Generally, the higher the etching temperature the greater the etch rates was observed for the substrates. The best etch rate was found in HBr etchant for MGC and BN, and the highest etch rate performance for SiC was found in H_3PO_4 etchant. For surface roughness, different substrates were found to be influenced by different variables. For MGC and BN, these substrates were affected by etching temperature and the best surface roughness occurred at high etching temperature of 90^oC. Etching duration was also found to be critical in determining the quality of SiC surface roughness during chemical machining.

Experimental data revealed that etching rate was closely correlated to surface roughness as well as the etching ratio. However, using the best etching rate it failed to yield the quality surface roughness, but produced the best etching ratio. Each variable presented different level of significance for each output of chemical machining. The results of etch rate and etch ratio also showed that etching temperature and etching duration imparted significant impact on the chemical machining of all substrates. In the analysis of surface roughness, etching temperature was found to be the critical variable in chemical machining of machinable glass ceramics. Etching temperature and etchant influenced the surface roughness of boron nitride whereas surface roughness of silicon carbide was more dependent on etching duration and etchant used.

Predictive models were developed using DE 7 once the analysis of data was completed. A total of 27 predictive models were developed for each substrate and each output. This predictive model can be used directly in the industry with the selected substrate and etchant. Optimisation of chemical machining was also performed. For machinable glass ceramic, the optimum of chemical machining happened at 100^oC in 10.5 molarity HCl etchant for 30 minutes. Results of chemical machining of machinable glass ceramics were obtained with optimal etching rate of 0.0008g/min, surface roughness improvement of 81.818nm (48% improvement) and

etching ratio of 3.403. In chemical etching of boron nitride, the best result occurred at 40^{o}C in 6 molarity HBr for 62 minutes. The etching rate obtained for BN is 0.00025g/min, with surface roughness improvement of 0.01nm (16% improvement) and etching ratio of 3.153. For the chemical etching of silicon carbide, the best performance occurred at 75^{o}C in 8.5 molarity of HBr for 240 minutes. The optimal value of etching rate for silicon carbide is 0.0009g/min, with surface roughness improvement of 128.71um (35% improvement) and etching ratio of 10.004.

Acknowledgement

I quit my permanent job with the Sony EMCS Sdn. Bhd. to commence a 4-year journey of PhD endeavour in 2008. Life could not have been better without the support from my parents, who have never lost their faith in me.

I would also want to thank my Supervisors, Associate Professor Chua Han Bing and Professor Khaled whom have given their encouragement and guidance throughout these 4 years of research.

My gratitude also goes to fellow lecturers in Curtin University of Sarawak Malaysia namely Dr. Alexander Gorin, Mr. Moola Mohan and Mr. Michael Ding for the contributions in their area of expertise.

Last but not least, special thanks goes to Dr. Paul for his training in “Advance in Design of Experiment”, which has enlightened me in the area of statistical studies.

Publications

Journal Papers

H.T. Ting, K.A. Abou-El-Hossein, H.B. Chua, 2009, *"Review of Micromachining of Ceramics by Etching"*, Transactions of Nonferrous Metals Society of China, Vol. 19, pp. S1-S16.

H.T. Ting, K.A. Abou-El-Hossein, H.B. Chua, 2009, *"Prediction of Etching Rate of Alumino-Silicate Glass by Response Surface Methodology and Artificial Neural Network"*, Journal of Scientific and Industrial Research, Vol. 68, pp. 920-924.

H.T. Ting, K.A. Abou-El-Hossein, H.B. Chua, 2010, *"Etch Rate and Dimensional Accuracy of Machinable Glass Ceramic in Chemical Etching"*, Advances in Science and Technology, Vol. 65, pp. 251-256.

H.T. Ting, K.A. Abou-El-Hossein, H.B. Chua, 20011, *"Etching Rate of Machinable Glass Ceramic"*, Advanced Materials Research, Vols. 264-265, pp. 1306-1311.

H.T. Ting, K.A. Abou-El-Hossein, H.B. Chua, 2011, *"Predictive Modelling of Etching Process of Machinable Glass Ceramics, Boron Nitride, and Silicon Carbide"*, Materials Sciences and Applications, Vols. 2, No.11, pp. 1601-1602.

Conference Papers

H.T. Ting, K.A. Abou-El-Hossein, H.B. Chua, 2008, *"Review of Micromachining of Ceramics by Etching"*, The 1st International Symposium on Hybrid Materials and Processing (Hymap 2008), Busan, Korean, October 2008.

H.T. Ting, K.A. Abou-El-Hossein, H.B. Chua, 2008, *"Application of Design of Experiment for Modelling of Etching of Ceramics – A Review*, The 2nd Engineering Conference (EnCON 2008), Kuching, Malaysia, December 2008.

H.T. Ting, K.A. Abou-El-Hossein, H.B. Chua, 2009, *"Etching Rate of Machinable Glass Ceramics"*, Advanced in Materials and Processing Technologies (AMPT 2009), Kuala Lumpur, Malaysia, October 2009.

H.T. Ting, K.A. Abou-El-Hossein, H.B. Chua, 2009 *"Chemical Etching of Machinable Glass Ceramics"*, 2nd CUTSE International Conference 2009, Miri, Malaysia, November 2009.

H.T. Ting, K.A. Abou-El-Hossein, H.B. Chua, *"Etch Rate and Dimensional Accuracy of Machinable Glass Ceramic in Chemical Etching"*, 12th International Ceramics Congress, Montecatini Terme, Italy, June 2010.

TABLE OF CONTENTS

CHAPTER 3 RESEARCH METHODOLOGY AND TECHNIQUES

List of Tables

List of Figures

Nomenclature

2^k	Two level
3^k	Three level
2FI	2 Factorial Interaction
AWJ	Abrasive Water Jet
ANN	Artificial Neural Network
AFM	Atomic Force Microscope
ANOVA	Analysis of Variance
BP	Backpropagation
BN	Boron Nitride
$Bi_4Ti_3O_{12}$	Bismuth Titanate
CHM	Chemical Machining
CrO_3^{2-}	Chromate
CVD	Chemical Vapor Deposition
CH_3COOH	Acetic acid
c-BN	Cubic Boron Nitride
CCD	Central Composite Design
CCI	Central Composite Inscribed
CCF	Central Composite Face Centered
CCC	Central Composite Circumscribed
DoE	Design of Experiment
DE	Design Expert
EBM	Electron Beam Machining
ECDM	Electrochemical Discharge Machining
EDM	Electrical Discharge Machining
EDTA	Ethylenediamine
ECM	Electrochemical Machining
$FeCl_3$	Ferric Chloride
GaN	Gallium Natrium
HAZ	Heat Affected Zone
HCl	Hydrochloric Acid
H_2O	Solvent/Water
HF	Hydrofluoric Acid
h-BN	Hexagonal Boron Nitride
ICs	Integrated Circuit
IPA	Isopropyl Alcohol
KOH	Potassium Hydroxide
KCl	Potassium Chloride
$K_2Cr_2O_7$	Potassium Dichromate
LN	Liquid Nitrogen
LAM	Laser Assisted Machining

LBM	Laser Beam Machining
LMA	Levenberg-Marquardt Algorithm
MgO	Magnesium Oxide
MEMS	Micro-Electromechanical Systems
MGC	Machinable Glass Ceramic
MSE	Mean-Squared Error
NaCl	Sodium Chloride
NN	Neural Network
OFAT	One-Factor-At-a-Time
PA	Ortho-Phosphoric Acid
PAC	Plasma Arc Cutting
PCD	Polycrystalline Diamond
PCHM	Photochemical Machining
RSM	Response Surface Methodology
RBSC	Reaction Bonded Silicon Carbide
RUM	Rotary Ultrasonic Machining
R^2	Coefficient of Determination
Si_3N_4	Silicon Nitride
SiC	Silicon Carbide
SSE	Sum of Square Error
SEM	Scanning Electron Microscopes
STEM	Shaped Tube Electrolytic Machining
Ti_3SiC_2	Titanium Silicon Carbide
TEA	Triethanolamine
TEM	Transmission Electron Microscope
TiB	Titanium Boride
USM	Ultrasonic Machining

Chapter 1 Introduction

1.1 BACKGROUND

Chemical machining has been used since 2500 B.C. as an engraving process. During engraving, chemical machining was employed to dissolve unwanted materials by masking or indentation. In patterning process, only selective areas are being attacked and this is controlled by masking or indentation. The development of chemical machining is growing with the advances in printed circuit board and growth of semiconductor industry. This is due to the micro and nano-patterning which is required in the patterning process. Chemical machining is also used in the aerospace industry to remove shallow layers of material from large aircraft components, missile skin panels, and extruded parts for airframes. The advantages of chemical machining are attributed to its cost effectiveness and absence of tool life problems.

The study of chemical machining of advanced ceramics focuses on the behaviour of the substrates that influence the efficiency and quality of chemical machining process. Hence, the development of advanced ceramics is the primary focus in the industry [1, 2]. The technology of advanced ceramics has improved as a result of the contribution from all the branches of industry with an interest in machining. Productivity has also increased through the replacement of conventional machining with non-conventional machining for some difficult-to-cut materials.

With the introduction of reliable electron microscopes and micro-probe analyzers in the 1950s, an extensive growth in physical metallurgy has been observed. The evolution of raw materials for mechanical and civil engineering has focused on the ceramics materials

[2]. With their ability to operate under high temperatures, their high resistance to abrasion, high corrosion resistance, and better dimensional stability, advanced ceramics have been widely used in industries, such as space shuttle building, power generation, and electronics industry [1, 3-5].

Increasingly, chemical machining is used in the industry to pattern advanced ceramics. The difficulties of chemical machining are related to its etch rate, surface roughness and accuracy. The etching variables and material properties are always of interest to researchers who aim to improve the production and the machining process efficiency. The etch rate is the main concern in terms of cost and productivity. The quality of etching will be affected significantly once any of the variables are varied [6-10]. Due to advanced ceramics physical properties, etch rate is always an issue and it does require thorough investigation in order to bring the chemical machining process to a more productive level. Surface quality with low value of roughness and without surface damage is desired. Accuracy and surface quality of etched materials is affected by the etch ratio due to the presence of indented and non-indented areas. Under certain condition, etch ratio is too low and affects the patterning or causes undercutting [11]. To optimise the process, chemical machining must be able to deliver product with high etch rate, good surface roughness and high accuracy in patterning.

The properties of microstructures of the etched material are known to be the uncontrollable parameters in this process. The material microstructure differs from one material to another, and it can strongly influence the physical properties, including the strength, toughness, and corrosion resistance of the material, which in turn govern the application of these materials in industrial practice. These properties are strongly related to the production of each material. Another problematic parameter is etchant quality. The quality of chemical etchant can significantly affect the result of chemical machining. The mixing process of etchant has to be very precise [6]. Thus, different results could be achieved for the same material etched in the same media when the same processing parameters were used. In addition, certain ranges of concentration are suited for specific ceramic materials. Besides, the results due to changes of the etchant concentration in

etching process at high temperature are difficult to predict due to the vaporisation and uncontrollable water content [7].

The objective of the current ceramic chemical machining study is to establish a predictive theory that would enable us to predict etch rate, surface roughness and accuracy. Thus, modeling and prediction of etching process will be carried out.

The statistical and artificial tools will be used in analysing and predicting etching process under various ranges of parameters. These models would be able to improve the etching process and reduce the number of experiments, which are used traditionally for tool design, process selection, and machinability evaluation. The predictive models generated will be used to predict the relationships and interaction of the variables involved.

1.2 MOTIVATION AND RESEARCH MAIN OBJECTIVES

Due to chemical machining history and the hazards in material preparation and processing, it rarely attracts the interest of researchers. Besides, it is also related to the substrate's mechanical properties (high resistance to abrasion and excellent hot strength), which discourage the researchers from applying chemical machining as the process method. The present research works focus mainly on the improvement of current method by adding stirring process or aided material to enhance the process. Substrates and etchants used are limited, and this further constrains the choice and development of advanced ceramics in the industry. However due to the growing demand of advanced ceramics and also the growth of patterning industry, there is still a good deal of motivation to extend the research studies to other types of advanced ceramics instead of the existing conventional substrates.

The motivation of this study is driven first, by the lack of information or reports on the performance of chemical machining of advanced ceramics. It is envisaged that this study would provide more insight on the performance of the chemical machining by establishing the relationships between key parameters such as etch rate, surface

roughness and dimensional accuracy of the machining process. From current reports, most of the research conducted focus on either one or two of the parameters and there remains a gap in the knowledge and understanding in regard to the performance of chemical etching of advanced ceramics. The study aspires to provide a more holistic understanding on the performance of chemical machining of advanced ceramic from the analysis of the etchant used and the results from the etch rate, surface roughness and dimensional accuracy studies.

The second motivation factor is that presently, no reports of any predictive models developed for the chemical etching of ceramic materials are available. Based on the statistical analyses of the results obtained from the machining performance for the selected number of advanced ceramics, predictive models can then be developed for the machining process. The models that are developed would strengthen the establishment of the relationship between the variables studied and output involved in the machining processes. Besides, the predictive model that is developed can be considered for application to mass production in the industry if the process is accurately assessed. This could save a lot of time and costing on the testing as well as resources.

Last but not least, this study would provide me with the opportunity to explore the use of micro-scratch technique for the patterning process in chemical machining. The old technique of patterning (mask patterning) is faced with challenges associated with undercutting, mask adhesive issues and its unstable resistivity against chemical reagents. This relatively new technique would be carried out to improve the patterning process. Similar technique, known as nano-scratch has been used for patterning in research field, but further improvement on the technique is required.

The major objectives of the current research work are summarized as follows:

a) To establish relationships for the chemical machining process of advanced ceramics in terms of etch rate, surface roughness and accuracy, based on specified range of variables involved.

b) To predict the cutting performance and optimise cutting parameters that would eventually lead to improved productivity.

1.3 SCOPE

The current study involved the developments of predictive models for etch rate, surface roughness and accuracy by employing the response surface method (RSM) and artificial neural network (ANN). The experiments were carried out with selected ranges of etching variables (etching temperature, etching duration, etchant and it concentration). The range of these variables was selected based on the preliminary experimentation. Chemical machining experiments were conducted according to the principles of design of experiment (DoE) so as to eliminate the large number of experiments that would otherwise be needed. Experimental data was then analysed with statistical method based on the response surface roughness – central composite method (CCM) and Artificial Neural Network (ANN).

1.4 THESIS OUTLINE

This thesis is organised into eight chapters as outlined below. The structure of the thesis is graphically presented in Figure 1-1.

- ***Chapter 1*** defines the motivation and objectives, scope, overall aims and the structure of this thesis.
- ***Chapter 2*** reviews the background areas relevant to this PhD research. It also covers the advantages and limitation of each machining method. This chapter also identifies the existing gaps, from which the specific objectives of this research are developed.
- ***Chapter 3*** summarises the research methodology, as well as the experimental and analytical techniques employed in this study. In this chapter, it describes the tools and equipment used in this research study.

- ***Chapter 4*** discusses the characterisation of the etch rate by analysing the ANOVA data and also discusses the relationship between the main variables with etch rate of each material.
- ***Chapter 5*** discusses the characterisation of the surface roughness by analysing the ANOVA data and also discusses the relationship between the main variables with surface roughness of each material.
- ***Chapter 6*** discusses the characterisation of the dimensional accuracy by analysing the ANOVA data and also discusses the relationship between the main variables with dimensional accuracy of each material.
- ***Chapter 7*** investigates the optimisation of chemical machining. This chapter also discussed the predictive mathematical models produced by RSM and ANN, and compared the results obtained by both analytical tools and with the experimental results.
- ***Chapter 8*** draws conclusion from this study and outlines the recommendations for future research.

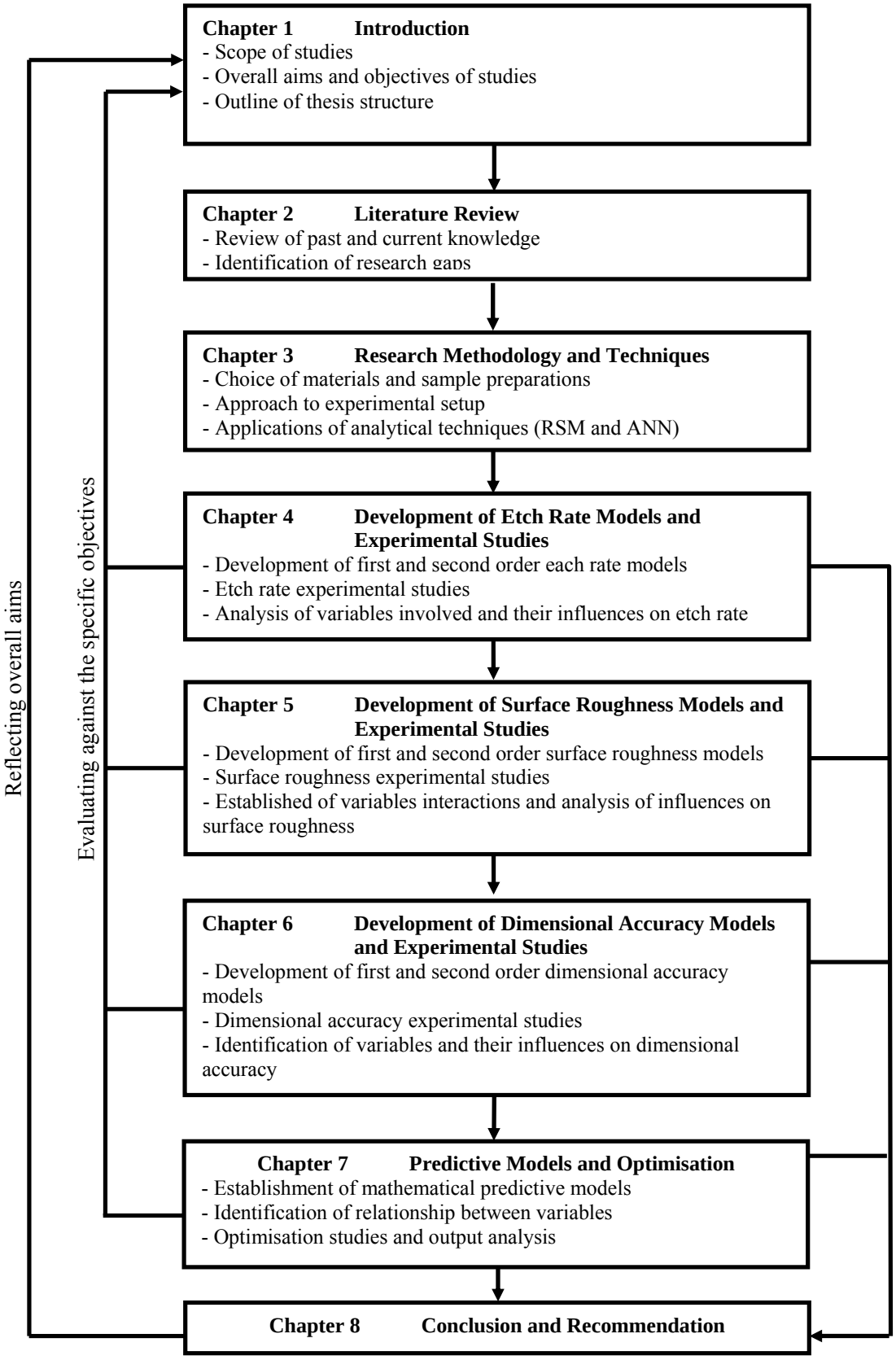

Figure 1-1 Thesis presentation

Chapter 2 Literature Review

2.1 INTRODUCTION OF ADVANCED CERAMICS

The term “ceramics” covers inorganic non-metallic materials that are formed by the action of heat to increase mechanical hardness and strength. Ceramics are classified into two types, namely, traditional ceramics and advanced ceramics (engineering ceramics). Nowadays, advanced ceramics can be classified into three distinct categories: oxides of (alumina, beryllium and zirconia), non-oxides (carbides, borides, nitrides and silicates), and composites (particulate reinforced combinations of oxides and non-oxides) [1].

The most common type of starting material for making ceramics is the chemically prepared powders. In the making of ceramics, additional materials are added to the powder to form the ceramic particles into the desired shapes. Some of the most common methods for processing ceramics include extrusion, slip casting, pressing and injection molding. Following these processes, ceramics are subject to heat treatment or sintering to increase the strength of the products formed [12].

2.2 ADVANCED CERAMICS

The development of advanced ceramics has opened a whole new approach to manufacturing industry. In the past, the applications of advanced ceramics were limited to certain industries due to their inherent properties. With the new tailored materials, engineers literally create the necessary materials and the structure for integrated manufacturing. Thus, with tailored materials, the old concept of materials, design and

fabrication processes are merged together into the new concepts of integrated design and manufacturing.

The 20th century has produced the greatest advancement in ceramics and material technology. The extensive metallurgical development in this period has now produced almost every conceivable combination of metal alloys and their capabilities are well known and continuously been exploited. The push for ever faster, more efficient, less costly production techniques continues up to today.

As the limits of metal-based systems are surpassed, new materials capable of operating under higher operating condition, longer service life and lower cost are required to keep pace with technological advancements. Metals, by virtue of their unique properties, such as, ductility, tensile strength, simple chemistry, and relatively low cost of production have occupied the vanguard position in regard to materials development. By contrast, ceramics are brittle by nature, having a more complex chemistry and requiring advanced processing technology and equipment to produce, and they perform best when combined with other materials, such as metals and polymers which can be used as support structures. This combination enables large shapes to be made. The Space Shuttle is a typical example of the application of advanced materials and an excellent testimony to the high capability of the advanced ceramics.

Given the advances in the understanding of ceramics and the knowledge gained from, crystallography analysis and their production in the ceramic industry, advanced ceramics have been widely used in many sectors of industry, especially in the electronics industry. The manufacturing techniques that involved metals previously were now considered applicable to ceramics systems. Many other techniques involving phase transformation, alloying, quenching and tempering techniques were applied to advanced ceramics production. As a result, the physical properties of advanced ceramics have been found to be significantly improved in terms of fracture toughness, ductility and impact resistance.

The new and emerging family of ceramics is referred to as advanced, and utilises highly refined materials and new forming techniques. These advanced ceramics posses several superior properties including high resistance to abrasion, excellent hot strength, chemical inertness and dimensional stability.

Advanced ceramics [12, 13] can be classified into three distinct material categories: oxides, non-oxides and composites. Each of these possesses unique properties and production method. Oxides ceramics contains alumina and zirconia, and these materials are highly resistant to oxidation, chemically inert and electrically insulating with low thermal conductivity. The production cost of zirconia is slightly higher compared to alumina. Non-oxides ceramics: carbides, borides, nitrides and silicates. They are extremely hard, chemically inert, and expensive and have high thermal conductivity, low oxidation resistance and electrical conductivity. Ceramic-based composites are particulate reinforced, combinations of oxides and non-oxides. These types of ceramics have great toughness, variable thermal and electrical conductivity, but the complex manufacturing processes involved require high cost.

To produce advanced ceramics, it requires demanding and complex procedure. High purity starting materials and precise methods of production must be employed to ensure the desired properties of these materials are achieved in the final product. As minor impurities can have a dynamic effect, for example, small amounts of Magnesium Oxide (MgO) can have a marked effect upon the sintering behaviour of alumina.

Oxide ceramics [1, 12, 14]are produced by using high purity starting materials. These materials are then cleaned or removed of unwanted impurities and other unnecessary compound with mineral processing technique. After the purification stage, small amounts of wax are added to bind the ceramic powder. Then, it undergoes heat treatment to produce a dense product. Production of non-oxide ceramics involves three stages of process: preparation of starting powders, mixing to create desired compounds, and formation and sintering of final component. The final stage has to be carefully controlled to ensure the absence of oxygen during heating as these materials will readily oxidise

during firing. As for the ceramic-based composites, they are produced from a combination of oxide ceramics and non-oxide ceramics or mixtures of different oxide ceramics or non-oxide ceramics respectively.

Advanced ceramics are now well established and their improvement in physical and chemical properties is clear evidence of their benefits. However, the production cost is high due the complex and precise production equipment. It is envisaged that the future ceramic materials will exploit the properties of polycrystalline phase combinations and composite ceramic structures to produce product of high and distinct quality.

2.3 MACHINING OF ADVANCED CERAMICS

The machining that is employed for ceramic shaping can be divided into two categories, namely conventional machining and non-conventional machining. Conventional machining includes grinding, drilling, turning, boring and milling, and non-conventional machining includes chemical machining, ultrasonic, abrasive water jet (AWJ), electrical discharge machining (EDM), laser beam machining (LAM). The type of machining used for ceramic shaping is dependent on the industry requirements. Industries such as aerospace and automobile require products with high strength, while semiconductor industry requires high dimensional accuracy and high surface quality product. Machining operations need to be chosen carefully in terms of time and cost efficiency, and the emerging environmental concerns.

2.3.1 Conventional Machining

Conventional machining is one of the most important material removal methods that uses mechanical energy. It can be classified as turning, milling, drilling and grinding. Each of these processes requires a sharp tool to mechanically cut the material to achieve the desired geometry. The disadvantages of conventional machining include the use of lubricant, which is environmentally unfriendly, long processing time, the use of high cost tools, high energy consumption and relatively low product quality, and, in some cases conventional machining is not feasible.

Turning operation is commonly used to produce cylindrical products from ceramics. A few studies have been conducted on turning operation of advanced ceramics. The major issues found are tool wear and surface damage. Tool wears that take place in machining of advanced ceramics are mainly affected by the tool materials and cooling condition [15]. The extremely high tool wear rate and surface damage of ceramics produced during machining are due to the high cutting temperature and the extreme hardness of the substrate. Wang et al. [16] introduced liquid nitrogen (LN) cooling to control the temperature in the cutting zone. The results showed that LN cooling was able to decrease the temperature in the cutting zone and better surface roughness was produced. Dabnum et al. [17] presented turning process in glass-ceramics using RSM method and showed that conventional machining was able to machine ceramics with some additives or supportive methods. He showed that the feed rate was the main influencing factor on the roughness, followed by the cutting speed and depth of cut. Yan et al. [18] indicated that the sintering temperature of ceramics materials plays a significant role in the turning process. It was found that polycrystalline diamond (PCD) tool is superior to the other tools, whilst the carbide inserts and the ceramics tool are unsuitable for machining ceramics. It was also found that turning ceramics with a sucker in cool and highly humid weather moistens the tool face and promotes tool wear. Few researchers have attempted to enhance the turning performance in ceramics materials. Vermaeulen et al. [19] designed an optical diamond turning machine to create the deterministic behaviour required for submicrometer shape accuracy and mirror surface quality, thereby minimizing tolerances in the manufacturing, and reducing requirements on conditioning of ambient temperature as well as the effort on software error compensation.

Grinding process tends to introduce strength-inhibiting defects into ceramics. A few methods have been used to prevent this damage, such as ‘ductile-regime’ grinding, lapping, polishing or ion beam implantation, but these processes resulted in raising the machining cost [20]. Pre-machining processes, such as surface polishing are known to weaken the flexural strength. There are doubts, however, as to the effectiveness or economics of such treatments, and alternative measures need to be undertaken. Huang

and Liu [21] investigated advanced ceramics machining characteristics and removal mechanisms. They observed that fractured and smeared areas were generated on Al_2O_3-TiO_3 surface after grinding process. These defects increased with smaller depths of cut. Chipping and cracking were clearly observed under SEM. The damage layer right underneath the machined surface seemed to be generated via 'chipping' [21]. The work at university of Tokyo [22] used a modified Norton Co. controlled milling centre and cast-iron-bonded diamond grinding tools for creep-feed grinding, and reported stock removal rates in complicated 3D shapes from Silicon Nitride (Si_3N_4) and Silicon Carbide (SiC). Tsutsumi et al. [23] found that the application of electric-discharge machining in grinding showed an increased in wheel cutting ability. The surface roughness of Si_3N_4 ground with the in-process decreases with decreasing grit diameter.

2.3.2 Non-Conventional Machining

Non-conventional machining is well known in ceramics processing due to its high productivity and cost effectiveness. In the past, many researchers have studied machining of advanced ceramics conducted by chemical machining (CHM), electrical discharge machining (EDM), laser assisted machining (LAM) and ultrasonic machining (USM). Non-conventional machining utilises other forms of energy different from mechanical energy. The energies used in non-conventional machining are thermal energy, chemical energy and electrical energy.

Chemical machining (CHM) is the oldest manufacturing technology. This process applies reactive etchants to remove unwanted part from the substrate surface. It is a corrosive-controlled process .Many studies have been done on CHM to investigate its etch rate, surface roughness and accuracy. CHM includes photochemical machining (PCHM). PCHM is a method of fabrication component using reactive etchants to corrosively oxidise selected areas of the component. This process can produce highly complex products with very fine details, at high accuracy and low cost. They present a number of advantages, such as simple set up, quick preparation and no tool is required, hence problems such as tool wear, machine tool deflections, vibrations and cutting forces are eliminated. In addition, chemical machining minimises the effect of ceramics brittleness

and low fracture. The disadvantages of chemical machining include chemical disposal, the presence of uncontrollable parameters, especially material structure and their rate of chemical reaction with etchants. In addition, high attention is required during processing. Zubel et al. [24] studied the silicon anisotropic etching process in water etchant of KOH and TMAH with and without both organic and inorganic addition. This study showed the etch rate was affected by the presence of organic and inorganic agents. Kim et al. [25] employed the etching process with a lower O_2 gas flow ratio and found that this action reduced etching damage to the low-*k* materials.

Abrasive water jet (AWJ) is a technique that involves forceful impingement of abrasive particles to achieve the removal of surface material. AWJ depends on the water jet pressure, stand-off distance, abrasive size and flow rate. However, these choices are significantly affected by external factors such as the machined material structure and geometry of the jet nozzle [20]. The most common advantage of AWJ is that it yields little heat during machining process and therefore, there is no heat affected zone (HAZ), and hence the process does not require heat treatment. Compared to traditional machining technologies, AWJ offers the following advantages: fast speed, able to cut thick material, good accuracy, finishing surface and it cuts virtually anything with no HAZ. Unfortunately, some burr will occur near the cutting area. AWJ is widely used in metal, glass, ceramic, marble and granite cutting machines. Gi and Gi [26] concluded in their research that AWJ has a great potential as a machining method for brittle and hard materials. Unfortunately, they found a large-scale fracture could easily develope on the backside of the substrate and affect surface finish. Although AWJ has been recognized as the most efficient method to machine ceramics, Chen et al. [27] reported that damage tends to occur in the lower zone of the surface, where a lot of pits were found and this reduced the surface quality. To overcome this problem, a new cutting head oscillation technique has been introduced. This technique applied to the cutting process produces superior results and shows the smooth zone depths increase by more than 30% with oscillation as compared to that without oscillation. However, further study is proposed to reduce the pits effect that occurs at the lower surface layer [28, 29].

Electrical discharge machining (EDM) uses spark erosion to remove small particles from electrically conductive material. The acceleration of EDM material removal rate is increased with the discharge current and working voltage, but decreased with increasing pulse duration. EDM is especially well-suited for cutting intricate contour that would be difficult to produce with traditional machining. Advantages of EDM include high dimensional accuracy, good surface finish, lack of burr and little HAZ. Ti_3SiC_2 with excellent electrical conductivity and thermal conductivity is easily machined by EDM, but high power is needed [30]. In order to obtain a high material removal rate and better surface roughness, Liu et al. [31] suggested using a suitable chemical additive, dielectric strength, washing capability and viscosity of the machining fluid. They also suggested using a water-based emulsion as the machining fluid since harmful gas is not generated during machining, and the equipment will not corrode. Another suggestion by Muttamara et al. [32] to improve the material removal rate is by employing positive polarity in case where the conductive layer is sufficient. Study on the EDM of conductive ceramics shows EDM performance is purely dependent on the level of intensity. It has been observed that increasing intensity will tend to increase surface roughness and electrode wear [33]. Hu et al. [30] investigated EDM on Titanium Silicon Carbide (Ti_3SiC_2) using water as dielectric and found typical thermal shock cracks and loose grains in subsurface, which resulted in about 25% of strength degradation.

Electrochemical Discharge Machining (ECDM) is a modification of EDM. Materials are removed or deposited with the transferring of ions based on the anodic dissolution mechanism, where high precision is achievable and it has the feasibility of micromachining. In order to obtain better machining accuracy and smaller machining size, much research has been done on electrolyte, electrode's insulation and systematic control of machining process [34-37]. Bhattacharyya et al. [38] found that machining rate and accuracy could be enhanced through effective and precise control of the spark generation. Taper side wall and flat front tool tip are the most effective parameters for controlled machining. The advantages of ECDM include higher material removal rate, use of nontoxic electrolyte components with very little changes in their composition during operation, minimal waste disposal, monitoring and control of electrolyte [39].

The laser assisted machining (LAM) is a thermal process. The laser is used as a heat source with the beam focused on the un-machined section of the substrate. The addition of heat softens the surface layer of the material, allowing ductile deformation rather than the brittle deformation to occur during cutting. LAM power requirements depend largely on the material and the nature of the machining process [40]. The possibility of vapourising material during LAM may cause surface problems due to its severity in much the same way as in discharge machining [20]. The advantages of laser are that it provides high speed and precise cut when cutting thin material and the method yields no burr and a little heat affected zone (HAZ). LAM has demonstrated its ability to reduce cutting force and lower dynamic forces, allowing less sharp segmented chip and smooth surface finish to be produced [41]. It is suitable to cut non reflection mild steel. LAM, however, requires high energy and cost to operate and must be conducted under a specified condition. The power of laser must be controlled properly to obtain a satisfactory result and a lot of power is needed to archieve this machining. Chang et al. [42] showed that LAM is able to predict the temperature distribution of difficult-to-machine materials during the machining process. Tool wear is a major factor affecting the surface roughness of the substrate. The authors [40] found that cutting resistance of processing aluminum oxide ceramics are extremely large, thus increasing the tool wear and reducing surface quality. Tsai et al. [43] reported that generation of tensile stress was concentrated at the edge of groove-crack and induced the extension of the groove-cracks during LAM. Black et al. [44] also showed that surface glaze usually possesses a different linear expansion rate to the underlying substrate. The large thermal gradient caused by the laser beam causes the lower substrate to expand at a different rate, resulting in cracking of the glaze.

Ultrasonic machining (USM) is a process where material is removed primarily by repeated impact of the abrasive particles. The main parameters, namely, static force, vibration amplitude, and grit size, have significant effects on the material removal rate [45-47]. Material removal occurs when the abrasive particles, suspended in the slurry between the tool and substrate, impact the substrate due to the down stroke of the vibrating tool. It is mentioned in many reports [45-47] that, for deeper cut, a vacuum-

assisted machining is strongly recommended to ensure adequate flow of the suspension. Another type of USM is rotary ultrasonic machining (RUM). RUM combines material removal mechanism of diamond grinding and USM. The difference between USM and RUM is in the tool used. USM uses a soft tool and slurry is loaded with hard abrasive particles while in RUM the hard abrasive particles are bonded on the tools. The major advantage of USM is that the machining does not involve thermal, chemical, or electrical process. Therefore, metallurgical, chemical and physical properties of the substrate remain unchanged. However, in USM, the material removal is considerably slow and even stops as penetration depth increases. The slurry may wear away the wall of the machined hole as it passes back towards the surface, which limits the accuracy and causes considerable tool wear. Efforts have also been made to develop models to predict the material removal rate in RUM from control variables [47, 48]. Zeng et al. [48] demonstrated that RUM tools could be designed in a way so that the lateral face is shorter. Tools with shorter latter face use less diamond grains and hence incurring lower manufacturing cost. The relationship between the cutting force and tool wear stage could be used indirectly to monitor tool wear during the machining processes. Thoe et al. [45] summarised that tool materials should have high wear resistance, good elastic and fatigue strength properties, and have optimum values of toughness and hardness for application. Table 2-1 below presents a summary of the non-traditional machining methods.

Table 2-1 Summary of Nontraditional Machining [14]

Process	Typical Penetration/ Feed rate mm/m (ipm)	Typical Surface finish AA, µm(uin.)	Typical accuracy, mm (in.)	Typical substrate or feature size, cm (in.)	Comments
Chemical					
Chemical milling	0.013-0.076 (0.0005-0.003)	1.6-6.35; as low as 0.2	Greater than 0.127 (0.005)	365x1524 (144x600) up to 1.27 (0.5) thick	• No burrs • No surface stresses • Tooling cost low

Process	Typical Penetration/ Feed rate mm/m (ipm)	Typical Surface finish AA, μm(uin.)	Typical accuracy, mm (in.)	Typical substrate or feature size, cm (in.)	Comments
Photochemical machining	As above	As above	0.025-0.05 (0.001-0.002)	30x30 (12x12) Up to 0.15 (0.06) thick	• Limited to thin material • Burr-free • Tooling cost low • Used in microelectronics
Electrochemical					
Electrochemical machining (ECM)	2.5-12.7 (0.1-0.5)	0.4-1.6 (16-63)	0.013-0.13 (0.0005-0.005) 0.05 (0.002) in cavities	30x30 (12x12) 5(2) deep	• Stress-free • Burr free • Tool design expensive • Disposal of wastes a problem • MRR independent of hardness
Electrostream drilling	1.5-3 (0.06-0.12)	0.25-1.6 (10-63)	0.025 (0.001)	Up to 0.5 (0.2) thick	• Charged high-velocity stream of electrolyte • Hole diameters down to 0.127mm • 40:1 hole AR
Shaped tube electrolytic machining (STEM)	As above	0.8-3.1 (32-125)	0.025-0.125 (0.001-.005)	Routinely up to 127 (5) thick	• Special form of ECM using conductive tube with insulated surface and acidic electrolyte • 300:1 hole AR • Hole diameters down to 0.5mm
Mechanical					
Abrasive jet machining	76 (3)	0.25-1.27 (10-50)	0.12 (0.005)	Up to 0.15 (0.06) thick	• Used for cutting brittle materials • Produces tapers • Inexpensive to implement • Can cut up to 6.3mm thick glass

Process	Typical Penetration/ Feed rate mm/m (ipm)	Typical Surface finish AA, μm(uin.)	Typical accuracy, mm (in.)	Typical substrate or feature size, cm (in.)	Comments
Abrasive waterjet machining	15-450 (0.6-18)	2.0-6.35 (80-250)	0.13-0.38 (0.005-0.015)	Up to 20(8) thick	• Used in glass, titanium, composites, nonmetals and heat-sensitive or brittle materials • Produces tapered walls in deep cuts • No burrs
Ultrasonic machining (impact grinding)	0.5-3.8 (0.02-0.15)	0.4-1.6 As low as 0.15	0.013-0.025 (0.005-0.001)	Up to 100cm^2 (16in^2)	• Most effective in hard materials • Rc>40 • Tool wear and taper limit hole AR at 2.5:1
Waterjet machining	250-200000 (10-7900) Soft material	1.27-1.9 (50-100)	0.13-0.38 (0.005-0.015)	Up to 2.5(1) thick	• Used on leather, plastics, and other nonmetals • Pressures of 60000pso and jet velocity of up to 3000ft/sec
Thermal					
Electrical discharge machining (EDM)	Up to 0.5 (0.02)	0.8-2.7 (32-105)	0.013-0.05 (0.0005-0.002)	Up to 200x200 (79x79); 5(2) deep	• Widely used and disseminated • Dies expensive • Cut all type of materials • Forms recast layer
Electron beam machining (EBM)	30-1500 (1.2-60)	0.8-6.35 (32-250)	0.005-0.025 (0.0002-0.001)	0.025-0.63 (0.01-0.25) thick	• Capable of micromachining thin materials • Hole sizes down to 0.05mm (0.002in) • 100:1 hole AR • High vacuum
Laser beam machining (LBM)	100-2500 (4-100)	0.8-6.35 (32-250)	0.013-0.13 (0.0005-0.005)	Up to 2.5 (1) thick	• Capable of drilling holes down to 0.127mm at 20:1 AR in seconds • Heat-affected zone and recast layers which may require removal •

Process	Typical Penetration/ Feed rate mm/m (ipm)	Typical Surface finish AA, µm(uin.)	Typical accuracy, mm (in.)	Typical substrate or feature size, cm (in.)	Comments
Plasma arc cutting (PAC)	250-5000 (10-200)	0.6-12.7 (25-500)	0.5-3.2 (0.02-0.125)	Up to 15(6) thick	• Clean rapid cuts and profiles in almost all plates • 5 to 10^{o} taper • Cheaper capital equipment
Precision PAC	As above	As above	0.25 (0.01)	Up to 1.5 (0.625) thick	• Special form of PAC limited to think sheets of material • Straighter & smaller kerf
Wire EDM	100-250 (4-100)	0.8-1.6 As low as 0.38	0.0025-0.1 (0.0001-0.004)	As large as 100x160 (40x65) Up to 45(18) thick	• Special form of EDM using traveling wire • Cuts straight narrow kerf • Wire diameters as small as 0.05mm (0.002in) • Permit complex geometries

2.4 THEORY OF CHEMICAL ETCHING (CHM)

CHM in the early years was mostly involved in the jewelry industry. Back in 4500 years ago, Egyptians used citric acid to etch jewelry [14]. Approximately 1000 years back in the region of United States, the Hohokam Indians used fermented cactus juice to etch jewelry. In 17th century, it was used for the first time as a manufacturing process of steel parts. Developments in chemistry provided significant advancement with the discovery of new type of acids during the 18th and 19th Century [49]. The first patent (British Patent: 565) was taken by William Fox Talbot (1982) using ferric chloride ($FeCl_3$) for etching copper. Later, John Baynes described chemical etching of materials from two sides in the US Patent 378,423 in 1888 [50].

Until late 1930s, CHM began with limited use of chemicals in manufacturing. In the 1940s, North American Aviation patented a process called chemical milling, which was used to fabricate aircraft wing panels. During the same period, CHM had begun to emerge in producing printed circuit boards. Major developments were noticed after the Second World War and the process has been widely used as manufacturing process since 1950s. First industrial application was conducted by North American Aviation, Inc. (California, USA) to etch aluminium components for rockets. The company named the process "chemical milling" and patented it (US Patent No: 2 739 047) in 1956. The process was used for removing excess mass from aluminium wing skins and other airframe parts [51].

Today, CHM is characterised as a process that uses acidic or alkaline etchants to dissolve materials in a controlled manner for purpose of milling or blanking parts. CHM is popular in producing complex configurations in thin materials and material that could be easily damaged by using conventional cutting tools [52]. There are two types of CHM, namely, chemical blanking and chemical milling.

Chemical blanking or photochemical machining is the process of producing metallic or nonmetallic parts by chemical action. This process consists of placing a chemical-resistance on the substrate and exposed it to chemical action. All exposed surface are dissolved except the desired part.

Chemical milling or chemical etching is the process used to shape substrate to an exacting tolerance by the chemical removal of substrate, rather than by conventional mechanical milling machining operations. The amount of material removed, or depth of etch, is controlled by the several independent variables. Location of the un-etched areas is controlled.

Chemical etching is categorised into etching in aqueous etchants and defect selective etching. There are two major classes of etching processes, namely, wet etching and dry

etching. The major differences are that wet etching is an isotropic process, which have selectivity that depends on crystallographic direction, masking and underlying layers.

Wet chemical etching techniques provide high degree of uniformity and repeatability, and adjustable etch rate by changing the ratio of components in the etching etchant. The versatility of this technique would enhance the etching process since the performance of chemical micromachining is determined by etch rate (material removal rate), etch ratio, surface roughness and accuracy. Generally, wet chemical etching involves removal of unwanted material by the exposure of the substrate to a corrosive etchant. The exposed material is oxidized by reactivity of the etchant to produce the reaction products [53]. The etch rate depends strongly on the kinetic and the reaction mechanism between the substrate and etchant involved.

There are two types of wet etching, namely, isotropic etching that involves etching the material in all direction and anisotropic etching, that involves etching in selective direction. The most popular anisotropic etchant is potassium hydroxide (KOH) given its low safety requirement. Anisotropic etching is mostly used in sophisticated design in conjunction with photoresist masks. The masks properties, however need to be compatible with the selected etchant [52].

Isotropic etchants having dissolution rates independent of orientation are also used. These chemical mixtures tend to uniformly remove material, and are limited by the mass transport of chemical species to the crystal surface. The actual surface reaction rates are so great that variations to atomic structure do not alter the reaction speed relative to chemical transport [54]. In order to obtain better results in terms of productivity and surface quality of machined ceramics, researchers have created many types of etchants. These include molten salt and Secco etch, which are commonly used in the industry and others include Dash etch, Jenkins Wright etch and Sponheimer etch.

A number of factors that influence etch rate are etchant properties, etchant concentration, etching duration, temperature, material properties, set up condition, agitation and stirring process [7, 8, 55]. A small change in each of these parameters will result in producing a

big different product at the end of the process. The nature of the etchants and their concentration are the main concerns. In order to obtain good results, etchant and substrate must be matched perfectly, in terms of their chemical properties. Due to ceramic mechanical properties, its grades are stable even at high temperature conditions. Thus, ceramics are always etched at extremely high temperature for several hours. Agitation and stirring process are considered as an additional process to stimulate the reactions and to enhance its performance. William et al. [6, 7] summarised the relationship between etchants and substrate after carrying out chemical etching process at different etching parameters. In their papers, they tested with a few variables, such as temperature, etchant types and etchant concentration. They highlighted that not all materials were etched in all the etchants and only specific etchants and concentrations are suited for certain materials [56].

The difficulties in micromachining of advanced ceramics are mostly related to etch rate, etch ratio, surface roughness and dimensional accuracy. Etch rate is the main concern in term of cost and productivity. Other external parameters are stirring process and aided material. From previous research works, it has been proven that stirring action was able to increase the etch rate by removing the ion concentration during etching process [57] and aided material, such as trithanolamine, supersonic aid, are able to increase the etch rate [55, 58, 59]. Undercut is a commonly known limitation phenomena in chemical etching. This is because wet isotropic etching has been chosen and this type of process etched the substrate at all directions at the same rate. In order to reduce the undercut effect, etch ratio between indented and non-indented area is being introduced [60].

Another difficulty mentioned above is the quality of micromachining. This is measured by substrate surface condition. With low value of roughness and less damage on surface, it is considered as good quality. A few uncontrollable parameters on surface quality are substrate microstructure and the chemical reaction between substrate and etchant [7]. Islands or isolated high spots can be formed due to the improper agitation [14]. Islands can also be formed due to the inadequate cleaning and inhomogeneity with the work

material. An overhang can result if the etchant is not properly agitated, particularly on deep cuts.

CHM is a very useful and economical method for weight reduction. With minimum set up procedures and equipments, CHM can be carried out easily because it does not require highly skill labour. During the process, CHM does not induce stress in substrates, nor affecting their mechanical properties. CHM, which is the oldest nontraditional machining method, can be applied to almost any material and parts of virtually any shape. Thin section, such as honeycomb, can be done because there are no mechanical forces involved in the process. In some applications, chemical machining can be an economical method for mass material removal because material is removed simultaneously from all surfaces of the part involved.

Although CHM is cost effective, it requires the handling of dangerous chemicals and the disposal of potentially harmful by-products although some recycling of chemicals may be possible. Besides, CHM may release existing residual stresses in the substrate and thus cause warpage. This is happening because of the different grain structure that exists near the welds, since weldments usually are not suitable for chemical machining.

2.5 ETCH RATE

Nowadays, manufacturing industries require high productivity. Thus, etch rate has become an important issue. Previous works summarised that etch rate varies as a function of temperature, elapsed time from the start of etch and etching period, etchant type and concentration, substrate properties and agitation [56]. Commonly, etch rate in CHM is very efficient compared with other nontraditional machining processes. However, etching proceeds on all exposed surfaces simultaneously which significantly increases the overall material removal rate on large parts.

Agitation has been proven to influence etch rate significantly. Additive materials have also been shown to affect etch rate in wet etching process. It was found that

ethylenediamine (EDTA), triethanolamine (TEA), pyrazine and hydrazine, have caused reduction in etch rates [55, 59]. These organic compounds probably are adsorbed on the silicon surfaces and they could restrict access of etching agent (OH^- or H^+ ion and water molecules). On the other hand, viscosity of the etching etchant might increase. This will lower the diffusion rate of the ions produced in the etching processes and decrease the etch rate. Cai et al. [61] added hydrochloric acid (HCl), potassium chloride (KCl) and sodium chloride (NaCl) into the etchant to investigate their influences on etch rates. Their experiments showed that addition of KCl increases etch rate, HCl had no effect on etch rate and NaCl had negative effects on etch rate. Peng et al. [57] studied etching process on gallium nitride (GaN) and etch rate proved to be increased significantly with photo-assisted process. Figure 2-1 [57] indicates both the solute (KOH) and solvent (H_2O) play an important role in the PEC etching of GaN. With an increase of the OH^- concentration, the hydration effect continuously reduces the H_2O concentration. These competing effects therefore produce a peak in the etch rate whose location is very sensitive to the mean hydration number of solute. Zubel and Barycka [62] found that etch rate was decreased significantly when conducting etching process without IPA. UV excitation can impart considerable energy to the photo-generated carriers at the GaN/electrolyte interface and enhance the oxidative dissolution process. For parts machined by immersion, the uniformity of the etchant concentration within the bath can be improved by agitation. If the bath is not agitated properly, several defect conditions can result, as island, or isolated high spots due to improper agitation on large parts [14]. Other defect such as dishing and pitting (due to unequal etch rates) can also be caused by improper agitation.

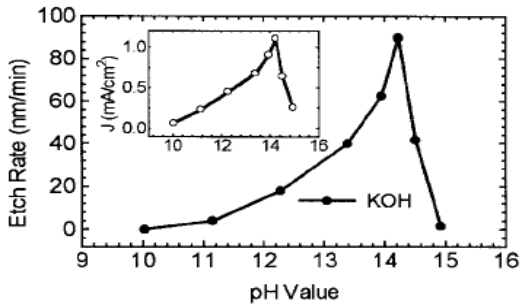

Figure 2-1 pH dependence of the GaN PEC etch rate in aqueous KOH etchants. Inset shows the pH dependence of the etch photocurrent density [57]

Stirring process is to increase the inflow of the active agent to the surface of silicon during etching in diluted etchants. During etching, substrate will react with etchant and release hydrogen ions. This reaction stops only when etch product blocks the chemical flow and causes an invisible wall between ions and substrate [63].

Substrate influences etch rate by its microstructure, film stress, and impurities in or on the material itself. Vartuli et al. [63] reported a decrease in etch rates with increasing crystal quality, as the reactions occurred favourably at the grain boundaries and defect sides. One of the most significant reasons for etch rate variation is the mechanical properties of the material, which are the result of the production method and subsequent processing. Etching process in the deposition method of pure materials tends to produce much greater differences in etch rate [7]. Other causes of unequal etch rates can also be due to selective etching at micro-cracks and grain boundaries in the materials [14].

Etchant affects etch rate by loss of reactive ions, loss of liquids to evaporation, etch product blocking in the chemical flow and concentration of etchant. William et al. [6, 7] provided the information of 620 etch rates of 53 materials in 35 etches that might be used in future fabrication of micro-electromechanical systems (MEMS) and integrated circuit (ICs). The etch rate in CHM is directly proportional to etchant concentration and directly adjacent to the area being machined [14]. Etchant concentration is related to the content of ion hydrogen in etchant. Higher concentration etchant or higher ion hydrogen facilitated in etching the substrate. This concept is applied to all type of etchants, either acidic or alkaline etchants. Zubel et al. [24, 62] concluded that etch rate of various plane in low concentration etchants are similar to one another due to the low anisotropy in KOH etchant. Peng et al. [57] studied the role of solvent or H_2O in etching and its role in etching. He concluded that etch rate was not solely depended on etchant concentrations. For hydrofluoric-acid-based (HF) etchant, William and Gupta [6] found that for weaker concentration of HF, the etch rate increased almost linearly with concentrations, but rose much faster with concentrated HF. Liu [64] indicated that etch rate, to a large degree, was limited by the removal rate of non-volatile components. This was supported by the observation that etch rate was increased significantly by increasing the concentration of

etchant. Yuan et al. [58] showed the differences between etchant concentrations through the heights of the micro-protuberance. He found the heights of micro-protuberance increased with increasing concentration.

Water content in low concentration etchant influences etch rate significantly. Makino et al. [56] showed that etch rate had a close relationship with the water content in the etchant. Etch rate decreased significantly in the open condition with high temperature compared to closed condition. During the open condition, water content in Ortho-phosphoric acid (PA) was vaporised when the process was carried out, which led to the change of water content in PA.

Period of etching affects etch rate significantly in two ways: elapsed time from the start of etch and prolonged etch. Temperature is another issue that affects the efficiency of chemical etching. Many research works have shown the temperature effect on etch rate at range from room temperature up to 800^{o}C for certain type of advanced ceramics [55-57, 61, 65]. Increasing temperature will increase etch rate and decrease surface quality. Niebuhr and Fang et al. [65, 66] observed similar results. An increase in temperature will tend to stimulate corrosive attack by increasing the rate of electrochemical reaction and diffusion processes. Gelder and Hauser [67] investigated etching of silicon nitride with silicon dioxide as a mask. They showed that etch rate was affected by water content and temperature. Etch rate of silicon nitride in refluxed boiling phosphoric acid was measured as a function of temperature and all etch rates increased with temperature.

2.6 SURFACE ROUGHNESS

Surface quality is concerned with surface roughness, surface damage and surface mechanical properties. Surface conditions determine the quality level of micromachining. A good surface has low value of roughness and without surface damage, such as pits. Surface quality is usually determined by scanning electron microscopes (SEM), atomic force microscope (AFM) or transmission electron microscope (TEM). Surface quality has a close relationship with etch rate. Researchers have found that surface quality

deteriorates with temperature due to higher etch rate. Increase in etch rate will cause the unevenly etching process and eventually higher surface roughness [55, 59]. Different etch rates will significantly result in different types of surface quality. Surface quality is also affected by etchant concentration, temperature, agitation and etching period [57].

Agitation is known to increase or decrease the etch rate, and thereby affecting the surface quality indirectly. Fadaei and Imanian [8] observed an improvement in surface finish by adding triethanolamine (TEA) which was able to decrease etch rate. This was due to the ability of TEA to decrease the difference between corrosion rate of grain and grain boundaries, thus reducing the pitting defects and producing better surface finish. Further agitation-isopropyl alcohol (IPA) will improve the surface finish [59, 63]. Besides, prolonged etching period is also known to increase etch rate and cause irregular hillocks and defects to appear on the material surface.

Vladuta [68] summarised the relationship between material properties, contact angle and surface quality with the surface energy. Surface energy is an important property that is affected by the chemical structure of the solid and influences the wettability of the material surface. The wettability also depends on the surface morphology and the contact liquid. The higher the surface energy is the better the surface quality and the finer the grain size.

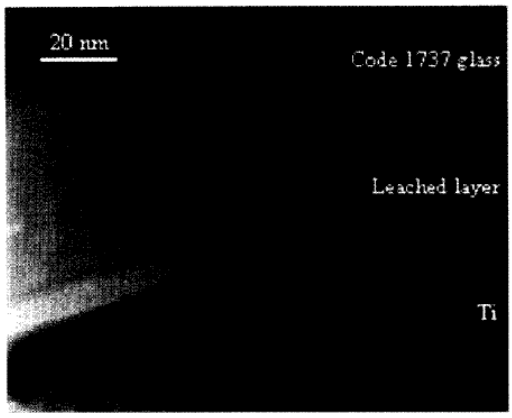

Figure 2-2 Cross-sectional STEM micrograph of RCA cleaned code 1737glass, showing leached surface layer [64]

Preparation before etching is a necessary procedure to improve the results at the end of the process. A few types of preparation methods have been carried out by researchers to improve substrate machinability by controlling the composition of ceramics, the type of '*green material*' used to produce ceramics, treatment and cleaning process. Kuech et al. [69] found the buried interfaces prepared through wet chemical processes resulted in a high concentration of traps localised at the interface. Liu et al. [64] applied treatment to glass ceramics due to its insensitivity to cleaning process. Through treatment process, the microstructure of the glass ceramic would be changed and creating a better machinability material. A thin SiO_2 layer, as shown in Figure 2-2 [64] was formed in glass ceramics during exposure to NH_4OH/H_2O_2. In the buffered HF dip, SiO_2 layer was dissolved and re-deposition of dissolved elements would take place in these areas.

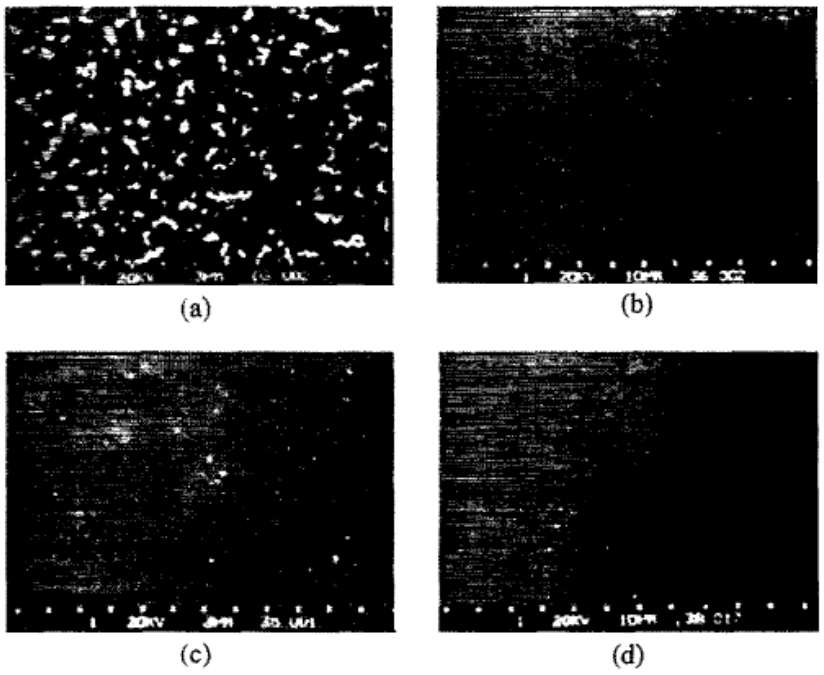

Figure 2-3 The surface of Si(100) - etching at 70^{o}C in (a) before etching in 5M KOH and (b) after etching in 5M KOH; and, (c) before etching in 10M KOH and (d) after etching in 10M KOH, respectively [24, 63]

Etchant concentration is determined by its content. The higher the hydrogen ion content the higher the concentration and vice versa. Figure 2-3 [24, 63] showed that quality of surface is strongly influenced by the etchant concentration. As the concentration increased, surface quality became smoother. This condition will become worse once etchant concentration is over the peak limit. Kinder and Tausley [55] found surface roughness of GaN reduced significantly while etching by KOH etchant concentration from 0.02M to 0.04M. During etching, reaction process takes place in between hydrogen ions and substrate to produce reaction material. Reaction material will increase if etchant concentration is too high and causing these insoluble reaction products to start forming and eroding the material surface [70]. A very smooth surface may be obtained when light intensity is high and etchant concentration is low. This corresponds to circumstances in which the reaction rate becomes limited by etchant concentration and the diffusion of reactants to the surface [71]. Kinder and Tausley [55] showed the surface roughness of GaN/SiC (0.2μm) etched surface with decreased KOH concentration. By reducing KOH concentration from 0.04M to 0.02M, the surface roughness was significantly reduced as seen in Figure 2-4 (surface roughness = 2.5μm while etching in 0.04M KOH). Cook et al. [71] studied the different ways of preparing four engineering ceramics to determine the most effective etching methods. All materials then underwent different types of etching methods. He summarised that SiC, Si_3N_4 and Sialon, which were polished using a Buehler Motopol polisher and underwent different stages of diamond paste on a Textmet cloth were etched excellently in molten salt etch. Figures 2-5 and 2-6 [71] are secondary electron image of thermally etched SiC, Si_3N_4 and Sialon. Microstructure in Figure 2-5 showed a fibrous nature, consisting of elongated, high aspect ratio SiC grains with finer grains in between them. The molten salt etch (Figure 2-6) removed the grain boundary phase and the Cr rich particles, leaving the matrix untouched.

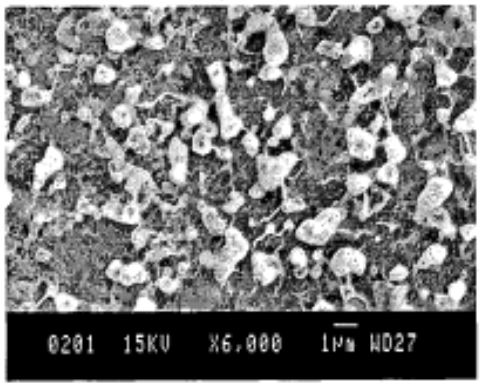

Figure 2-4 SEM image of GaN/SiC (0.2um) etched surface [55]

Figure 2-5 Secondary Electron image of molten-salt-etched SiC [71].

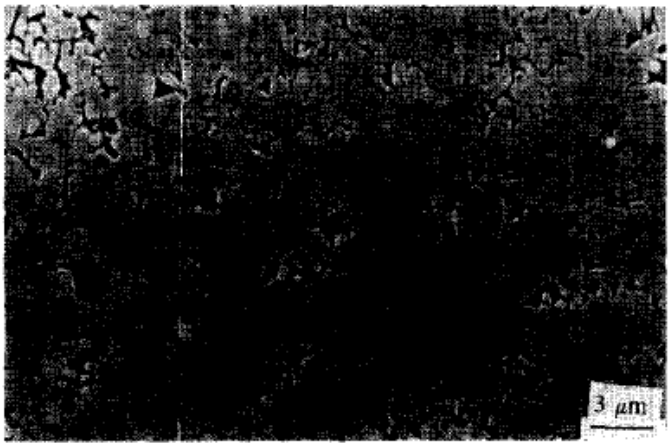

Figure 2-6 Backscattered eletron image of molten-salt-etched Si3N4 [71].

Temperature plays a crucial role in surface roughness during ion reaction. Temperature changes affect material morphology at the end of the process and thus indirectly affecting the surface quality. Many researchers have shown that increasing temperature allows one to obtain better surface quality in various concentration of etchant [24, 56, 58, 62-64, 72, 73]. Increasing temperature will stimulate reaction and increase the surface quality. Jardiel et al. [74] observed the shape of grains changed from rounding plate-like grain to platelets after etching thermally.

Photoresist is the light-sensitive material used in photolithography and photoengraving to form patterned coating on a surface. Indirectly, the adhesive of photoresist change the quality of surface roughness at the end of the process. It sometimes produces chemical reaction with the chemical etchant during the process that is carried out. This also causes peel off of photoresist. Thus, adhesive of photoresist has to be highly resistant to the chemical etchant used. Liu et al. [64] reported the surface roughness was closely related to photoresist's adhesive quality. Their results showed that better surface roughness was found in chromium photoresist, compared to fused silica wafer.

2.7 DIMENSIONAL ACCURACY

In previous years, masking is used to protect substrate surface from chemical etchant and also for fabrication purpose. However, the difficulty and complicated methods in applying maskant onto the material surface and defects raised by maskant during CHM have increased the production cost and processing period. Thus, direct micro-fabrication technique is being introduced to meet the increasing demand of multi-kind and small-quantity production.

Direct micro-fabrication technique which combines micro-indention and CHM has been proposed [75-77]. One of the reasons that direct patterning has received attention from industry is that the demand of multi-kind and small-quantity production is increasing in the market. The key point of this technology is that the change in etch rate arises from the

non-indentation area which facilities contact with the chemical etchant. By applying this technique, dimensional accuracy is measured in terms of etch ratio, which is the ratio of etch rate at non-indented area to indented area.

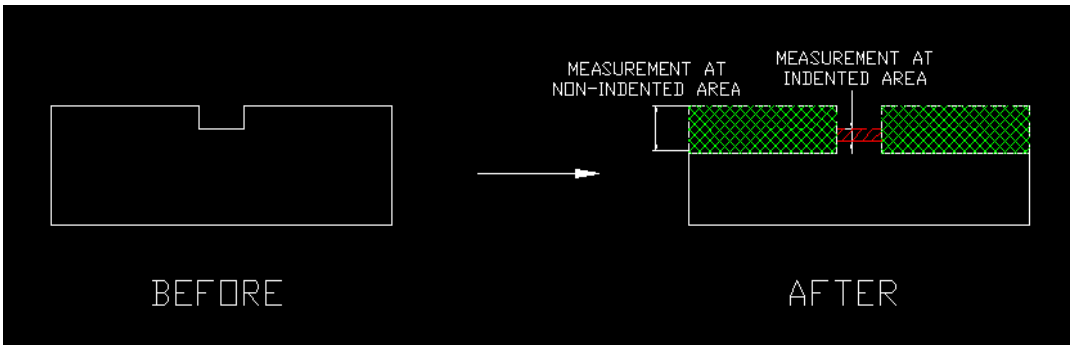

Figure 2-7 Schematic diagram of the cross section at the glass surface before and after CHM

The micro-patterning and CHM presents potential maskless fabrication technique because of its operation versatility, low costs for initial facilities, simplicity of process and material selectivity. Kurachi et. al. have proposed a novel micro-fabrication technique without using photomask on glass surface, which is a combination of micro-indentation and CHM process [78]. Youn and Kang fabricated the micro-pattern on the Pyrex glass by suing nano-scratch with HF etching [77]. These research studies showed that patterning on the glass surface becomes possible due to etch rate difference between indented and non-indented area. Saito et al. proposed the mechanism for alumino-silicate glass in that etch rate change is attributed to the change of leaching reaction. The leaching of the glass components other than SiO_2 occurred with HF etching was restricted by micro-indentation [75]. In their further inspection, they found that etch rate changed with the material composition. They indicated etch ratio increased with increasing ratio of Al_2O_3 to SiO_2 [76].

2.8 ETCHANT

The selection of an etchant is dependent upon numerous factors, some of which are: material to be etched, depth of etch, surface finish required, potential damage to or

alteration of metallurgical properties of the material, speed of material removal, permissible operating environment, economics of material removal [79].

The simplest example of a molten salt would be to take sodium choride (table salt) and heat it to a red heat (801^{o}C) where it would melt into liquid. This liquid is stable, has a heat capacity similar to water and flows much like water does [54]. Molten salt functions are not limited to solvent, its properties include good heat transfer characteristics. It is also able to attain very high temperatures. Molten salt technology has been used commonly in industries, such as diverse technologies, electrochemistry, heat transfer, chemical oxidation and nuclear reactors.

Secco etch mainly consists of hydrofluoric and chromium oxide. There are a few types of Secco etch being used today, their differences are controlled by their acid composition. As an example, Jacque [80] used Secco etch of 2ml Hydrofluoric (HF) and 1ml chromate (Cr_2O_3) to etch Si_3N_4 and Ravi [54] used 2ml HF, 1ml potassium dichromate ($K_2Cr_2O_7$) and 1ml acetic acid (CH_3COOH) in etching advanced ceramics. Secco etch is used to delineate crystalline defects on silicon substrate of water. It is a useful chemical etching method for characterisation of defects on surface of bare silicon wafer [81]. However, Hua [82] concluded that Secco etch alone did not fully de-process the die to substrate where crystalline defects may be covered by the oxide. 152 Secco etchant consists of hydrofluoric acid and potassium dichromate, its composition is 67%HF: 33% 0.15M $K_2Cr_2O_7$ in water (H_2O). This mixture is the innovation of Secco etch, which is created by Chu [81] for etching of silicon wafer. 152 Secco etch has the advantages of delineating crystalline defects through two main processes, which are well-defined etching pits with elliptical shape, and its preparation is simple, fast and reliable. The disadvantage of 152 Secco etch is that it cannot identify the orientation of wafer plan compared to the other Secco etch [83].

Thermal etch involves heating of polished ceramic specimens to around 200^{o}C of the sintering temperature. It is performed under argon in vertical tube furnace with silicon carbide hearth. The specimens are then annealed in vacuum or inert atmosphere and used

primarily in high temperature [80]. Thermal etching is not normally applied to non-oxide ceramics owing to problems with oxidation and it should be carried out under vacuum or inert atmosphere. From previous researchers, pressure-less-sintered β-SiC produced by sintering SiC powders were successfully etched [74]. Cook et al. [74] successfully built a useful guideline in fabricating engineering ceramics. They found that only SiC was successfully thermally etched and gave a low value of surface roughness. Jardiel et al. [74] tested bismuth titanate ($Bi_4Ti_3O_{12}$) and it changed from rounding plate-like grain to platelets under the action of the chemical agent [74].

Other etchants are Sirtl etchant, which contains 1ml HF:1ml C_2O_3 [80]; Silver etch- 2ml HF:1ml HNO_3:2ml$AgNO_3$ [54]. Dash etchant with 1ml HF: 3ml HNO_3 : 1ml CH_3COOH; Jenkins Wright, which contains 60ml HF: 30ml HNO_3 : 60ml CH_3COOH : 30ml (1g CrO_3 : 2ml H_2O) [84]; Sponheimer Mills, contains 5mg H_3IO_6 : 5mgKI : 50ml H_2O : 2ml HF [39]; Copper etch, contains 600ml HF : 300ml HNO_3 : 28g $Cu(NO_3)_2$: 3ml H_2O [80]; Copper displacement, contains 55g $CuSO_4$: SH20 : 950ml H_2O : 50ml HF; CP-4, contains 3ml HF : 5ml HNO_3 : 3ml CH_3COOH [6]; and, Sailer etchant, contains 300ml HNO_3 : 600ml HF : 2ml BS : 24g Cu $(NO_3)_2$: dilute 10:1 with H_2O [85].

2.9 ADVANCED CERAMICS

2.9.1 Machinable Glass Ceramics (MGC)

The first practical glass ceramics were developed nearly fifty years ago. These glass ceramics are prepared by the controlled crystallisation of special glasses. The original glass ceramics were produced by inducing volume nucleation in melt-derived bulk silicate glasses, usually by the addition of nucleating agents. Since that time, a wide variety of applications of these versatile materials have been developed as a result of their many outstanding properties and the distinct advantages of the glass ceramic method, in certain circumstances, over conventional ceramics processing routes [86]. Stookey is the first person to produce glass ceramics industrially in the 1950s.

More recently, glass ceramic processing has been greatly extended to include non-silicates and even non-oxide compositions, and also the preparation of the precursor glasses by sol-gel techniques [86]. Ordinary glass is non-crystalline. Glass ceramics however, are polycrystalline materials that are manufactured by controlled crystallisation of suitable base glasses [87]. Glass ceramics represent an extreme case because the material, originally a glass, is deliberately heat treated to transform it into a new material whose polycrystalline structure gives rise to totally different set of properties. Because of these dependencies, glass properties are listed for glasses in the annealed state, and the properties of glass-ceramics are given on the basis of the manufacturer's standard production process [88, 89].

Glass ceramics are mechanically strong material and can sustain repeated and quick temperature change up to 800-1000^{o}C. At the same time, they have very low heat conduction coefficient and can be nearly transparent for radiation in the infrared wavelengths. Chemical durability of glass ceramics is strongly dependent upon their composition. In addition, previous thermal history and mode of forming can have pronounced effects. For glass ceramics, the amount and composition of the crystalline and glass phases, as well as the microstructure, have effects that may well substantially alter the intrinsic durability expected on the basis of the overall bulk composition [88, 89].

Glass ceramics are useful in thermally hazardous conditions. This glassy material contains crystalline lattices, which give the distinct properties of glass ceramics. Glass ceramics possess good resistance to erosion and pressure, as well as excellent hardness, and make them widely used in industrial purposes. Moreover, glass ceramics are very good electrical insulator [88, 90].

Machinable glass ceramic (MGC) is a problem solving material combining the performance of a technical ceramic with the versatility of a high performance glass. MGC's outstanding property is that its main crystal phase forms micas or other plate-like crystals which are easily cleavable. When pieces of these glass ceramics are machined with conventional metal-working tools they do not break into pieces as normal glasses

typically do, but they can be machined easily to the desired shape. The MGC has this ability because the cracks which are created during the machining process do not run catastrophically through the whole piece but are deviated at the small plate like crystals and, at the same time, split into several others so that the energy which is introduced into working piece is absorbed by the formation of many small cracks [91-94]. MGC is influenced by the amounts of diopside-based glass quantity, which itself had the lowest sintering temperature. This came from the enhancement of crystalline phase in the sintered specimens when diopside-based glass was added to the other one gradually [95].

MGC can be applied in very different areas. One area is the photo-typing of components for new equipment or systems in those cases in which fabrication of the few pieces needed from the material of optimal choice are too expensive at that time. Other applications concern medical areas, for example, dental restoration or bone restoration. For these applications, the original idea to produce a MGC has been further extended to materials which are at the same time biocompatible or bioactive [92].

Research works done on machining of machinable glass ceramics by chemical etching is limited due to their resistance to the chemical effects, and they have become the last material to be used in chemical etching. Dry etching of glass had been reported by using SF_6 [96]. Watanabe obtained a linear relationship between etch rate and temperature while compared between wet etching and mechanomachining [97]. Williams et al. [6] found that not all materials were etched in all etchants due to time limitations. This was probably caused by the limited chemical reaction. Gaiseanu et al. [98] found good agreement in the relationship between etching time and etch rate on his analytical and experimental result. While, Minhao et al. [99] presented a result at constant etching period and reported that the obtained etch rate was surprisingly linear. They concluded that a minor change of etching time had slightly changed the linear shape of etch rate to curvature; and Olsen et al. [100] also indicated that increase in etching time would decrease the bond strength by increasing etch rate.

2.9.2 Boron Nitride (BN)

Boron nitride is a binary compound of boron which consists of equal proportions of boron and nitrogen atoms. It is a synthetic material that has been discovered in the early 19th century but was not developed as a commercial material until the latter half of the 20th century. In 1842, BN was first obtained by Balmain by heating boron trioxide with cyanide of potassium. Founded in 1952, Warren Diamond powder is a manufacturer of micron-sized and fine-mesh diamond and cubic boron nitride (c-BN) for grinding and polishing applications. Boron and nitrogen are neighbours of carbon in the periodic table with same number of outer shell electrons. Atomic radii of boron and nitrogen are similar to that of carbon. Thus, BN and carbon exhibit similarity in their crystal structure. Similar to carbon, BN can be synthesised in hexagonal (h-BN) and cubic forms (c-BN).

The synthesis of h-BN powder is achieved by ammonia of boric oxide at elevated temperature. h-BN is the equivalent in structure of graphite. As shown in figure 2-8, it is the most stable and softest among BN polymorphs, and its layered lattice structure give it good lubricating properties. In hot pressed state, h-BN is readily machinable using conventional metal cutting techniques; hence complex shaped components can be fashioned from hot pressed billet. Generally, h-BN has high dielectric breakdown strength, high volume resistivity and good chemical inertness. H-BN is resistant to sintering and is usually formed by hot pressing. It is frequently shaped into electrical insulators and melting crucibles. It can be applied with a liquid binder as temperature-resistant coating for metallurgical, ceramics, or polymer processing machinery [101].

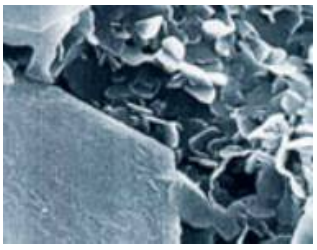

Figure 2-8 h-BN powder

C-BN is formed by high pressure, high temperature treatment of h-BN. C-BN has the same structures as diamond and its properties mirror those of diamond. Indeed c-BN is the second only to diamond in hardness. C-BN is first synthesised in 1957, but it is only in the last 15 years that commercial production of c-BN has developed. Commonly, c-BN has high thermal conductivity, excellent wear resistance and good chemical inertness. It is like synthetic diamond, often bonded onto metallic or metallic-ceramic cutting tools for the machining of hard steels. Owing to high oxidation temperature, it has a much higher working temperature than diamond [101].

Because of excellent thermal and chemical stability, BN ceramics are traditionally used as parts of high-temperature equipment. With high dielectric breakdown strength and volume resistivity, h-BN has been used as an electrical insulator. However, its tendency to oxidise at high temperatures often restricts its use to vacuum and inert atmosphere operation. Its chemical inertness leads to applications, such as thermocouple protection sheaths, crucibles and linings for reaction vessels though as above oxidation must be avoided. BN ceramics have great potential in nanotechnology. Nanotubes of BN can be produced that have a structure similar to carbon nanotubes, however, the properties are very different. BN ceramics also applied in moulds and evaporating boats, as machine cutting tools and abrasives, as substrates for electronic devices and wear resistant coatings.

Research work of chemical machining on BN is relatively less compared to other materials and machining methods. Gaiseanu et. al. [98] concluded that etch rate decreased with increasing etching duration. He also concluded that the relationship between etching and etching duration depended on the material properties of boron nitride or the composition of boron. Lavrenko and Alexeev found that the difference in oxidation behaviour of powder compacts and pyrolytic BN was due to the pore structure of the former sample and to the BN vaporisation from the surface of the latter one [102].

2.9.3 Silicon Carbide (SiC)

In year 1891, American inventor Edward G. Acheson created silicon carbide, later sold under the trade name Carborundum, by heating a mixture of clay and coke (almost pure carbon) [103]. He also developed the electric batch furnace by which silicon carbide (SiC) is still made today and formed The Corborundum Company to manufacture bulk SiC, initially for use as an abrasive [103]. Historically, the first use of SiC was as an abrasive, and then followed by electronic applications. In the beginning of 20^{th} century, SiC was used as detector in the first radios, and in 1907 Henry Joseph Round produced the first light emitting diode by applying a voltage to a SiC crystal and observing yellow, green and orange emission at cathode [104].

SiC is available in reaction bonded and sintered forms respectively. Both materials are ultra hard and have high thermal conductivity. This has led to increased hardness and conductivity improved seal and bearing performance. SiC materials exhibit good erosion and abrasive resistance, and these properties can be utilised various applications such as spray nozzles, shot blast nozzles and cyclone components [105]. SiC is derived from powder or grain, produced from carbon reduction of silica. It is produced as either fine powder or a large bonded mass, which is then crushed. It is washed with hydrofluoric acid to purify the powder or grain. Then, it will undergo fabrication [106]. SiC can be grouped into four types depending on the processing methods used in the production of solid forms, namely, reaction-bonded or reaction-sintered, hot-pressed, sintered, and chemical vapor deposition (CVD) [107].

Reaction bonded silicon carbide (RBSC) is being developed to meet the need of the industry, where high temperature strength and high stiffness to weight ratios are required. The demand of more energy efficient engines and the need to replace critical metals drove RBSC to faster path of development. The primary characteristic of RBSC is the 8-12% free silicon found in the structure [20, 108]. Reaction bonding is a method for producing ceramic matrix composites [109]. This is accomplished by using silicon powder as the starting material followed by porous carbon or graphite with molten silicon. In reaction-bonding process, a mixture of SiC powder, graphite and a plasticizer is

pressed in a mold to prepare a porous product, and silicon metal, as a liquid or vapour, is infiltrated into the pores. The reaction between silicon and carbon forms SiC. The finished product is almost fully dense; it contains a mixture of Si, C and reaction-formed SiC between original SiC particles. The densification process does not produce any shrinkage, so dimensional tolerances are easily achieved. The primary advantage of RBSC is the relatively low cost [107, 109, 110].

For 50 years, Carborundum was the second hardest substance known. Mechanical properties of RBSC depend on the amount of free silicon and carbon. In the case of a fully dense SiC-Si composite, the material demonstrates good bend strength (400MPa) at room temperature. RBSC is resistant to wear (tolerates a wide range of acids and alkalis) and oxidation. Besides, it has good abrasion resistant; has good thermal shock resistant due to low thermal expansion coefficient and high thermal conductivity, and has good dimensional control of complex shapes [110].

RBSC has a wide variety of industry applications. It is being produced as low mass kiln supports due to its high temperature strength, oxidation resistance and thermal shock resistance. This component also lowers the thermal mass of kiln cars. It is an ideal material for wear components, thrust bearing and precision components. RBSC is ideal to be used as seal face material. Under conditions of seal face contact, this free silicon will vaporise, leaving behind free carbon atoms at the interface. This reduces the frictional heat at the faces, and promotes good wear characteristic. The disadvantage to RBSC is also the free silicon, which reduces chemical resistance. Chemical like caustic or hydrofluoric acid will leach out the free silicon and severely limit good seal performance [108, 111, 112].

Research of chemical machining on SiC is relatively limited compared to other machining methods. Many studies have been reported on surface roughness of SiC to minimise the replication of substrate defects into homoepitaxial SiC active device layers [113-115]. Kim and Lee studied the relationship between etch rate and roughness of etching of SiC. They found that roughness of material surface was correlated to etch rate.

It formed a quadratic relationship, where surface roughness achieved an optimum point before becoming rougher [112]. Wang et al. reported etching of SiC and stated that SiC is the most mature candidate to be used in semiconductors by etching process [116].

2.10 ADVANCED CERAMICS APPLICATION

It was forecast that demand of advanced ceramics in U.S. will increase by 7.0% per year to over $12 billion in 2010 [117]. The higher profit as a result will spur more growth for industries as advanced ceramics continue to penetrate several applications, such as capacitors, cutting tools, joint implants and membranes. The growth of advanced ceramics relies heavily on the technology and the brilliance of its application, especially in electronic component and electrical equipment industries. Tables 2-2 and 2-3 show the prediction of advanced ceramics demand in 2010 compared to 2000 and 2005.

Table 2-2 U.S. advanced ceramics demand by market (million dollars).

				% Annual Growth	
	2000	2005	2010	2000-2005	2005-2010
Total demand	9050	8625	12100	-1.0	7.0
Electronic components	3750	2820	4130	-5.5	7.9
Electrical equipment	1670	1680	2370	0.1	7.1
Industrial machinery	1124	1160	1500	0.6	5.3
Transportation equipment	1060	1135	1600	1.4	7.1
Other markets	1446	1830	2500	4.8	6.4

Table 2-3 U.S. advanced ceramics demand in the industrial (million dollars).

				% Annual Growth	
	2000	2005	2010	2000-2005	2005-2010
Total demand	9050	8625	12100	-1.0	7.0
Monolithic ceramics	7980	7530	10600	-1.2	7.1
Ceramics coatings	740	770	1050	0.8	6.4
Ceramic matrix composites	330	325	450	-0.3	6.7

Cordierite, titanite and glass ceramics have recorded the most rapid rates of growth due to their use in environmental, medical product and electronic component markets. However,

other advanced ceramics, such as alumina, beryllia, silicon carbide and silicon nitride materials showed low average gains due to environmental concerns, competition from other ceramics and a reliance on slower-growing markets.

Advanced ceramics have demonstrated their reliable applications in various industries with their great service life, cost effectiveness and excellent properties, such as the capability to operate under high temperature, high resistance to abrasion, high corrosion resistance, longer tool life and dimensional stability.

The production of high technology I.T. devices will continue to spark the demand for semiconductors, capacitors and other ceramics-containing electronic components. In 2005, 38% of total demand was contributed by the insulators and permanent magnets usage. Other advanced ceramic electrical equipment includes igniters, heating elements, heat shielding components, connectors and seals [118].

Advanced ceramics, which possess great strength and high resistance to heat, are mainly applied in the industrial machinery. The market projected an increment of 5.3% per year through 2010 from a weak 2000 base. As users of machine tools begin benefiting from the generally stronger macroeconomic environment, the need to expand supply brings idled capacity back online and performing of upgrades to existing equipment will provide market opportunities for producers of ceramic wear parts. Advanced ceramics are also used as cutting tool, which is more of a consumable item. The economic recovery will mean greater demand for the tools necessary to cut and form metal.

With good features of resistance to corrosion and wearing, advanced ceramics are also used throughout the steel production processes [119]. Oxide-based ceramics of aluminum, zirconium, chromium, and magnesium are primarily used in a part of the process where contact is made with molten steel and low contamination is desired. Non-oxide ceramics of silicon, titanium, tungsten, and aluminum are utilised for hot handling because of their inherent thermal shock resistance to acidic species or wear.

Advanced ceramics have found greater use in the chemical and plastic market, with the most growth arising from the production of membranes. In this application, growth has the potential to accrue due to ceramic's performance advantages such as toleration of high temperatures and its ability to overcome more difficult processing conditions. The demand is also being driven by greater penetration into specialty applications such as natural gas purification and filtration of molecules in liquids. The effort to reduce the dependence on oil for energy production will provide opportunities for advanced ceramics in the environmental market. Emerging applications include the use of ceramic bearings in wind turbines.

In the transportation equipment market, advanced ceramics are used in catalytic converter substrates, engine bearings, ceramic armor for military vehicles, diesel engine particulate filters and ceramic matrix composite brakes. Advanced ceramics, such as alumina, silicon nitride, and aluminum nitride are currently being used to manufacture critical aerospace components because of their unique physical properties. These inorganic, non-metallic materials retain dimensional stability through a range of high temperatures and exhibit very high mechanical strength. They also demonstrate excellent chemical resistance and stiffness-to-weight ratio, thereby providing manufacturers with the ability to design components that offer optimum performance in their application.

2.11 STATISTICAL METHOD (DESIGN OF EXPERIMENTS)

Design of Experiment (DoE) is a combination of mathematical and statistical techniques. Mathematical models can be used to predict and better analyse result behaviour in different condition with a limited number of experimental tests [120]. DoE techniques can be used to analyse different kinds of experiments such as two-level factorial design, fractional design, response surface methodology and others. Basically, their concepts are similar to each other. The differences are in their statistical model and characteristics (Figure 2-9).

DoE is used in various industrial applications to optimise processes. In the industry, DoE is used to enhance the productivity and product quality. As automation systems become

more complex, they can only be analysed using DoE method. DoE also reduces process cost and time of trial-an-error. According to Baldassari et al. [121], DoE approach was able to reduce the effect of mixing time and enhance the quality of their specimens. Pierlot et al. [122] concluded that DoE was able to express the influence of the process parameters on the response and statistical method to determine the significance of the coefficients of the regression equation. In certain circumstances, DoE is used in simulation to enhance data accuracy, and filter out the errors and unnecessary factors. Montevechi et al. [123] found that DoE was able to improve the simulation process by avoiding the trial-and-error techniques to seek etchants. In their process, they also found the significance effects of the interactions were confirmed, aiding the managerial decision making process.

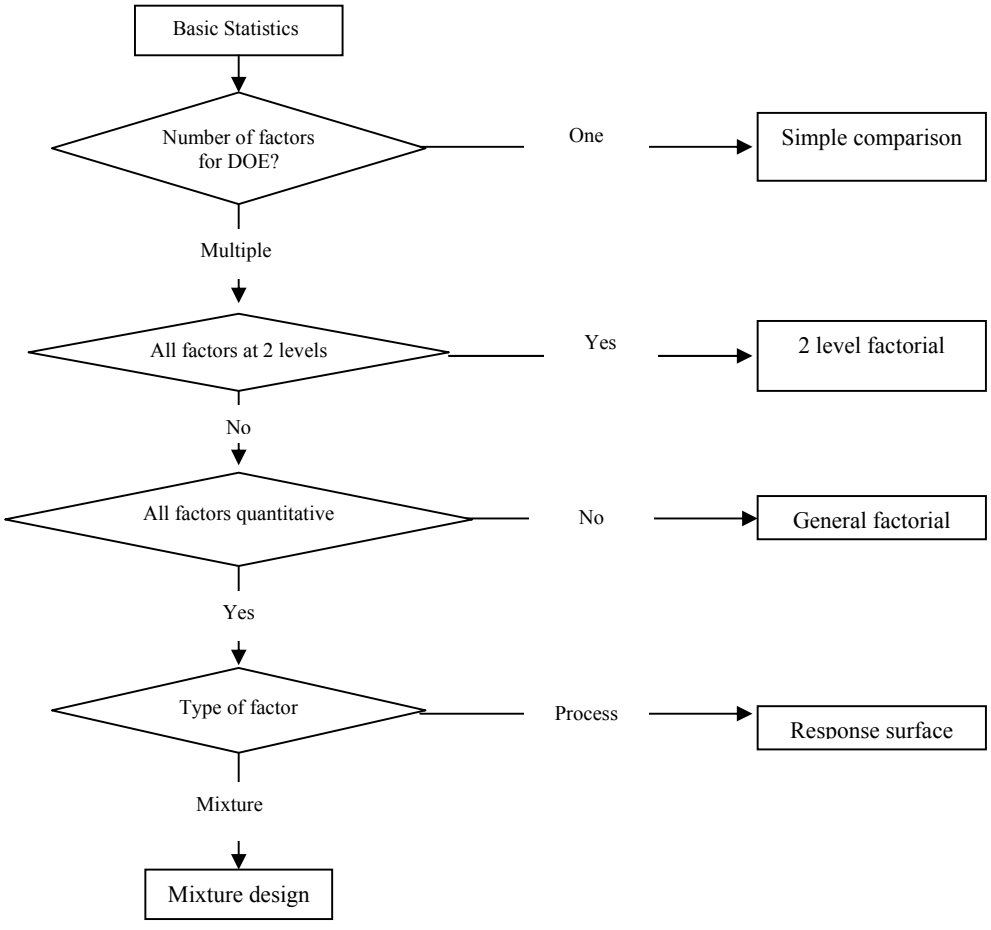

Figure 2-9 shows the flowchart guide to DoE [124]

DoE techniques can be divided into three major categories: comparative objective, screening objective, and response surface objective [117]. Comparative objective is used when experiment goal is primarily to make a conclusion about one a-priori factor, and the question of interest is whether the factors is "significant". Screening objective is chosen when primary purpose of the experiment is to select a few important main effects from the many less important ones. While, response surface objective is used to optimise the process and to make the process more robust against external and non-controllable influences. Table 2-4 shows the design selection guideline.

Table 2- 4 Design selection guidelines [117].

Number of factors	Comparative Objective	Screening Objective	Response Surface Objective
1	One factor completely randomized design	-	-
2-4	Randomized block design	Full/ Fractional factorial design	Central composite/ Box-Behnken
5 or more	Randomized block design	Fractional factorial/ Plackett-Burman	Screen first to reduce number of factors

2.11.1 Full Factorial Design

In statistics, factorial experiment is an experiment whose design consists of two or more factors, each with discrete possible values, and whose experimental units take on all possible combinations of these levels across all such factors. Factorial design is a tool that allows experimenters to experiment on many factors simultaneously. In this design, a few assumptions are made to study the process: the factors are fixed, the designs are completely randomized, and the usual normality assumptions are satisfied.

The simplest factorial design is two-level factorial which involves a few factors at two levels or values (lower and upper bounds). In some cases, they involve different types of levels, such as quantitative (temperature, pressure & time); or quantitative (two machines, or two operators). A complete replicate of such a design requires 2^k observations and is called two-level (2^k) factorial design, where k is the number of factors in design.

Similarly, if the midpoints are included, the design is called 3^k factorial design as schematically shown in Figure 2-10.

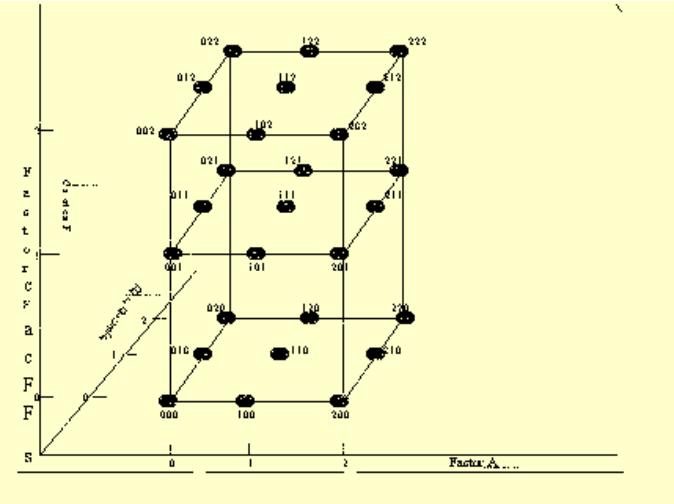

Figure 2-10 3^3 Factorial Design Schematic.

Factorial design can be used in fitting second-order model to improve the optimization process. A general second-order model is defined as [120, 125]:

$$y = a_0 + \sum_{i=1}^{n} a_i x_i + \sum_{i=1}^{n} a_{ii} x_i^2 + \sum_{i=1}^{n} \sum_{i=1}^{n} a_{ij} x_i x_j + \ldots \qquad \text{(eq. 2-1)}$$

where x_i and x_j are the design variables and a_{pq} is the etching parameters.

The construction of a quadratic response surface model in N variables requires the study at two levels so that the etching parameters can be estimated. Generally, for a large number of variables, the number of experiments grows exponentially and becomes impractical. A full factorial design typically is used for five or fewer variables [120, 124, 125].

Compared to one-factor-at-a time (OFAT), 2^k design provides wider inductive basis, which covers a broader area or volume to draw interferences about the process, and it

reveals interactions of factors [125]. One of the major disadvantages is 2^k factorial design is that it limits all factors at two levels, thus assuming that the response is approximately linear over the range of the factor level chosen.

2.11.2 Response Surface Methodology (RSM)

Response Surface Methodology (RSM) is useful for modeling and analysis of problems in which a response interest is influenced by several factors [124]. This is a methodology of constructing approximations of the system behavior using results of the response analyses calculated at a series of points in the variable space. The objective is to optimise a series of responses which are influenced by varied independent variables.

The concept of RSM involves the response variable, y, and several independent variables $x_1, x_2, x_3, \ldots, x_k$, which can be expressed as [120, 124, 125]:

$$y = f(x_1; x_2; x_3; x_4) + \varepsilon \qquad \text{(eq. 2-2)}$$

where y is etching performance, x_1 is the etching temperature, x_2 is the etching duration, x_3 is the etchant concentration, x_4 is the type of etchant, and ϵ is the noise or error in response.In this methodology, all independent variables are assumed to be continuous and controllable by the experimenter with negligible error, dependent variable is assumed to be a random variable.

Usually a low order polynomial (first-order and second-order) in some regions of the independent variables is employed. The first-order model is expressed as [120, 124, 125]:

$$y = \beta_o + \sum_{i=1}^{k} \beta_i x_i + \varepsilon \qquad \text{(eq. 2-3)}$$

and the second-order model [120, 124, 125],

$$y = \beta_o + \sum_{i=1}^{k} \beta_i x_i + \sum_{i=1}^{k} \beta_{ii} x_i^2 + \sum_i \sum_j \beta_{ij} x_i x_j + \varepsilon \quad \text{(eq. 2-4)}$$

are generally utilized in RSM problems. The β_{pq} parameters of the polynomials are estimated [120, 124, 125].

RSM is an economical and user-friendly tool to be used and has been employed by many researchers. Bezerra et al. [119] summarized that the application of RSM in optimisation was largely diffused and consolidated principally because of its advantages over experimentation approach that is based on classical one-variable-a-time optimisation. Hung et al. [126] applied RSM to investigate effect of various controlled factors on performance of silicon trench etches on $Cl_2/HBr/O_2$ predicting surface roughness of machinable glass ceramic. The result of analysis was that all independent variables were found to influence the etch rate positively.

Mead and Pike [127], and Hill and Hunter [128] reviewed the earlier work on RSM. They used RSM for tool life modeling, surface roughness modeling, and in other machining processes. Dabnun et al. [17] concluded that TSM was useful techniques for surface roughness tests. Relatively, a small number of designed experiments are required to generate much useful information that is used to develop the predicting equations for surface roughness.

Desai et al. [129] summarised the application of RSM in fermentation production and found that RSM is useful in getting insight information of a system directly, and interactions between different components. Benardos et al. [130] stated that the experimenter was able to optimise the process after running RSM and knowing whether or not transformations on the responses or any of the process variables were required.

Though RSM is a highly recommended method, it still shows data inaccuracy; less generalization capability and its performance is not consistent compared to other methods.

RSM techniques are being classified into: central composite design (CCD), box-behnken and 3^3 design.

2.11.2.1. Central Composite Design (CCD)

CCD is the most common experimental design tool, which is used to construct second-order model. CCD techniques are divided into central composite circumscribed (CCC), central composite inscribed (CCI) and central composite face centered (CCF). CCC design is the original form of CCD, with axial points at certain distance, α (distance from the centre of the design space) from the center based on the properties desired for the design and the number of factors in the design [120, 124]. CCI design uses the factor settings as the axial points and creates a factorial or fractional design within those limits. It is a scaled down CCC design with each factor level of the CCC design divided by α to generate the CCI design. In CCF design, start points are the center of each face of the factorial space. This variety requires three levels of each factor. Figure 2-11 denotes a CCD model.

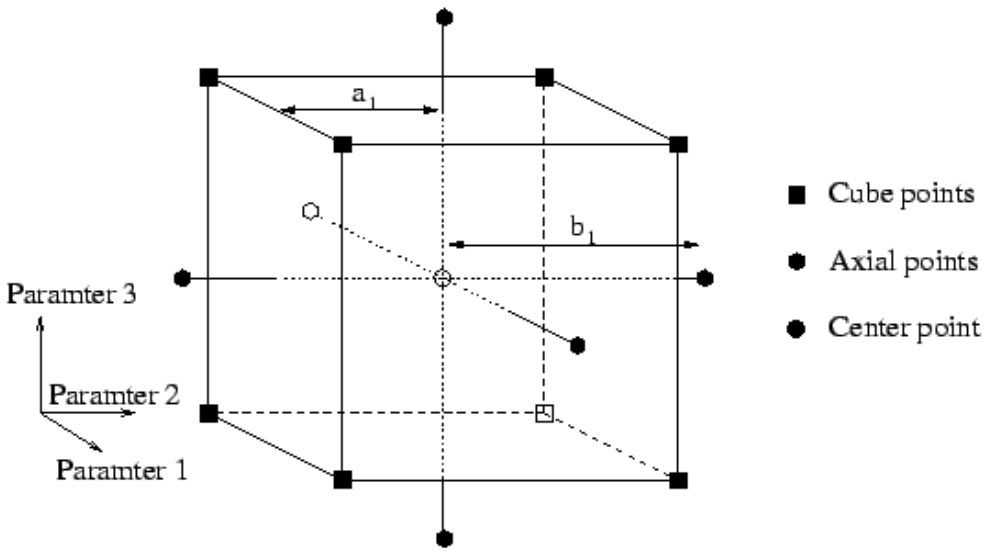

Figure 2-11 Central Composite Model with three input parameters

In Figure 2-11, the design involves 2^N factorial points, 2^N axial points and 1 central point. CCD presents an alternative to 2^N design in the construction of second-order model

because it reduces the number of experiments as compared to full-factorial design. Overall, CCD is the most popular of the many classes of RSM designs due to its ability to be partitioned naturally into two subsets of points; the first subset estimates linear and two-factor interaction effects while the second subset estimates curvature effects. CCDs are efficient, in providing much information in a minimum number of required runs. They are also flexible due to their variety of choices that enable them to be used under different conditions

2.12 NEURAL NETWORK

2.12.1 Introduction to Neural Network

Artificial neural network (ANN), usually called neural network (NN) has a history of six decades but has found solid application only in the past few years. In 1943, McCulloch and Pitts tried to develop the first ANN model based on their understanding of neurology. They developed this neuron model based on the fact that the output of the neuron is unity if the weighted sum of its inputs is greater than a threshold values, otherwise the output is zero [131]. In 1954 Farley and Clark, and in 1956 Rochester and Haibit attempted to develop ANN model using computer simulations. They proposed some modification to the McCulloch-Pitts neuron model. Instead of a binary output, they created a model with real-valued output representing the average firing rate of the cell. Since then, study of neural network has rapidly developed. Especially the study in mid of 80's, it has become the key of development in the field of machine learning. Thus, it is distinctly different from the fields of control systems or optimisation, where the terminology, basic mathematics, and design procedures have been established and applied for many years [132-134].

In engineering, ANN serves two important functions: as pattern classifier and as nonlinear adaptive system. Pattern classifier is the act of taking in raw data and taking an action based on the category of the pattern. It aims to classify data (or patterns) based on statistical information extracted from the patterns. The patterns to be classified are

usually groups of observations, defining points in an appropriate multidimensional space [135].

As a nonlinear adaptive system, ANN learns to perform functions (an input or output map) from data. Adaptive means the system parameters are changed during operation, normally called the training phase [136]. After training phase, ANN parameters are fixed and system is deployed to solve the problem at hand (testing phase).

This is a system based on the structure and functioning of the biological nervous recognition, complex networking and high degree of parallel computing capability [133-135, 137]. Purpose of the model is to capture the relationship between a historical set of model inputs and corresponding outputs [133-135, 138]. ANN assumes that the following information processing occurs in a number of simple elements called neurons, signals are transmitted between neurons over connection links, each connection link has an associated weight that multiplied the signal transmitted; and, each neuron applies an activation function to the incoming signal to determine its output signal [139].

The basic unit of brain is the neuron [133, 134, 136, 137]. Each neuron receives signals through synapses (connection) that control the effects of the signal on the neuron. These synaptic connections are believed to play a key role in the behavior of the output. The input/output training data are fundamental in ANN because they convey the necessary information to discover the optimal operating point.

An input is presented to the ANN and corresponding desired target set at the output. An error is composed to the difference between the desired target and the system output. System parameters are then adjusted when the error information is fed back. This process is repeated until the performance is acceptable. Training of ANN includes supervised learning, unsupervised learning and reinforcement learning.

The fundamental building block in an ANN is the mathematical model of a neuron as shown in Figure 2-12. The three basic components of the artificial neuron are [135, 140]:

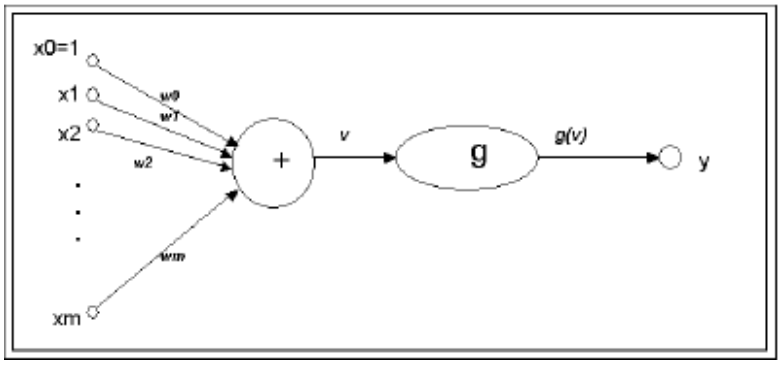

Figure 2-12 Three basic components of Artificial neuron

1. The synapses or the connecting links that provide weights, w_j to the input values, x_i for $j = 1, \ldots m$;
2. An adder that sums the weighted input values to compute the input to the activation function $\upsilon = \omega_o + \sum_{j=1}^{m} \omega_i x_i$, where ω_o is called the bias (not to be confused with statistical bias in prediction or estimation) and is a numerical value associated with neuron. It is convenient to think of the bias as the weight for an input χ_o whose value is always equal to one, so that $\upsilon = \omega_o + \sum_{j=1}^{m} \omega_i x_i$;
3. An activation function g that maps υ to $g(\upsilon)$ the output value of the neuron. This function is a monotone function.

ANN is a learning process and does not require reprogramming, it can be implemented in any application without any problem [136]. When an element of ANN fails, its operation can continue without error due to its parallel structure nature. ANN also has the ability to manage noisy or incomplete data with ease; the process of information is distributed over the neurons which operate in parallel, therefore resulting in increase computational power in contrast to the sequential operation of today computers.

Unlike most available statistical method, ANN does not need predefined mathematical equations of the relationship between model inputs and corresponding outputs, and rather

use the data alone to determine the structure of the model and unknown model parameters [112, 138]. This enables ANN to overcome the limitation of existing modeling methods. Disadvantages of ANN are that the network needs training to operate and it requires high processing time for large networks.

2.12.2 Layers

Neurons, which are the processing unit in ANN, are organized into layers as shown in figure 2-13. The common type of ANN consists of a layer of "input" units that is connected to a layer of "output" units by layers of "hidden" units. The activity of input units represents the raw data that is fed into the network, activity of each hidden units is determined by the activities of the input units and the weights on the connections between the input and hidden units, and output units is dependant on the activity of hidden units and weights between hidden and output units. Each weight between input and hidden units determine when each hidden unit is active, and so by modifying these weights, a hidden unit can choose what it represents and proceeds to next layers.

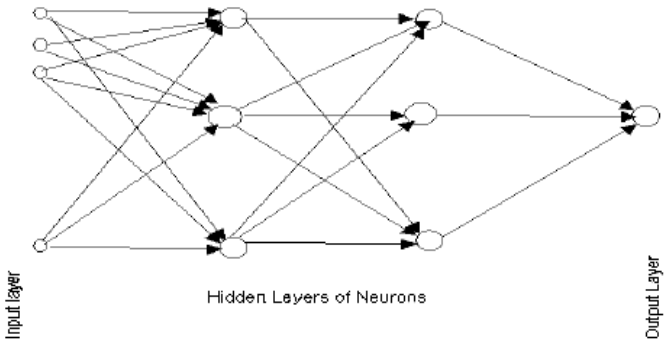

Figure 2-13 Architecture of neural network

2.12.3 Neuron

Neurons can exhibit complex global behavior, determined by the connections between the processing elements and element parameters. The original inspiration for the technique came from examination of the central nervous system and the neurons which constitute one of its most significant information processing elements. In ANN model,

simple nodes (neurons) are connected together to form a network of nodes [133, 135]. The general mathematic definition is as shown in equation (5):

$$y(x) = g\left(\sum_{i=D}^{n} \omega_i x_i + b_i\right) \qquad \text{(eq. 2-5)}$$

where x_1 is neuron with n is input dendrites (x_o ... x_n), one output axon $y(x)$, w_i is the weights, b is biases and g is the transfer function that weight how powerful the output should be from the neuron, based on the sum of the input.

The output neuron of each proceeding neuron is modulated by a corresponding weight and bias before moving to next hidden layer. This activity is then modified by the transfer function. This signal is then propagated to the next layer of the neuron and the same procedure is repeated until the end of the hidden layer as shown in figure 2-14.

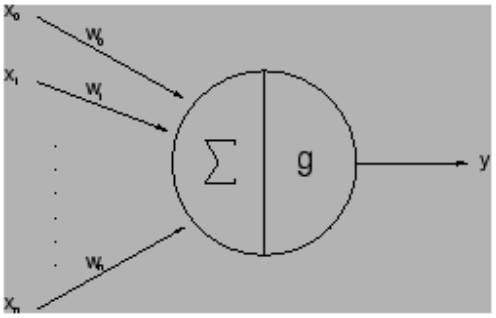

Figure 2-14 Activity of single layer neuron

2.12.4 Connection

Connections are the paths where all information flows within a ANN model [133, 135]. Learning, repetition of a task can cause the connection strengths to change, some neuron connections becoming reinforced and new ones being created, others weakening or in some cases disappearing altogether. Besides that, essential element of neural connectivity is the excitation or inhibition distinction. It is like human brains, each neuron is either excitatory or inhibitory, which is to say that its activation will either increase the firing rates of connected neurons, or decrease the rate, respectively. Nevertheless, transfer

function plays an important role in determining neuron's response. Transfer function describes how a neuron's firing rate varies with the input it receives. Each of these behaviors can be represented mathematically.

2.12.5 Weights and Bias

As mentioned previously, connections are where information is being stored. Each connection is equipped with weight and bias, which are used to modify the signal flow on respective connection. Weight is determined the suitable input weight for next layer and bias is worked out as an adjustment by which the product of weight and output from preceding layer is added. These are important in determining the trend of the model [133-135].

2.12.6 Transfer Function

ANN behavior is dependant on both weights and transfer function that are specified for the units [131, 133-135]. This function typically falls into one of three categories: linear (or ramp), threshold and sigmoid as depicted in figure 2-15.

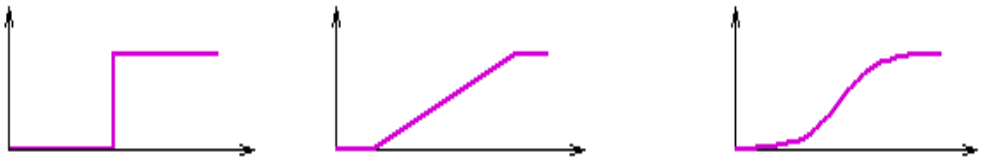

Figure 2-15 Typical transfer function.

For linear transfer function, the output activity is proportional to the total weight output. Threshold units is where the output is set at one of the two levels, depending on whether the total input is greater than or less than some threshold value. In a sigmoid unit, the output varies continuously but not linearly as the input changes. The most common sigmoid units used are log-sigmoid and tan-sigmoid.

2.12.7 Learning

Learning process in ANN can be viewed as the problem of updating network architecture and connection weights with bias so that a network can efficiently program a specific task. The network usually learns the connection weights and bias from available training patterns. Performance is improved over time by iteratively updating the weights in the network. Design of learning process for ANN includes following components: understanding learning paradigm in which ANN operates, and how the network weights are updated from layer to layer [131, 133].

Learning paradigm contains supervised learning, unsupervised learning and hybrid learning. Supervised learning, that is, network is provided with correct output for every input pattern and weights are determined to provide accurate output. This is of network does not require a correct answer associated with each input pattern in the training data set. This learning explores underlying structures of data and organises patterns into categories from these correlations. For hybrid learning, it is the combination of supervised and unsupervised learning in term of weights [131].

2.12.8 Training

Training is the process of fitting the network to the experimental data. It consists of optimising the value of the weight associated with each connection between neurons. The strength of the signal of the synapse multiplied by weight of the synapse defines the contribution of that synapse to the activation of the neuron for which it is an input. Usually, experimental data is divided into three sets: training set, test set and cross validation set [141]. During training, it is important to avoid over training in an effort to obtain the best fit. This is a potential problem with the use of powerful non-linear regression methods in NN modeling. An over-trained model tends to remember the relationship between input and output variables and therefore lacks generalisation capability [137].

2.12.9 Neural Network Type-Feed-Forward Neural Network

ANN can be classified by their learning paradigm. Each of these classifications is dependant upon input's behavior, input's pattern, transfer functions and network topology required. Feed-forward neural network is one of the most common and simplest types of ANN devised. It is a network where connections between the units do not form a directed cycle. In this network, the information moves in only one direction, forward, from the input unit, through the hidden unit and to the output unit. There are no cycles or loops in the network. Feed-forward neural network can be categorized into single layer perceptron and multi-layer perceptron.

Single layer perceptron consists of a single layer of output units; the inputs are fed directly to the output via a series of weights. The sum of the products of the weights and inputs is calculated in each node, and if the values are above some threshold (typically 0) the neuron fires and takes the activated value (typically 1); otherwise it takes the deactivated value (typically -1). Neurons with this kind of activation function are called McCulloch-Pitts neurons or threshold neurons [131, 133].

Multilayer perceptron (MLP) is used a variety of learning techniques, the most popular being backpropagation. MLP have become popular technique for modeling manufacturing processes, among many other applications. It has been theoretically proven that any continuous mapping from an *m*-dimensional real space to an *n*-dimensional real space can be approximated within any given permissible distortion by the three-layered feedforward neural network with enough intermediate units [142-145].

MLP is a supervised learning network, that is, output values are compared with the correct answer to compute the value of some predefined error-function. This error is then fed back through the network and reduced the error function by adjusting the weight of each connection. This process is repeated for a sufficiently number of training cycles, the network is then converged to some state where the error is minimized [131, 133, 143].

One of the advantages of MLP is its efficiency in modeling process mean and process variation simultaneously using one integrated MLP model.

2.13 NEURAL LEARNING USING BACKPROPAGATION

Backprogation (BP) was first described by Arthur and Yu in 1969 and Rumelhart et al. described this method through their works in 1986 [146]. The original procedure used the gradient descent algorithm to adjust the weights toward convergence using the gradient. Because of this, the term "backpropagation" is used to denote an ANN training algorithm using gradient descent as the core algorithm.

BP is used to adjust the weights and biases to solve a particular problem. BP network is made up of a large number of interconnected neurons. The neurons are arranged in one input layer, one output layer, and one or more hidden layer(s). Each neuron in the input layer is connected to a neuron in the output layer. There is no connection between neurons in the same layers. The connection between two neurons is called synapse, and each synapse has a strength or weight attached to it which influences the output of the neuron. Neurons in the input layer receive the input variables. The neurons in the hidden layer receive the output of the input neurons and a non-linearity in the relationship between input and output parameters is introduced at the hidden neuron. The output of the hidden neuron is sent to the output neuron. The more the number of hidden neurons, the more complex the model becomes. The predicted output is compared with the desired output and the error is sent back to the hidden layer for improving the prediction. The cycle is repeated until the overall error value drops below predetermined threshold [131, 137, 144, 147].

BP can also be considered as a generalisation of the delta rules for non-linear activation function and MLPs. In order for hidden layer to serve any useful function, MLP must have non-linear activation function for the multilayers. Equations (6) [131, 133, 144]:

$$\delta_o^p = (d_o^p - y_o^p)\,\mathcal{F}_o{}'(s_o^p) \quad \text{and} \quad \delta_h^p = \mathcal{F}'(s_h^p)\sum_{o=1}^{N_o}\delta_o^p w_{ho}. \qquad \text{(eq. 2-6)}$$

where each output unit, δ_o and each hidden unit, h_o. Equation 6 gives a recursive procedure for computing the δ's for all units in the network, which are then used to compute the weight changes according to equation. The procedure constitutes the generalized delta rule for a feed-forward network of non-linear units.

Advantages of BP are:

- It allows quick convergence on satisfactory minimum error in the kind of networks to which it is suited
- It is the generalized delta rule, which allows for adjustment of weights leading to the hidden layer neurons in addition to the usual adjustments to the weights leading to the output layer neurons.

Techniques of BP can be shown in figure 2-16.

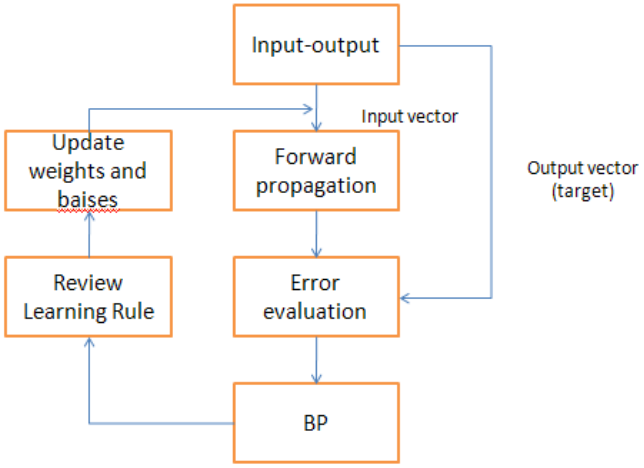

Figure 2-16 Back propagation schematic design

2.14 LEVENBERG-MARQUARDT ALGORITHM (TRAINLM)

Levenberg-Marquardt algorithm (LMA) provides a numerical solution to the problem of minimising a function, generally nonlinear, over a space of parameters of the function. LMA is a very popular curve-fitting algorithm and it is more robust compared to the others because it is able to find a solution even if it starts far off the final minimum.

Limitations of LMA are its sensitivity to initial network weights; outliers are not included in the data, which may lead to overfitting noise; and, it requires the storage of some matrices that can be quite large for certain problems [148-150].

LMA is designed to approach second-order training speed without having to compute the Hessian matrix. As stated earlier, it can be approximated as:

$$H = J^t J \quad \text{(eq. 2-7)}$$

and gradient can be computed as

$$g = J^t e \quad \text{(eq. 2-8)}$$

Principally, LMA involves in solving the following equation:

$$(J^t J + \lambda I)\delta = J^t e \quad \text{(eq. 2-9)}$$

where $\boldsymbol{J}$ is the Jacobian matrix for the system, $\boldsymbol{\lambda}$ is the Leverberg's damping factor, $\boldsymbol{\delta}$ is the weight update vector and $\boldsymbol{e}$ is the error vector containing output errors for each input vector used in training the network. The $\boldsymbol{\delta}$ provides information on the changes of network weights to achieve better solution/output. $\boldsymbol{\lambda}$ is adjusted at each iteration, and guides the optimisation process. If reduction of $\boldsymbol{e}$ is rapid, a smaller value can be used, bringing the algorithm closer to the Gauss-Newton algorithm, whereas if iteration gives insufficient reduction in residual, $\boldsymbol{\lambda}$ can be increased, giving a step closer to the gradient descent direction [148-150].

LMA main contribution to the method was the introduction of the damping factor, $\boldsymbol{\lambda}$. This value is summed to every member of the approximate Hessian diagonal before the system is solved for the gradient. Then, LMA equation is solved, weights are updated using $\boldsymbol{\delta}$ and the network errors for each entry in the training set are recalculated. If the new sum of square error (SSE) has decreased, λ is decreased with the iteration ends. If it has not,

then the new weights are discarded and the method is repeated with higher value for λ. λ is adjusted by using an adjustment factor, ν [148-150].

As stated earlier, LMA consists basically in solving different λ values until in SSE decreases. So, each learning iteration (epoch) will consist of the following steps:

1. Compute Jacobian matrix
2. Compute error gradient, g
3. Approximate the Hessian using cross product of Jacobian, H
4. Solve $(H + \lambda I)\delta = g$ to find δ.
5. Update the network weights by δ.
6. Recalculate SSE with updated weights.
7. If SSE increased, discard new updated weights and increased λ. Else decrease λ and stop.

2.15 APPLICATION OF NEURAL NETWORK

An ANN is an adaptive system that learns relationship through repeated presentation of data and is capable of generalising to new, previously unseen data. Neural networks have been trained to perform complex functions in various fields, including pattern recognition, identification, classification, and speech, vision, and control systems [132]. In the past, researchers have reported the excellent performance of ANN in analyzing and predicting data of process [142, 151, 152].

Kim et al. applied ANN to characterised oxide film etched in gas chemistry and examined etch mechanisms as a function of process factors [112]. Shie and Yang focused on the optimisation of photoresist coating process by ANN to identify the process parameters in wafer fabrication. Results showed relationship between coating duration and coating chemistry was important factor with least MSE. Liao had proved the efficiency of ANN in modeling by study of the process mean and process variation simultaneously using one integrated MLP model [143].

Mehmet et al. reported that ANN had the ability to predict the output of unseen test data accurately. They found that MLP architecture with BP learning algorithm could be used as a tool to predict mechanical properties [153]. Shahin et al. too, have good agreement with the capability of ANN in accurately predicting the unseen test data. Their results indicated accuracy of ANN predicting data in ultimate bending capacity of fabricated and cold-formed steel circular tubes [138]. Balestrassi et al. tested the effectiveness of ANN and RSM. They pointed out the lack of use of RSM in simulation due to the system not being able to read RSM data. It was a real-world experimental tool than a simulation tool [154].

Paliwal et al. had carried out literature review of comparative studies on ANN and traditional statistical techniques in various filed of applications. ANN application in various fields was listed by them, which showed the success of ANN. The review clearly pointed out the potential of ANN being used as a tool for classification and in prediction problems. One of the advantageous was that ANN could automatically approximate any nonlinear mathematical function. However, the determination of various parameters, such as number of hidden layer, nodes in the hidden layer etc. associated with ANN was not straightforward and finding the optimal configuration of ANN was very time consuming process [155].

2.16 Concluding Remarks

Upon review of the literature, it is concluded that:

- The previous studies performed on the machining of advanced ceramics generally required high technology tool, such as electrode beam, laser beam and so on. Each tool has certain life span and maintenance is required throughout the service. In term of cost effectiveness, these methods are generally quite high.
- 7% increment of advanced ceramics demand by 2010 [118] is an attractive figure. The gain of advanced ceramics demand certainly will benefit as advanced ceramics continue to penetrate several applications, such as micro-electromechanical, semiconductor, cutting tools, joint implants and membranes. It also motivates the

study of machining of advanced ceramics aiming to obtain high output with better quality and decrease the overall cost.

- Chemical machining as the oldest advanced machining method is commonly used in patterning industry. This method has been applied since 2500 B.C. till the current day. The reason is that chemical machining does not required complicated set up and the procedure of chemical machining is simple. However, it has to be carefully handled. Problem raised in chemical machining is mostly related to the chemical etchant involved. Etchants used are both acid-based and alkali-based, which are hazardous and thus requires the process to be carried out in the fume hood. The disposal of etchant also has to be carefully handled to avoid unnecessary damage.
- Precise dimensional accuracy is important in the patterning industry. Currently in industry, mask patterning is the most common patterning method. The problem of this masking patterning is related to the masking properties and adhesive properties. In order to produce a precise and smooth patterning, the masking has to be resistant to the chemical reagent. Thus, the usage or choice of chemical reagent is limited due to the masking. New method – nano-scratch technique has been introduced and a few studies have shown its versatility [11, 75]. By applying this method, the masking cost can be reduced and the problem raised by masking can be eliminated as well as to reduction in the hazardous resulting from mask application because the process of mask application involves toxic materials.
- Quality of chemical machining is measured by the etch rate and surface roughness. In some cases, the dimensional accuracy is also the key of success, especially in patterning industry. A small change in the parameters will cause a huge difference in the end product. Etch rate, which is related to the speed and time required for the whole process is the most important measurement. Without etch rate, it means that the process is not working. Of course, the higher the etch rate is, the better is the process. Unfortunately, in most of the studies, high etch rate would decrease surface roughness quality [20].
- In micro- and nano-patterning industry, surface roughness is the key of success. With poor surface roughness, the end product will be rejected and cause the increase of production cost.

- Dimensional accuracy is directly influenced by the quality of surface roughness and it is associated with etch rate. The higher the etch rate, the higher the etch ratio. This is a preferable phenomena but this might lead to poor surface roughness (as discussed above). Though undercut can be eliminated by applying nano-scratch patterning, a few questions are being raised, such as how much load should be applied on indented area, what is the best etch ratio for the process and is it able to perform any types of patterning design.
- The use of statistical tool to study the performance of the processes is quite common in both the industry and research fields. This is because it can reduce the time consumed in trial-and-error tests and also increase the effective analysis of the results. RSM is commonly used in most of the research field due to its feasibility to fit into all type of experiments and it is user friendly [126, 156, 157]. ANN, which is also an analytical tool, is less frequently used compared to RSM in machining field. The benefit is that it is able to produce significant analysis result, although it requires large number of inputs.

Chapter 3 Research Methodology and Techniques

3.1 INTRODUCTION

The literature review discussed in Chapter 2 provides an overview of the present understanding of CHM and advanced ceramics as well as its applications and existing machining methods. The review indicated that there is a need to perform further research to better understand the CHM of advanced ceramics as well as the analytical tools and predictive model. The finding will help in mitigating the chemical machining problems and provide better understanding in achieving optimisation of the chemical machining in industries. Thus, it is necessary to study the CHM and also produce the predictive model for each substrate. This chapter outlines the research methodology, experimental approach and analytical techniques that were used to achieve these purposes.

To study the characteristic of advanced ceramics in CHM, sample preparation is required prior to experimentation and analysis. Atomic force microscopy (AFM) was employed for the surface roughness measurement. Measurement of etching rate was based on the weight loss of substrate following CHM and that of etching ratio was carried out using the digital micrometer. Analysis of experiments data and predictive model were performed by RSM and ANN. Accuracy of output was adjusted to 95% confidence level.

3.2 WORKPIECE AND MATERIALS

This study will focus on three types of advanced ceramics namely machinable glass ceramics, silicon carbide and boron nitride. These substrates are selected as they have not been well-researched and also due to their availability in the industry. Additionally, none of these substrates have been analysed by ANN nor has predictive model been developed for the CHM process.

3.2.1 Machinable Glass Ceramics (MGC)

MGC used is manufactured by Goodfellow.Inc. with 46% of SiO_2, 16% of Al_2O_3, 17% of MgO, 10% of K_2O and 7% of B_2O_3. The properties of MGC produced by Goodfellow.Inc are almost similar to the rest, which is able to remain rigid at high operating temperatures with low thermal conductivity and useful as high temperature insulators. It has excellent electrical insulation and is widely used in the semiconductor and MEMs industries. Besides, it is white in colour and can be highly polished without damage to its properties and this enhances MGC values as manufacturing materials in the medical and optical devices [158, 159]. Additionally, outgassing in ultra-high vacuum environments can be eliminated, if MGC is degassed before use and since it is non-wetting, it can be bonded to itself as well as to various metals, if the surfaces are first metalised. Compared to other advanced ceramics, MGC has greater resistance to surface damage and brittle fracture.

MGC's chemical resistance towards acid is poor, especially concentrated acid. However, dielectric properties of MGC are excellent with 5.9 dielectric constant, 40kVmm^{-1} strength of dielectric, and more than 10^{14} volume resistivity. Its compressive strength is 345MPa, hardness-vickers is 400kgf mm^{-2} and tensile modulus is 67GPa. MGC possesses 13x10^{-6} K^{-1} thermal expansion coefficient, 790 J K^{-1} kg^{-1} of specific heat, and 1.5Wm^{-1}K^{1} thermal conductivity and density of 2.52gcm^{-3} without apparent porosity.

3.2.2 Boron Nitride (BN)

BN used in this research is manufactured by Goodfellow.Inc. It has a hexagonal structure and is sometimes known as white graphite, due to its lubricity, anisotropic properties, heat resistance, and high thermal conductivity. This latter property, combined with a low

thermal expansion, leads to excellent resistance to thermal shock. For this reason, BN is used as crucibles for molten metal. BN used here is produced by densification of powder. BN differs from graphite in having a high dielectric strength (40-200kVmm^{-1}) and low dielectric constant (4.3) and is often used as an electrical insulator at very high temperatures. Chemically it is moderately resistant to dilute and concentrated acid. It is also non-toxic and transparent to microwaves. Mechanically, BN has good compressive strength (30-120MPa), shear strength (12-25MPa) and average tensile modulus (20-35MPa). Compare to MGC, BN has 2-15% of apparent porosity and with density of 1.9gcm^{-3}.

3.2.3 Silicon Carbide (SiC)

Reinforced Bonded Silicon Carbide (RBSC) used is manufactured by Goodfellow.Inc. Silicon is infiltrated into a pre-formed silicon carbide/carbon powder green body which is then fired. This gives rise to around 10% free silicon, which fills the pores. The resulting microstructure has low porosity and very fine grain. After firing, RBSC is difficult to machine. It has high strength up to 1350^{o}C which results in its use as high temperature gas turbine components. The high hardness (harder than tungsten carbide) means that it is used extensively for bearings and seals. The high thermal conductivity combined with low thermal expansion leads to good thermal shock resistance. RBSC can tolerate a wider range of acids and alkalis than either MGC or BN. Its oxidation resistance helps to give long service life in furnace applications. Mechanical properties of RBSC: 200-3500MPa compressive strength, 2500-3500kgfmm^{-2} hardness-Vickers, and 410GPa tensile modulus. Like MGC, RBSC has no apparent porosity with density of 3.10gcm^{-3}.

3.3 ETCHANT

Selection of etchant was done by pre-experimentations to confirm that each chosen substrate was able to react with the etchant. Due to the limited choice of etchant, hydrochloric acid, hydrobromic acid and hydrophosphoric acid were selected following the pre-experimentations.

3.3.1 Hydrochloric acid (HCl)

Research studies conducted on etching of advanced ceramics using HCl as etching etchant is relatively less extensive. This might be due to the hazard caused by HCl and the need for extra precautions during handling and the etching process. Cook et al. studied the etching performance of a few etchants (molten salt bath, HCl and KOH) with different advanced ceramics. Their results showed that performance of HCl was relatively poor compared to other etchants [71].

3.3.2 Hydrobromic acid (HBr)

Hydrobromic acid (HBr) is a strong acid formed by dissolving the diatomic molecule hydrogen bromide in water. HBr used contains 47.6% HBr by weight with highest concentration of 9M. This is the reason HBr is a stronger acid than HCl, but not as strong as hydroiodic acid. HBr acid is also known as the strongest mineral acids.

3.3.3 Hydrophosphoric acid (H_3PO_4)

H_3PO_4 is a deliquescent solid at room temperature. It is supplied at 49% concentration with greatly reduced vapour pressure. This enhances personal safety and also allows room-temperature storage in unpressurised containers [56].

3.4 EXPERIMENTAL APPARATUS

3.4.1 Set-up Glassware

Figure 3-1 Set-up of chemical machining. (A) Glass reaction vessel, (B) solution, (C) substrate holder, (D) Heating mantle, (E) Water-cooled condenser, (F) Temperature controller, (G) Glass encased thermocouple and (H) Outlet Valve.

Figure 3-1 illustrates the laboratory-scale CHM system by employing boron silicate glass reaction vessel in this study. Selected etchant was filled in before top glass cover was closed and substrate was fed into the vessel by the substrate holder. Condensation unit was added to the set-up to reduce the changes of etchant's concentration. Experiments were then carried out as designed by RSM described in Section 2.11.2.

Selection of chemical machining set-up is very important as the concentrated acid is corrosive toward glass materials as well as ceramics during the process. This is critical at high temperature. Therefore, boron silicate glassware is used. Boron silicate glass has low coefficient of thermal expansion, making it resistant to thermal shock, about one-third that of ordinary glass. This reduces material stress caused by temperature gradients, thus making it more resistant to breaking. Although this material is known to be slightly etched by the etchants, it is sufficient for laboratory scale experimentation. As shown in Figure 3-2, the etch rate of boron silicate is one of the lowest compared to the rest. This indicates that these materials would be suitable for the glassware of an etching apparatus.

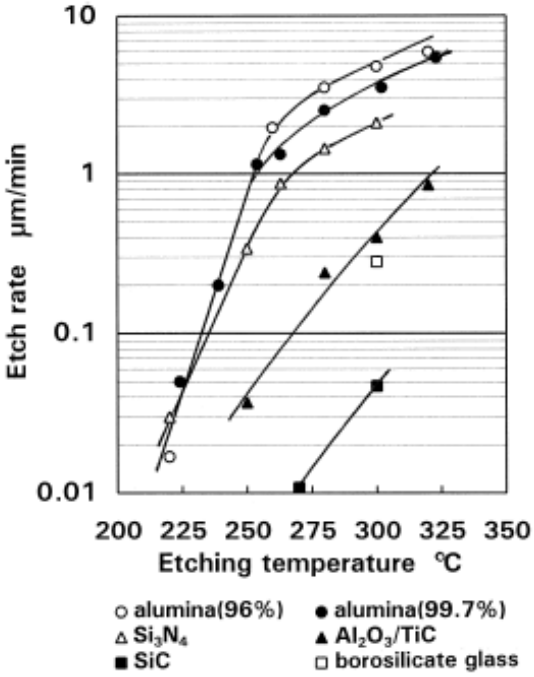

Figure 3-2 Etch rate of various ceramic materials in refluxed boiling etchant[56]

3.4.2 Heating Mantle

Figure 3-3 Heating mantle model MS-E103

The etchant in boron silicate glass reaction vessel was heated by the heating mantle. The heating mantle (Figure 3-3) used in this study is MS-E103 with the temperature controller. Its heating element is made of the glass fiber, which is able to minimise the damage of flask during etching process. The heating efficiency is promoted greatly because of being in good contact between heating element and glass vessel. This heating mantle can heat up to 450^{o}C.

3.4.3 K-Type Thermometer

Figure 3-4 K-type thermocouple model EA11A

The temperature in the solution was checked by K-type thermocouple model EA11A (Figure 3-4). This model offers a single K-type thermocouple with multifunction LCD display. This meter is fully tested and calibrated and, with proper use, will provide years of reliable service. The measurement range is from -50°C to 1300°C with multi-function LCD (Table 3-1).

Table 3-1 Accuracy specification

Units	Range	Accuracy (@23 ± 5°C)
°F	0°F to 1832°F	± (0.3% reading + 2°F)
	-58°F to 0°F and 1832°F to 1999°F	± (0.5% reading + 2°F)
°C	0°C to 1000°C	± (0.3% reading + 1°C)
	-50°C to 0°C and 1000°C to 1300°C	± (0.5% reading + 1°C)

3.4.4 Atomic Force Microscopy (AFM)

Atomic force microscopy (AFM) is used to measure the surface roughness of substrate before and after CHM process. AFM is a high resolution type of scanning probe microscopy, with demonstrated resolution of fractions of a nanometer. Binnig, Quate and Gerber invented the first AFM in 1986 [160-162]. Today, most AFMs use a laser beam

deflection system, introduced by Meyer and Amer, where a laser is reflected from the back of the reflective AFM lever and onto a position-sensitive detector. AFM tips and cantilevers are micro-fabricated from silicon or silicon nitride with a tip radius of curvature on the order to nanometers. When the tips is brought into proximity of a sample surface, the forces between the tip and sample lead to a deflection of the cantilever [163]. Depending on the situation, forces that are measured in AFM include mechanical contact force, van der Waals forces and magnetic forces [161-163].

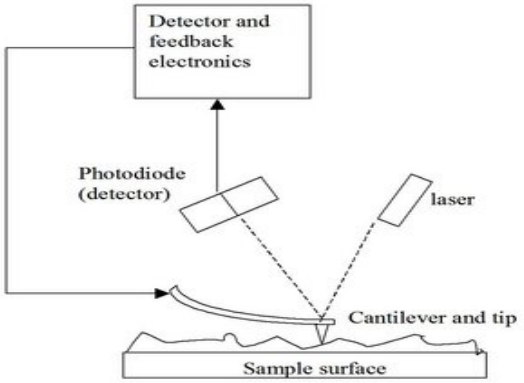

Figure 3-5 The principles of AFM [164]

The measurement of AFM relies on the forces between the tip and sample. Yet, this is a non contact scanning where the force is not measured directly. Thus, the force is calculated by measuring the deflection of the lever, and knowing the stiffness of the cantilever. Hook's law gives F = -kz, where F is the force, k is the stiffness of the lever, and z is the distance the lever is bent [162, 164] as shown in Figure 3-6.

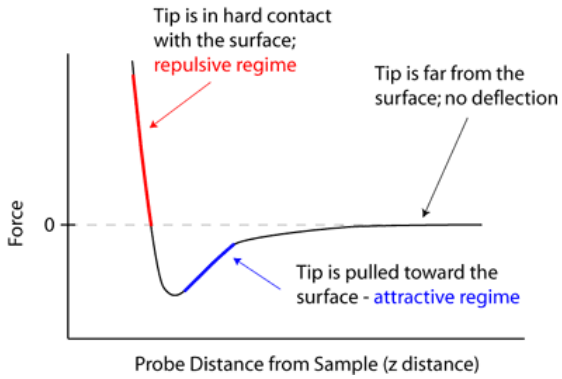

Figure 3-6 Measurement of AFM [164]

If the tip were scanned at constant height, there would be a risk that the tip would collide with the surface, causing damage. Hence, in most cases a feedback mechanism is employed to adjust the tip-to-sample distance to keep the force between the tip and the sample constant. This can be achieved by mounting the sample on a piezoelectric crystal [164]. AFM, however, has the advantage of imaging almost any type of surface and provides a true three-dimensional surface profile [162]. Additionally, samples viewed by AFM do not required special treatment that would actually destroy the sample and prevent its reuse. The main disadvantage of AFM is that it produces a small image size. AFM can only show a maximum height on the order of micrometers and a maximum area of around 100 by 100 micrometers.

The AFM is one of the foremost tools for imaging, measuring, and manipulating matter at the nanoscale. The brand of AFM used in this research is Shimadzu and model name is SPM 9500-J2. This is a non-contact scanning with air as the medium. A stiff cantilever is oscillated in the attractive regime, meaning that the tip is quite close to the sample, but not touching it. The forces between the tip and sample are quite low, on the order of pN (10^{-12}N). The detection scheme is based on measuring changes to the resonant frequency or amplitude of the cantilever. The cantilever used here is monolithic silicon with aluminum coating on the detector side. The scanning rate is 2Hz with 256 x 256 images resolution. Surface profiles data is measured in arithmetical mean deviation, R_a. The average roughness or deviation of all points from a plane fit to the test part surface, as shown in equation 10. R_a is available for profile and area data.

$$R_a = \frac{1}{L}\int_O^L |z(x)|dx \qquad \text{(eq. 3-1)}$$

where L is substrate length, z is individual peak to valleys from sample length, and x is the distance from the peak to valleys wave within sampling length.

3.4.5 Roller tool

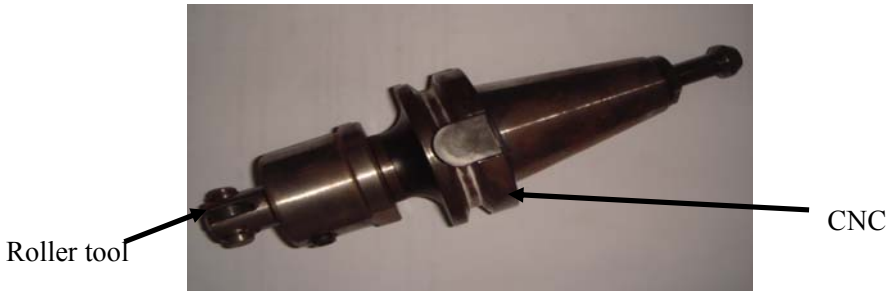

Figure 3-7 Roller tool for the indentation.

A new tool - roller tool was designed and fabricated for the purpose of micro-indentation as illustrated in Figure 3-7. This roller was designed to be used in CNC machine and the insert of CNC machine is shown in Figure 3-8. The fabricated roller tool was attached to this insert tool and worked together in the CNC machine. CNC machine is chosen because of its ability to accurately apply the required force on the substrate.

Figure 3-8 CNC insert

Figure 3-9 EZO-6800rs Roller

Figure 3-10 Stainless steel spring

Roller tool is a simple tool, which contains only EZO-6800rs roller (Figure 3-9) and also a stainless steel spring (Figure 3-10) with spring constant of 0.5 Nm^{-1}. The width of EZO-6800rs roller is 5mm with 15mm diameter and has a weight of 5.24g. All parts are changeable in the roller tool.

The mechanism of the roller tool is simple as shown in Figure 3-11. The roller portion is movable and the length of this portion is depends on the stainless steel spring. Before

indentation, the depth of indented concave was decided and force was calculated by using $F = kx$, where k is spring constant and x is the displacement of the spring's end from its equilibrium position. Roller tool moved through the substrate surface and created the indented concave with required depth (as shown in Figure 3-12).

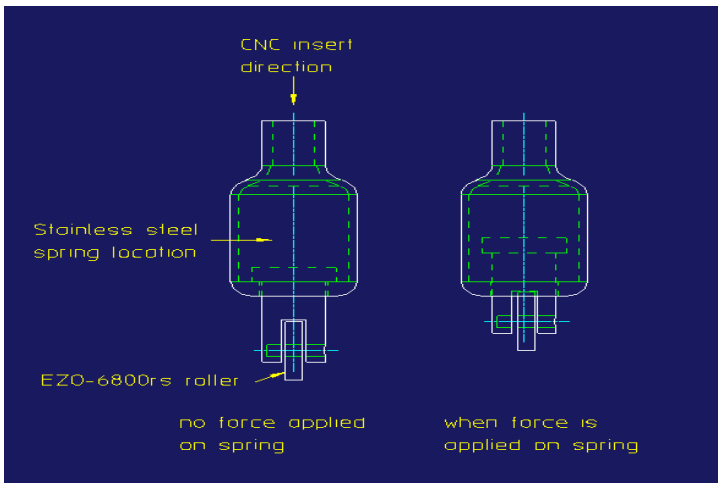

Figure 3-11 Roller tool structure (left) without force and (right) with force.

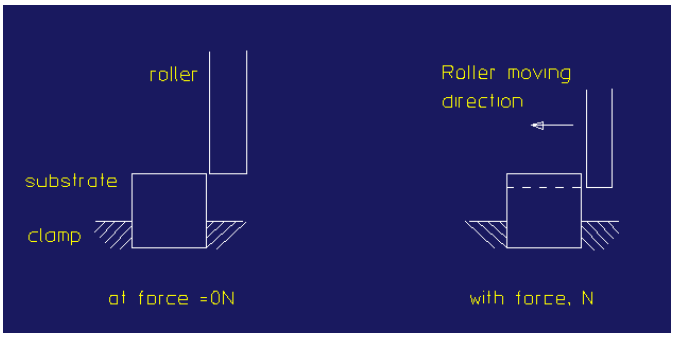

Figure 3-12 Mechanism of roller tool before and after force is applied.

3.5 EXPERIMENTATION

3.5.1 Introduction

The scope of our research involved studies of chemical machining of advanced ceramics in terms of etching rate, surface quality and dimensional accuracy. The main objective of the research is to establish the relationships between the above variables with etching

temperature, etching duration, chemical reagents and its concentration. Using the experimental data obtained, predictive models were developed by RSM based on the etching variables studied, namely temperature, etching duration, type of chemical reagent and its concentration.

A few assumptions have been taken in RSM to study this experimental process: errors are assumed to approximate the normal distribution that has a zero mean and a constant variance. Predictive models for etching rate, surface quality and dimensional accuracy were subsequently established. The result obtained from the predictive mathematic models was compared with previous experimental data and verified by Artificial Neural Network (ANN). These predictive models would be very valuable to the industry since there is no need to run experiments to estimate the output variables.

The difficulties of CHM of advanced ceramics lie in controlling the variables of this process. The combination of these variables directly influences the etching rate, surface quality and dimensional accuracy and therefore the quality of CHM. As mentioned earlier, a few uncontrollable variables included the quality of substrates and chemical reagents, since they were sourced from different manufacturers. External variables such as stirring process and aided material also indirectly influence the quality of CHM. In order to avoid unnecessary influence, each material was cleaned to eliminate the contamination on top of them, and statistical method was used to verify the result of CHM process.

3.5.2 Experimental design

3.5.2.1 Preparation

Each substrate was cut into 10mm X 10mm X 10mm dimension and cleaned with distilled water for 10 minutes and then dried in the oven for an hour. This procedure was to ensure no contamination on the substrate's surface and no dust on top of the surface after cutting process.

Then, all the substrates proceeded to the indentation process, where substrate was indented by a roller tool as shown in Figure 3-12. This rolling tool was fabricated to fit

into the specific application. The details of this tool are explained in the earlier section. Indentation of substrate was carried out by inserting the roller tool into the CNC insert. After setting up the CNC machine and force needed, the roller tool was rolled over the substrate and a straight line concave was created. Before proceeding to take the essential parameters, the substrate was cleaned and dried for about an hour. Figure 3-13 illustrates the process of indentation on the substrate by CNC and roller tool.

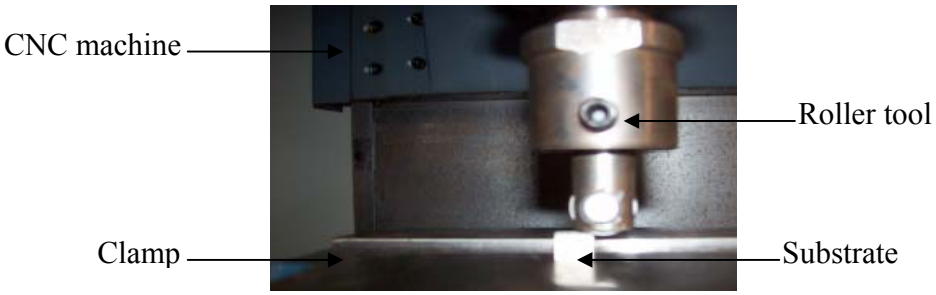

Figure 3-13 Indentation of substrate by the CNC with roller tool

After that, each substrate was sent for measurement before CHM was carried out. In this study, parameters involved were etching rate, surface roughness and etching ratio. Etching rate was measured by the differentiation of substrate's weight before and after CHM experiment. The weight of substrate was measured by weighing balance – Sartorius BT224S (Figure 3-14) with 0.1mg resolution internal calibration. It can measure up to three decimal points in gram.

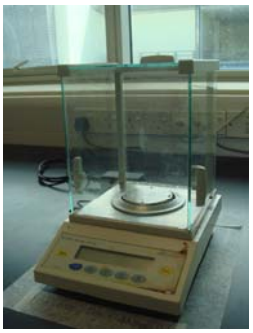

Figure 3-14 Sartorius BT 224S weighing balancer

Measurement of surface roughness was done by local government agency – SIRIM. AFM - Shimadzu-SPM 9500-J2 was used to measure surface roughness. As mentioned previously, surface roughness was measured in μm with deviation of ± 1.5nm. Figure 3-15 shows the work place for AFM and where the result was obtained during the measurement of one of the substrates.

Figure 3-15 AFM from Shimadzu-SPM 9500-J2

Lastly, measurement of the depth of indented concave and indented surface were taken by digital micrometer – KEN3313010K (Figure 3-16). This apparatus is manufactured by Kennedy with accuracy of 0.001mm. Etching ratio is the ratio between depths at indented concave compared to the non-indented surface.

Figure 3-16 Micrometer

The last step before proceeding to the CHM experiment was the experimental design by 2^k factorial design and CCD. DE 7 was employed as the software to analyse experiment all data. For first-order model, thirteen numbers of experimental runs were designed and all running sequences were randomised. Each material was investigated with three different etchants (HCl, HBr and H_3PO_4). Then, data was analysed. For second-order model, CCD was selected with three numerical variables (etching temperature, etching

duration and solution's concentration) and one categorical variable (etching solution). In this study, variables investigated were etching temperature (0^{o}C to etchant's boiling point), etching duration (30 minutes to 270minutes), etching etchant (HCl, HBr and H_3PO_4) and etchant concentration (lowest, medium and highest). 95% confidence level was chosen and a table of the experimental run was created by DE 7 (as shown in Table 3-2 and Table 3-3). All experiments were randomly organised to make sure the observation was independently distributed.

Table 3-2 Experimental table generated by 2^k Factorial Design for CHM of MGC

run	temperature	period	concentration	etching rate	surface roughness	etching ratio
1	64	0	1			
2	28	180	-1			
3	64	105	-1			
4	64	105	0			
5	100	105	-1			
6	28	105	0			
7	64	105	0			
8	64	105	0			
9	28	30	1			
10	100	30	0			
11	64	210	1			
12	100	180	1			

Table 3-3 Experimental table generated by RSM-CCD for CHM of MGC

run	temperature	duration	concentration	etchant	Etching rate result	Surface roughness result	Etching ratio result
1	100	30	-1	HCl			
2	100	135	0	HBr			
3	19	30	-1	HCl			
4	19	240	1	HCl			
5	62	0	0	HCl			
6	100	135	0	H_3PO_4			
7	19	30	1	HCl			
8	19	30	1	H_3PO_4			
9	19	30	1	HBr			
10	19	240	1	H_3PO_4			
11	19	240	1	HBr			
12	62	135	0	H_3PO_4			

run	temperature	duration	concentration	etchant	Etching rate result	Surface roughness result	Etching ratio result
13	100	30	-1	H_3PO_4			
14	62	135	1.68	HCl			
15	62	135	0	HCl			
16	62	135	0	H_3PO_4			
17	0	135	0	HCl			
18	62	135	0	HBr			
19	100	30	-1	HBr			
20	100	240	-1	H_3PO_4			
21	62	135	0	HCl			
22	62	135	0	HBr			
23	100	240	-1	HBr			
24	19	30	-1	H_3PO_4			
25	19	30	-1	HBr			
26	0	135	0	H_3PO_4			
27	0	135	0	HBr			
28	62	135	-1.68	HCl			
29	62	135	1.68	H_3PO_4			
30	62	170	0	HBr			
31	100	30	1	H_3PO_4			
32	62	135	0	HCl			
33	100	30	1	HBr			
34	62	135	0	H_3PO_4			
35	62	135	0	HBr			
36	100	30	1	HCl			
37	62	135	-1.68	H_3PO_4			
38	62	310	0	HCl			
39	62	135	-1.68	HBr			
40	62	135	1.68	HBr			
41	62	300	0	H_3PO_4			
42	62	310	0	HBr			
43	19	240	-1	H_3PO_4			
44	19	240	-1	HBr			
45	100	240	-1	HCl			
46	19	240	-1	HCl			
47	62	135	0	H_3PO_4			
48	100	135	0	HCl			
49	100	240	1	H_3PO_4			
50	100	240	1	HBr			
51	62	0	0	H_3PO_4			

run	temperature	duration	concentration	etchant	Etching rate result	Surface roughness result	Etching ratio result
52	62	0	0	HBr			
53	62	135	0	HCl			

3.5.2.2 Chemical machining process

CHM experiment was started by pouring 500ml of selected etchant into the boron silicate glass vessel and heated until the desired temperature. Then, substrate was inserted to the vessel and CHM started as shown in Table 3-2. At the end of the experiment, substrate was removed from the vessel and etchant was removed to a disposal bottle. This was followed up by cleaning and drying process. Measurements for etching rate and etching ratio were taken after the drying process in the laboratory. For surface roughness measurement, samples were sent to SIRIM.

3.5.2.3 Analysis

The last procedure was to analyse all results by inserting this data into DE 7 and ANN. Analysis of Variance (ANOVA) and *p*-value were generated and results were analysed. This was started with the first order model (2^k factorial design), where data was analysed to determine the behaviour of the process. If this is the linear process, curvature term shown in ANOVA with *p*-value is more than 0.5 or insignificant. Information shown in ANOVA was sufficient to study the process. Otherwise, this would be followed by second order model (CCD) to proceed on the higher level model (quadratic, cubic and etc). At this stage, ANOVA was studied and followed by monitoring the changes of each dominant factor and examining the generated graphs. The parameter studied and the models' lacks of fit were as indicated and assessed respectively. Predictive empirical model on this experimental model was also generated.

3.6 DESIGN OF EXPERIMENT

DoE is the combination of mathematical and statistical techniques. Mathematical models can be used to predict and better analyse result behaviour in different condition with a limited number of experiment tests [120]. Software Design Expert (DE 7.0) was used.

3.6.1 Factors, Levels and Ranges

Three materials were used: machinable glass ceramic, boron nitride, and silicon carbide. As mentioned in previous section, factors chosen in this research are etchant, etchant's concentration, etching temperature and etching duration. These factors can be categorised as one categorical factor (etchant), and three numerical factors (etchant concentration, etching temperature and etching duration). Each of these factors is at two levels, which are their maximum and minimum values. Selection of range for each numerical factor was based on the pre-experiment-two factorial design. Central points were added to the experimental design to determine the trend of the process.

3.6.2 Selection of the Response Variable

Based on research works and the industry requirements, the most important quality of machining of advanced ceramics was discussed. Response variables, which were chosen here were etching rate (g/min), surface roughness (μm/min) and dimensional accuracy (etching ratio). The measurement of each weight, surface roughness and dimensional of indented and non-indented areas was taken before and after the etching process.

3.6.3 Choice of Experimental Design

DoE is divided into three categories: comparative objective, screening objective and response surface objective [8]. Comparative objective is chosen if the primary goal of the process is to study whether selected factor is significant. Screening objective was chosen when primary purpose of the experiment was to select the few important main effects from the many less important ones. Whereas, response surface objective was used to find and optimise the process and troubleshoot process problems to make the process more robust against external and non-controllable influences.

Experimental design was started with the screening objective, which was the two-level (2^k) factorial design. This was to determine the important factors, the range of factors and trend of experimental process. In statistics, factorial experiment is an experiment whose design consists of two or more factors, each with discrete possible values, and whose experimental units take on all possible combinations of these levels across all such factors.

Factorial design is a tool that allows experimenters to experiment on many factors simultaneously. The simplest factorial design is two-level factorial which involves a few factors at two levels or values.

3.6.3.1 Planning stage for 2^k factorial design [4]

The planning stage for 2^k factorial design was carried out as below:

1. Factors to be investigated were determined.
2. A 2^k factorial experiment was designed and run in a localised region of the response surface.
3. Estimates of the effects and the coefficient of the linear model were calculated:
   $y = b_o x_o + b_1 x_1 + b_2 x_2 + b_3 x_3 + \varepsilon$ (eq. 3-2)
4. A reference factor was selected and it was used as a guide in determining the appropriate steps along the direction of each factor in order to continue moving along the path of steepest ascent.
5. A few experimental conditions along the path response of steepest ascent were selected and trials were run to determine if the response continued to increase. If the response ceased to increase, a new path should be generated.
6. If a new path was needed, a new 2^k factorial experiment was designed and run again. All previous steps were repeated until no substantial improvement in the response was obtained.

In this analysis, it will determine either this is a linear or quadratic model. If this is a linear process, study of the process can proceed with the ANOVA obtained. Otherwise, this is followed with comparative objective, where RSM is required. RSM is useful for modeling and analysis of problems in which a response of interest is influenced by several factors [2]. There are a few types of RSM: central composite design (CCD), Box-Behnken and 3^3design. For this case, central composite design was chosen as the experimental design method. CCD is intended for sequential experimentation, thus making it flexible for industrial process development. The reasons are due to CCD's ability to be partitioned naturally into two subsets of points; the first subset estimates linear and two-factor interaction effects while the second subset estimates curvature

effects. CCD is efficient, in providing much information in a minimum number of required runs, and flexible due to its variety of choices that enables the design tool to be used under different operability.

3.6.3.2 Planning stage for CCD

1 A three-level factorial experiment in the region was designed and executed, where the path of the steepest scent yields no substantial improvement in response.

2 The coefficients of the model was computed:

$$y = b_o x_o + b_1 x_1 + b_2 x_2 + b_3 x_3 + \varepsilon \quad \text{(eq. 3-3)}$$

3 Using the above model, the nature of the stationary point of the response surface was determined. The stationary point was the one where the gradient vanished.

3.7 ARTIFICIAL NEURAL NETWORK

ANN was also used to study the process of CHM and to compare the results with CCD. The neural network learns complex data both adaptively and nonlinearly without any formulation on the causal relationship between the input and output patterns. Such learning ability can be attributed to the fact that the neural network, possessing many simple parallel processing units (neurons), resembles the architecture of the human brain. These neurons are interconnected in such a way that knowledge is stored in the weights of the connections. Each neuron contains the weighted sum of the inputs filtered by a transfer functions. The main characteristics of ANN are the neurons arrangement in the network architecture that dictates what type of problem can be dealt with and method of determining the weights of the connections [139]. In this process, it is assumed that information processing occurs in a number of simple elements called neurons. The signals are transmitted between neurons over connection links, each connection link has an associated weight that multiplied the signal transmitted, and each neuron applies an activation function to the incoming signal to determine its output signal [139].

NeuroSolutions 5 with excel was used and this is a highly advanced simulation environment capable of supporting users with varying levels of expertise. A conceptual

understanding of the fundamentals of ANN theory is deemed necessary. This software is user friendly and making explicit the level of user knowledge required.

3.7.1 Planning of ANN

1 Type of problem was chosen before proceeded on the design. One of the designs was function approximation, which was used to determine a continuous value for each input pattern.

2 Input and output files selection. All input values and outputs were determined, identified the symbolic data if available.

3 Cross validation: data was divided into training set and test set. Each of these was used to train and checking the network quality.

4 Data was trained by selecting type of transfer function, number of hidden layers, number of epochs and others. A pre-saved hidden layer multilayer perceptron (MLP) would be opened for modeling this data. Training data was used to train the network. It would continue as setting set when the training was run.

5 The table of training and cross validation mean-squared error (MSE) was tested.

6 Test data: The true test of a network is how well it can classify samples that it has not seen before. This was used to check the performance of ANN. Again, the MSE was checked.

Chapter 4 Development of Etch Rate Models and Experimental Studies

4.1 INTRODUCTION

The etch rate of a substrate to be patterned must be known while designing a new fabrication process. It is also an important indicator on the quality of chemical machining. Generally, the faster the etch rate, the better is the quality. Besides, the quality of chemical machining was also found to be correlated to the magnitude of surface roughness and etching ratio. This will be discussed in Chapter 5 and 6. Preliminary study showed that etch rate of substrate was difficult to control due to the complex variables involved. In this study, etch rate was measured in g/min, which is the difference of substrate's weight taken before and after the chemical machining process.

The development of first and second order models of etch rate and the experimental etch rate studies were presented in this chapter. First order model was used to decide the nature of the model (as mentioned in section 3.6.3.) If the curvature term in ANOVA is significant, data is then analysed by the second order model (CCD). This is because the first order model is insufficient to analyse the data given. In the etch rate experimental studies, the relationships between variables including the etching temperature, etchant concentration, the type of etchant, and the etching duration and the etch rate were investigated.

4.2 DEVELOPMENT OF FIRST ORDER ETCH RATE MODEL

In this design, 95% confidence interval was set and p-value was used to analyse the significance of corresponding variables. Each p-value has to be less than 0.05 (or 5%) and the smaller the magnitude of p-value, the more significant the model. 2^k factorial design is a screening process which is specifically suited for linear process. This means that each variable is independent of each other. This is always the first step of experiment design to study the relationship between a fixed variable and range of each variable in the process. If the curvature term is significant, all data provided in the ANOVA of 2^k factorial design are useless because these results are analysed linearly and each variable is assumed to be independent.

Many researchers found that there are interactions between variables in chemical machining process of advanced ceramics [6, 7, 9, 71, 165-169]. Tables 4-1, 4-2 and 4-3 depict curvature values that are significant in machining of MGC in all etchants. This implies interaction between variables exists in these processes and RSM is required to study the collected data. Tables 4-4, 4-5 and 4-6 show the results of first order model of etch rate of BN in all etchants. These results revealed that RSM is needed to proceed on to further analysis of these experimental data. This is because p-values of curvature are less than 0.05 and augmentation is required in these processes. Tables 4-7, 4-8 and 4-9 suggest augmentation of etch rate of SiC to RSM instead of linear modeling. Curvature terms are significant in the etching process of SiC with different etchants.

Table 4-1 ANOVA for selected factorial model for etch rate of MGC in H_3PO_4

Source	Sum of Squares	df	Mean Square	F Value	p-value	
Model	2.27E-08	1	2.27E-08	2.5269	0.163	not significant
B-duration	5.18E-08	1	5.18E-08	5.7535	0.0534	
Curvature	1.13E-07	1	1.13E-07	12.5130	0.0123	significant

Table 4-2 ANOVA for selected factorial model for etch rate of MGC in HBr

Source	Sum of Squares	df	Mean Square	F Value	p-value	
Model	0.01308	1	0.013081	28.9522	0.0017	significant
B-duration	0.01566	1	0.015667	34.67674	0.0011	
Curvature	0.00429	1	0.004296	9.507459	0.0216	significant

Table 4-3 ANOVA for selected factorial model for etch rate of MGC in HCl

Source	Sum of Squares	df	Mean Square	F Value	p-value	
Model	0.00623	2	0.003	22.43	0.007	significant
B-duration	0.00603	1	0.006	43.40	0.003	
C-concentration	0.00008	1	0.000	0.56	0.497	
Curvature	0.00187	1	0.002	13.45	0.021	significant

Table 4-4 ANOVA for selected factorial model for etch rate of BN in H_3PO_4

Source	Sum of Squares	df	Mean Square	F Value	p-value	
Model	0.0034	1	0.0034	867.43	0.022	significant
B-duration	0.0039	1	0.0039	987.49	0.020	
Curvature	0.0008	1	0.0008	193.56	0.046	significant
Residual	0.0000	1	0.0000			

Table 4-5 ANOVA for selected factorial model for etch rate of BN in HBr

Source	Sum of Squares	df	Mean Square	F Value	p-value	
Model	0.002678	1	0.0027	69.98	0.004	significant
B-duration	0.003168	1	0.0032	82.77	0.003	
Curvature	0.000921	1	0.0009	24.07	0.016	significant
Residual	0.000115	3	0.0000			

Table 4-6 ANOVA for selected factorial model for etch rate of BN in HCl

Source	Sum of Squares	df	Mean Square	F Value	p-value	
Model	1.2005E-05	1	1.2E-05	0.0666192	0.8205	not significant
C-concentration	0.000012005	1	1.2E-05	0.0666192	0.8205	
Curvature	0.00372076	1	0.00372	20.647567	0.0452	significant
Residual	0.000360407	2	0.00018			

Table 4-7 ANOVA for selected factorial model for etch rate of SiC in H_3PO_4

Source	Sum of Squares	df	Mean Square	F Value	p-value	
Model	8.2E-08	1	8.2E-08	3.09	0.177	not significant
B-duration	1.7E-07	1	1.7E-07	6.25	0.088	
Curvature	2.9E-07	1	2.9E-07	10.72	0.047	significant
Residual	8.0E-08	3	2.7E-08			

Table 4-8 ANOVA for selected factorial model for etch rate of SiC in HBr

Source	Sum of Squares	df	Mean Square	F Value	p-value	
Model	1.068E-07	1	1E-07	63660000	< 0.0001	significant
C-concentration	6.000E-08	1	6E-08	63660000	< 0.0001	
Curvature	8.824E-08	1	9E-08	63660000	< 0.0001	significant
Residual	0.000E+00	3	0E+00			

Table 4-9 ANOVA for selected factorial model for etch rate of SiC in HCl

Source	Sum of Squares	df	Mean Square	F Value	p-value	
Model	6.1E-09	1	6.1E-09	1.84	0.308	not significant
B-duration	1.6E-07	1	1.6E-07	49.00	0.0198	
Curvature	1.8E-07	1	1.8E-07	52.56	0.0185	significant
Residual	6.7E-09	2	3.3E-09			

4.3 DEVELOPMENT OF SECOND ORDER ETCH RATE MODEL

As shown in the previous section, the etch rate of all materials in etchants studied was augmented to second-order model due to the significant curvature is observed in ANOVA. Thus, CCD was carried out with the collected data with different higher level model fitting. Each of these was checked at 95% confidence interval and p-value was used to determine the significance of the model fitting. It was found that all models fitted well with no lack of fit in all results. The main variables as mentioned earlier were determined by evaluating their p-value.

Table 4-10 shows the etch rate ANOVA for chemical machining of MGC. This process is fitted well to 2 factorial interaction (2FI) model. With 99.99% fitness, etching temperature and etchant are dominant variables, followed by interaction between etching temperature and etchant and etching duration. Equation (11)-(13) are the predictive model generated by DE 7 for etch rate in H_3PO_4, HBr and HCl.

Table 4-11 presents ANOVA for etch rate of BN. Etch rate of BN is fitted 99.98% to 2FI model with etchant as the dominant variable and followed by etching temperature. This is similar to the etch rate of MGC. The other significant variable is the interaction between the individual etchant and its concentration. Predictive models generated are as follows: equations (14)-(16) are chemical machining of BN in H_3PO_4, HBr and HCl respectively.

The etch rate of SiC was studied and ANOVA data is presented in Table 4-12. The result indicates that etching temperature is the most significant variable with 99.48% confidence and etchant with 95% confidence in the etch rate of SiC. Once again,

interaction between etchant and etchant's concentration appears to be an important variable. Equations (17)-(19) are etch rate's predictive models for SiC in etchants, namely H_3PO_4, HBr and HCl respectively.

Predictive model for MGC's etch rate in the respective etchant:

Etch rate in of MGC H_3PO_4 = -2.57E-4 - 4.30E-6(T) + 1.23E-6(t) + 1.32E-4(c) - 3.1E-8(T)(t) - 1.46E-6(T)(c) - 1.91E-7(t)(c) + 1.05E-7(T^2) + 2.25E-5(c^2) (eq. 4-1)

Etch rate of MGC in HBr = 4.032E-5 + 9.01E-7(T) - 6.79E-7(t) + 1.29E-4(c) - 1.49E-6(T)(c) - 1.91E-7(t)(c) +1.05E-7(T^2) + 2.25E-5(c^2) (eq. 4-2)

Etch rate of MGC in HCl = - 4.71E-5 - 6.45E-7(T) + 5.93E-5(c) - 1.49E-6(T)(c) - 1.91E-7(t)(c) + 1.052E-7(T^2) + 2.25E-5(c^2) (eq. 4-3)

Predictive model for BN's etch rate in respective etchant:

Etch rate of BN in H_3PO_4 = - 9.34E-4 + 4.59E-6(T) + 3.98E-6(t) - 7.88E-4(c) - 3.53E-8(T)(t) + 1.54E-6(T)(c) (eq. 4-4)

Etch rate of BN in HBr = - 1.807E-4 + 8.766E-6(T) + 1.89E-6(t) - 2.27E-4(c) - 3.53E-8(T)(t) + 1.54E-6(T)(c) + 1.38E-6(t)(c) (eq. 4-5)

Etch rate of BN in HCl= - 2.63E-4 + 9.88E-6(T) + 1.38E-6(t) - 2.38E-4(c) - 3.53E-8(T)(t) + 1.54E-6(T)(c) + 1.39E-6(t)(c) (eq. 4-6)

Predictive model for SiC's etch rate in the respective etchant:

Etch rate of SiC in H_3PO_4 = - 0.038 + 7.66E-4(T) - 2.76E-4(t) + 0.015(c) + 1.92E-8(T)(t) + 2.57E-6(T)(c) - 5.094E-4(t)(c) - 6.438E-6(T^2) + 2.9E-6(t^2) + 0.032(c^2) (eq. 4-7)

Etch rate of SiC in HBr = 0.0995 + 7.611E-4(T) - 1.296E-3(t) + 0.122(c) + 1.92E-8(T)(t) + 2.57E-6(T)(c) - 5.094E-4(t)(c) - 6.44E-6(T^2) + 2.92E-6(t^2) + 0.032(c^2) (eq. 4-8)

Etch rate of SiC in HCl = 0.0996 + 7.64E-4(T) - 1.297E-3(t) + 0.00122(c) + 1.92E-8(T)(t) + 2.57E-6(T)(c) - 5.096E-4(t)(c) - 6.44E-6(T^2) + 2.92E-6(t^2) + 0.032(c^2) (eq. 4-9)

Table 4-10 ANOVA for Response Surface 2FI Model for MGC

Source	Sum of Squares	df	Mean Square	F Value	p-value	
Model	4.81E-06	17	2.83E-07	12.93857	< 0.0001	Significant
A-temperature	2.05E-06	1	2.05E-06	93.6329	< 0.0001	
B-duration	1.33E-07	1	1.33E-07	6.06528	0.0192	
C-concentration	6.43E-09	1	6.43E-09	0.293934	0.5914	
D-etchant	1.04E-06	2	5.21E-07	23.82329	< 0.0001	
AB	3.87E-07	1	3.87E-07	17.69015	0.0002	
AD	2.39E-07	2	1.19E-07	5.460201	0.0089	
BD	2.19E-07	2	1.09E-07	4.999168	0.0127	
Residual	7.22E-07	33	2.19E-08			
Lack of Fit	6.05E-07	25	2.42E-08	1.652124	0.2354	not significant

Table 4-11 ANOVA for Response Surface 2FI Model for BN

Source	Sum of Squares	df	Mean Square	F Value	p-value	
Model	8.21E-06	14	5.87E-07	4.993748	0.0002	significant
A-temperature	6.42E-07	1	6.42E-07	5.466191	0.0274	
B-duration	2.09E-08	1	2.09E-08	0.177808	0.6767	
C-concentration	4.5E-08	1	4.5E-08	0.383452	0.5411	
D-etchant	3.51E-06	2	1.75E-06	14.92901	< 0.0001	
AB	4.38E-07	1	4.38E-07	3.727926	0.0645	
BC	4.07E-07	1	4.07E-07	3.461199	0.0742	
CD	1.06E-06	2	5.3E-07	4.512148	0.0208	
Residual	3.05E-06	26	1.17E-07			
Lack of Fit	3.04E-06	24	1.27E-07	16.38762	0.0591	not significant

Table 4-12 ANOVA for Response Surface Quadratic Model for SiC

Source	Sum of Squares	df	Mean Square	F Value	p-value	
Model	9.89E-05	17	5.81E-06	15.20579	< 0.0001	significant
A-temperature	4.09E-06	1	4.09E-06	10.6982	0.0052	
B-duration	1.31E-07	1	1.31E-07	0.342155	0.5673	
C-concentration	5.01E-07	1	5.01E-07	1.309221	0.2705	
D-etchant	2.98E-06	2	1.49E-06	3.897953	0.0433	
BD	7.19E-05	2	3.59E-05	93.95018	< 0.0001	
Residual	5.74E-06	15	3.82E-07			
Lack of Fit	8.62E-07	8	1.08E-07	0.154753	0.9913	not significant

4.4 ETCH RATE STUDIES

In general chemical machining process is dependent on the chemical reaction rate and diffusing rate of etchant molecules [170]. These two parameters are relatively sensitive to etching temperature and etching duration. However, in this experiment, diffusion is not a critical factor because all etchants' concentration was kept constant and condensation was applied in the setup of chemical machining, which would minimise the changes of concentration, especially at high temperature. Etch rate can be influenced by many independent variables and interactions between these variables. The aim of etch rate studies is to assess the influence of a number of physicochemical conditions on the quality of chemical machining. If etch rate is zero, it shows that no chemical reaction is happening between etchant and substrate or no chemical machining has occurred.

4.4.1 Effect of Etching Temperature

Temperature was found to be the most significant variable influencing etch rate in chemical machining of MGC, BN and SiC as demonstrated by ANOVA which shows that the influence of temperature is 99.99% significant in MGC, 97.3% in BN and 99.5% in SiC.

Figures 4-1, 4-2 and 4-3 show the profile of etch rate for MGC, BN and SiC respectively with temperature. Generally the etch rate increased with increase in the etching temperature. Tehrani and Imanian [8] reported that high temperature greatly increased the oxidizing power, which caused a rapid increase in the etch rate. Similarly, Makino et al. [56] found that the etch rates in all ceramic materials tested increased with increasing etching temperature. Significant faster etch rates at higher temperatures observed are typical, but less ideal etching behaviour is also common with more aggressive etch rate [85, 171]. However, for SiC the rate was observed to increase, but more sharply than MGC and BN to a peak of about 60^{o}C and then dropped dramatically thereafter. This phenomenon was not observed for MGC and BN at the range of temperature tested. Similar phenomenon has been observed and reported by Vartuli et al. [63] in the case of advanced ceramics wet etching that no etching was found at etching temperature up to 75^{o}C. The reason for this trend is not clear, but it seems to suggest that

the heat dependent etching of SiC may follow a different reaction mechanism from that of MGC and BN. The decline in the etch rate at higher temperature for SiC might be attributed to the accumulation of the etching product that could form as a barrier at the surface of the ceramic substrate thus limiting the etching reaction [8, 177].

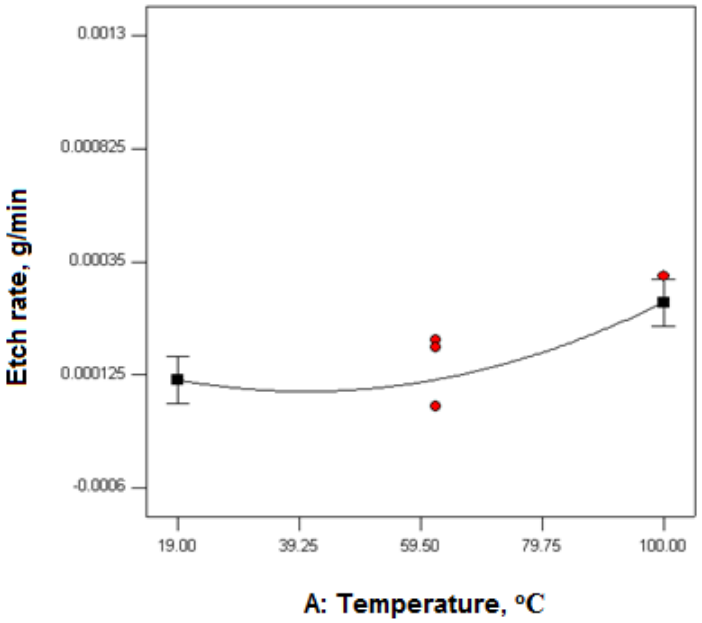

Figure 4-1 MGC etch rate (g/min) versus etching temperature (^{o}C)

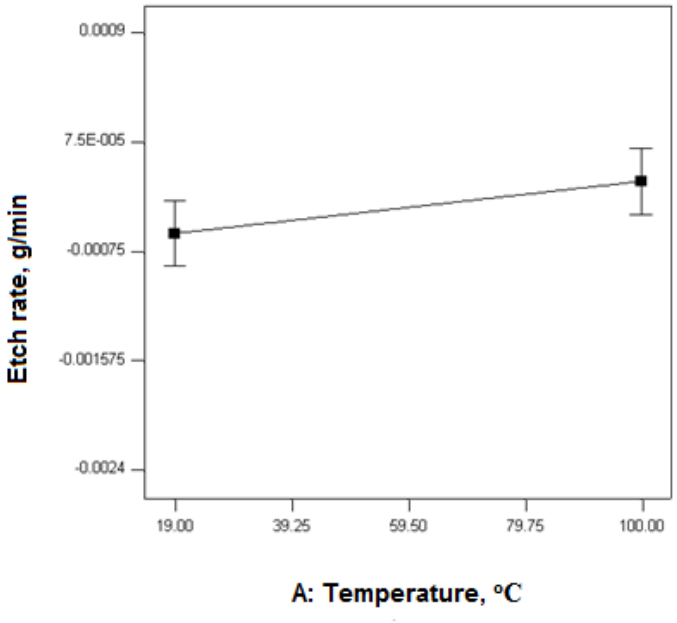

Figure 4-2 BN etch rate (g/min) versus etching temperature (^{o}C)

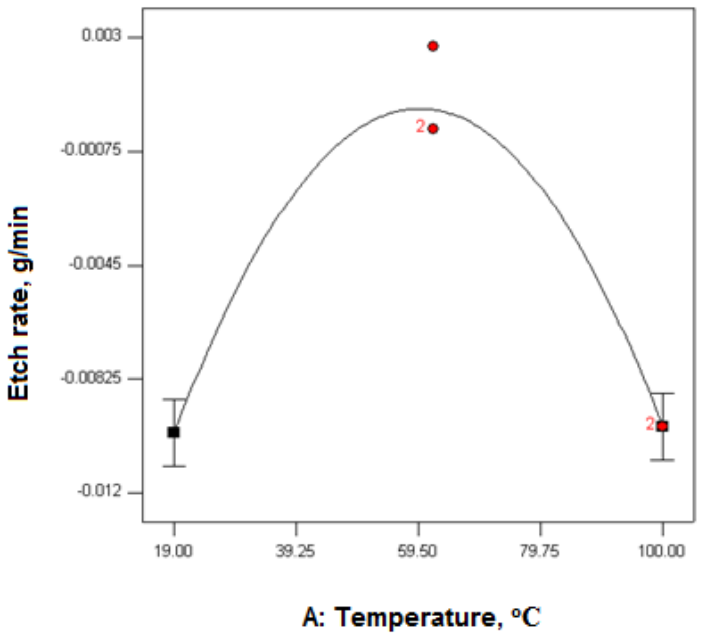

Figure 4-3 SiC etch rate (g/min) versus etching temperature (^{o}C)

The Arrhenius plots shown in Figures 4-4, 4-5, and 4-6, further confirm that etch rate shows strongly dependency on etching temperature and that a reaction-controlled etching process dominates. Thus it is necessary to employ reaction-limited etching in the manufacture of devices because it is relatively easy to control other variables in wet etching [172]. The changes of etch rate are due to the increase in the chemical reaction rate of etchants and frequency of molecules' collision with etching temperature. Arrhenius law stated that the rate of a chemical reaction increases exponentially with the absolute temperature [173]. It is well known that chemical machining processes are limited by either chemical machining reaction or by the diffusion rate of etchant molecules. Diffusion limited processes are relatively insensitive to temperature at lower activation energies and are usually encountered at high concentration [174]. Arrhenius law's equation is given as follows:

$$R = R_o \exp(-E_a/kT) \qquad \text{(eq. 4-10)}$$

where R is the etch rate, R_o is the pre-exponential variable, E_a is the activation energy, k is the Gasconstant (8.3145 J/mol K) and T is temperature. R_o is taken as the attempt

frequency for reaction between anion of etchant and materials' surfaces. E_a is the minimum amount of energy needed to activate molecules to a condition in which it is equally likely that they will undergo chemical reaction. This is listed in Table 4-13.

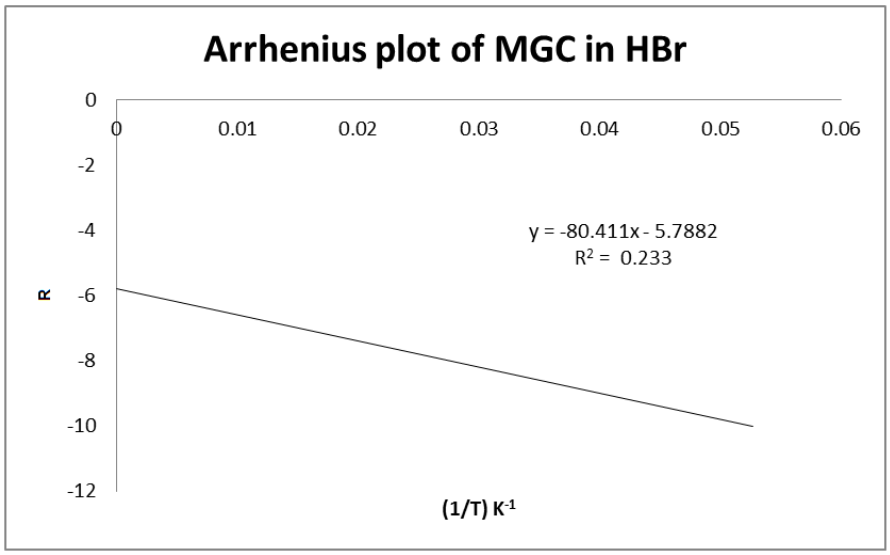

Figure 4-4 Arrhenius plot of MGC in HBr

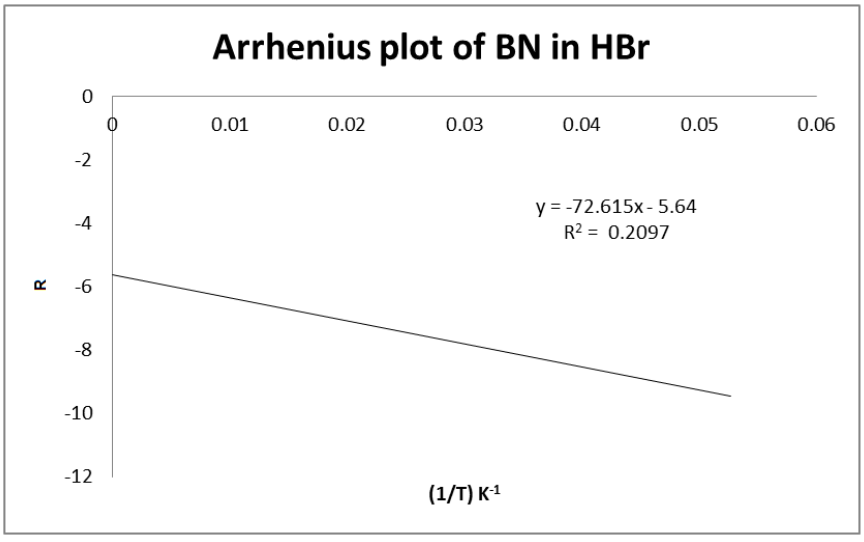

Figure 4-5 Arrhenius plot of BN in HBr

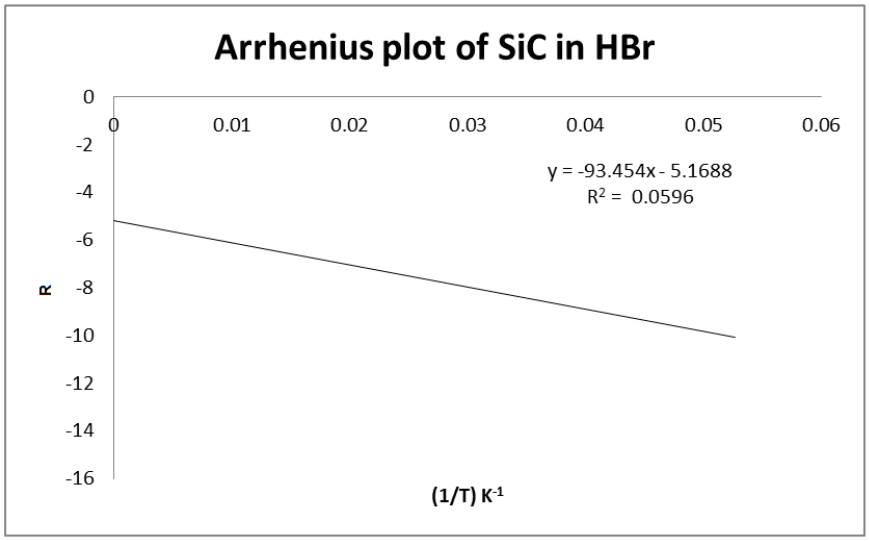

Figure 4-6 Arrhenius plot of SiC in HBr

Table 4-13. E_a value of Arrhenius plot (kJ/mol)			
	HCl	HBr	H_3PO_4
BN	0.1132	0.6037	0.00132
MGC	0.4592	0.6685	0.1329
SiC	0.4978	0.7769	0.1548

The results from the Arrhenius plots for MGC, BN and SiC indicate the etching process for the selected substrates with different etchants are temperature dependent. The different *E*a values obtained for the three substrates suggest that reaction mechanisms involved in the etching process with the individual etchant are different. Among the three substrates, BN exhibited the lowest E_a for all the etchants used and this is in agreement with the higher rate of etching observed for BN at 19.5^{o}C as compared to the others. It can be seen that etch rate of BN started at the fastest rate at 0.0075 g/min and with MGC at 0.000125 g/min and SiC at 0.0010 g/min. Another significant finding as shown in Table 4-13 is that among the three etchants used H_3PO_4 exhibited the lowest E_a value for the three respective substrates tested. This observation further supports the results obtained from the ANOVA analysis showing significant influence of temperature on the etching rate and the strong interactions between temperature and etchant variables. From

this study we can see that the choice of the etchant and the temperature that we use are important considerations prior to carrying out the chemical etching process.

4.4.2 Effect of Etchant

From the earlier study, the rate of etching has been shown to be temperature and etchant dependent. In this study the effect of the etchant on the rate of etching for MGC, BN and SiC was investigated with respective to medium concentration (10M for HCl etchant, 12M for H_3PO_4 etchant and 6M for HBr etchant) of etchant at 65^{o}C.

Table 4-14 shows the list of some chemical reactions taking place during etching of MGC with the etchants involved namely, HCl, HBr and H_3PO_4. Figures 4-7, 4-8 and 4-9 illustrate how the individual etchant affects the etching rate of MGC, BN and SiC. The highest etch rate of MGC was observed in HBr etchant, followed by the HCl and H_3PO_4. Similar trend was observed for the etch rate of BN, with the maximum etch rate at 0.00008g/min in HBr. For SiC, the respective etch rate in the three etchants used are similar. The results showed that HBr served as the best etchant for MGC and BN.

The different etching rate observed with different etchants is possibly attributed to their inherent reactivity toward the substrate. Simon et al. [71] tested four advanced ceramics in different etchants and found different etching properties exhibited in these materials. Three materials were well etched in molten-salt whereas one material performed better with electrolytic etching method. Substitution of Al_2O_3 for SiO_2 enhanced the leaching reaction of the alumino silicate glass with HF acid, resulting in an increase of etch rate [76]. The different chemical composition and structure of the substrates are other factors that are likely to influence the reaction mechanism and reactivity of the etchants involved. The different E_a values obtained for the different etchants in the earlier study seem to support this idea, although more detail kinetic studies are warranted to establish the mechanisms involved.

Table 4-14 Chemical reactions taking place in HCl, HBr and H_3PO_4.

Material		HCl	HBr	H_3PO_4
MGC	SiO_2	$SiO_2 + HCl \rightarrow SiCl_4 + 2H_2O$	$SiO_2 + HBr \rightarrow SiBr4 + 2H_2O$	$3SiO_2 + 4H_3PO_4 \rightarrow Si_3(PO_4)_4 + 6H_2O$
	B_2O_3	$B_2O_3 + HCl \rightarrow 2BaCl_3 + 3H_2O$	$B_2O_3 + HBr \rightarrow 2BaBr_3 + 3H_2O$	$B_2O_3 + 2\ H_3PO_4 \rightarrow 2BPO_4 + 3H_2O$
	Al_2O_3	$Al_2O_3 + HCl \rightarrow 2AlCl_3 + 3H_2O$	$Al_2O_3 + HBr \rightarrow 2AlBr_3 + 3H_2O$	$Al_2O_3 + H_3PO_4 \rightarrow 3AlPO_3 + 3H_2O$
	K_2O	$K_2O + 2HCl \rightarrow KCl_2 + H_2O$	$K_2O + 2HBr \rightarrow KBr_2 + H_2O$	$3K_2O + 2H_3PO_4 \rightarrow 2K_2PO_3 + H_2O$
BN	BN	Information on reactions for BN and SiC is not available.		
SiC	SiC			

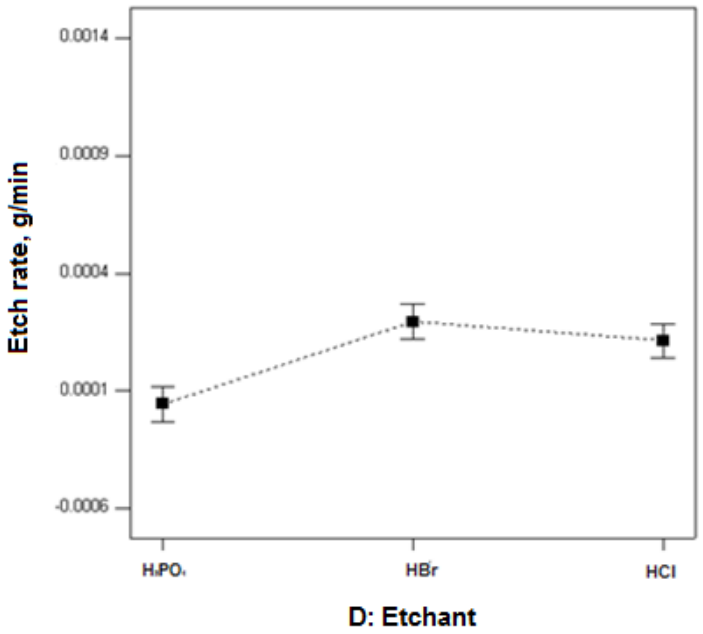

Figure 4-7 MGC etch rate (g/min) versus etchant

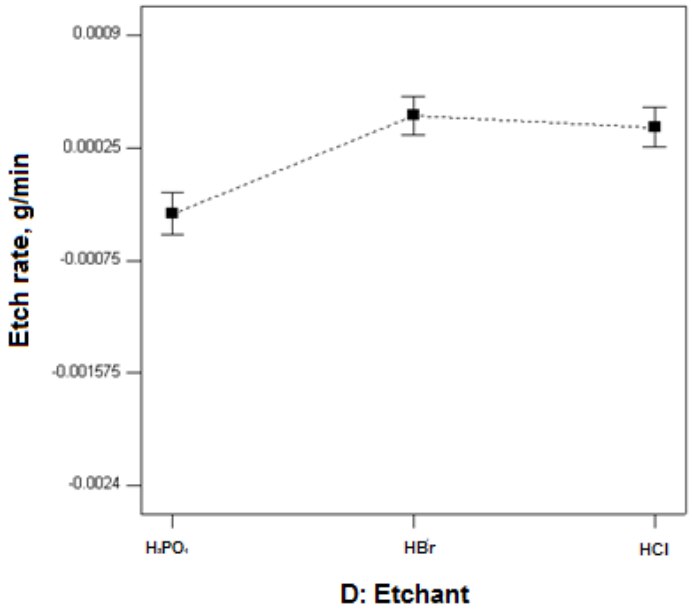

Figure 4-8 BN etch rate (g/min) versus etchant

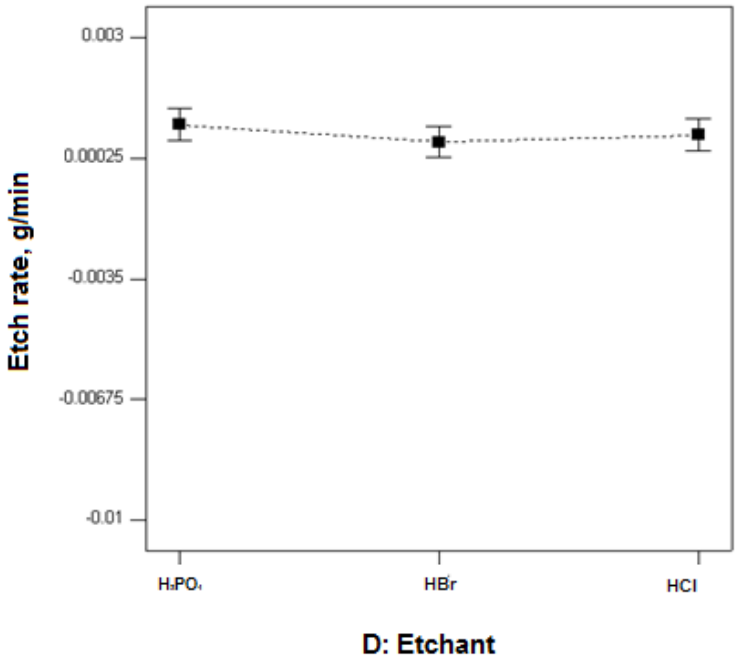

Figure 4-9 SiC etch rate (g/min) versus etchant

4.4.3 Effect of Etching Duration

Etching duration appears to be a significant variable in MGC etch rate from the initial ANOVA analysis. Figure 4-10 shows the profile of the etch rate against the duration of etching. In the early stage of etching, etch rates did not show any significant increase until a period of about 2 hours. Hirota et al found that increase of etch rate was proportional to the etching duration [175]. Peng et al. [172] found that etch rate of machinable glass ceramics was decreased slightly at the beginning of the process and the result become stable after an extended duration. This indicates that an induction time might be necessary for etching to go through the diffusion barrier as reported. [56, 61, 176] . This observation seems to be consistent with the notion that at longer etching duration, more reactions are taking place with less disruption due to greater extent of dissociation of acid. More comprehensive studies are required to established this notion.[98]. However, under certain condition, prolonged etching duration might cause damage on the material surface and increase materials' surface roughness [85, 98]. Besides temperature and etchant, the etching duration is worth considering in order improving quality of chemical etching.

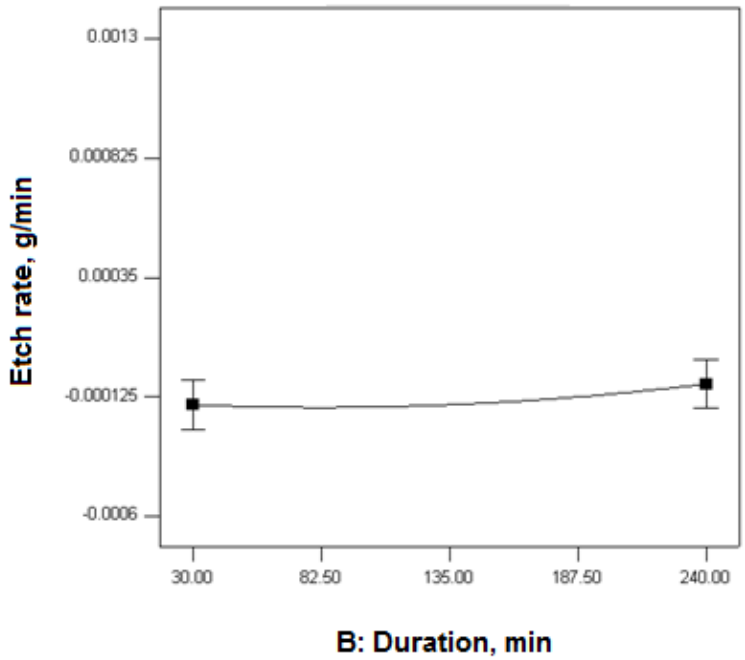

Figure 4-10 MGC etch rate (g/min) versus etching duration (min)

4.4.4 Effect of Etchant's Concentration

In Tables 4-10, 4-11 and 4-12, etchant's concentration appears to be the least significant variables for all substrate as the *p*-values are more than 0.05. With 95% confident interval, the *p*-value of variables have to be less than 0.05 to become significant. This is explained earlier, which means that 95% of the time the interval will contain the true parameter value. As shown in Figure 4-10, the changes of etch rate in MGC is relatively small compared to the other substrates. The non-significance of etchant's concentration can be due to condensation that is applied in the chemical machining setup, which reduces the changes of etchant's concentration, especially at high temperature. Besides, reactivity of the etchant toward the substrate and nature of the reaction mechanism involved could contribute to the etchant's concentration being the least affected variable in etch rate.

In contrast to MGC, the etch rate of BN and SiC decreased dramatically with increased etchant's concentration as shown in Figures 4-12 and 4-13. It is not clear what causes the rate of etching to fall when the concentration of the etchant is increased. One possibility is that an increase in the etchant concentration could reduce the ionisation of the etchant resulting in a lower concentration of the H^+ ions that are essential for the etching process. Noor et al. [177] found the etch rate of silicon decreased with increased etchant's concentration. Cakir et al. [60] also found that high etchant's concentration also decreased etch rate of studied chemical machining of Cu-ETP copper. Kendall and Shoultz reported that higher concentration of KOH reduced the etching rate of Si based on the following rate equation that they developed [178].

$$R_{100} = (2.6\text{x}10^{6})(W^{2.5})\exp\text{-}(W/300+0.48)/k^{*}(\text{T}+273)\ [\mu\text{m/hr}] \qquad \text{(eq. 4-11)}$$

where R is the etch rate, W is the actual concentration of KOH (wt%) in water, k is Boltzmann's contant $8.617\text{x}10^{-5}$ eV/K and T is the temperature in ^{o}C. This observation is reflected in Figure 4-14.

Further studies are required to develop a kinetic model for the etching reaction of BN and SiC in order to understand how changes of the etchant's concentration affect the rate of etching.

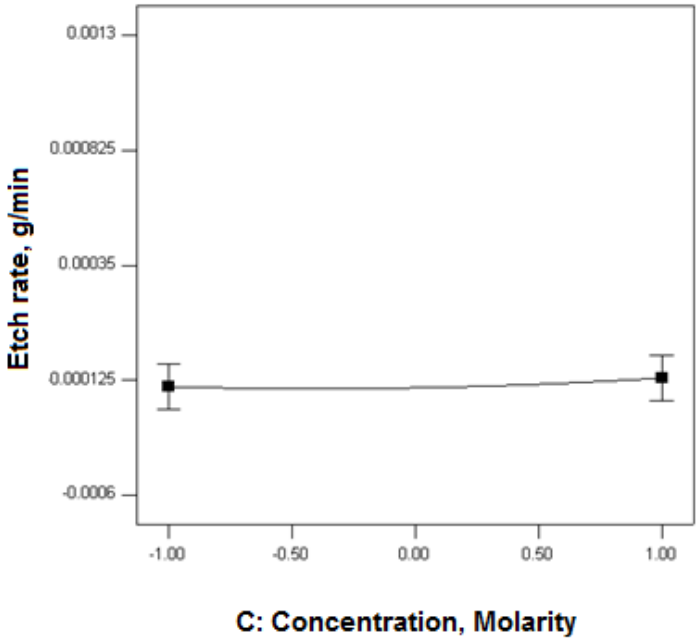

Figure 4-11 MGC etch rate (g/min) versus etchants' concentration (Molarity)

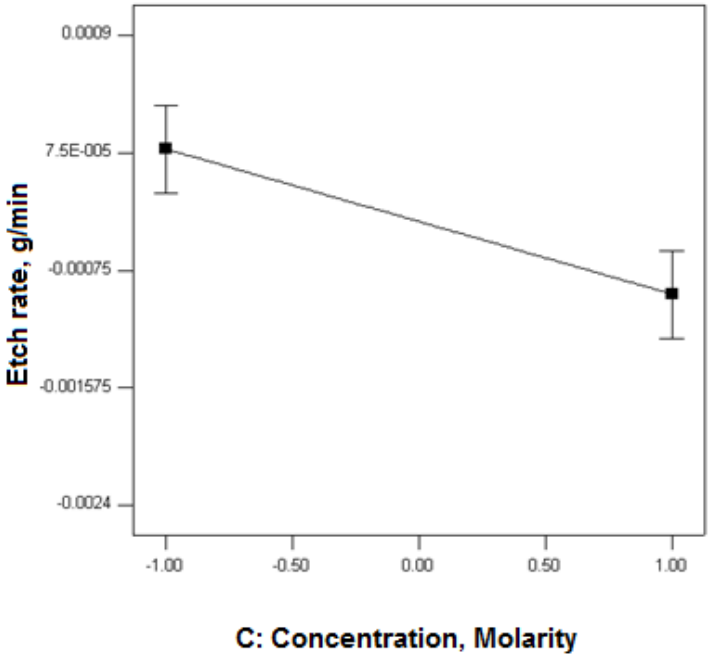

Figure 4-12 BN etch rate (g/min) versus etchants' concentration (Molarity)

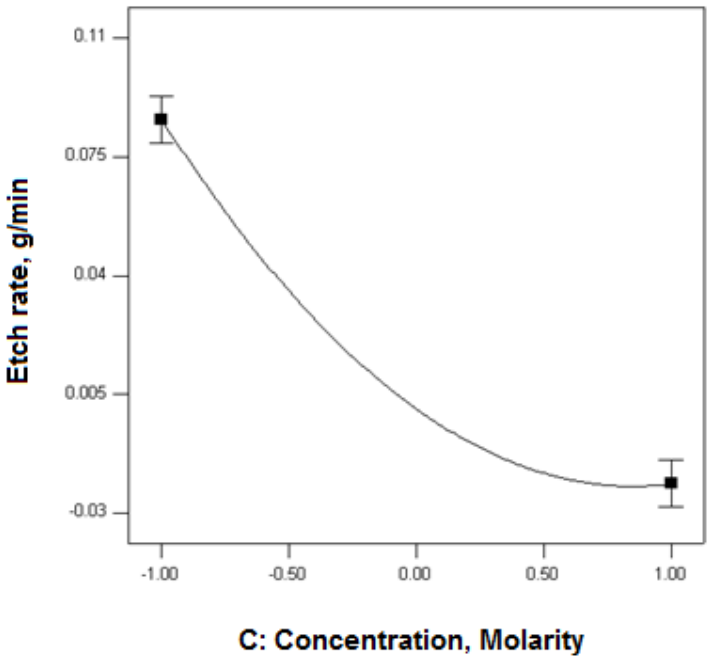

Figure 4-13 SiC etch rate (g/min) versus etchants' concentration (Molarity)

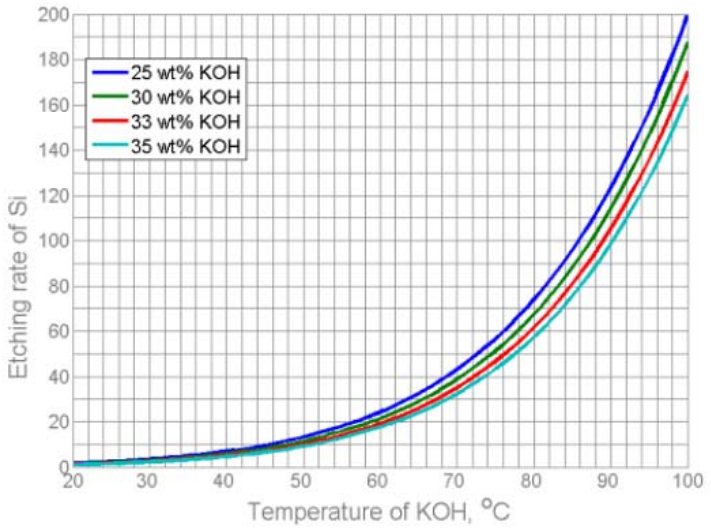

Figure 4-14 Etch rate of silicon in KOH for different concentration and temperatures [178].

4.5 CONCLUSION

From the results obtained we are able to conclude that etch rate was influenced by etching temperature and etchant used for the selected materials. In MGC, etch rate was also influenced by the etching duration. For SiC, the etch rate shows dependency on the on both the etching duration and individual etchant involved. Results also showed that etch rate increased with the increase of etching temperature for MGC and BN with exception of SiC was obtained. MGC and BN show the best result while etching in HBr etchant; and, SiC's best etch rate occurred in H_3PO_4 etchant. The difference etch rate was observed for the substrates suggests that the reaction mechanism involved for the individual etching process could be different, however further kinetic data are required to support this notion. Additionally, the findings confirm that selection of the right etchant for specific substrate is important in achieving the best etching result.

Chapter 5 Development of Surface Roughness Models and Experimental Studies

5.1 INTRODUCTION

Surface roughness is an important measurement in chemical machining. It affects the mechanical properties (friction and wear) of substrates and therefore, it would have significant impact on substrate application, notably on the substrate bonding. The mechanism of direct substrate bonding at room temperature has been attributed to the short range intermolecular and interatomic attraction forces, such as Van de Waals forces. High surface roughness will result in small real area of contact, and therefore yield voids at the bonding interface. When the surface roughness exceeds a critical value, the substrates will not bond at all.

In this study, surface roughness (R_a) was measured in nm by AFM before and after the CHM process. The measurement assessed the improvement of surface roughness after the chemical machining process. Thus, the value obtained either is negative (the surface roughness getting poorer after chemical machining) or positive (the surface roughness getting better after the chemical machining). Consequently, the higher the positive value of surface roughness, the better it is. Analytical study of surface roughness is similar to etch rate, where its first and second order models were developed with DE 7. This is followed by surface roughness studies, where the relationships between surface roughness and variables such as etching temperature was assessed as well as their influence on the surface roughness was investigated.

The present study mainly focused on the micro-patterning method, which is used to replace mask patterning. AFM is used because this tool functions by measuring a local property such as height, optical absorption or magnetism and is equipped with a probe or tip placed very close to the sample. Also, it is possible to take measurement over a small area as the substrates used in this study which is only 10 mm cube. AFM operates by measuring the attractive or repulsive forces between a tip and the sample. In its repulsive contact mode, the instrument lightly touches a tip at the end of cantilever to the sample. As a raster-scan drags the tip over the sample, the detection apparatus measures the vertical deflection of the cantilever, which indicates the local sample height. The, R_a value obtained is a measure of the surface roughness of substrates. The lower R_a value indicates a better surface quality. Although SEM can provide information on the surface topography, grain distribution and size, it is not able to determine and analyse the surface roughness of the etched materials.

5.2 DEVELOPMENT OF FIRST ORDER SURFACE ROUGHNESS MODEL

First order models for surface roughness are presented in Tables 5-1, 5-2 and 5-3 for MGC in H_3PO_4, HBr and HCl respectively; Tables 5-4, 5-5, 5-6 for BN in H_3PO_4, HBr and HCl respectively; and Tables 5-7, 5-8, 5-9 for SiC in H_3PO_4, HBr and HCl respectively. The curvature term for each test is significant as shown in the tables below, which means that chemical etching of MGC, BN and SiC has to proceed to CCD for analysis.

Table 5-1 ANOVA for selected factorial model for surfce roughness of MGC in H_3PO_4

Source	Sum of Squares	df	Mean Square	F Value	*p*-value	
Model	23689.41	1	23689.41	17.22	0.0089	significant
B-duration	29447.14	1	29447.14	21.40	0.0057	
Curvature	12597.04	1	12597.04	9.15	0.0292	significant
Residual	6880.31	5	1376.06			
Lack of Fit	6880.31	4	1720.08			

Table 5-2 ANOVA for selected factorial model for surface roughness of MGC in HBr

Source	Sum of Squares	df	Mean Square	F Value	*p*-value	
Model	8523.5	1	8523.5	22.72	0.00	significant
C-concentration	7727.5	1	7727.5	20.59	0.00	
Curvature	2201.5	1	2201.5	5.87	0.04	significant
Residual	3001.8	8	375.2			
Lack of Fit	3001.8	7	428.8			

Table 5-3 ANOVA for selected factorial model for surface roughness of MGC in HCl

Source	Sum of Squares	df	Mean Square	F Value	*p*-value	
Model	5386.9	1	5386.9	28.71	0.00	significant
C-concentration	6033.9	1	6033.9	32.16	0.00	
Curvature	1528.5	1	1528.5	8.15	0.04	significant
Residual	938.1	5	187.6			
Lack of Fit	938.1	4	234.5			

Table 5-4 ANOVA for selected factorial model for surface roughness of BN in H_3PO_4

Source	Sum of Squares	df	Mean Square	F Value	*p*-value	
Model	5101.81	1	5101.81	7.63	0.0328	significant
B-duration	7206.30	1	7206.30	10.78	0.0168	
Curvature	4369.57	1	4369.57	6.53	0.0431	significant
Residual	4012.44	6	668.74			
Lack of Fit	4012.44	5	802.49			

Table 5-5 ANOVA for selected factorial model for surface roughness of BN in HBr

Source	Sum of Squares	df	Mean Square	F Value	*p*-value	
Model	92309.5	1	92309	39.1	0.00	significant
B-duration	78572.8	1	78573	33.2	0.00	
Curvature	14258.3	1	14258	6.0	0.04	significant
Residual	18906.8	8	2363			
Lack of Fit	18906.8	7	2701			

Table 5-6 ANOVA for selected factorial model for surface roughness of BN in HCl

Source	Sum of Squares	df	Mean Square	F Value	*p*-value	
Model	76429.29	1	76429	149.48	< 0.0001	significant
B-duration	78364.46	1	78364	153.27	< 0.0001	
Curvature	10804.01	1	10804	21.13	0.0059	significant
Residual	2556.49	5	511			
Lack of Fit	2556.49	4	639			

Table 5-7 ANOVA for selected factorial model for surface roughness of SiC in H_3PO_4

Source	Sum of Squares	df	Mean Square	F Value	p-value	
Model	1637.00	1	1637.00	143.85	0.0012	significant
B-duration	1341.34	1	1341.34	117.87	0.0017	
Curvature	117.37	1	117.37	10.31	0.0489	significant
Residual	34.14	3	11.38			
Lack of Fit	34.14	2	17.07			

Table 5-8 ANOVA for selected factorial model for surface roughness of SiC in HBr

Source	Sum of Squares	df	Mean Square	F Value	p-value	
Model	3790.00	1	3790.00	245.819	< 0.0001	significant
B-duration	3460.56	1	3460.56	224.452	0.0001	
Curvature	155.36	1	155.36	10.077	0.0337	significant
Residual	61.67	4	15.42			

Table 5-9 ANOVA for selected factorial model for surface roughness of SiC in HCl

Source	Sum of Squares	df	Mean Square	F Value	p-value	
Model	114.71	1	114.7	9.41	0.037	significant
C-concentration	114.71	1	114.7	9.41	0.037	
Curvature	868.86	1	868.9	71.26	0.001	significant
Residual	48.77	4	12.2			
Lack of Fit	48.77	3	16.3			

5.3 DEVELOPMENT OF SECOND ORDER SURFACE ROUGHNESS MODEL

The second-order surface roughness model is required because all the models did not fit to the linear model in first-order analysis. In surface roughness analysis, data was obtained by inspecting the surface roughness under AFM with power of 5μm. The values of surface roughness before and after were marked and the reduction of surface roughness was noted and analyzed. Thus, the higher the reduced surface roughness is, the better the surface roughness after etching process.

Tables 5-10, 5-11, 5-12 represent ANOVA data for the reduced surface roughness for MGC, BN and HCl respectively. Each of them shows different behaviour and responses with different significant factors. Yet, all models fitted well without any lack of fit. Equations (21)-(29) are predictive models for reduced surface roughness of MGC, BN and SiC when treated with H_3PO_4, HBr and HCl respectively. Temperature was found to be the most critical factor in reducing surface roughness of MGC and BN, but for BN and SiC, the type of etchant is crucial in determining the quality of the surface roughness. The other important factors include the interaction between etchant and its concentration for MGC and SiC, interaction between etching temperature and duration, etchant and its concentration for BN and SiC respectively and etching duration for SiC.

Predictive models for surface roughness of MGC in the respective etchant are as follows:

Reduced surface roughness of MGC in H_3PO_4 = - 69.95 + 0.803(T) + 0.095(d) - 11.9(c) + 4.71E-3(T)(t) - 0.41(T)(c) - 0.395(t)(c) (eq. 5-1)

Reduced surface roughness of MGC in HBr = 74 - 0.759(T) - 0.286(t) + 89.8(c) - 0.405(T)(c) + 4.71E-3(T)(t) - 0.395(t)(c) (eq. 5-2)

Reduced surface roughness of MGC in HCl = - 5.005 + 0.323(T) - 0.235(t) + 119.22(c) + 4.706E-3(T)(t) - 0.405(T)(c) - 0.395(t)(c) (eq. 5-3)

Predictive models for surface roughness of BN in the respective etchant are as follows:

Reduced surface roughness of BN in H_3PO_4 = 14.76 - 0.53(T) - 0.069(t) - 6.54(c) + 2.12E-4(T)(t) + 0.19(T)(c) + 0.028(t)(c) + 9.35E-3(T^2) - 1.46E-3(t^3) + 2.59(c^2) - 0.69(c^3) - 2.39E-4(T)(t)(c) - 4.96E-5(T^2)(t) - 1.89E-6(t^3) - 5.82E-4(T^2)(c) + 5.07E-5(T)(t^2) - 0.098(T)(c^2) -2.82E-4(t^2)(c) + 0.043(t)(c^2) -3.41E-5(T^3) (eq. 5-4)

Reduced surface roughness of BN in HBr = 7.803 - 0.698(T) + 0.21(t) - 8.27(c) - 8.79E-4(T)(t) + 0.223(T)(c) + 0.011(t)(c) + 0.011(T^2) - 2.55E-3(t^2) + 3.95(c^2) - 1.89E-6(t^3) - 2.39E-4(T)(t)(c) - 4.9E-5(T^2)(t) - 5.82E-4(T^2)(c) + 5.07E-5(T)(t^2) - 0.69(c^3) - 0.098(T)(c^2) - 3.41E-5(T^3) - 2.82E-4(t^2)(c) +0.04(t)(c^2) (eq. 5-5)

Reduced surface roughness of BN in HCl = 11.20 - 0.83(T) + 0.29(t) - 3.31(c) - 3.41E-5(T^3) -9.99E-4(T)(t) + 0.113(T)(c) + 0.049(t)(c) + 0.012(T^2) - 2.93E-3(t^2) + 0.73(c^2) - 1.89E-6(t^3) - 2.39E-4(T)(t)(c) - 4.96E-5(T^2)(t) - 0.69(c^3) - 5.82E-4(T^2)(c) + 5.07E-5(T)(t^2) - 0.098(T)(c^2) - 2.8E-4(t^2)(c) +0.04(t)(ct^2) (eq. 5-6)

Predictive models for surface roughness of SiC in the respective etchant are as follows:

Reduced surface roughness of SiC in H_3PO_4 = 886.76 - 45.95(T) - 16.1(t) - 43.05(c) + 0.28(T)(t) - 0.66(T)(c) - 3.81(t)(c) + 0.69(T^2) + 0.1(t^2) + 12.07(c^2) + 2.62E-3(T)(t)(c) - 2.21E-3(T^2)(t) + 0.015(T^2)(c) - 8.62E-5(T)(t^2) - 2.79(T)(c^2) + 0.0165(t^2)(c) + 1.42(t)(c^2) - 2.822E-3(T^3) - 2.89E-4(t^3) + 76.54(c^3) (eq. 5-7)

Reduced surface roughness of SiC in HBr = 946.2 - 47.46(T) - 17.47(t) + 183.24(c) + 0.29(T)(t) - 1.043(T)(c) - 4.56(t)(c) + 0.698(T^2) + 0.11(t^2) - 36.54(c^2) - 2.21E-3(T^2)(t) + 2.63E-3(T)(t)(c) + 0.015(T^2)(c) - 8.62E-5(T)(t^2) - 2.79(T)(c^2) + 0.0165(t^2)(c) + 1.42(t)(c^2) - 2.823E-3(T^3) - 2.89E-4(t^3) + 76.54(c^3) (eq. 5-8)

Reduced surface roughness of SiC in HCl = 345.12 - 25.93(T) - 19.66(t) - 152.87(c) + 0.259(T)(t) + 0.034(T)(c) - 3.25(t)(c) + 0.55(T^2) + 0.15(t^2) + 118.98(c^2) - 2.21E-3(T^2)(t) + 2.63E-3(T)(t)(c) + .015(T^2)(c) - 8.62E-5(T)(t^2) - 2.79(T)(c^2) + 0.016(t^2)(c) + 1.42(t)(c^2) - 2.82E-3(T^3) - 2.89E-4(t^3) + 76.54(c^3) (eq. 5-9)

Table 5-10 ANOVA for Response Surface 2FI Model for MGC

Source	Sum of Squares	df	Mean Square	F Value	*p*-value	
Model	121552.4	14	8682.3	2.5557	0.0168	significant
A-temperature	17775.5	1	17775.5	5.2324	0.0299	
B-duration	1844.5	1	1844.5	0.5429	0.4673	
C-concentration	4242.8	1	4242.8	1.2489	0.2733	
D-etchant	4137.2	2	2068.6	0.6089	0.5510	
CD	83076.7	2	41538.3	12.227	0.0002	
Residual	95121.2	28	3397.1			
Lack of Fit	46332.5	24	1930.5	0.1582	0.9987	not significant

Table 5-11 ANOVA for Response Surface Cubic Model for BN

Source	Sum of Squares	df	Mean Square	F Value	*p*-value	
Model	97.504	39	2.5001	6.5717	0.0002	significant
A-temperature	9.248	1	9.2486	24.310	0.0002	
B-duration	1.1819	1	1.1819	3.1069	0.0998	
C-concentration	0.5380	1	0.5380	1.4142	0.2541	
E-etchant	4.8290	2	2.4145	6.3467	0.0109	
AD	4.7197	2	2.3598	6.2032	0.0118	
BD	11.3842	2	5.6921	14.962	0.0003	
CD	0.4958	2	0.2479	0.651	0.5363	
Residual	5.3260	14	0.3804			
Lack of Fit	0.5797	3	0.1932	0.447	0.7238	not significant

Table 5-12 ANOVA for Response Surface Quadratic Model for SiC

Source	Sum of Squares	df	Mean Square	F Value	*p*-value	
Model	169781	39	4353.358	7.776016	0.008	significant
A-temperature	1096.908	1	1096.908	1.95931	0.2111	
B-duration	10337.54	1	10337.54	18.46504	0.0051	
C-concentration	656.899	1	656.899	1.17336	0.3203	
D-etchant	7486.236	2	3743.118	6.685999	0.0297	
AD	14103.91	2	7051.955	12.59628	0.0071	
CD	18305.84	2	9152.921	16.34905	0.0037	
Residual	3359.065	6	559.8442			
Lack of Fit	741.5918	4	185.3979	0.141662	0.9513	not significant

5.4 SURFACE ROUGHNESS STUDIES

Advanced ceramic plays an important role in semiconductor industries. As nano-implantation is required in the semiconductor industry, material surface roughness after machining is one of the key issues because rough surface will affect the performance of the end product. Thus, lower surface roughness is required. Poor surface roughness is often caused by extremely high etching rate [151]. The aim of surface roughness study is to investigate relationship between surface roughness and selected variables and also to obtain better quality of surface roughness at faster rate of etching.

5.4.1 Effect of Etching Temperature

The selection of etching temperature is important in achieving quality surface finish. In industrial application of chemical etching, highest temperature is used to machine the substrate because of the better surface roughness that is produced [60].

In our present study, etching temperature was found to significantly influence the surface roughness of MGC and BN. As shown in Figures 5-1, 5-2 and 5-3, reduction of surface roughness for MGC, BN and SiC was increased with etching temperature. Reduction of surface roughness takes place mainly due to the chemical reaction at the desired surface area [76, 77]. This phenomenon is similar to etching rate in all materials where it increases with rising etching temperature. For MGC and BN (Figures 5-1 and 5-2), better surface roughness is obtained at a higher temperature while the best surface roughness of SiC was obtained at 80°C (Figure 5-3). However, above this temperature, the surface roughness increased and it is considered to be over-etched. This might be due to the higher rate of dissociation of etchant into its anions and cation as discussed in Chapter 4, which created a protective layer at the etching surface and thus hindering the etching reaction [61].

Generally, a positive reduced surface roughness was observed when temperature was increased. Figure 5-4 (a)-(e) are AFM images of MGC in 5M HBr for 180 minutes at different temperatures. Reduced surface roughness is around -17nm at 19^{o}C, 30 nm at 65^{o}C and 77.5 nm at 100^{o}C. For BN and SiC, a quadratic trend was obtained with a peak

point of reduced surface roughness, but the roughness increased after 80^{o}C. Figures 5-5 (a)-(e) are AFM images of BN and SiC in 7.5M of HBr for 75 minutes, and Figures 5-6 (a)-(e) in 6M of HBr for 180 minutes at different etching temperature. The reduced surface roughness of BN at 19 ^{o}C is around -10nm, 1.7 nm at 65^{o}C, and 3.5nm at 100^{o}C. The reduced surface roughness of SiC is 126nm at 19 ^{o}C, 151 nm at 65^{o}C and 96 nm at 100^{o}C.

Etching temperature has also been found to significantly influence the degree of transformation of the surface [179]. More extensive etching is expected to occur at higher temperature due to the increasing rate of etchant dissociation with temperature. However, higher etching temperature does not necessarily produce better quality surface roughness. Poor surface roughness is reported at higher etching temperature [179, 180]. They found that all the treated surfaces were rougher than that of the untreated surface [60]. As temperature of etch increased near to boiling point, roughness values increased to about 15nm Ry due to preferential etching of the grain boundary areas [56].

However, several researchers found that the lower surface roughness was obtained at the beginning of the process and increased after certain etching temperature. Jardiel et al. found that increasing temperature up to 50^{o}C improves etching and new grain boundaries and other structures are clearly observed [74]. Platelets show sharp boundaries instead of rounded ones observed in the thermally etched samples.

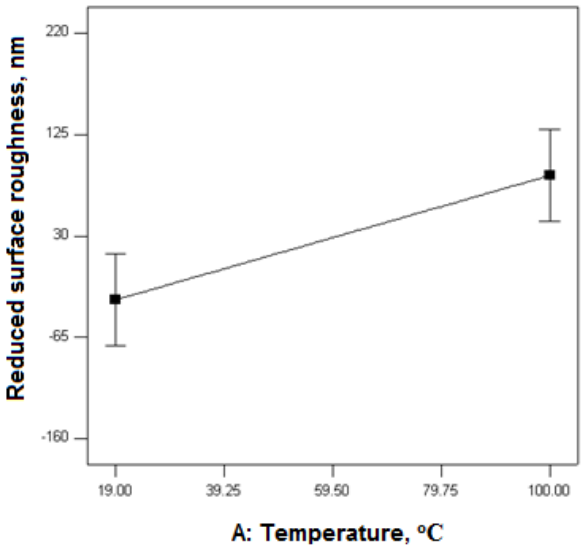

Figure 5-1 MGC reduced surface roughness (nm) with etching temperature (^{o}C)

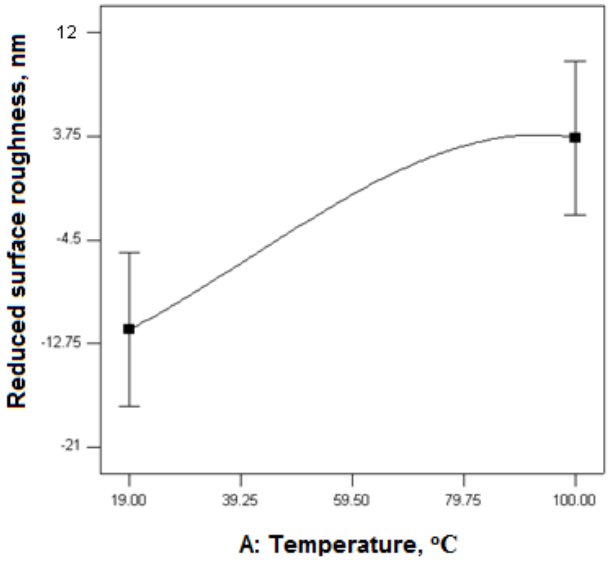

Figure 5-2 BN reduced surface roughness (nm) versus etching temperature (^{o}C)

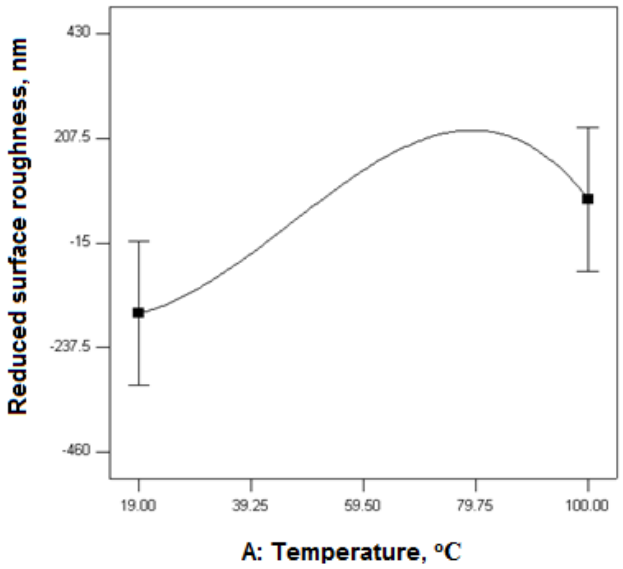

Figure 5-3 SiC reduced surface roughness (nm) versus etching temperature (^{o}C)

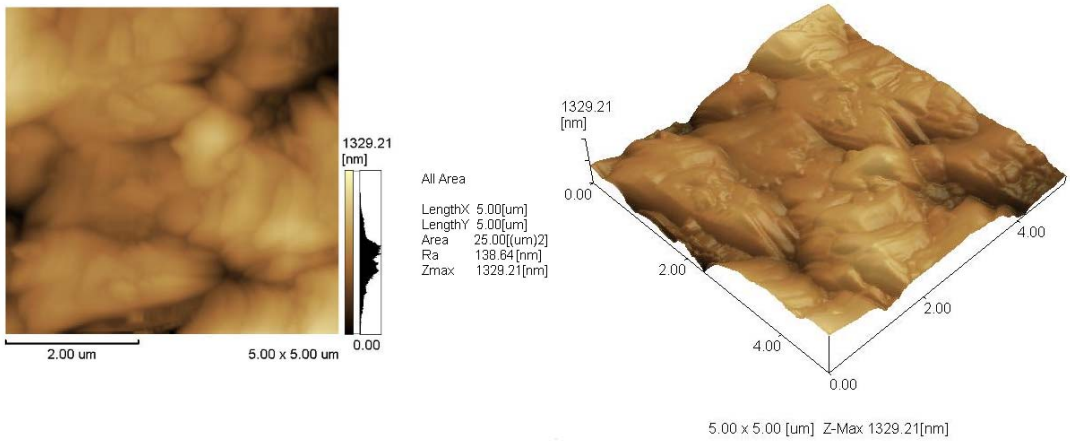

Figure 5-4 (a) AFM images of MGC before etching in 5M HBr for 180 minutes in 19^{o}C, R_a = 138.64nm

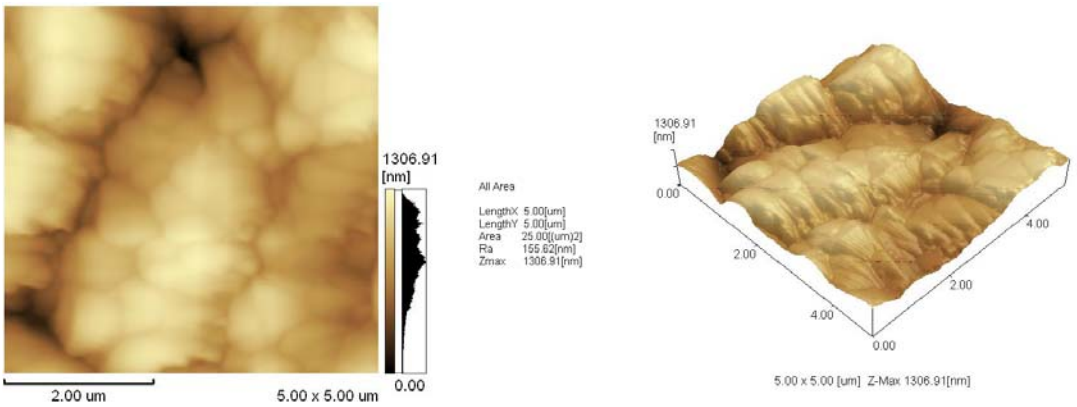

Figure 5-4 (b) AFM images of MGC after etching in 5M HBr for 180 minutes in 19°C, R_a = 155.62nm

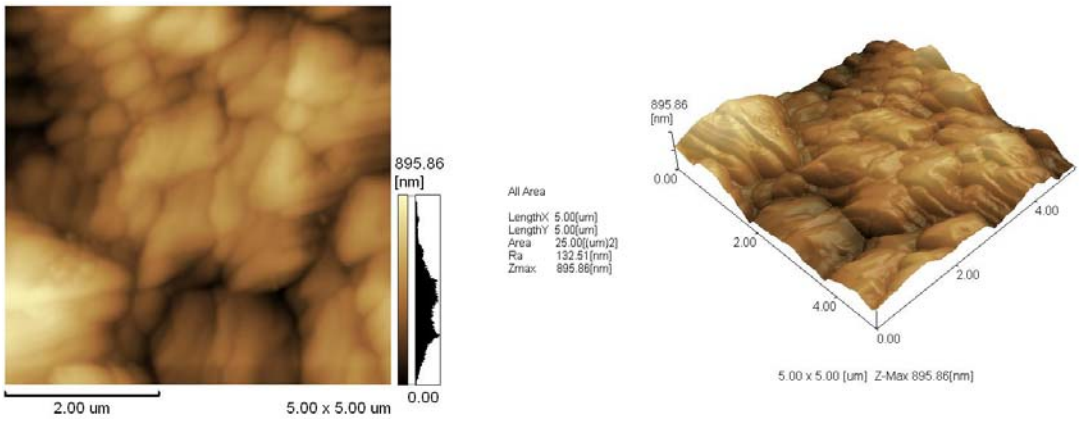

Figure 5-4 (c) AFM images of MGC before etching in 5M HBr for 180 minutes in 65°C, R_a = 132.51nm

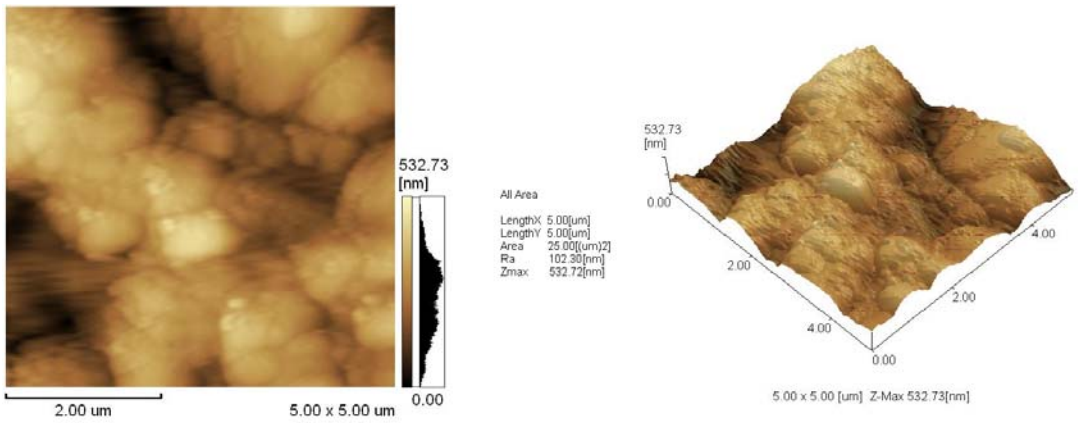

Figure 5-4 (d) AFM images of MGC after etching in 5M HBr for 180 minutes in 65°C, R_a= 102.30nm

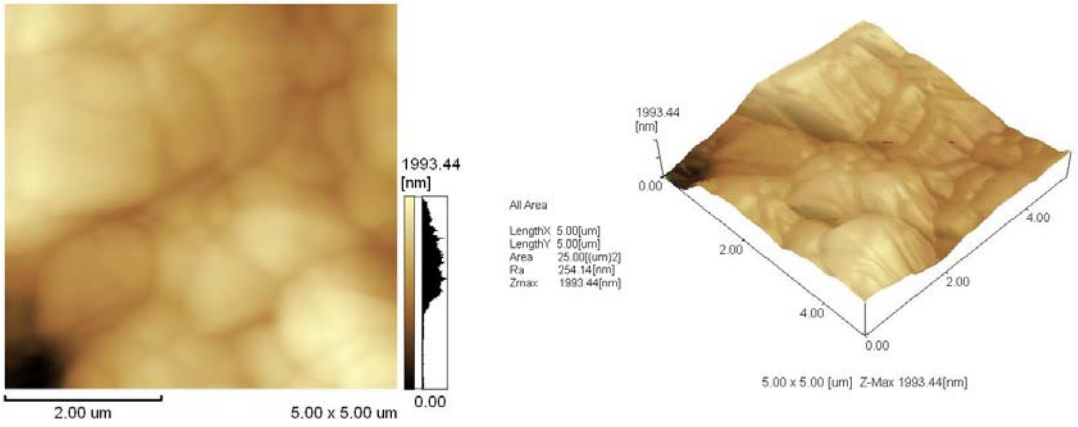

Figure 5-4 (e) AFM images of MGC before etching in 5M HBr for 180 minutes in 100°C, R_a = 254.14nm

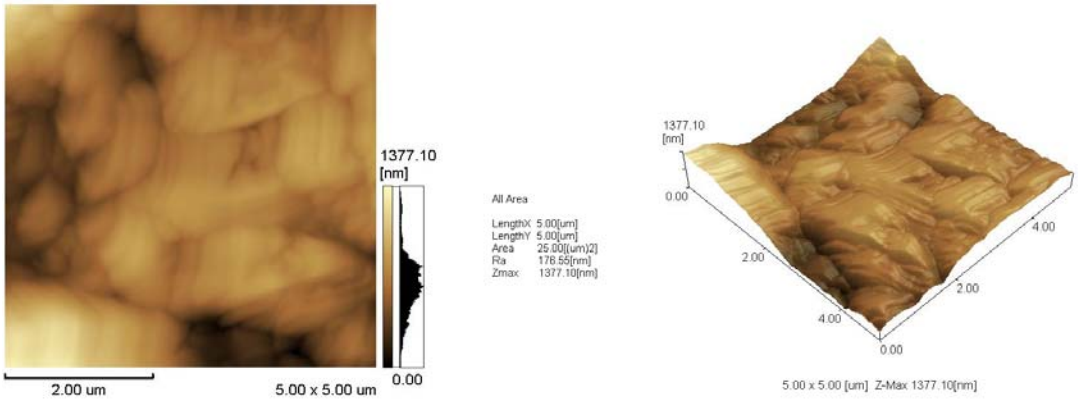

Figure 5-4 (f) AFM images of MGC after etching in 5M HBr for 180 minutes in 100°C, R_a = 176.55nm

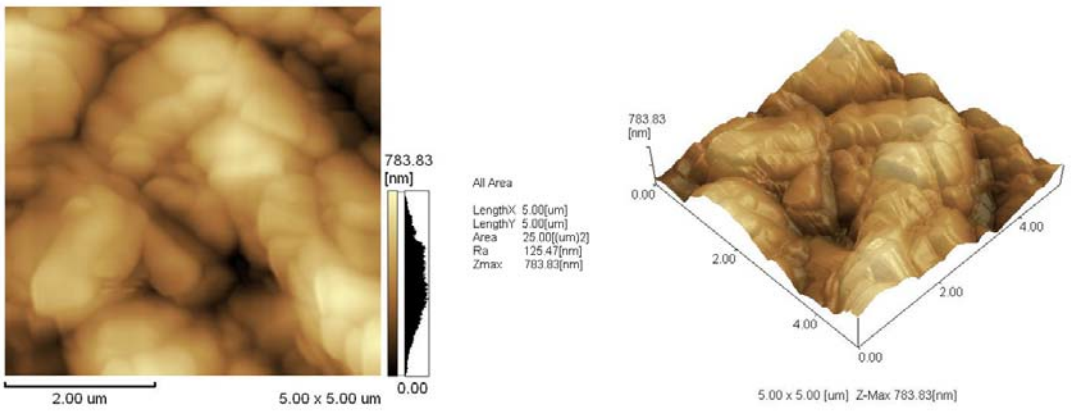

Figure 5-5 (a) AFM images of BN before etching in 7.5M HBr for 75 minutes in 19°C, R_a = 125.47nm

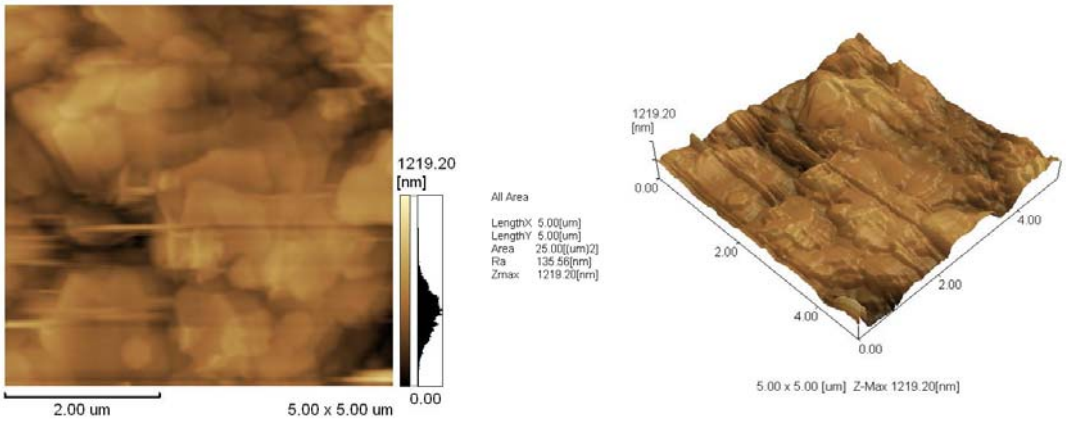

Figure 5-5 (b) AFM images of BN after etching in 7.5M HBr for 75 minutes in 19°C, R_a=135.56nm

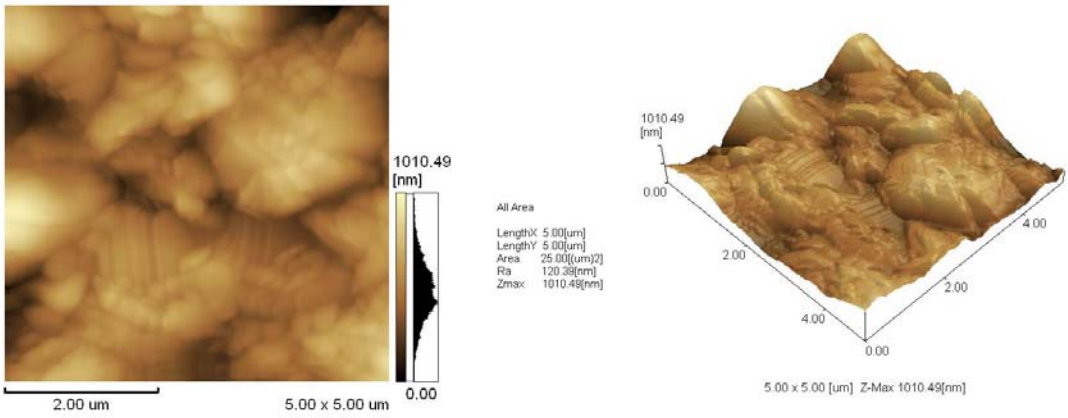

Figure 5-5 (c) AFM images of BN before etching in 7.5M HBr for 75 minutes in 65°C, R_a= 120.39nm

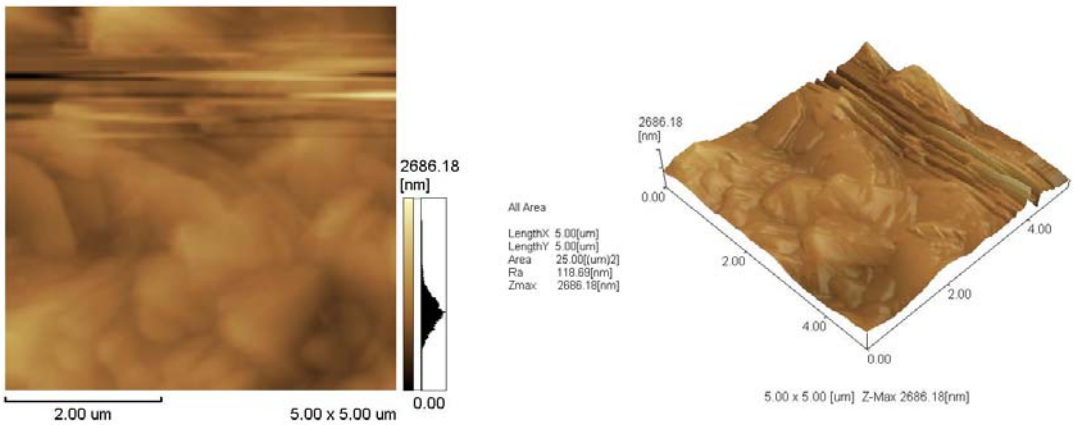

Figure 5-5 (d) AFM images of BN after etching in 7.5M HBr for 75 minutes in 65°C, R_a=118.99nm

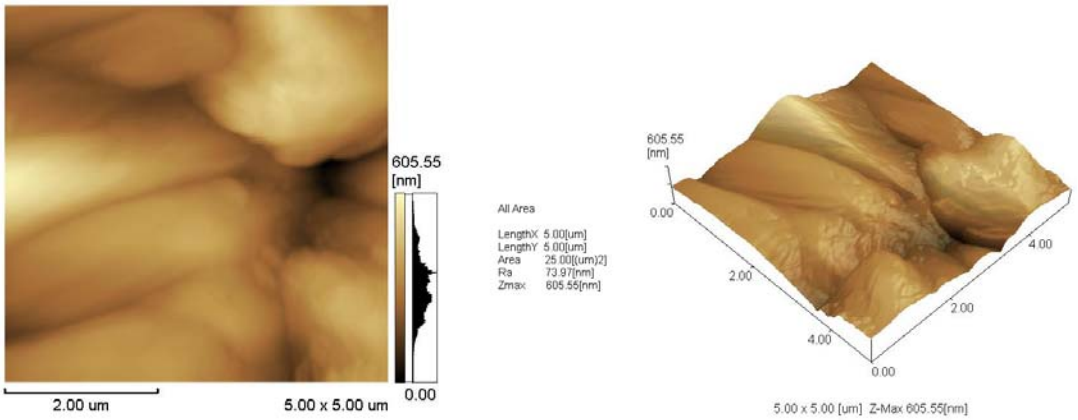

Figure 5-5 (e) AFM images of BN before etching in 7.5M HBr for 75 minutes in 100°C, R_a = 73.97nm

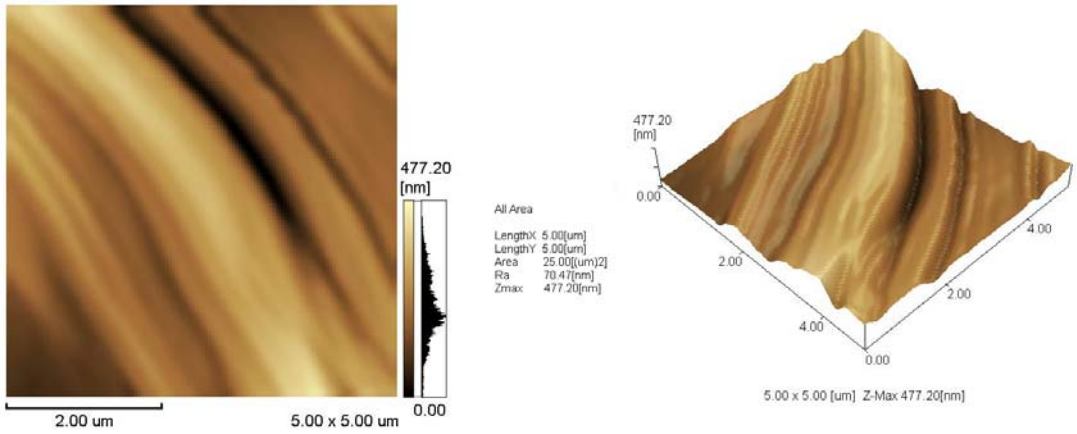

Figure 5-5 (f) AFM images of BN after etching in 7.5M HBr for 75 minutes in 100°C, R_a= 70.47nm

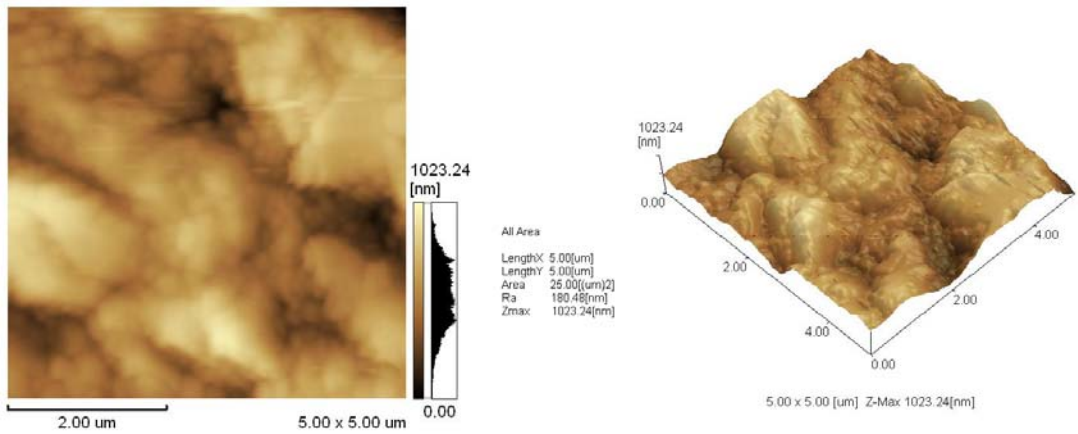

Figure 5-6 (a) AFM images of SiC before etching in 6M HBr for 180 minutes in 19°C, R_a= 180.48nm

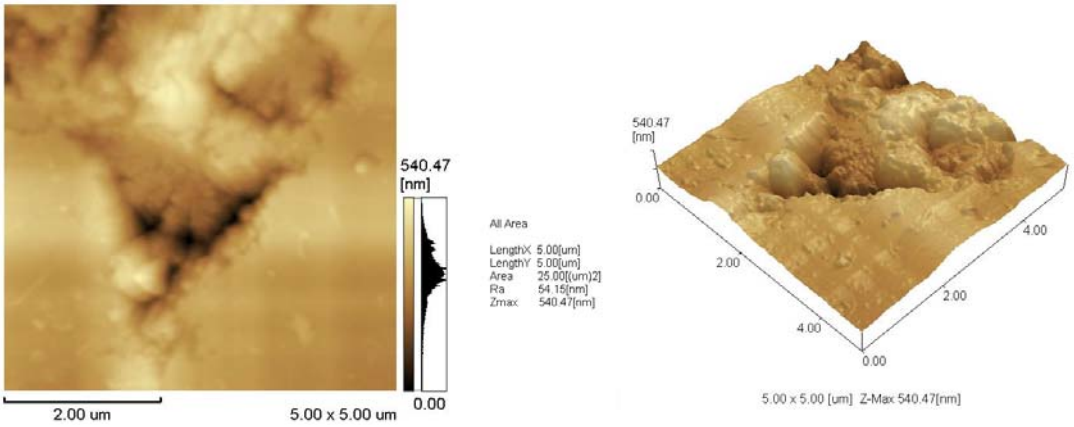

Figure 5-6 (b) AFM images of SiC after etching in 6M HBr for 180 minutes in 19°C, R_a=54.15nm

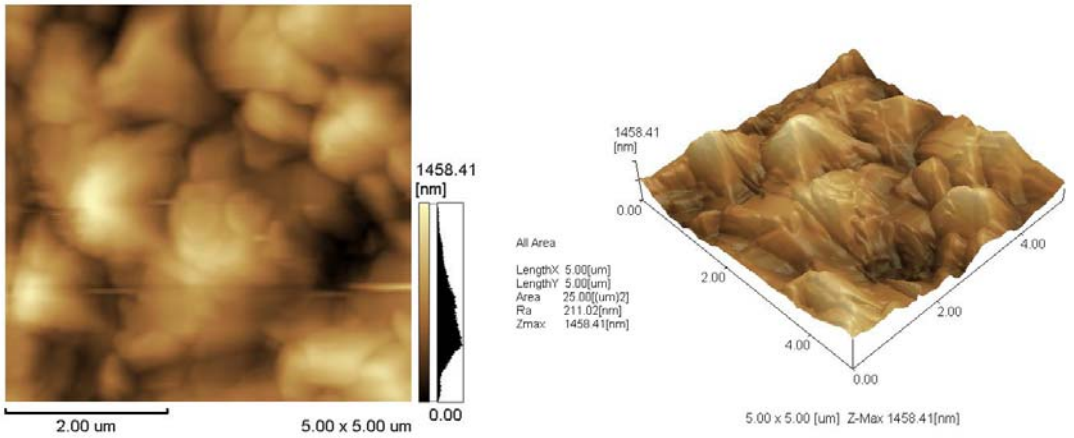

Figure 5-6 (c) AFM images of SiC before etching in 6M HBr for 180 minutes in 65°C, R_a=211.02nm

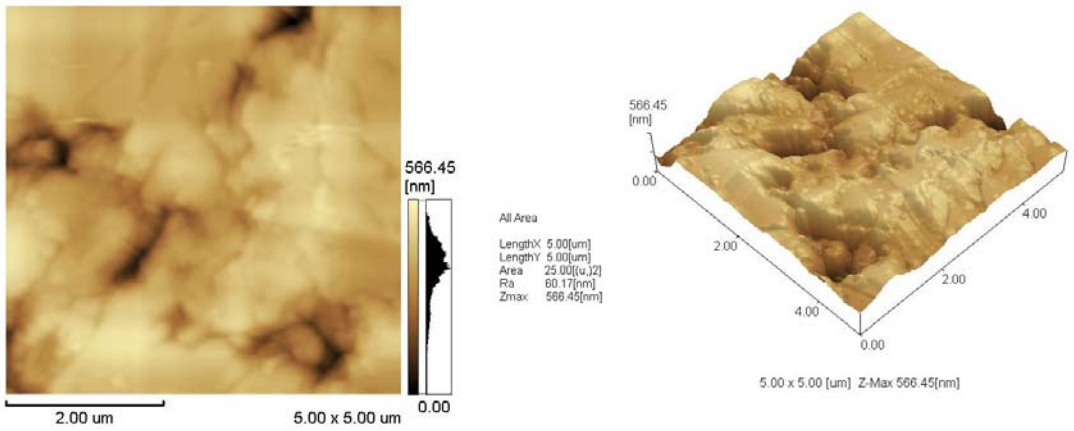

Figure 5-6 (d) AFM images of SiC after etching in 6M HBr for 180 minutes in 65°C, R_a=60.17nm

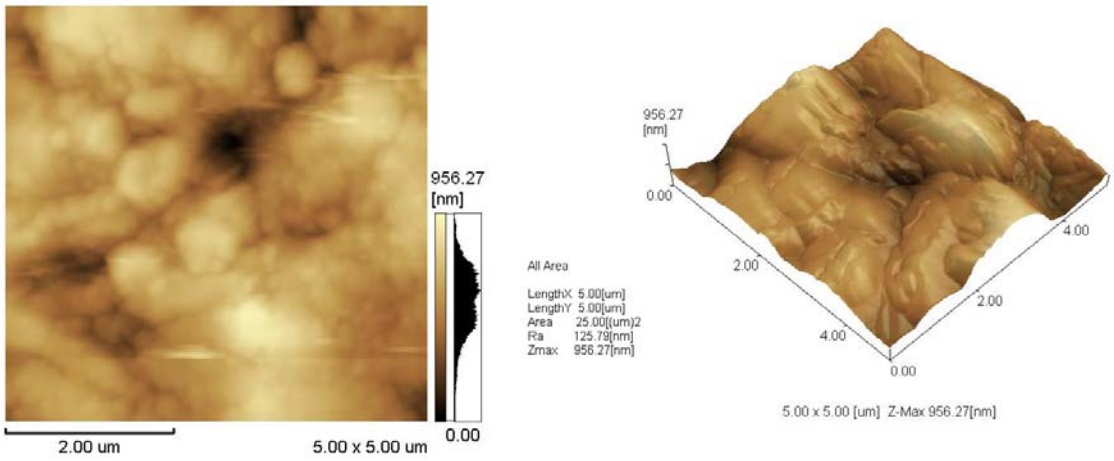

Figure 5-6 (e) AFM images of SiC before etching in 6M HBr for 180 minutes in 100°C, R_a = 125.79nm

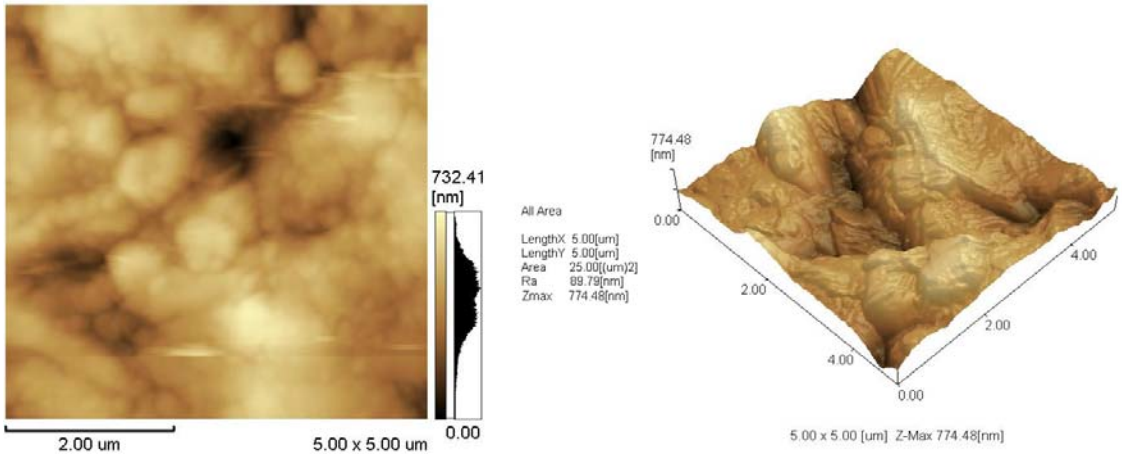

Figure 5-6 (f) AFM images of SiC after etching in 6M HBr for 180 minutes in 100°C, R_a= 89.79nm

5.4.2 Effect of Etchant

Etching process relied on the reaction between anion of the etchant and the material composition. For this reason, the effect of etchant, namely HBr, HCl and H_3PO_4 on the etching and surface roughness of the MGC, BN and SiC was performed. The experimental results and the AFM analysis on the effect of the etchants concerned are as depicted from Figures 5-7 to 5-12 respectively and is summarized in Tables 5-12 and 5-13. From Figures 5-10 to 5-12, the effect of etchant was compared at moderate

concentration (0 level) of each etchant with temperature and duration are fixed. Thus, the effect of etchant towards the substrate can be studied precisely.

The result shown in Figure 5-7 is in good agreement with the result obtained in Table 5-1 that *p*-value of etchant in MGC is more than 0.05. Thus, it is not a significant variable in the affecting surface roughness of MGC. However, with BN and SiC as indicated in Figure 5-8 and 5-9 the etchant is a significant variable and has influenced on surface roughness in chemical etching of BN and SiC. The etching of BN in H_3PO_4 gave the best performance with 1.55nm improvement of surface quality. This is followed with 0.15nm improvement in HCl and 1nm detriment in HBr etchant on BN's surface. For SiC, it is best etched in the HCl with the improvement of 50nm on the surface roughness. As shown in Figure 5-9, H_3PO_4 contributed 15nm improvement on surface quality and HBr gave 10nm of surface's improvement. The difference of surface roughness observed for each substrate could be attributable to the difference in the microstructure of substrate and their reactivity towards the anions of etchants. Structurally, all materials are crystalline, partially crystalline, or amorphous. These substrates are made up of a large number of small crystals, or grains, and separated from one another by the grain boundaries.

Table 5-13 Result of surface roughness for MGC at 65^{o}C following 120minutes etching process (Figure 5-10 (a)-(f))

0 level etchant concentration	Before (nm)	After (nm)	Surface roughness (nm)
10M HCl	163.89	142.98	+ 28
6M HBr	131.34	101.81	+ 37
12M H_3PO_4	281.64	224.54	+ 42

Table 5-14 Result of surface roughness for BN at 65^{o}C for 120minutes etching process (Figure 5-11 (a)-(f))

0 level etchant concentration	Before (nm)	After (nm)	Surface roughness (nm)
10M HCl	125.47	145.28	- 12
6M HBr	84.61	108.56	- 38
12M H_3PO_4	204.36	159.62	+ 13

Table 5-15 Result of surface roughness for SiC at 65^{o}C for 120minutes etching process (Figure 5-12 (a)-(f))

0 level etchant concentration	Before (nm)	After (nm)	Surface roughness (nm)
10M HCl	35.47	29.94	+ 5.53
6M HBr	102.01	102.98	- 0.97
12M H_3PO_4	33.82	32.64	+ 1.18

The different effect of the individual etchant on the surface roughness improvement from the AFM analyses suggest that, the extent of etching caused by the etchant on the surface of the respective material is different. This observation also implies a distinct reactivity of the etchant towards the material microstructure that is attributable to the different trend of surface roughness properties exhibited by MGC, BN and SiC. With the same type of etchant and other independent variables, the only difference between these materials is their microstructure and composition. Williams et al. summarised that the degree of roughening probably depends on the microstructure and thus varies with the method of material preparation [6]. Prudhomme et al. [181] also found that roughness of the same material is different from two etchants used proving that the chemical reactivity is not the same at the solid-liquid interface.

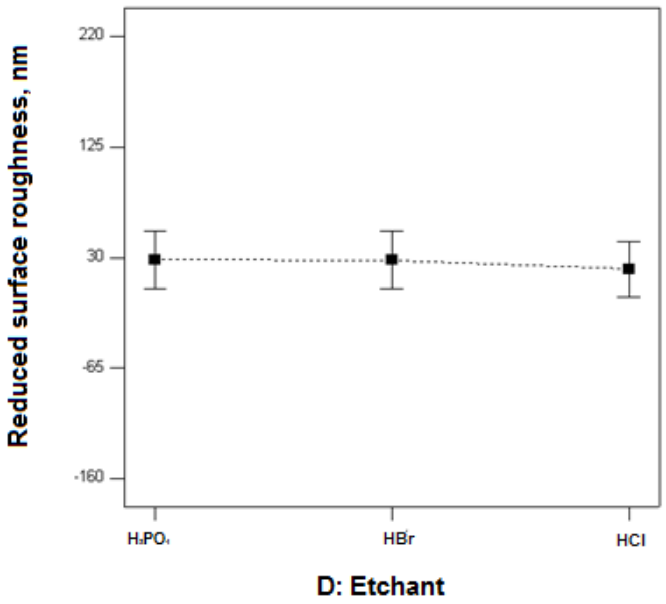

Figure 5-7 MGC reduced surface roughness (nm) versus etchant

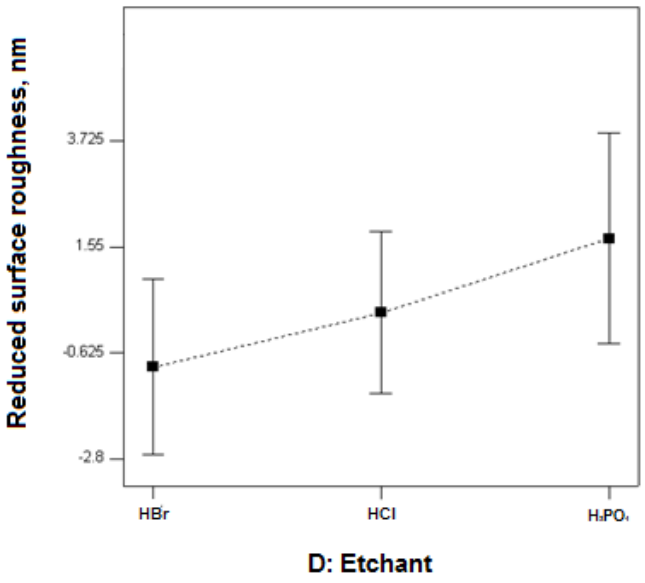

Figure 5-8 BN reduced surface roughness (nm) versus etchant

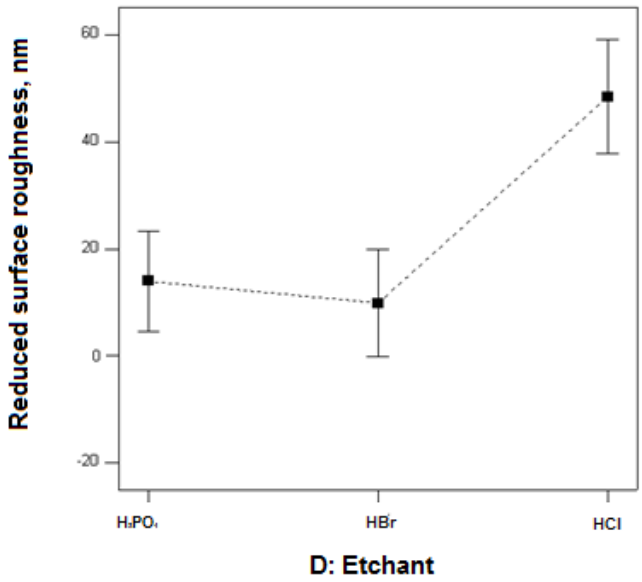

Figure 5-9 SiC reduced surface roughness (nm) versus etchant

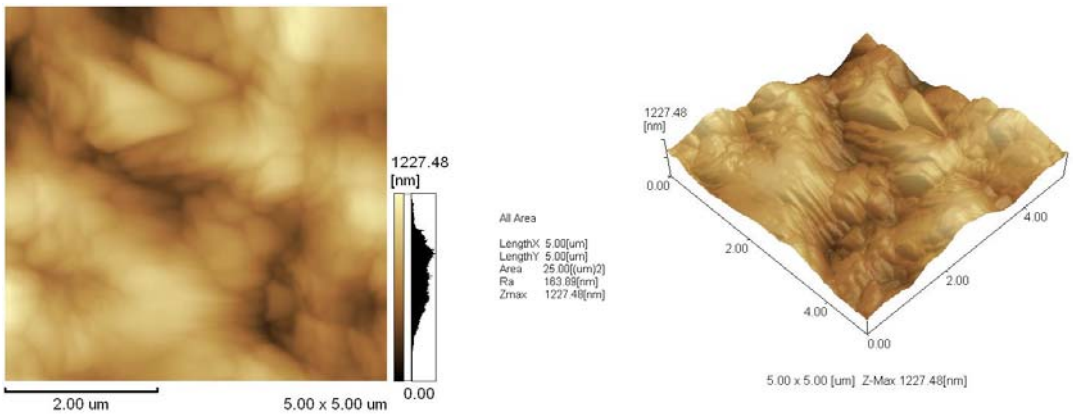

Figure 5-10 (a) AFM images of MGC before etching at 65^{o}C for 120 minutes in 0 level etchant - 10M HCl, R_a = 163.89nm

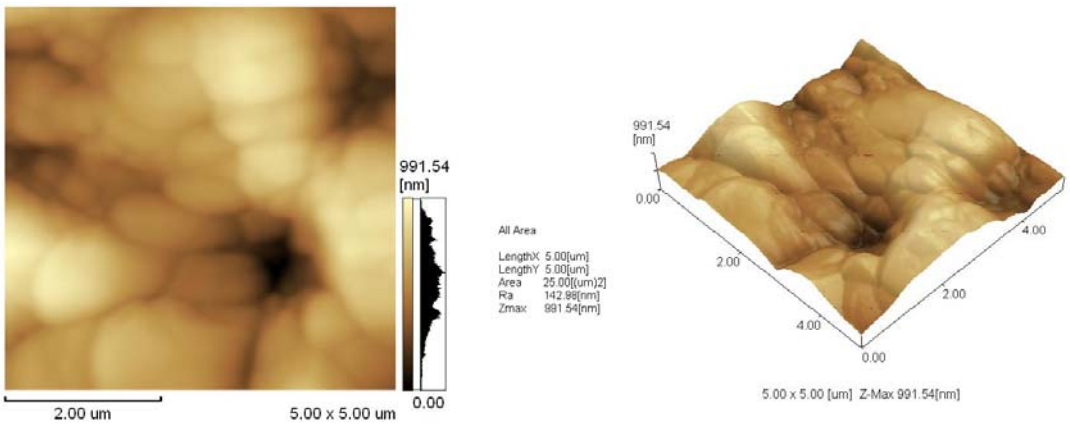

Figure 5-10 (b) AFM images of MGC after etching at 65°C for 120 minutes in 0 level etchant - 10M HCl, R_a = 142.98nm

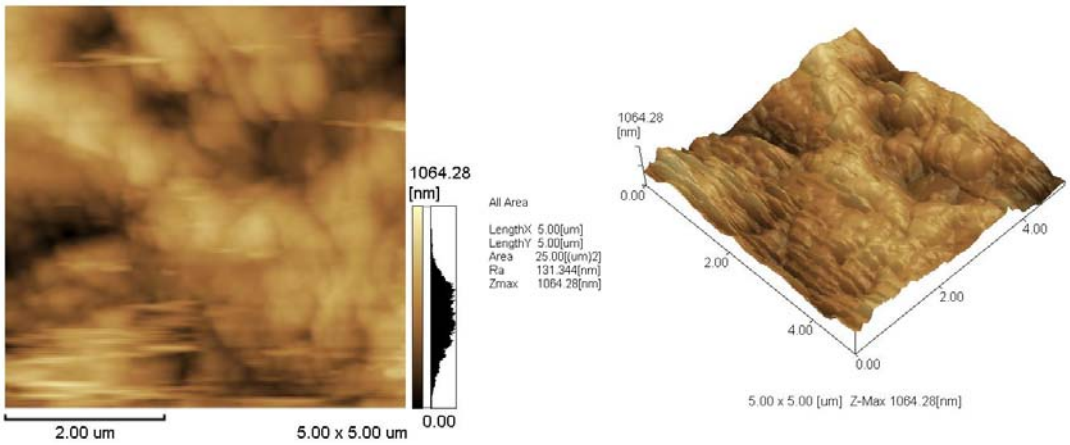

Figure 5-10 (c) AFM images of MGC before etching at 65°C for 120 minutes in 0 level etchant - 6M HBr, R_a = 131.34nm

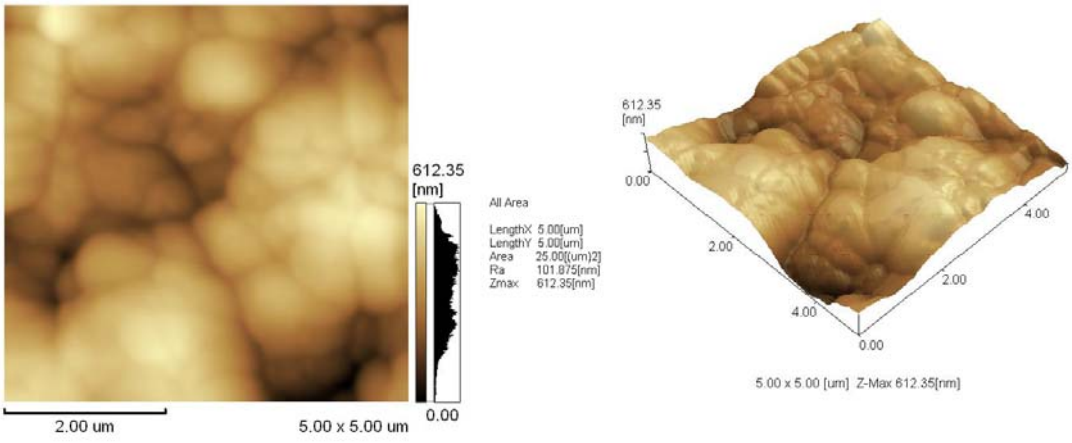

Figure 5-10 (d) AFM images of MGC after etching at 65°C for 120 minutes in 0 level etchant - 6M HBr, R_a = 101.81nm

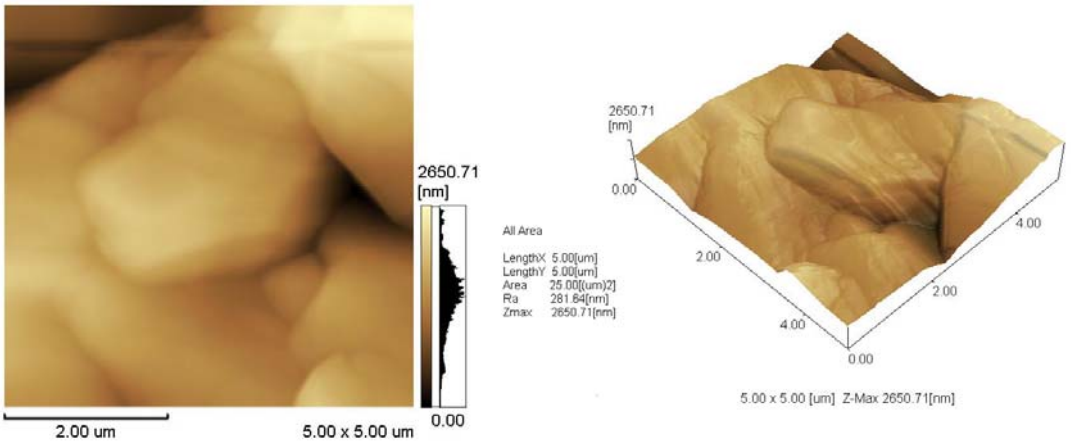

Figure 5-10 (e) AFM images of MGC before etching at 65°C for 120 minutes in 0 level etchant - 12M H_3PO_4, R_a = 281.64nm

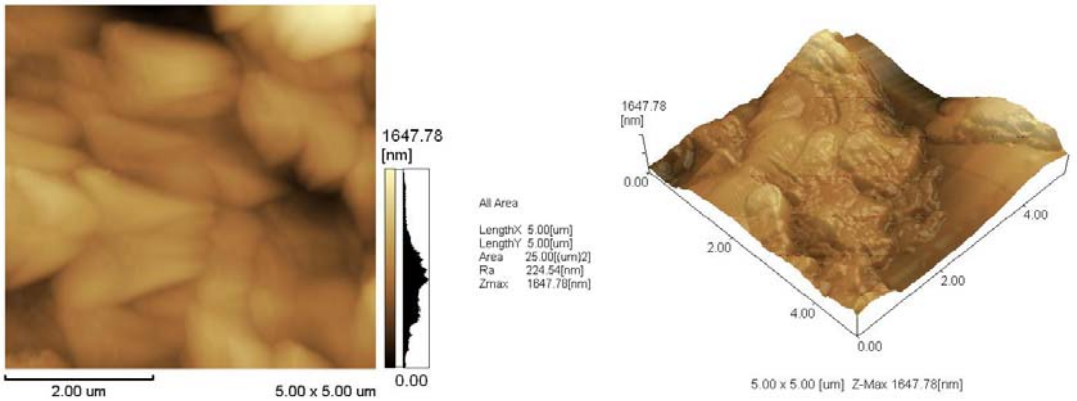

Figure 5-10 (f) AFM images of MGC after etching at 65°C for 120 minutes in 0 level etchant - 12M H_3PO_4, R_a = 224.54nm

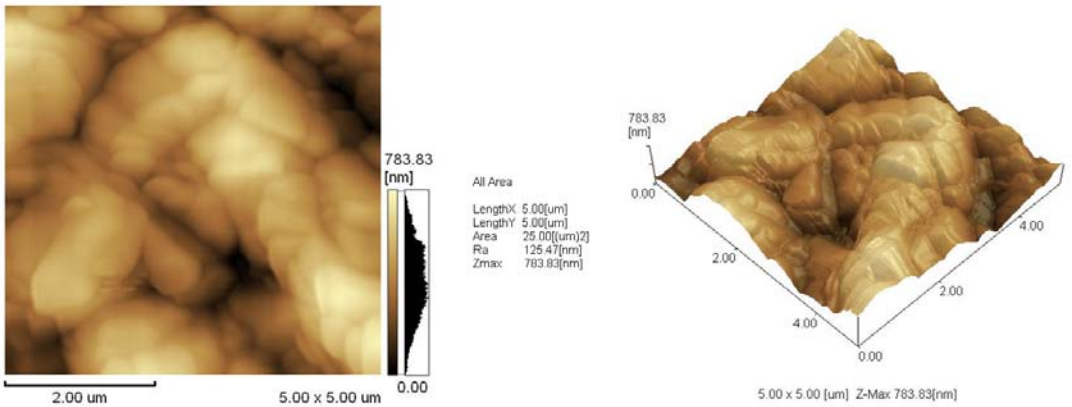

Figure 5-11 (a) AFM images of BN before etching at 65°C for 120 minutes in 0 level etchant - 6M HCl, R_a = 125.47nm

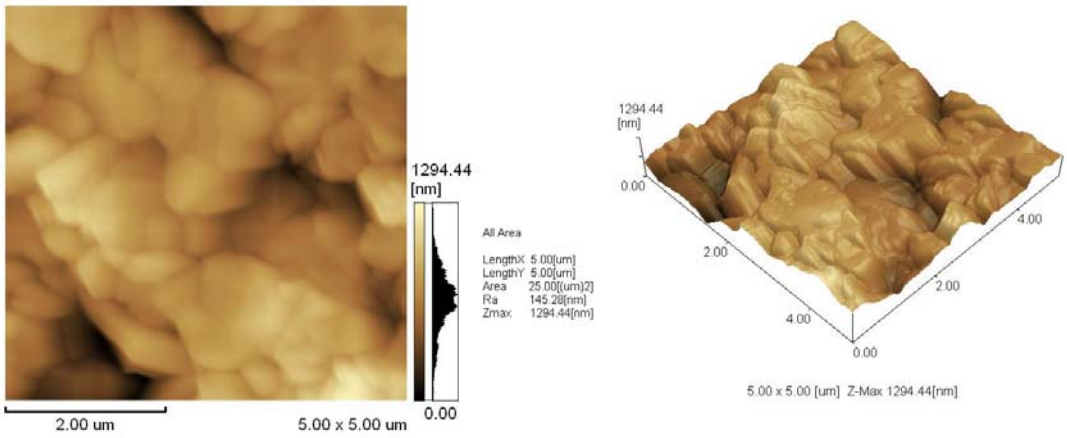

Figure 5-11 (b) AFM images of BN after etching at 65°C for 120 minutes in 0 level etchant - 10M HCl, R_a = 145.28nm

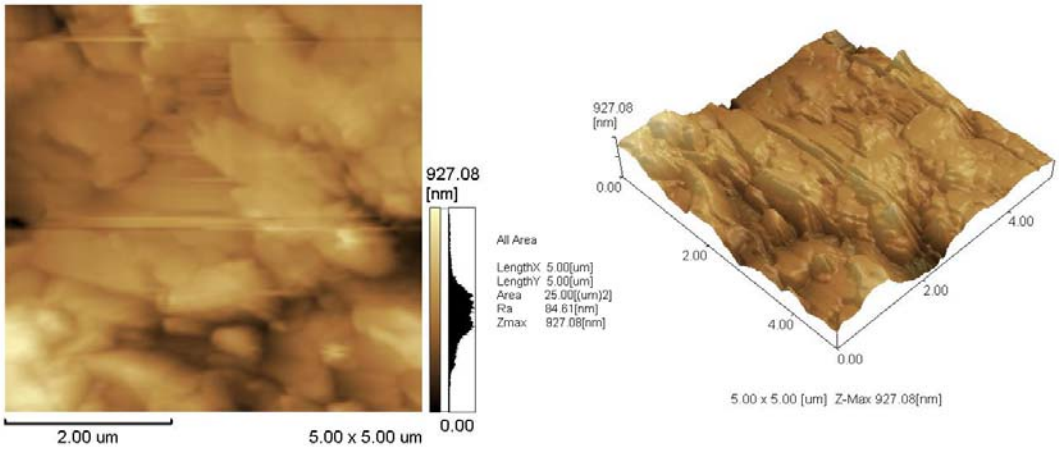

Figure 5-11 (c) AFM images of BN before etching at 65°C for 120 minutes in 0 level etchant - 6M HBr, R_a = 84.61nm

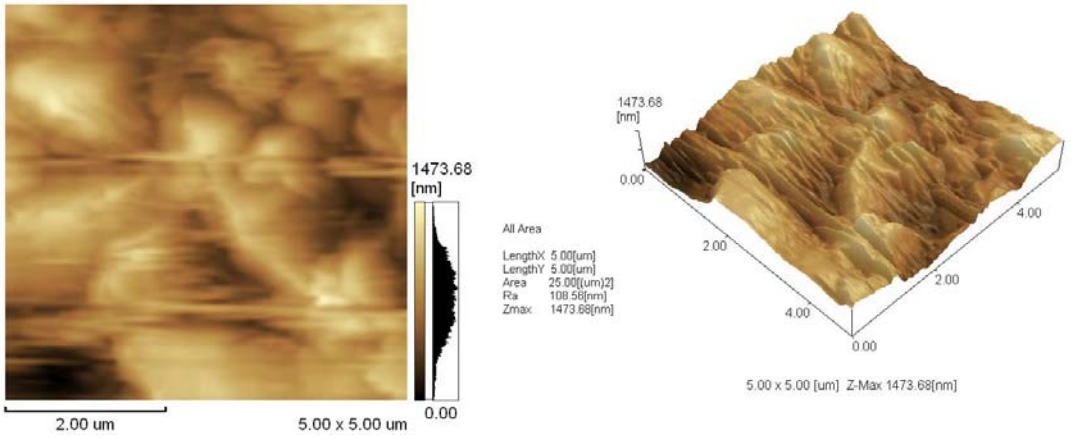

Figure 5-11 (d) AFM images of BN after etching at 65°C for 120 minutes in 0 level etchant - 6M HBr, R_a = 108.56nm

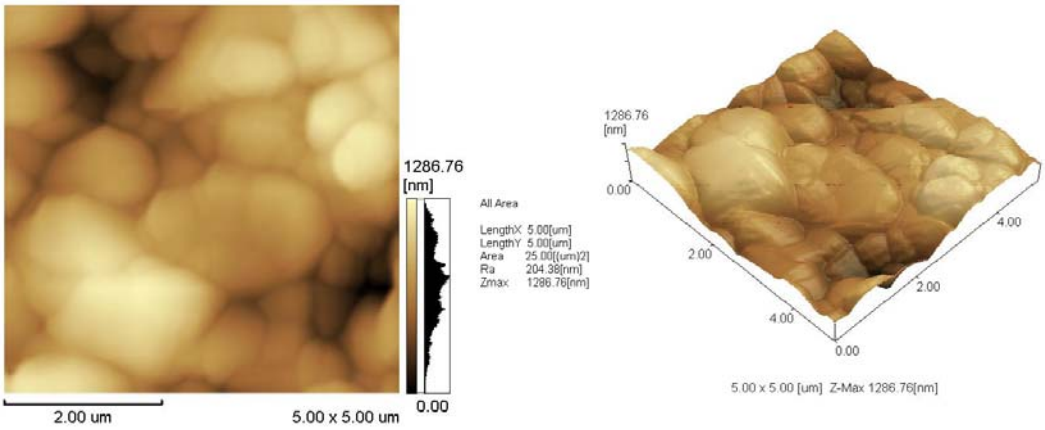

Figure 5-11 (e) AFM images of BN before etching at 65°C for 120 minutes in 0 level etchant - 12M H_3PO_4, R_a = 204.36nm

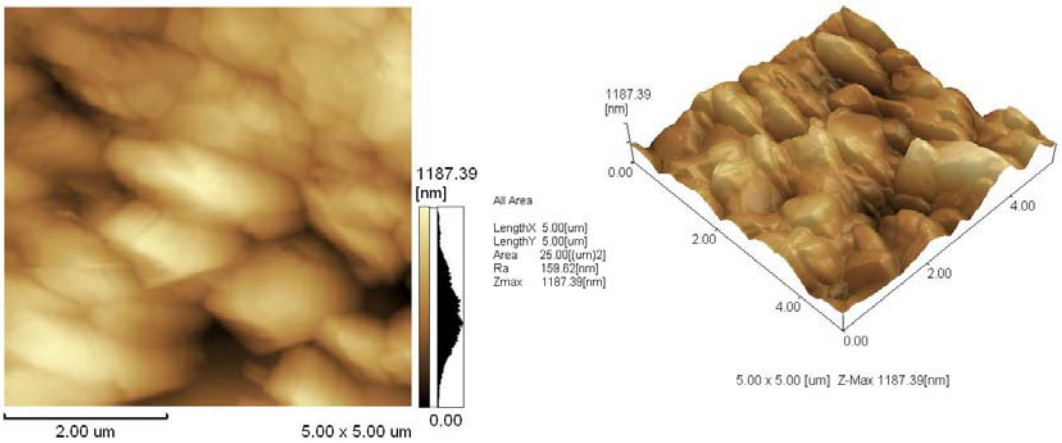

Figure 5-11 (f) AFM images of BN after etching at 65°C for 120 minutes in 0 level etchant - 12M H_3PO_4, R_a = 159.62nm

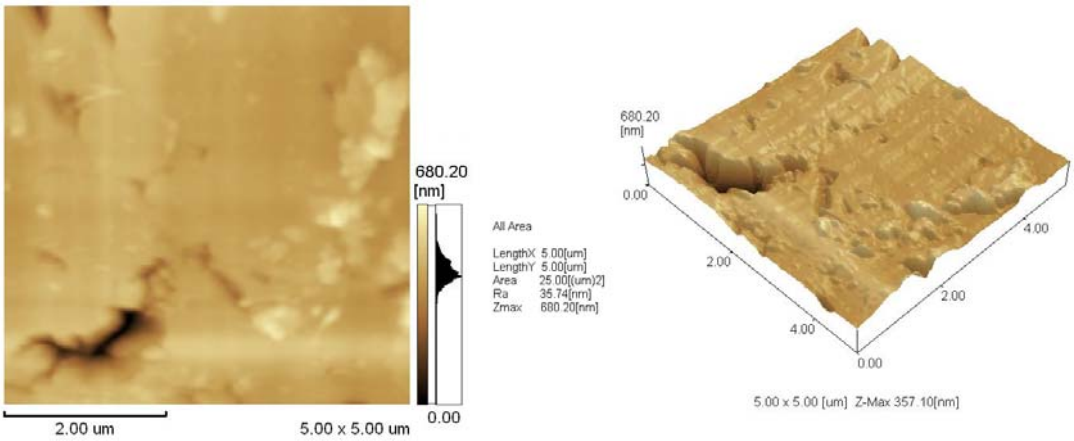

Figure 5-12 (a) AFM images of SiC before etching at 65°C for 120 minutes in 0 level etchant - 10M HCl, R_a = 35.47nm

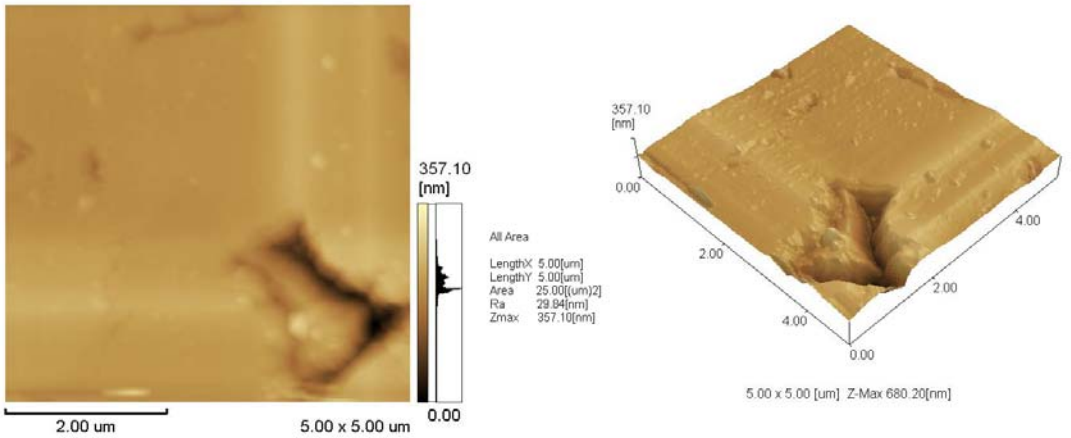

Figure 5-12 (b) AFM images of SiC after etching at 65°C for 120 minutes in 0 level etchant - 10M HCl, R_a = 29.94nm

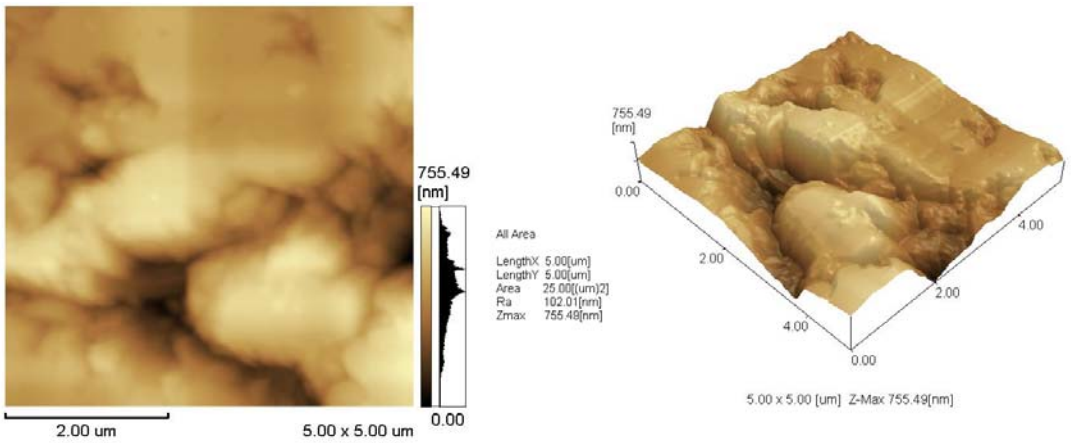

Figure 5-12 (c) AFM images of SiC before etching at 65°C for 120 minutes in 0 level etchant - 6M HBr, R_a = 102.01nm

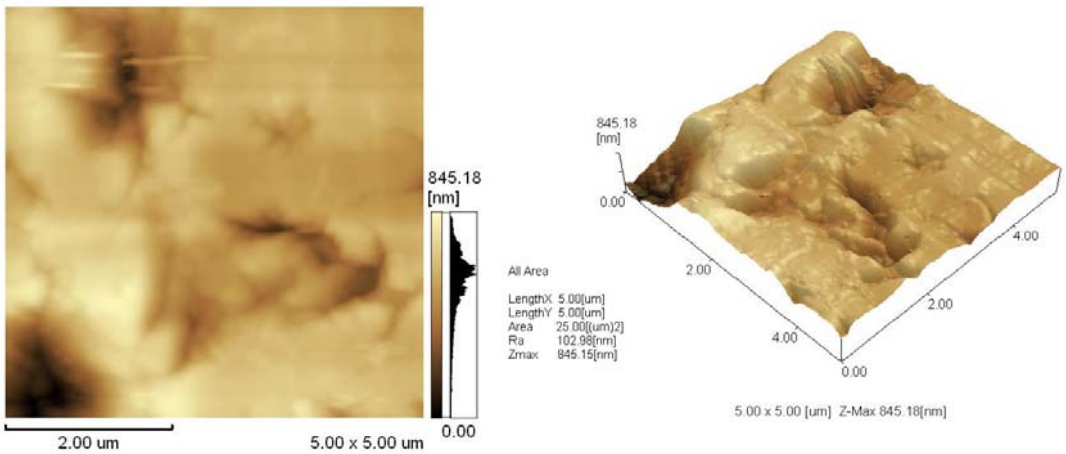

Figure 5-12 (d) AFM images of SiC after etching at 65°C for 120 minutes in 0 level etchant - 6M HBr, R_a = 102.98nm

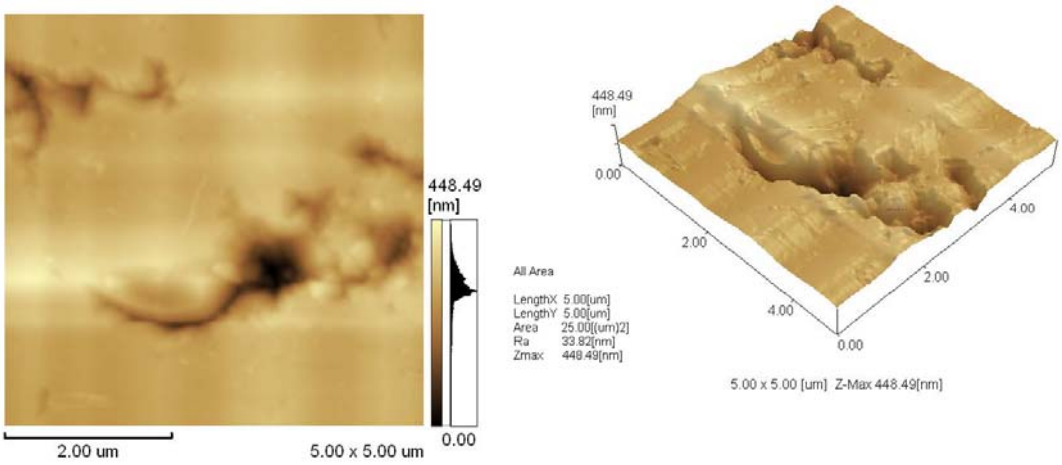

Figure 5-12 (e) AFM images of SiC before etching at 65°C for 120 minutes in 0 level etchant - 12M H_3PO_4, R_a = 33.82.64nm

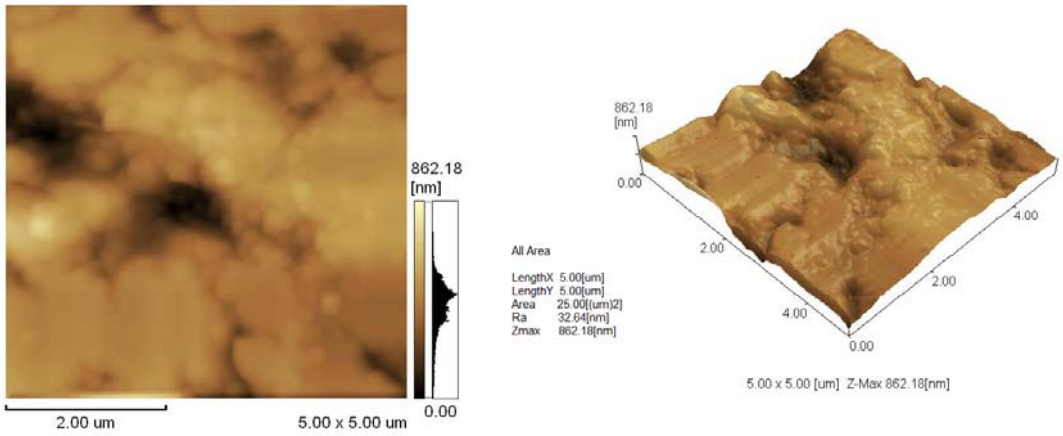

Figure 5-12 (f) AFM images of SiC after etching at 65°C for 120 minutes in 0 level etchant - 12M H_3PO_4, R_a = 32.64nm

5.4.3 Effect of Etching Duration

In the earlier study, the etching duration has been shown to influence the etching rate. The possible effect of etching duration on the surface roughness of the ceramic materials was investigated. A significant reduction of the surface roughness in chemical etching of SiC was observed as shown in Figure 5-15. Figures 5 (-13, -14 and -15) show similar reduction of the surface roughness with etching for all substrates. Figures 5 (-16, -17 and -18) are AFM images of each material at different duration. Figures 5-16 (a)-(c) are AFM

images of MGC in 6M HBr at 100^{o}C at different etching duration. The surface roughness improved at different rate: 30nm for 60 minutes, 19.8nm for 120 minutes, and 45.75nm for 180 minutes etching. The summary of result from Figure 5-17 (a)-(c) and Figure 5-18 (a)-(f), is shown in Table 5-16 and 5-17 respectively.

Figures 5-17(a)-(c) are AFM images of BN in 6M HBr at different duration. Surface roughness is improved from 17.58nm (at 30 minutes) to 46.4nm (at 75 minutes), and next the improvement of surface roughness is lower, which is 29nm (at 150 minutes). Image of SiC surface roughness is shown in Figures 18(a)-(c). The surface roughness in 6M HBr for 40 minutes is 14.41nm, for 120 minutes is 20.96nm and for 230minutes is 20.86nm.

Table 5-16 Result of surface roughness for BN at 100^{o}C in 7M HBr (Figure 5-17(a)-(f))

Duration of etching (min)	Before (nm)	After (nm)	Surface roughness (nm)
30	108.56	90.98	+ 17.58
75	120.39	73.97	+ 46.40
150	79.97	44.91	+ 29.00

Table 5-17 Result of surface roughness for SiC at 100^{o}C in 6M HBr (Figure 5-18(a)-(f))

Duration of etching (min)	Before (nm)	After (nm)	Surface roughness (nm)
40	54.97	50.56	+ 14.41
120	80.12	59.16	+ 20.96
230	106.41	85.55	+ 20.86

Overall, surface roughness with the exception of BN tends to improve with initial etching duration of about 2 hours, but decline upon extended duration of etching.

The results from Prudhomme et al. [182] and Cakir et al. [60, 180] are in good agreement with the results that we obtained. One possible explanation for this trend is the improvement in the surface state that might occur when the solute was dissolved in the etchant at longer etching period, which in turn would increase the energy gap for generating etch figure and reduce the damage of material's surface. It was reported that longer etching period produce a more stable etching process in the case of aluminium

etching (187). Baranova and Dorosinskii [70] also observed that as the duration of etching was extended , insoluble reaction products started forming and the surface of the sample started to erode. This observation is consistent with the poor surface roughness that we observed from the AFM analysis upon extended etching for MGC, BN and SiC.

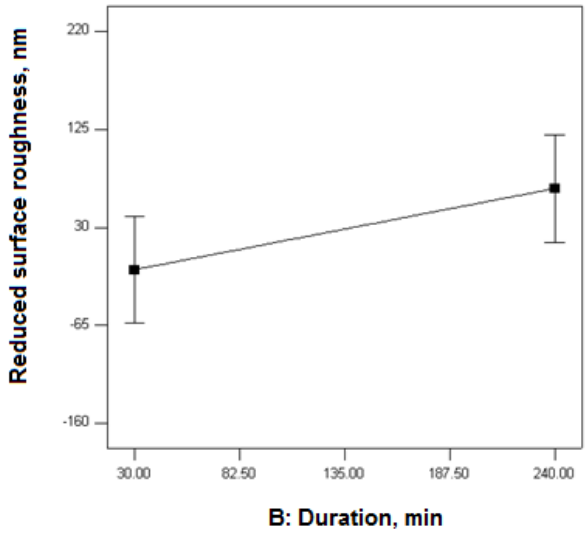

Figure 5-13 MGC reduced surface roughness (nm) versus etching duration (minutes) in HBr

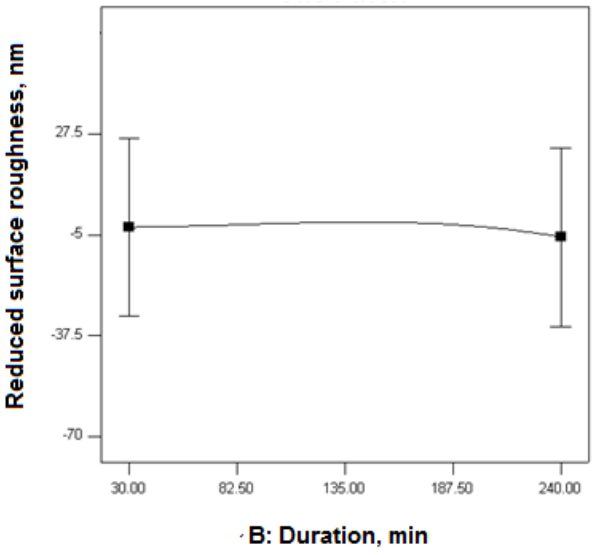

Figure 5-14 BN reduced surface roughness (nm) versus etching duration (minutes) in HBr

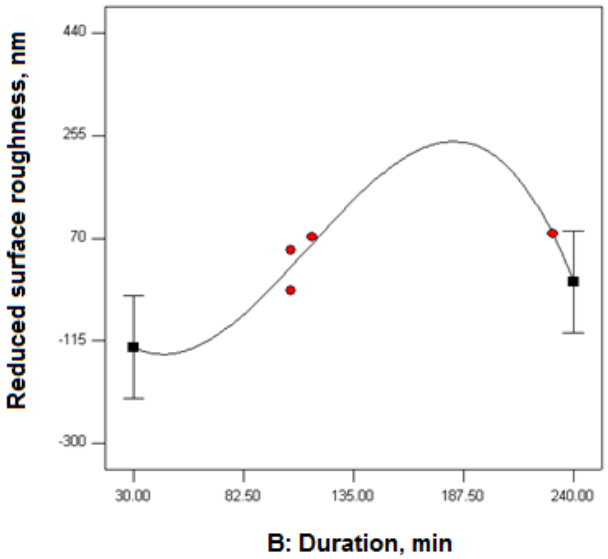

Figure 5-15 SiC reduced surface roughness (nm) versus etching duration (minutes) in HBr

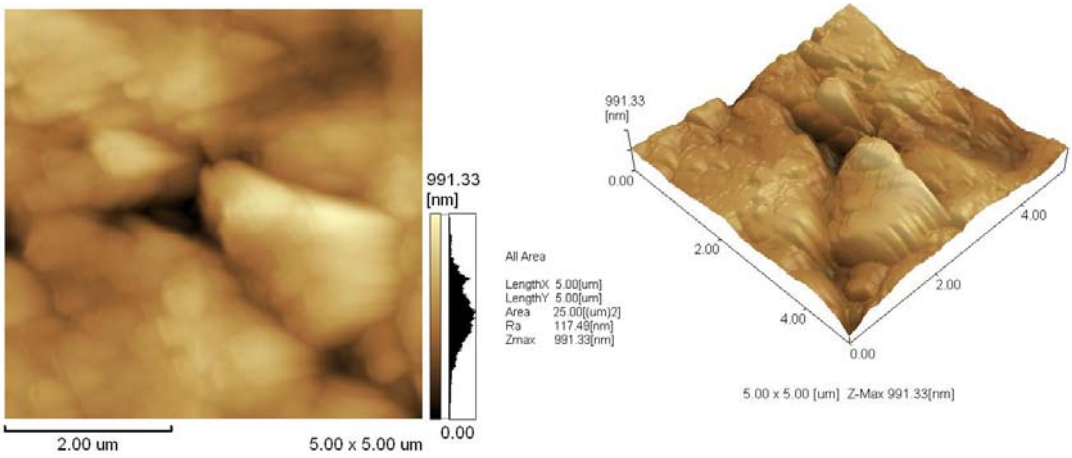

Figure 5-16(a) AFM images of MGC before etching in 6M HBr at 100^{o}C for 60 minutes, R_a = 117.49nm

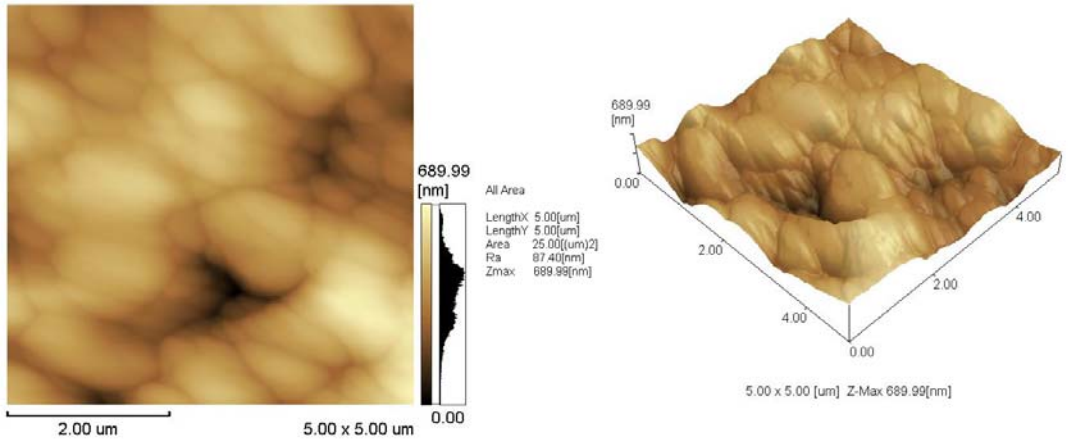

Figure 5-16(b) AFM images of MGC after etching in 6M HBr at 100°C for 60 minutes, R_a = 87.40nm

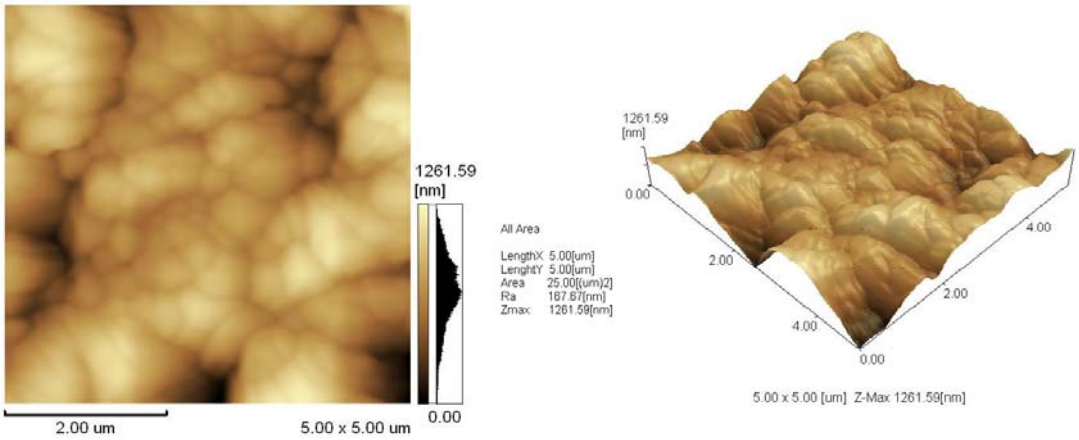

Figure 5-16(c) AFM images of MGC before etching in 6M HBr at 100°C for 120 minutes, R_a = 167.67nm

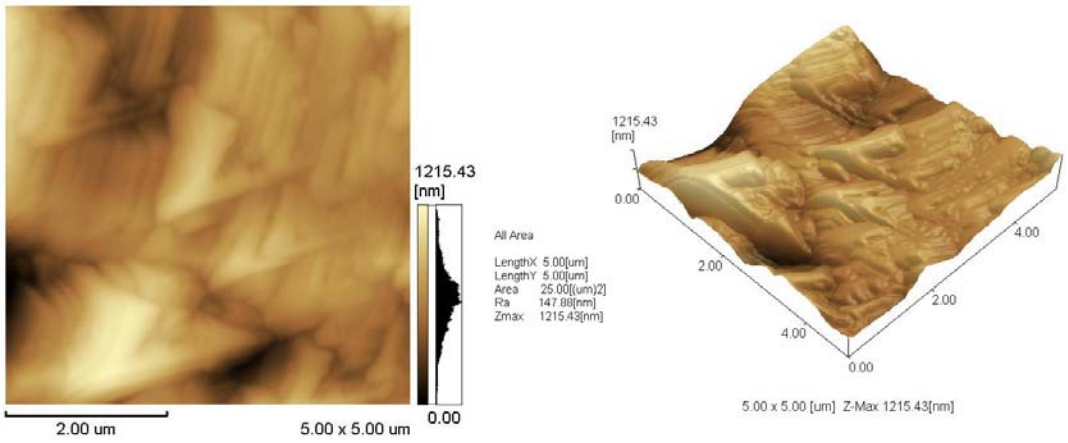

Figure 5-16(d) AFM images of MGC after etching in 6M HBr at 100°C for 120 minutes, R_a = 147.86nm

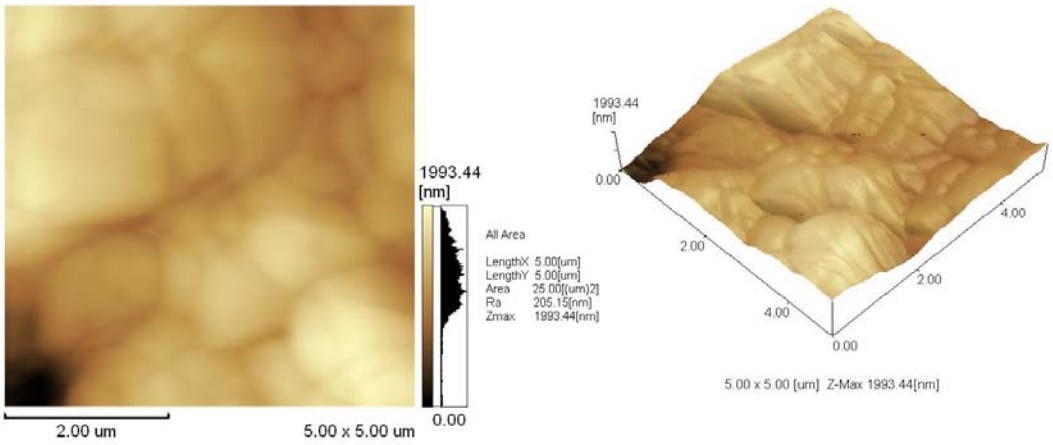

Figure 5-16(e) AFM images of MGC before etching in 6M HBr at 100°C for 180 minutes, R_a = 205.15nm

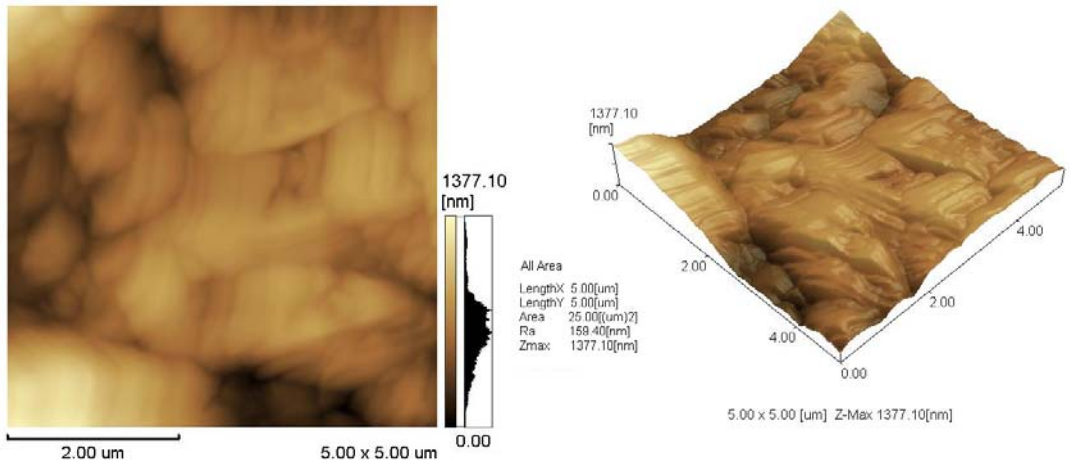

Figure 5-16(f) AFM images of MGC after etching in 6M HBr at 100°C for 180 minutes, R_a = 159.40nm

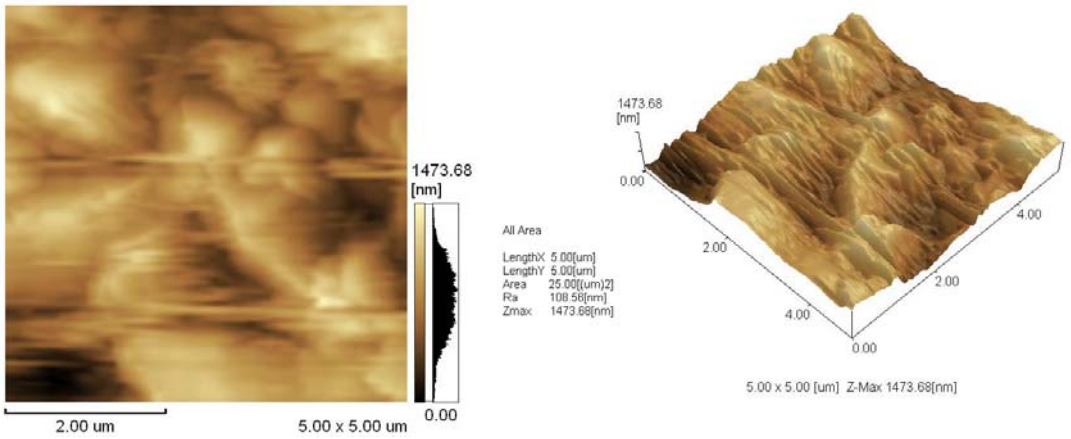

Figure 5-17(a) AFM images of BN before etching in 7M HBr at 65°C for 30 minutes, R_a= 108.56nm

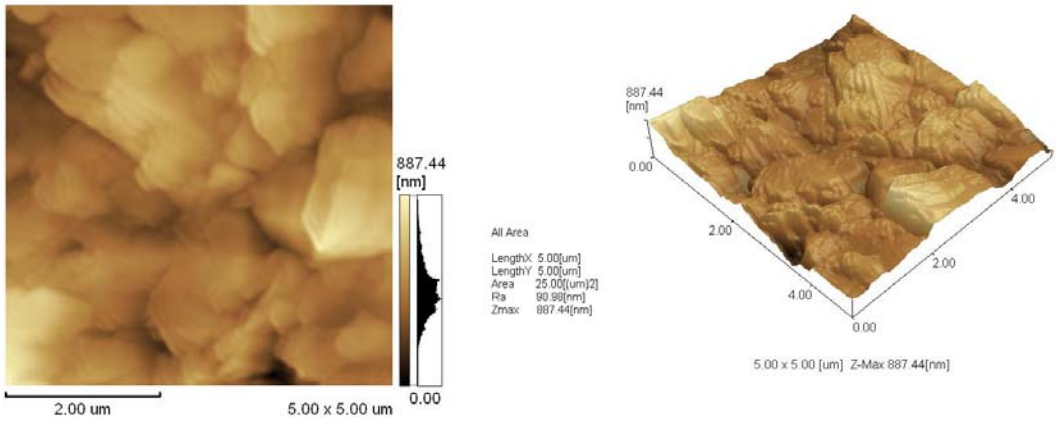

Figure 5-17(b) AFM images of BN after etching in 7M HBr at 65^{o}C for 30 minutes, R_a=90.98nm

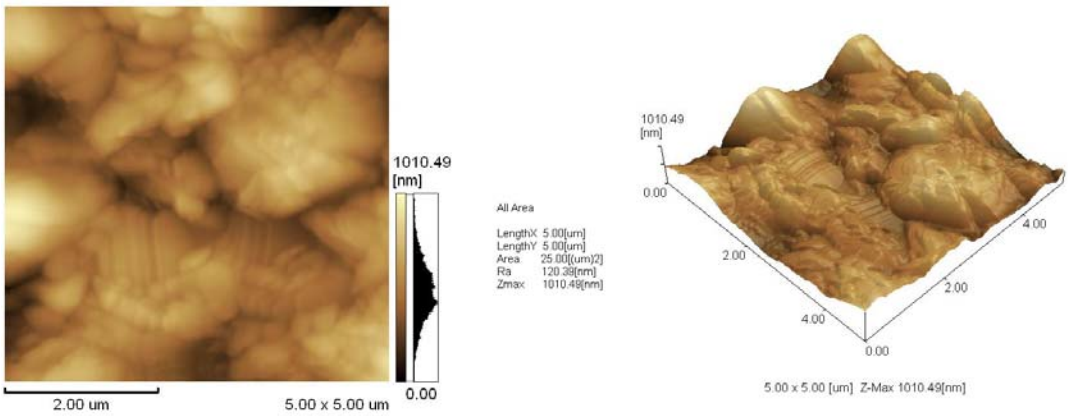

Figure 5-17(c) AFM images of BN before etching in 7M HBr at 65^{o}C for 75min, R_a=120.39nm

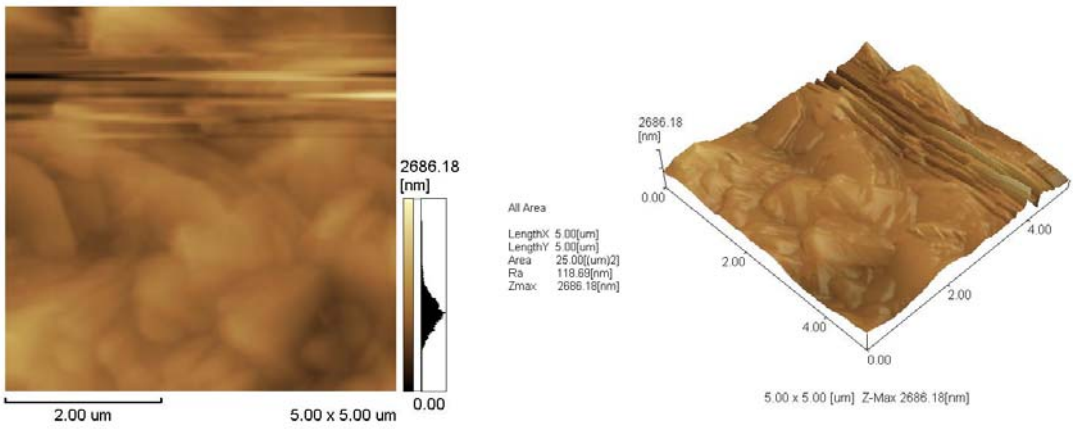

Figure 5-17(d) AFM images of BN after etching in 7M HBr at 65°C for 75min, R_a=73.97nm

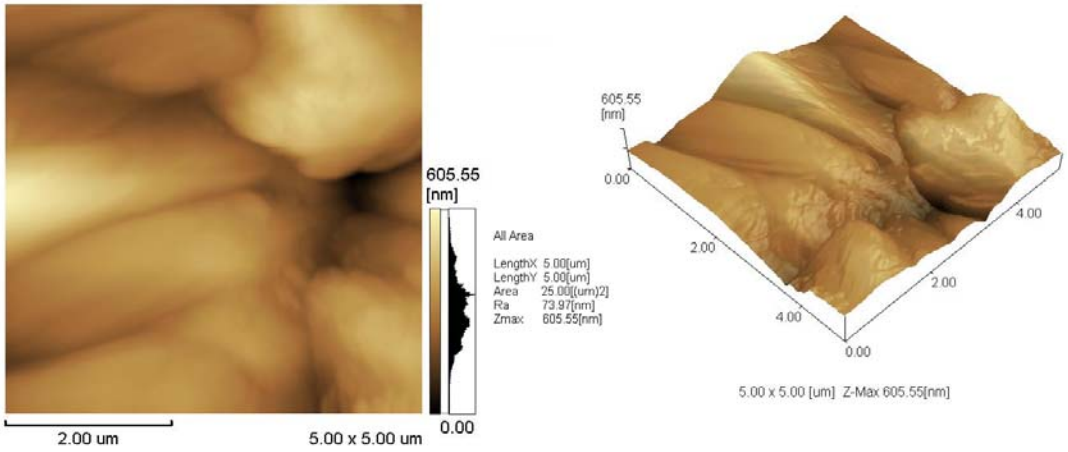

Figure 5-17 (e) AFM images of BN before etching in 6M HBr at 65°C for 150 minutes, R_a = 73.97nm

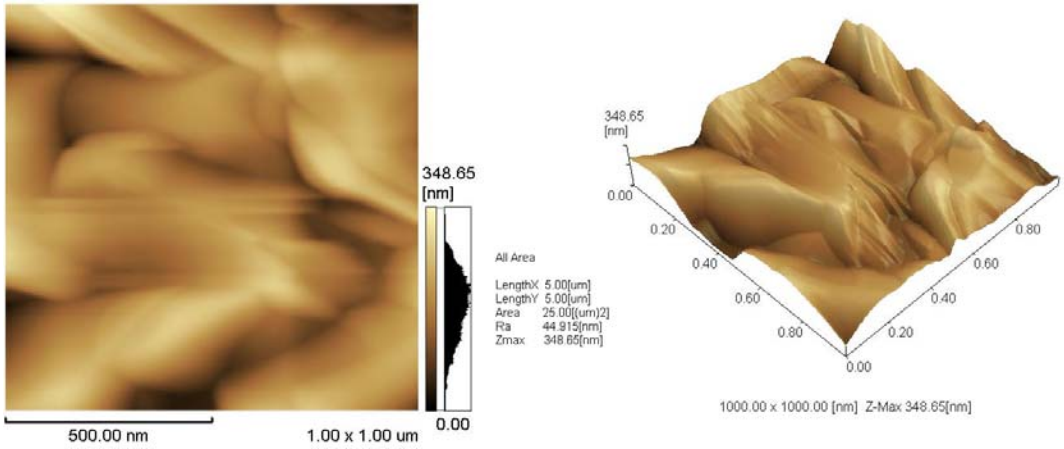

Figure 5-17 (f) AFM images of BN after etching in 6M HBr at 65°C for 150 minutes, R_a=44.91nm

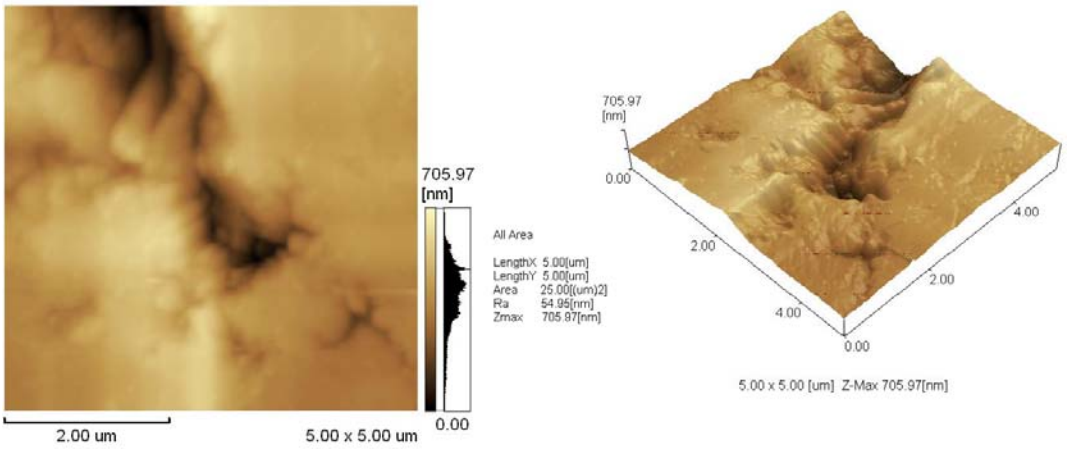

Figure 5-18 (a) AFM images of SiC before etching in 6M HBr at 65°C for 40 minutes, R_a= 54.97nm

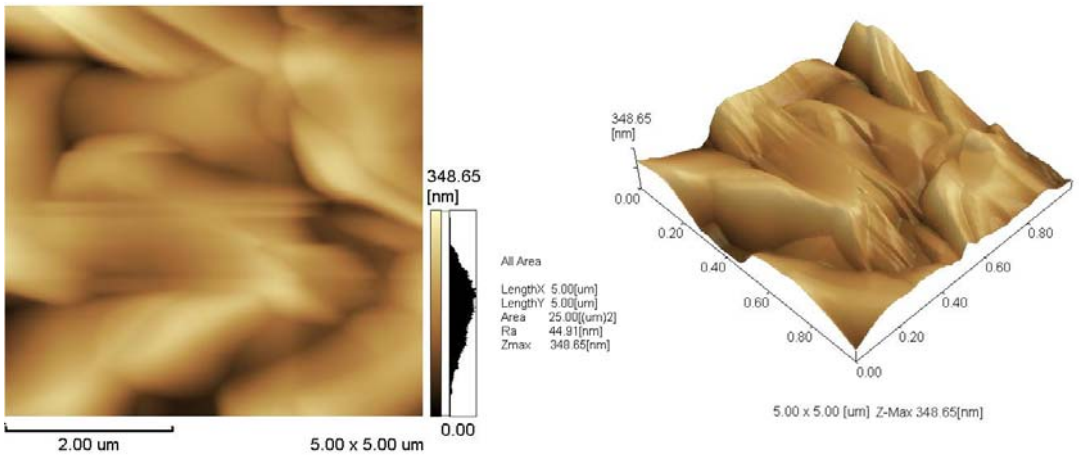

Figure 5-18 (b) AFM images of SiC after etching in 6M HBr at 65°C for 40 minutes, R_a = 50.56nm

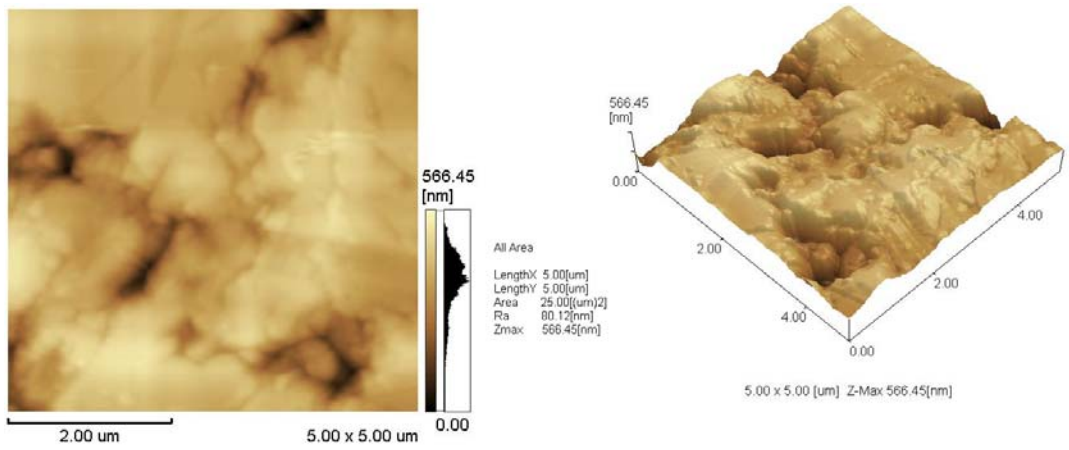

Figure 5-18 (c) AFM images of SiC before etching in 6M HBr at 65°C for 120 minutes, R_a = 80.12nm

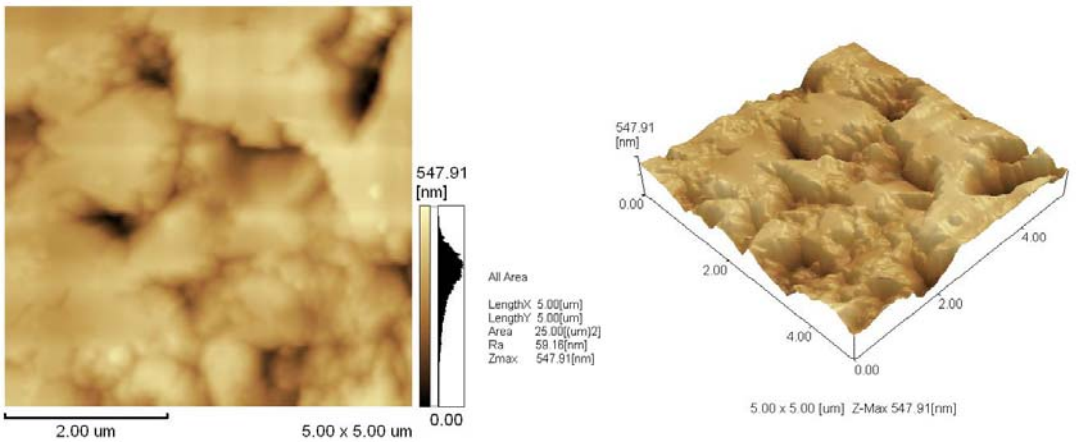

Figure 5-18 (d) AFM images of SiC after etching in 6M HBr at 65°C for 120 minutes, R_a= 59.16nm

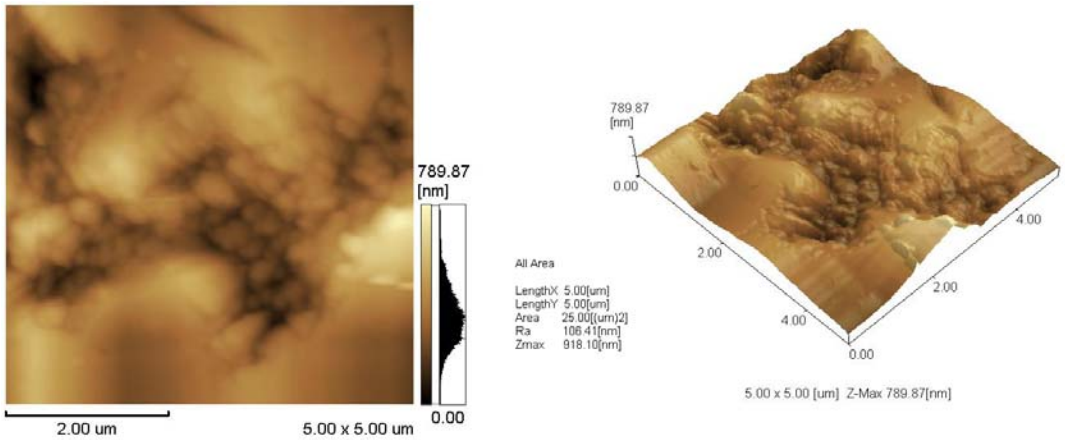

Figure 5-18 (e) AFM images of SiC before etching in 6M HBr at 65°C for 230 minutes, R_a= 106.41nm

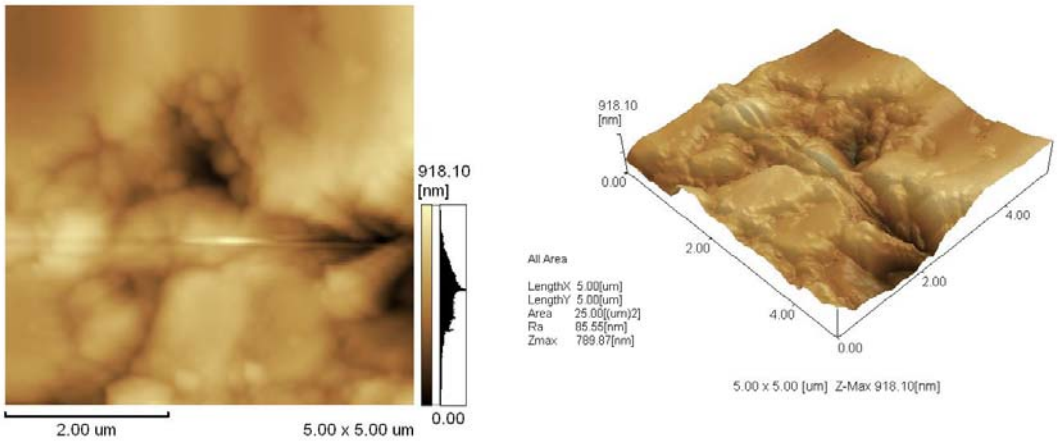

Figure 5-18 (f) AFM images of SiC after etching in 6M HBr at 65^{o}C for 230 minutes, R_a=85.55nm

5.4.4 Effect of Etchant's Concentration

The effect of etchant's concentration on the surface roughness of MGC, BN and SiC was also investigated during the etching process. In Tables 5-1, 5-2 and 5-3, ANOVA indicated that the influence of etchant's concentration is less than 80%. Interaction of etchant and its concentration was found to be more important in reducing surface roughness. Figures 5-19, 5-20 and 5-21 show the graphs of reduced surface roughness versus etchant's concentration of MGC, BN and SiC. All the figures show smoother surface roughness at lower etchant's concentration. The higher the concentration of etchant used the higher the surface roughness was obtained. This might be due to the etch rate drop with increasing etchants' concentration. The lower etch rate might result in rougher surface roughness being obtained because less surface layer is being removed.

It was reported that poorer material surface was achieved when higher concentration of etchant is used [177, 182]. Sundararaman et al. [174] also observed that etching at high concentration produced a rougher surface. Others also reported that after etching with concentrated HCl etchant, the surface roughness of the materials involved increased by approximately 10^2nm in height [168, 183].

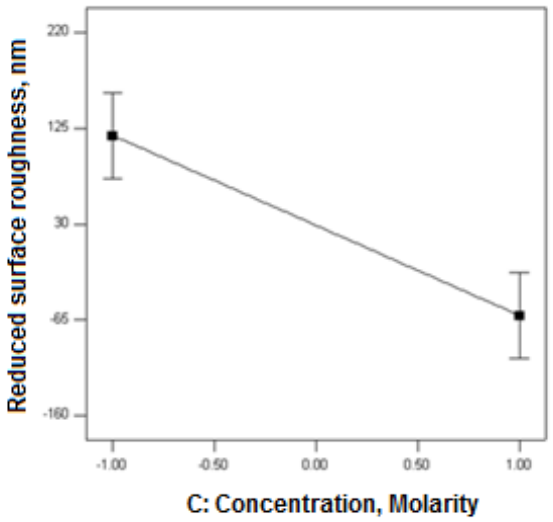

Figure 5-19 MGC reduced surface roughness (nm) versus etchant's concentration (Molarity)

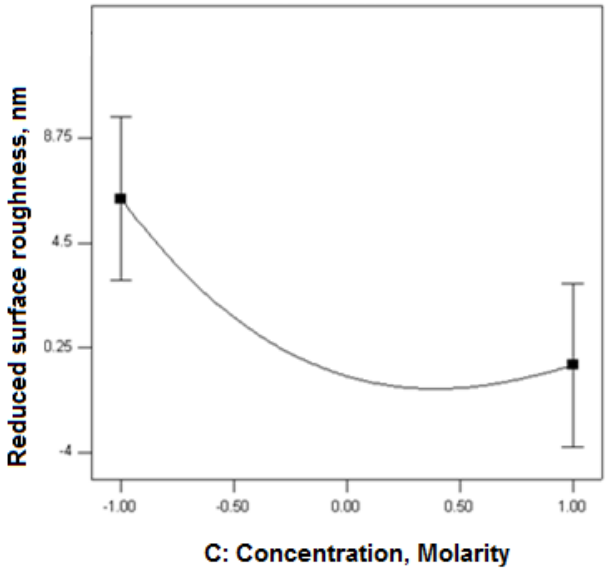

Figure 5-20 BN reduced surface roughness (nm) versus etchant's concentration (Molarity)

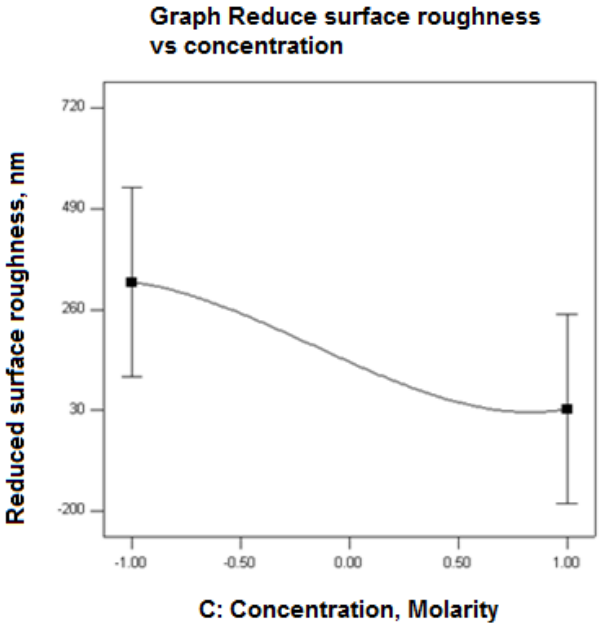

Figure 5-21 SiC reduced surface roughness (nm) versus etchant's concentration (Molarity)

5.5 CONCLUSION

Our results showed that surface roughness of MGC is solely affected by etching temperature. Generally, better surface roughness was obtained at higher temperature. In etching of BN, etching temperature and etchant are the main factors affecting surface roughness. Our results showed that better surface roughness of BN was obtained in H_3PO_4 etchant. This was observed when etching process occurred at the high temperature zone. For etching of SiC, surface roughness was influenced by etching duration, etchant and the interaction between the etchant and its concentration. The best surface roughness was obtained in HCl etchant with 6 Molarity concentration following an etching duration of 180 minutes.

Chapter 6 Development of Dimensional Accuracy Models and Experimental Studies

6.1 INTRODUCTION

Dimensional accuracy in this research is defined by the etch ratio representing the ratio between etch rate of non-indented area compared to indented area on the surface of a substrate. It forms the basis for obtaining a successful pattern on the surface of a substrate. A successful pattern is created when the etch rate at indented area is lower than non-indented area. This would correspond to obtaining an etch ratio of greater than 1. Patterning of substrate is to design and produce a desirable pattern on the substrate surface. A few methods have been introduced in the industry for micro- and nano-patterning, such as dry and wet mask patterning. Recently, a new technology has been introduced to replace mask by micro-indentation. This technique is versatile due to its low cost for initial facilities and manufacture, simplicity of process and substrate selectivity [75-77, 167, 184].

Dimensional accuracy model is established based on the etch ratio. In this study, the first and second order model were developed for etch ratio by CCD. First order model is used to study linear model and this is also to determine the nature of the process, whether the process is linear or it requires higher level model as identified by the curvature term shown in ANOVA of first order model. ANOVA in first order model will be used as analytical tool if curvature term is shown to be insignificant. Otherwise, CCD is needed to study the process. In this study, CCD is needed because this process is not linear. Thus, discussion of etch ratio is based on the result of the second order model. Predictive

models were generated for each substrate in different etchants. Experimental studies to establish relationships between substrates and etchants were reported in the later Section 6.4.

6.2 DEVELOPMENT OF FIRST ORDER DIMENSIONAL ACCURACY MODEL

First order models for etch ratio are represented in the following Tables for MGC, BN and SiC in H_3PO_4, HBr and HCl. Curvature term is significant in all the analyses shown below, which means that chemical machining of MGC, BN and SiC have to proceed to CCD for analysis.

Table 6-1 ANOVA for selected factorial model for etch ratio of MGC in H_3PO_4

Source	Sum of Squares	df	Mean Square	F Value	p-value	
Model	14.34	1	14.34	31.30	0.0113	significant
C-concentration	24.00	1	24.00	52.36	0.0054	
Curvature	25.50	1	25.50	55.64	0.005	significant

Table 6-2 ANOVA for selected factorial model for etch ratio of MGC in HBr

	Sum of Squares	df	Mean Square	F Value	p-value	
Model	25.00	1	25.00	7.58	0.07	not significant
B-duration	25.00	1	25.00	7.58	0.07	
Curvature	35.59	1	35.59	10.80	0.05	significant

Table 6-3 ANOVA for selected factorial model for etch ratio of MGC in HCl

Source	Sum of Squares	df	Mean Square	F Value	p-value	
Model	10.49	1	10.5	21.3	0.004	significant
B-duration	14.84	1	14.8	30.2	0.002	
Curvature	4.47	1	4.5	9.1	0.024	significant
Lack of Fit	2.95	5	0.6			

Table 6-4 ANOVA for selected factorial model for etch ratio of BN in H_3PO_4

Source	Sum of Squares	df	Mean Square	F Value	p-value	
Model	0.0313	1	0.0313	10.339	0.19	not significant
C-concentration	0.0313	1	0.0313	10.339	0.19	
Curvature	0.8352	1	0.8352	276.314	0.04	significant

Table 6-5 ANOVA for selected factorial model for etch ratio of BN in HBr

Source	Sum of Squares	df	Mean Square	F Value	p-value	
Model	0.0036	1	0.004	0.006	0.9445	not significant
C-concentration	0.8438	1	0.844	1.459	0.3505	
Curvature	15.5402	1	15.540	26.880	0.0352	significant

Table 6-6 ANOVA for selected factorial model for etch ratio of BN in HCl

Source	Sum of Squares	df	Mean Square	F Value	p-value	
Model	0.002060	1	0.00206	0.1536	0.7213	not significant
C-concentration	0.002604	1	0.0026	0.1942	0.6892	
Curvature	0.153612	1	0.15361	11.4579	0.0429	significant
Lack of Fit	0.026331	2	0.01317	0.9479	0.5876	not significant

Table 6-7 ANOVA for selected factorial model for etch ratio of SiC in H_3PO_4

Source	Sum of Squares	df	Mean Square	F Value	p-value	
Model	0.563	1	0.563	2.7	0.1989	not significant
B-duration	0.563	1	0.563	2.7	0.1989	
Curvature	4.688	1	4.688	22.5	0.0178	significant

Table 6-8 ANOVA for selected factorial model for etch ratio of SiC in HBr

Source	Sum of Squares	df	Mean Square	F Value	p-value	
Model	3.54	1	3.54	3.353	0.1645	not significant
C-concentration	8.17	1	8.17	7.737	0.0689	
Curvature	18.13	1	18.13	17.173	0.0255	significant
Lack of Fit	1.17	2	0.58	0.292	0.7947	not significant

Table 6-9 ANOVA for selected factorial model for etch ratio of SiC in HCl

Source	Sum of Squares	df	Mean Square	F Value	p-value	
Model	0.50	1	0.50	63660000	< 0.0001	significant
C-concentration	0.50	1	0.50	63660000	< 0.0001	
Curvature	0.25	1	0.25	63660000	< 0.0001	significant

6.3 DEVELOPMENT OF SECOND ORDER DIMENSIONAL ACCURACY MODEL

Based on the dimensional accuracy model the higher the etch ratio, the more accurate is the dimensional accuracy. As shown above, the first order model showed that this process is not a linear function model. As such, a second-order model was developed to further understand the process.

Equations (30)-(38) are predictive model developed for etch ratio in H_3PO_4, HBr and HCl for MGC, BN and SiC respectively. They are all empirical models and no special unit is required. Tables 6-10, 6-11 and 6-12 are ANOVA data for etch ratio for MGC, BN and SiC. MGC and BN were fitted to 2FI model with 96.4% and 95.6% respectively without lack of fit. While, SiC was fitted almost perfectly at 99.99% to quadratic model. Etching duration is the main factor affecting the etch ratio of MGC, BN and SiC. Other than that, BN and SiC were affected by the etchant's concentration. Other significant factors are interaction between etching temperature and etchant, etching temperature and etchant's concentration.

Etch ratio of MGC in H_3PO_4 = -1.91 + 0.042(T) + 0.023(t) - 1.40(c) - 2.62E-4(T)(t) + 0.023(T)(c) -5.71E-3(t)(c) (eq. 6-1)

Etch ratio of MGC in HBr = - 4.12E-3 + 0.017(T) + 0.029(t) - 0.68(c) - 2.62E-4(T)(t) + 0.023(T)(c) - 5.71E-3(t)(c) (eq. 6-2)

Etch ratio of MGC in HCl = - 2.16 + 0.042(T) + 0.027(t) - 0.85(c) - 2.62E-4(T)(t) + 0.023(T)(c) - 5.71E-3(t)(c) (eq. 6-3)

Etch ratio of BN in H_3PO_4 = 26.51 - 0.715(T) + 0.043(t) - 6.52(c) + 5.56E-4(T)(t) + 0.03(T)(c) + 0.025(t)(c) + 4.81E-3(T^2) - 4.55E-4(t^2) - 1.53(c^2) (eq. 6-4)

Etch ratio of BN in HBr = 61.71 - 1.18(T) + 0.093(t) - 9.76(c) + 5.56E-4(T)(t) + 0.03(T)(c) + 0.025(t)(c) + 4.81E-3(T^2) - 4.55E-4(t^2) - 1.53(c^2) (eq. 6-5)

Etch ratio of BN in HCl = 19.21- 0.69(T) + 0.071(t) - 8.34(c) + 5.56E-4(T)(t) + 0.03(T)(c) + 0.0247(t)(c) + 4.81E-3(T^2) - 4.55E-4(t^2) - 1.53(c^2) (eq. 6-6)

Etch ratio of SiC in H_3PO_4 = 0.191 - 5.788E-3(T) - 4.085E-4(t) - 2.55(c) + 7.38E-5(T)(t) - 6.405E-4(T)(c) + 8.157E-3(t)(c) (eq. 6-7)

Etch ratio of SiC in HBr = - 5.84 + 0.0582(T) + 0.0303(t) + 0.932(c) + 7.378E-5(T)(t) - 6.405E-4(T)(c) + 8.158E-3(t)(c) (eq. 6-8)

Etch ratio of SiC in HCl = 0.389 - 4.91E-3(T) - 1.62E-3(t) – 2(c) + 7.38E-5(T)(t) - 6.405E-4(T)(c) + 8.157E-3(t)(c) (eq. 6-9)

Table 6-10 ANOVA for Response Surface 2FI Model for MGC

Source	Sum of Squares	df	Mean Square	F Value	p-value	
Model	110.344	14	7.8817	2.17495	0.0376	significant
A-temperature	0.00045	1	0.0004	0.00012	0.9912	
B-duration	24.1194	1	24.119	6.6557	0.0152	
C-concentration	3.67303	1	3.673	1.0135	0.3224	
D-etchant	12.2488	2	6.1244	1.6900	0.2022	
AB	24.0021	1	24.002	6.6233	0.0154	
AC	17.2937	1	17.293	4.7721	0.0372	
Residual	105.092	29	3.6238			
Lack of Fit	95.4480	24	3.9770	2.0618	0.216	not significant

Table 6-11 ANOVA for Response Surface 2FI Model for BN

Source	Sum of Squares	df	Mean Square	F Value	p-value	
Model	227.07	17	13.35748	7.0012	0.0044	significant
A-temperature	7.2948	1	7.294831	3.8235	0.0863	
B-duration	32.692	1	32.69273	17.1357	0.0033	
C-concentration	20.530	1	20.53049	10.7609	0.0112	
D-etchant	12.550	2	6.27511	3.2890	0.0907	
AB	28.961	1	28.9611	15.179	0.0046	
AC	5.7031	1	5.70311	2.9892	0.1221	
Residual	15.262	8	1.90787			
Lack of Fit	9.4126	4	2.35316	1.6089	0.3281	not significant

Table 6-12 ANOVA for Response Surface Quadratic Model for SiC

Source	Sum of Squares	df	Mean Square	F Value	p-value	
Model	60.668	14	4.333448	32.23	< 0.0001	significant
A-temperature	7.265	1	7.26539	54.04	< 0.0001	
B-duration	4.7716	1	4.771665	35.49	0.0001	
C-concentration	1.2381	1	1.238174	9.21	0.0126	
D-etchant	14.496	2	7.248152	53.92	< 0.0001	
AB	0.5943	1	0.594312	4.42	0.0618	
AC	0.0031	1	0.003176	0.02	0.8809	
Residual	1.344	10	0.134423			
Lack of Fit	0.796	8	0.099509	0.36	0.877	not significant

6.4 DIMENSIONAL ACCURACY STUDIES

In a typical dimensional accuracy experimental study a load is applied on the substrate surface where patterning is required. Then, it undergoes the etching process. At the end of the process, measurement is taken at the indented area and non-indented area. Etch rate between non-indented area and indented areas is compared, which is called the etch ratio. Etch rate at indented area has been shown to be slower compared to normal surface area (non-indented area) because the surface that has been densified by stress enhanced the bonding of the substrate structure and delayed the chemical reaction at the indented area [6]. With different etch rate happening at indented area and non-indented area, the desired patterning is represented as shown in Chapter 2, Figure 2.7.

To achieve a higher dimensional accuracy for the development of patterning, a higher etch ratio is required, where higher etch rate occurred at non-indented area and lower etch rate at indented area. Figures 6-1, 6-2 and 6-3 show plots of etch rate at indented and non-indented area for MGC, BN and SiC. These figures indicate that etch rate at non indented area is always higher than indented area with increasing etching period. The slower rate of etching observed at the indented surface of all the substrates studied is consistent with the literature reports [76] [77]. For MGC, the peak etch rate occurred after an etching period of about 250 minutes for surface of non-indented and 180 minutes for indented surface respectively. Etch rate at both surfaces decreases simultaneously after the respective etching periods. The etch ratio in SiC shows a similar trend with etching period. The only exception is the etch ratio of BN. This actually agrees with the results presented in Section 4.4.3, where etch rate increases with etching duration. The lower etch rate at the higher etching duration is possibly due to the insoluble deposit at the indented area, which might be formed on the substrate surface with etchant [75].

In Figure 6-1 and 6-3, the etch rate for both areas are increased to a peak duration of about 190 minutes duration and decreased dramatically thereafter for MGC and SiC. The result is consistent with the observation made by Hirota et. al. where the thickness reduction of the substrate was proportionally increased with etch duration without defects [175]. In Figure 6-2, etch ratio in BN is at its highest at duration of 140 minutes longer than those observed for MGC and SiC. The longer time required for the etch ratio to peak in BN is probably due to the lower relative reactivity at the densified surface compared to the other two substrates. Another reason might be due to the contamination on substrate's surface that occurs during the indented process, which forms a protective layer on its surface and delays the etching reaction [61].

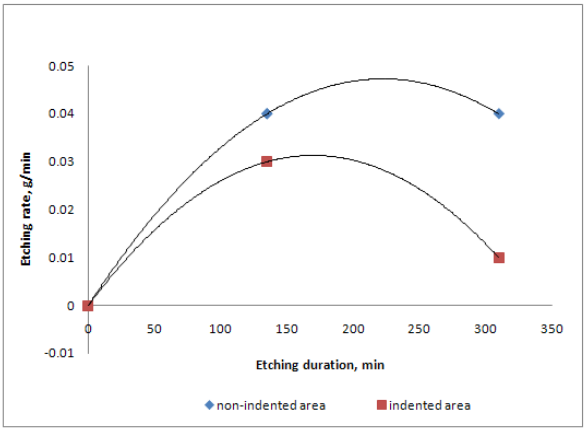

Figure 6-1 MGC etch rate of indented area and non-indented area versus etching duration (minutes)

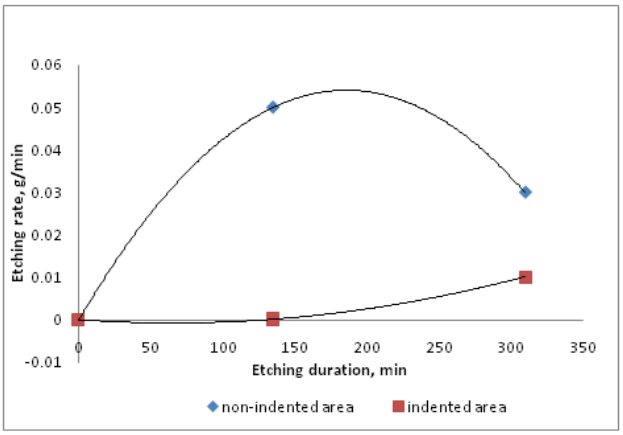

Figure 6-2 BN etch rate of indented area and non-indented area versus etching duration (minutes)

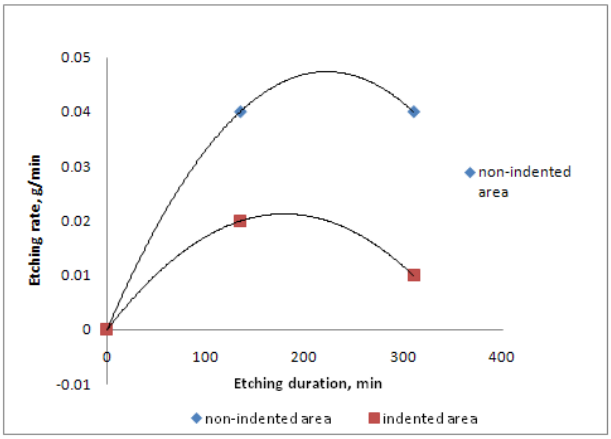

Figure 6-3 SiC etch rate of indented area and non-indented area versus etching duration (minutes)

Nagai et al. [185] successfully conducted experiment on macro-size patterning and chemical machining, which led to the formation of well-ordered patterns of surface crystal steps. Youn and Kang [77] fabricated Pyrex glass by micro-indentation with HF etching. Saito et al. [75, 76, 184] proved the feasibility of micro-machining process in fabricating glass ceramic in HF etching. These research studies showed that patterning on the glass ceramic surface become possible due to etch rate difference between indented and non-indented area. One of the key issues of this technology is to increase and control the difference of etch rate between intended and non-indented area.

6.4.1 Effect of Etching Duration

ANOVA revealed that etching duration has a significant impact on the dimensional accuracy or the etch ratio for MGC and SiC during the chemical machining process. The results presented in Figures 6-4 and 6-6, show that the etch ratio for MGC and SiC increased linearly with etching duration. Cakir et al. observed that etch ratio of non-indented to indented area increased with etching process. Similar phenomena were also observed in many research studies [75-77, 167, 184].

In this study, the best ratio of 3 was obtained for MGC and 2.3 for SiC at the respective duration of 240 minutes. The lower ratio observed for SiC could be due to the greater

hardness and the lower reactivity of the substrate to the etchant involved. For BN, it fitted well to quadratic model with 99.56%. Its peak etch ratio of 5.5 occurred around 90 minutes, but there is a notable decrease in the etch ratio thereafter. .The decrease in the etch ratio is consistent with a significant increase in the etch rate at the indented surface of BN in Fig 6.2 when the etching duration was extended beyond 200 minutes. . The protective layer formed as a result of product accumulation at the non-indented reaction site might attribute to the lower etch ratio observed in BN following the prolonged etching period. More detailed kinetic studies are required to establish the real cause for the observed phenomenon.

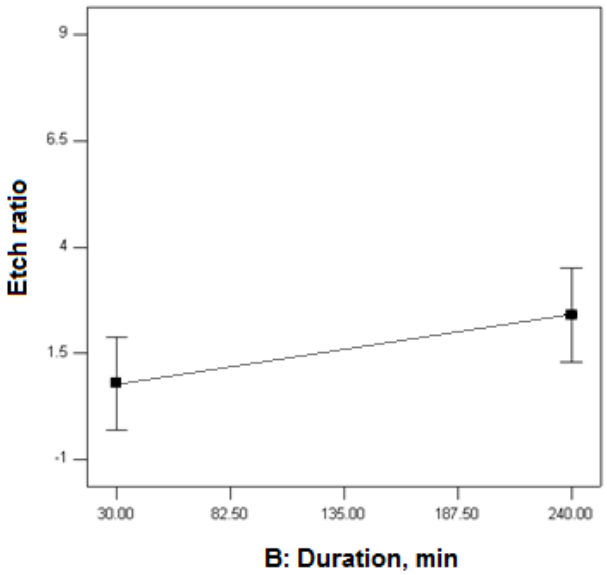

Figure 6-4 MGC etch ratio versus etching duration (minutes)

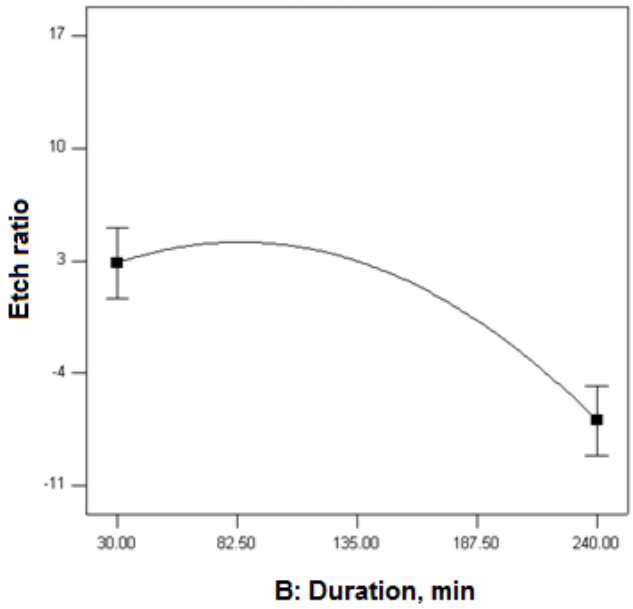

Figure 6-5 BN etch ratio versus etching duration (minutes)

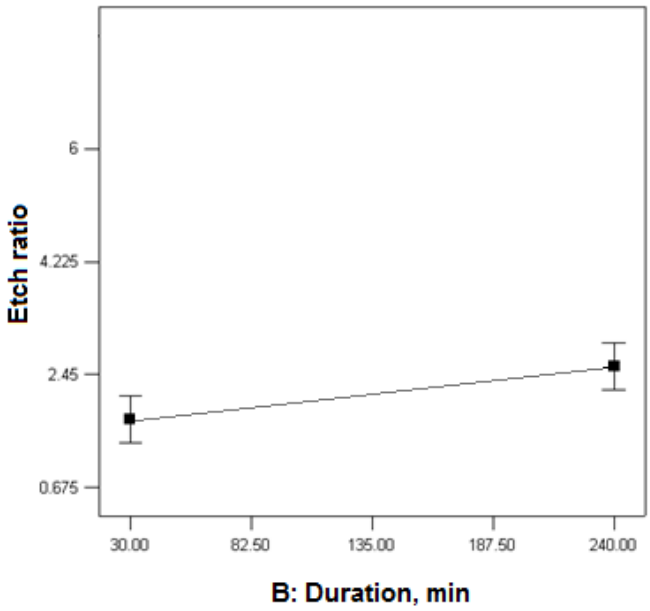

Figure 6-6 SiC etch ratio versus etching duration (minutes)

6.4.2 Effect of Etchant's Concentration

With less than 0.05 *p*-value, etchant's concentration is considered as one of the key influencing factors on etch ratio of MGC, BN and SiC. Overall, etch ratio decreased with etchant's concentration. A peak etch ratio was found in the etching of BN, occurring around 6 Molarity HBr. This means that higher etch rate difference between non-indented and indented areas could be obtained at lower etchant's concentration. Saito et al. found that higher etch ratio for glass ceramic was obtained at lower pH region [75, 76]. They also suggested that etch ratio can be controlled by etchant's concentration. The results (Figures 6-7, 6-8 and 6-9) also suggest that, in higher etchant's concentration region, the leaching reaction scarcely occurred even at non-indented area, resulting in the decrease of etch rate ratio. Leaching reaction is a technique which converts the substrate into soluble salts in aqueous media. The etching reaction of the substrate and the leaching reaction are considered to be competitive reaction. When leaching preceded the etching reaction, the etch rate would be increased. This happens when ions diffuse into the leached layer to enhance the dissolution rate. Saito et al. [184] also reported that not only alkali and alkali earth metal oxide, but also alumina in alumino silicate glass were leached out in HF etchant.

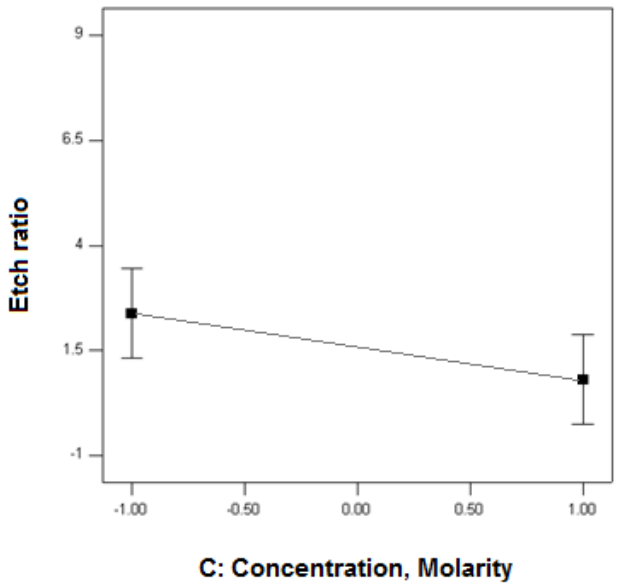

Figure 6-7 MGC etch ratio versus etchant's concentration (Molarity)

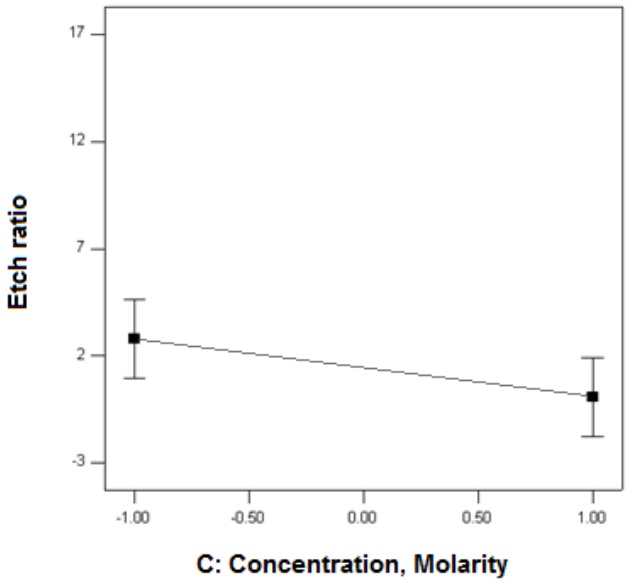

Figure 6-8 BN etch ratio versus etchant's concentration

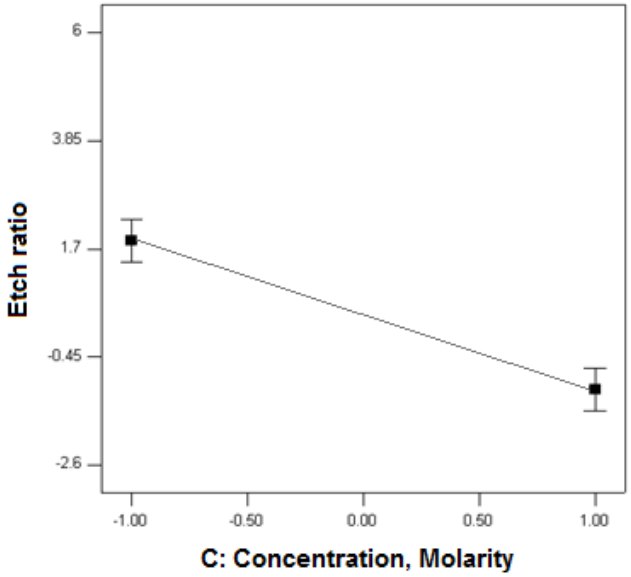

Figure 6-9 SiC etch ratio versus etchant's concentration

6.4.3 Effect of Etching Temperature

Figures 6-10, 6-11 and 6-12 show plots of the etch ratio versus etching temperature of MGC, BN and SiC. Although etching temperature plays an important role in the etch rate and surface roughness of the substrates, their influence toward the etch ratio for MGC and BN is relatively less compared to other variables studied above including the etchant concentration and etching duration. The *p*-value of temperature in MGC and BN is more than 0.05. With 95% confident interval, this means that temperature is not a significant variable bearing little influence on the etch ratio. This is also clearly reflected in Figure 6-10 and 6-11 where the changes of etch ratio is relatively small. Although higher etching temperature should lead to higher etch rate, it does not seem to affect the etch ratio significantly. Etch ratio for MGC is about 1.4 and BN is about 0.2 at room temperature. As temperature rises, etch ratio of MGC and BN showed minor increment. One of the reasons is because etch ratio is calculated by dividing etch rate at non indented area over indented area. If the etch rates for both area are increased with similar rate, this will create a phenomenon where etch ratio is relatively low or near to 1.

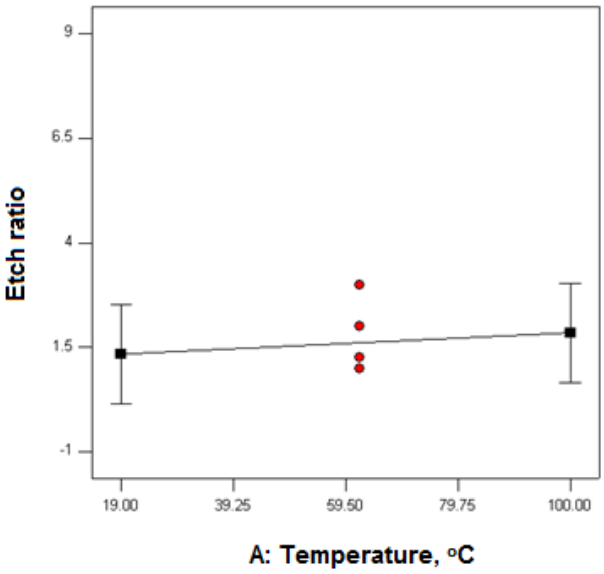

Figure 6-10 MGC etch ratio versus etching temperature (^{o}C)

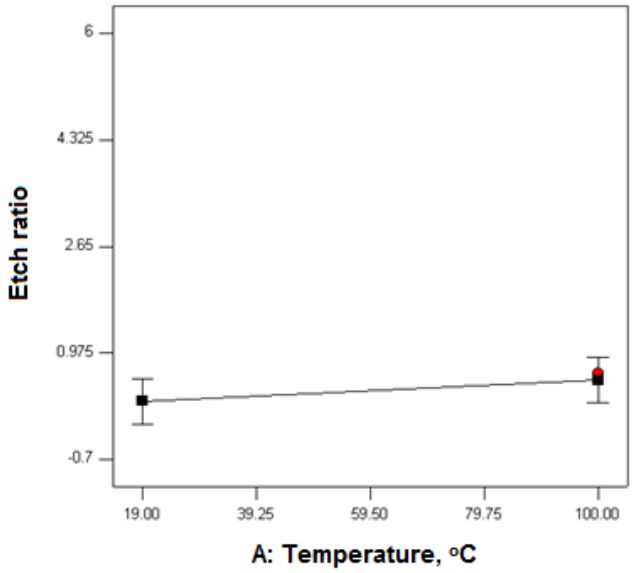

Figure 6-11 BN etch ratio versus etching temperature (^{o}C)

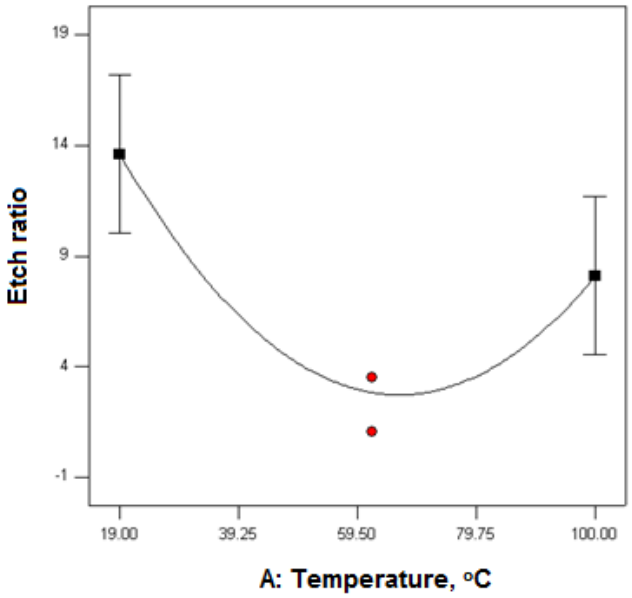

Figure 6-12 SiC etch ratio versus etching temperature (^{o}C)

Figure 6-12 shows the relationship between SiC's etch ratio and etching temperature. The etch ratio for SiC did not increase linearly with temperature as observed for MGC and

BN. Instead the etch ratio decreased from a value of 13 at 19^{o}C to a value of 3 at 65^{o}C and increased again to 8.5 at 100^{o}C. The results suggested that at lower temperature ranging from about 20^{o}C to 65^{o}C, the reactivity of the indented part of the SiC appeared to increase with temperature. However, it is interesting to note that above 65^{o}C the trend was reversed. This observation seemed to suggest that a different reaction mechanism could be involved at the higher temperature at 65^{o}C and above. Saxena and Dwivedi [166] observed that thermal annealing process was governed by two independent mechanisms, which were characterised by activation energies of 22kJmol^{-1} and 9kJmol^{-1} at switch over temperature of about 150^{o}C. A more in-depth kinetic study is warranted to support the idea of dual reaction mechanisms of SiC involved at the lower and higher range of temperature respectively.

6.4.4 Effect of Etchant

Figures 6-13, 6-14 and 6-15 show the relationship between the etch ratio and etchant in CHM of MGC, BN and SiC. The results show that the best etch ratio was obtained for all the substrates when they were etched in HBr. Data shown earlier in Table 6-10 reveals that the influence of etchant on the etch ratio is relatively small compared to the etching duration. In BN, p-value of etchant is 0.0907, which is higher than 0.05. This shows that it was less influenced by the etchants involved. However, in SiC etching, the etchant appeared to have a significant impact on the etch ratio obtained as shown in Table 6-10. As highlighted by William, not all materials were etched in all the etchants due to different material properties, and only specific solutions and concentrations are suited for certain materials [56].

Etch ratio of SiC in HBr is about 17, which is the highest value obtained compared to other etchants suggesting again the low etch rate at the indented area of SiC. For etching of SiC in HCl and H_3PO_4, the etch ratios obtained are similar, but lower at the respective values of 2.75 and 3.0. From this study we concluded that HBr served as the most effective etchant compared to HCl and H_3PO_4 for the substrates involved. However, to achieve the required patterning, proper control towards the relative etch rate at the indented and non-indented surface is necessary. Therefore, the choice of the etchant and

concentration used is critical in order to ensure a successful and the required patterning on a specific substrate.

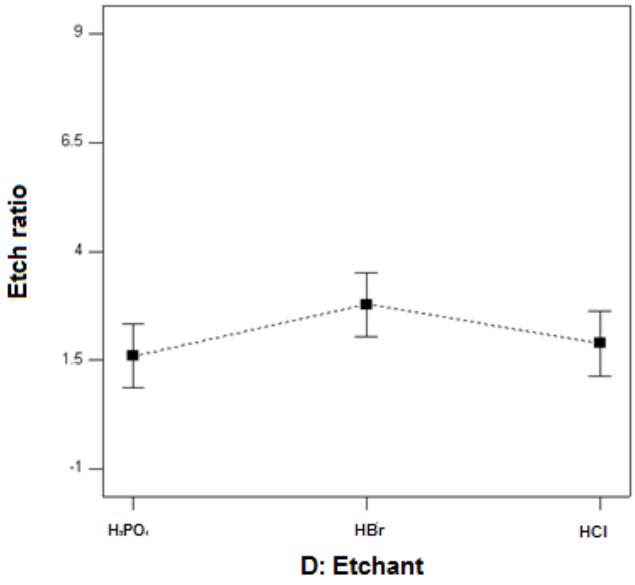

Figure 6-13 MGC etch ratio versus etchant

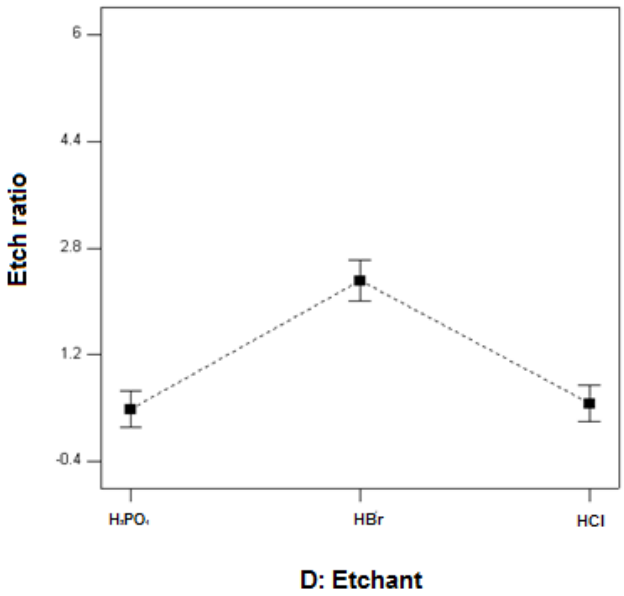

Figure 6-14 BN etch ratio versus etchant

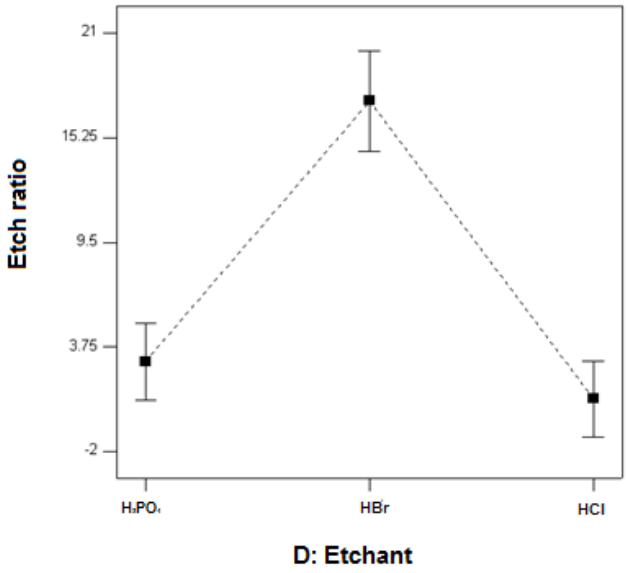

Figure 6-15 SiC etch ratio versus etchant

6.5 CONCLUSION

We concluded that the etch ratio for MGC is mainly influenced by etching duration and favourable etch ratio can be achieved at prolonged etching. For BN's etch ratio, it is strongly influenced by etching duration and the concentration of etchants. Higher etch ratio was observed at the etching duration of about 100 minutes and at relatively low etchant concentration. The etch ratio for SiC was significantly influenced by etching temperature, and etchant concentration and type of etchants, but relatively less by etching duration. Higher etch ratio was observed for SiC at prolonged etching with low etchant concentration. Relatively higher etch ratio values were observed at temperature of 19^{o}C and 100^{o}C with a minimum etch ratio at 65^{o}C. Generally, lower etch rate was found at indented area compared to non-indented area due to less reactivity at the densified areas where stronger bonding occurs between the particles at the surface of the material. Further study using a variety of load pressure would yield better patterning results.

Chapter 7 Predictive Models and Optimisation

7.1 INTRODUCTION

In this chapter, the main objective is to verify the predictive models generated by CCD. For this purpose, ANN was employed using NeuroSolution 5 as the verification software. The method for performing ANN is described in Section 3.7.1and MLP neural network was chosen for this study. The advantage of MLP is due to its ability to model the process mean and process variation simultaneously using one integrated MLP model. The ANN results will be discussed in Section 7.2.1 and this will be followed with the comparison of the ANN, RSM and the experimental results obtained respectively.

Optimisation of chemical machining of advanced ceramics is important in terms of cost and time consumed. Currently, manufacturing industries, especially semiconductor sectors require high performance of machining with less time consumed and lower production cost. In our studies, optimisation of chemical machining of all substrates is performed by using optimisation tool in DoE.

7.2 PREDICTIVE MODELS

7.2.1 ANN Results

In performing ANN, MLP was applied in the study of CHM of MGC, BN and SiC. Training of data is part of the MLP analysis. This is to estimate the parameters of the model and ensure data is not over-trained. It is then followed by validation, which is monitoring the training with a subset of the training exemplars set aside. The data would

then proceed on the testing to determine its ability to generalise. At the end of the process, mean squared error (MSE) and coefficient of determination (R^2) were checked in the training and testing. In training, MSE will decrease from the beginning of training until the lowest MSE value, where data is well trained. Sometimes, the MSE value would increase at the end of the training due to over-training. This is not a preferable scene where data has to be trained again. In testing, result of R^2 is important to determine the goodness of fit of a model. An R^2 of 1.0 indicates that the model perfectly fits with the respective data. Yet, this is not possible in reality. So, the closest value of R^2 to 1.0, the better the data fits to the respective model. Each substrate is trained with 1000 number of epochs with learning rate of 0.05. The input layer consists of four neurons (corresponding to etching temperature, etching duration, etchant and etchant's concentration) and three neurons in the output layer (corresponding to etch rate, surface roughness and etch ratio).

7.2.2 ANN Result for Boron Nitride

In the analysis of BN etch rate as shown in Figure 7-1, it was found that the MSE in training is 0.00989 without over-training. Seven set of experimental data were used as testing and the result is shown in Figure 7-2. R^2 obtained in the testing is 0.9124 and this shows that ANN model reproduces the adsorption in this system, within experimental ranges adopted in the fitting model.

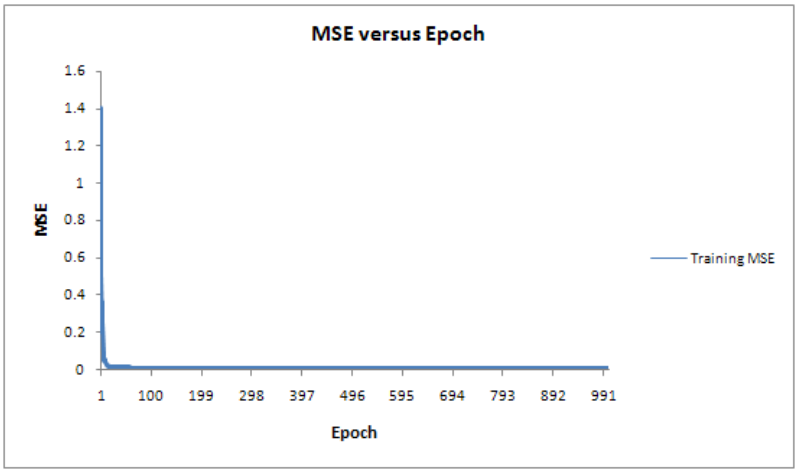

Figure 7-1 BN etch rate's variation of mean square error (MSE) in training of ANN

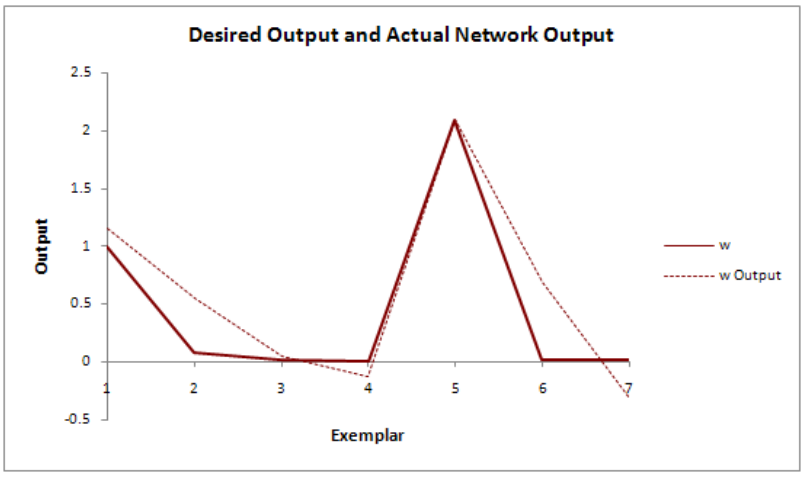

Figure 7-2 Comparison of ANN predicted and the measured of average value of BN etch rate for testing patterns.

Graph of MSE versus epoch for BN surface roughness training set is shown in Figure 7-3 and the final MSE obtained is 0.0409 without being over-trained. The fitting of model is shown in Figure 7-4, where R^2 of 0.987 was obtained with five data for testing purpose. They fit well to MLP model.

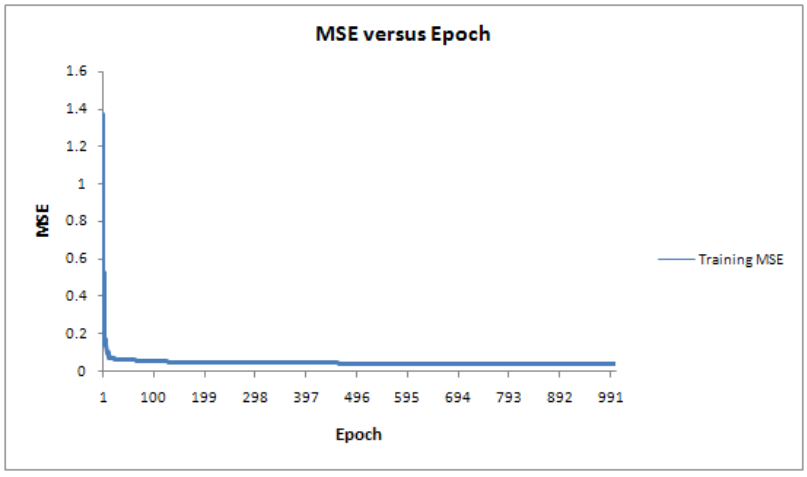

Figure 7-3 BN surface roughness's variation of mean square error (MSE) in training of ANN

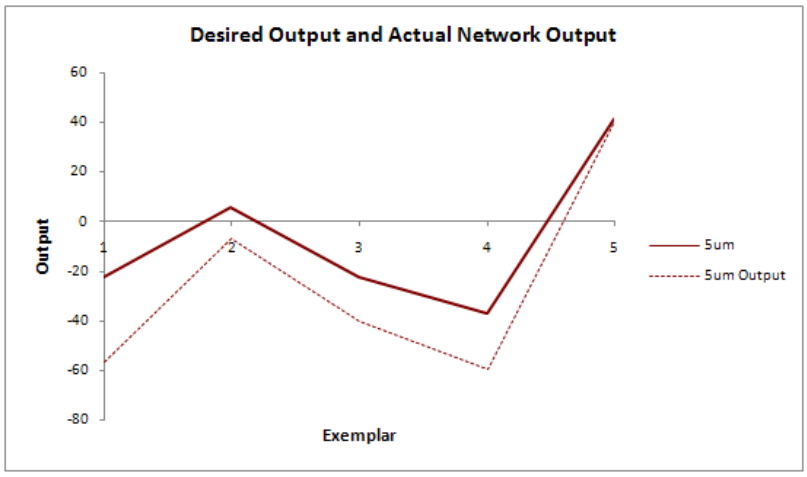

Figure 7-4 Comparison of ANN predicted and the measured of average value of BN surface roughness for testing patterns.

The best MSE obtained in training of BN etch ratio is 0.011834 with 1000 number of epochs without being over-trained (Figure 7-5). Compared to etch rate and surface roughness analysis, etch ratio required longer period to train the data. For the fitting of etch ratio model, R^2 is 0.936 as shown in Figure 7-6.

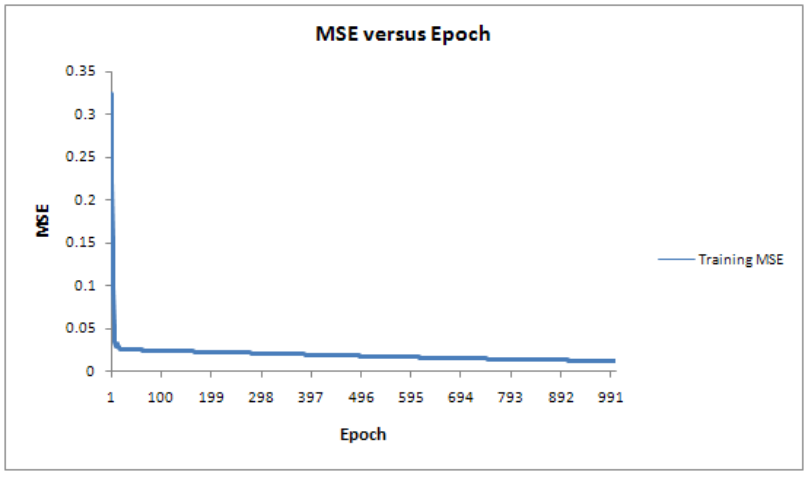

Figure 7-5 BN etch ratio's variation of mean square error (MSE) in training of ANN

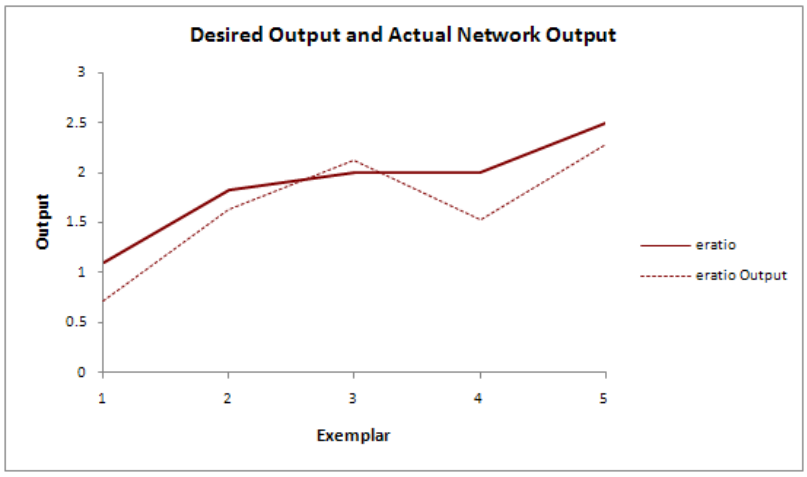

Figure 7-6 Comparison of ANN predicted and the measured of average value of BN etch ratio for testing patterns.

7.2.3 ANN Result for Machinable Glass Ceramic

Etch rate of MGC was well trained in MLP with MSE of 0.0095 and the line shown in Figure 7-7 is stable at the end of the training. Testing of MGC etch rate data is shown in Figure 7-8. It is found that the data fitted well to the model with R^2 of 0.943.

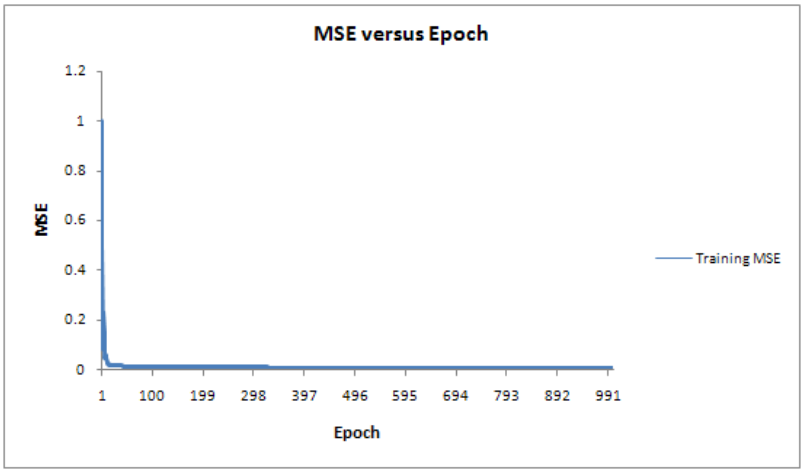

Figure 7-7 MGC etch rate's variation of mean square error (MSE) in training of ANN

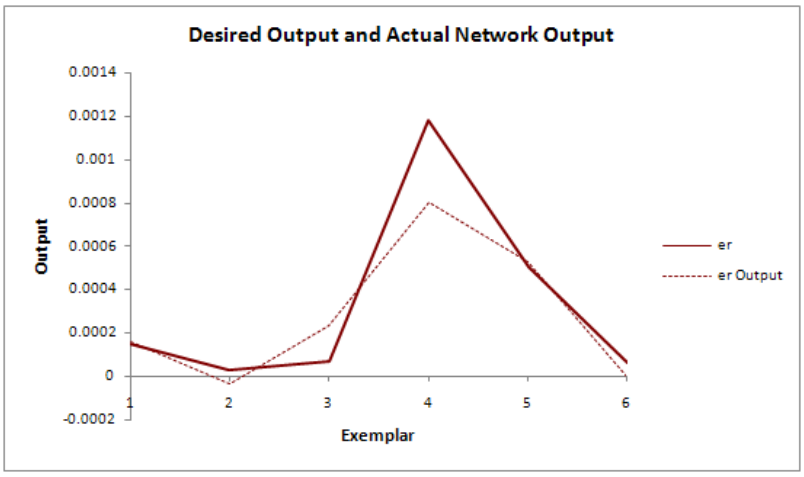

Figure 7-8 Comparison of ANN predicted and the measured of average value of MGC etch rate for testing patterns.

The MGC surface roughness training graph is shown in Figure 7-9 and the testing graph is shown in Figure 7-10. From the result obtained, it was found that the MSE for surface roughness training is 0.00125 and R^2 for testing data is 0.9823. This result shows that MLP model was able to predict the surface roughness of MGC and the data obtained fitted well to the model.

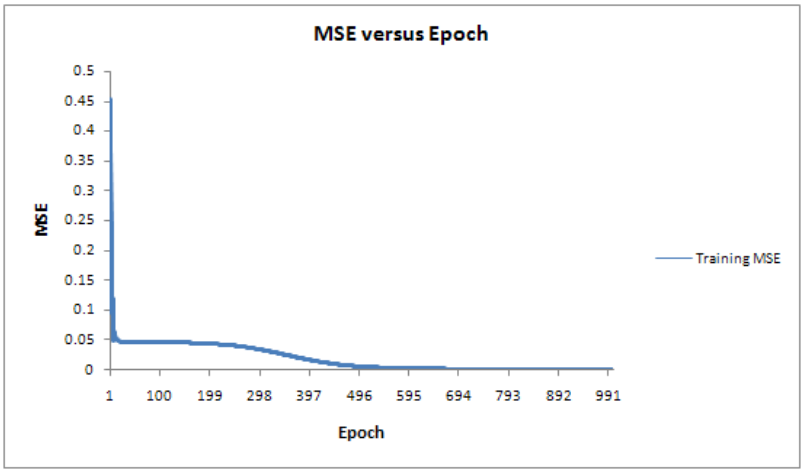

Figure 7-9 MGC surface roughness's variation of mean square error (MSE) in training of ANN

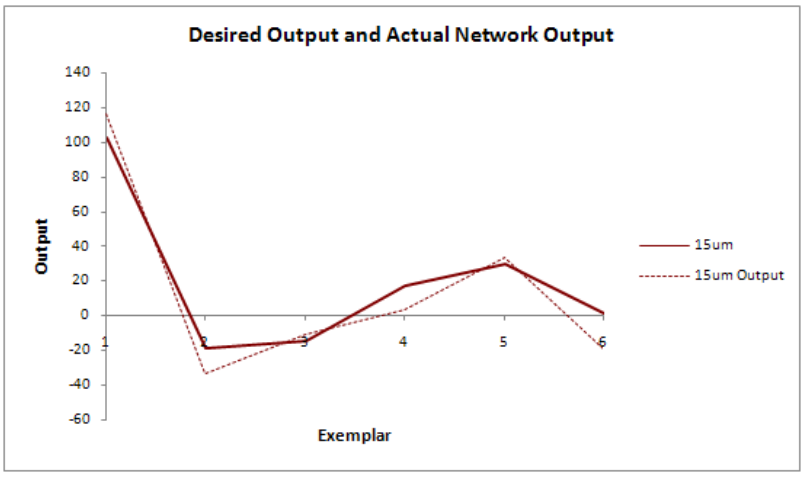

Figure 7-10 Comparison of ANN predicted and the measured of average value of MGC surface roughness for testing patterns.

The training graph of MGC etch ratio shown in Figure 7-11indicates that it was well trained with MSE of 0.0183 and there was no sign of being over-trained. As for testing, the graph of predicted result versus experimental result is depicted in Figure 7-12. R^2 of 0.967 was obtained which demonstrated that MGC etch ratio experimental data fitted well to the MLP model.

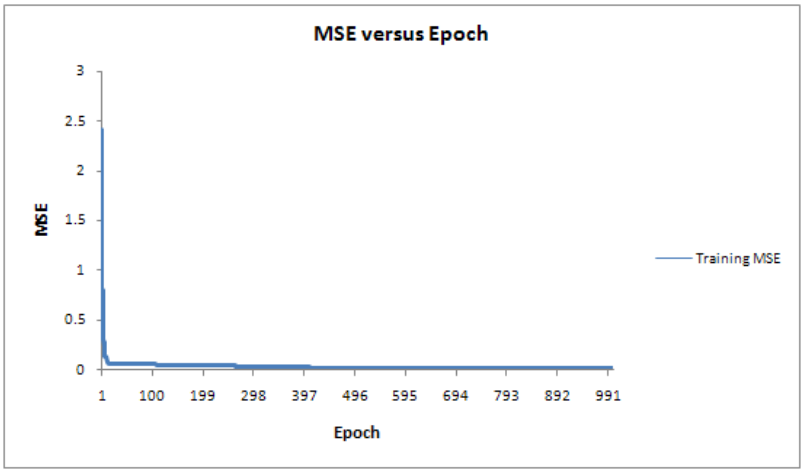

Figure 7-11 MGC etch ratio's variation of mean square error (MSE) in training of ANN

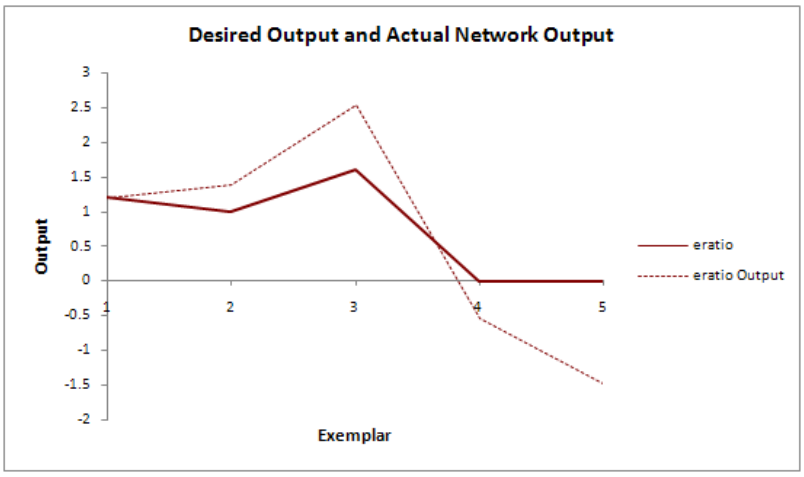

Figure 7-12 Comparison of ANN predicted and the measured of average value of MGC etch ratio for testing patterns.

7.2.4 ANN Result for Silicon Carbide

From the overall ANN analysis, SiC gives the best result compared to that of MGC and BN. In the training of SiC for etch rate, a relatively low value of MSE was obtained (0.0098) and no over-train was found in the training graph (Figure 7-13). Figure 14 shows a comparison of experimental data with predictive model of MLP. It is found that the data almost fitted perfectly or 98.9% to the predictive model.

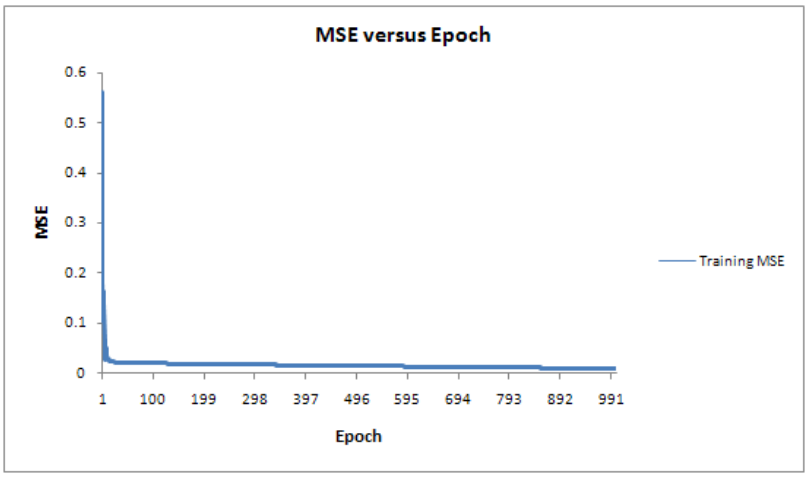

Figure 7-13 SiC etch rate's variation of mean square error (MSE) in training of ANN

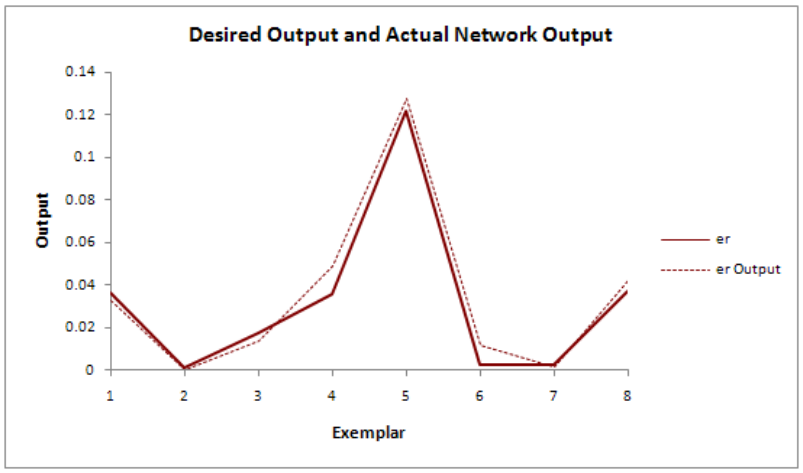

Figure 7-14 Comparison of ANN predicted and the measured of average value of SiC etch rate for testing patterns.

Figure 7-15 shows the training graph of SiC surface roughness in MLP. MSE obtained is 0.00139 and no over-train is found in the graph. This shows that SiC's surface roughness was well trained. The predictive model of MLP is shown in Figure 7.16, where R^2 of testing is 0.996.

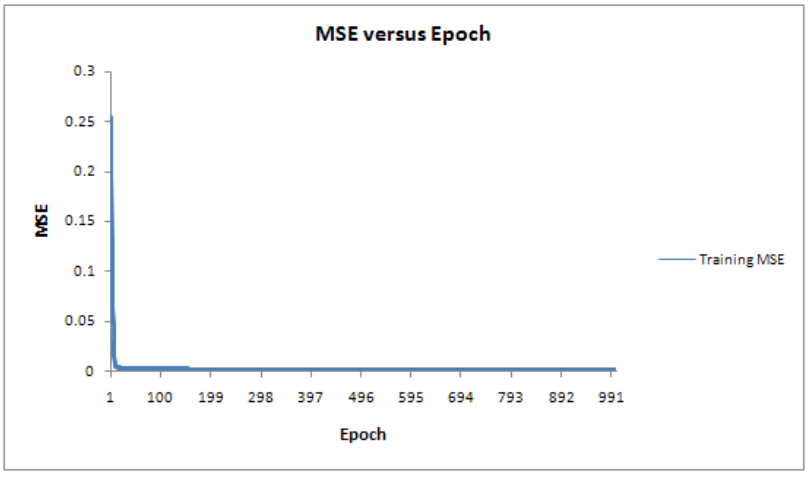

Figure 7-15 SiC surface roughness's variation of mean square error (MSE) in training of ANN

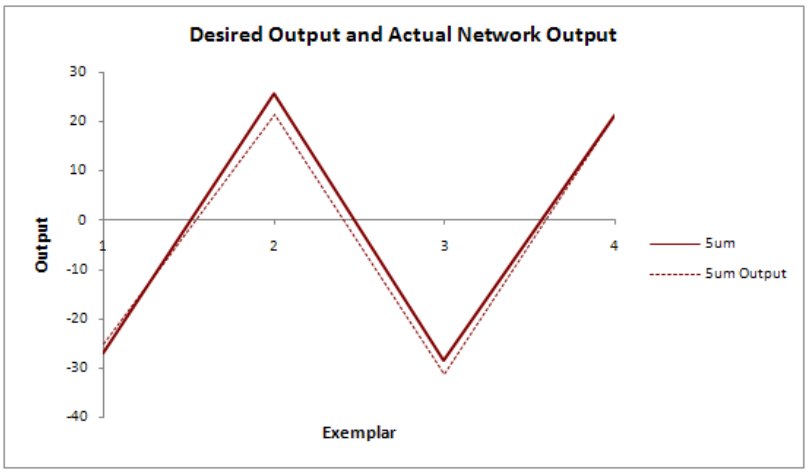

Figure 7-16 Comparison of ANN predicted and the measured of average value of SiC surface roughness for testing patterns.

Training of SiC etch ratio showed that the data is well trained with MSE of 0.0021. Figure 7-17 shows that training line of SiC etch ratio is stable at the end of the epoch. Testing of SiC etch ratio is shown in Figure 7-18, where R^2 of 0.961 was obtained. Data is well fitted to the predictive model.

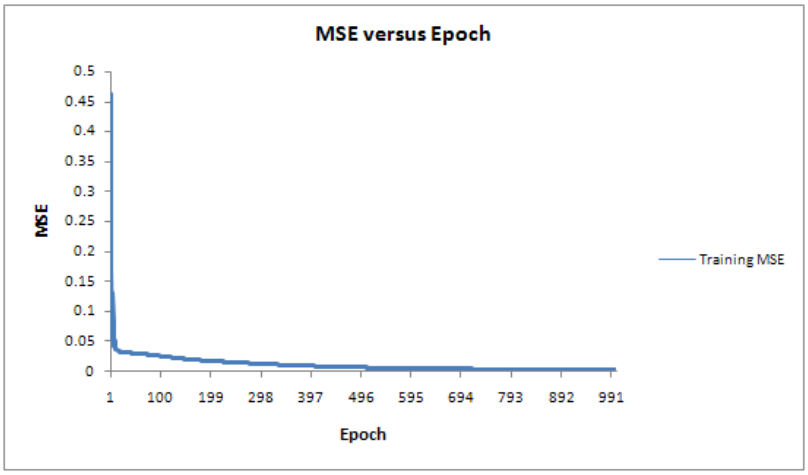

Figure 7-17 SiC etch ratio's variation of mean square error (MSE) in training of ANN

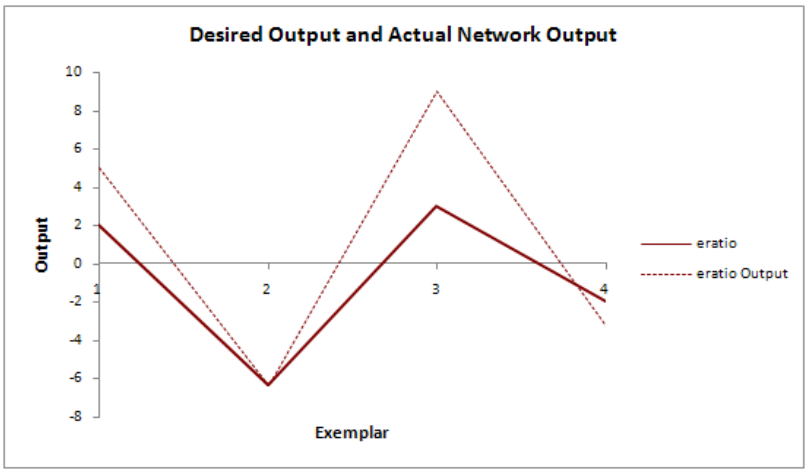

Figure 7-18 Comparison of ANN predicted and the measured of average value of SiC etch ratio for testing patterns.

7.2.5 Comparison between Artificial Neural Network and Response Surface Method

The Artificial Neural Network (ANN) analysis on the data above was performed and a predictive model was generated. These results were then drafted in the graph to facilitate comparison of results obtained from the CCD predictive model and experimental study (as shown in Tables 7-1, 7-2 and 7-3). These graphs are shown as follows: Figures 7-19, 7-20 and 7-21 show comparison for etch rate of MGC, BN and SiC respectively; Figures 7-22, 7-23 and 7-24 show comparison for reduced surface roughness of MGC, BN and SiC respectively; and, Figures 7-25, 7-26 and 7-27 show comparison of graphs for etch ratio of MGC, BN and SiC respectively.

The results obtained by CCD's predictive model clearly showed its positive impact as indicated in Figures 7-19, 7-22, 7-24 and 7-25. Overall, both techniques demonstrate a good agreement with the experimental result. With less than 10% error, CCD's predictive model performed better.

Table 7-1 Data comparison between Experimental, Predictive model by RSM and ANN for BN

	Etchant	Temp (°C)	Duration (minutes)	Etchant concentration	ETCH RATE (g/min)			SURFACE ROUGHNESS(nm)			ETCH RATIO		
					Experiment	RSM	ANN	Experiment	RSM	ANN	Experiment	RSM	ANN
1	HBr	62	135	7	0.0005	0.0003	-0.0053	-168.00	-105.73	-31.38	-0.500	15.984	-3.84
2	H_3PO_4	100	30	10	0.0000	0.0001	-0.0027	0.03	-13.99	-46.07	0.000	6.843	18.93
3	H_3PO_4	100	240	10	0.0000	-0.0001	0.0040	101.58	-11.78	-48.58	0.000	-3.426	8.52
4	H_3PO_4	62	135	12	0.0000	-0.0004	0.0022	12.98	-1.02	-32.58	0.000	2.831	-21.04
5	H_3PO_4	62	135	12	0.0000	-0.0004	0.0022	12.98	-1.02	-32.58	0.000	2.831	-21.04
6	H_3PO_4	19	30	14	0.0000	-0.0015	-0.0024	27.10	56.26	7.81	0.000	9.125	18.57
7	HCl	100	30	7	-0.0001	0.0007	0.0063	2.65	55.55	-41.50	0.000	4.684	-5.93
8	HCl	62	135	9	0.0000	0.0002	0.0011	-12.28	-30.23	-41.27	0.000	0.830	2.66
9	HCl	62	135	6	0.0000	0.0002	0.0133	-0.17	17.77	-31.96	0.250	1.743	-4.38
10	HBr	100	135	7	0.0001	0.0005	-0.0084	-166.63	-93.67	-26.35	0.500	3.578	-5.84
11	HBr	100	240	8	0.0004	0.0006	-0.0066	3.72	-174.87	-37.63	0.500	-0.993	96.74
12	H_3PO_4	62	300	12	0.0001	-0.0001	0.0039	-39.75	-45.95	-38.81	0.500	-17.020	52.12
13	H_3PO_4	62	135	12	0.0002	-0.0004	0.0022	12.98	-1.02	-32.58	0.500	2.831	-21.037
14	H_3PO_4	100	240	14	0.0000	-0.0007	-0.0023	-75.18	-30.67	-54.46	0.571	1.481	18.380
15	HBr	62	135	9	0.0005	0.0004	-0.0106	3.72	-90.51	-89.06	0.667	4.044	-9.992
16	HCl	62	0	9	0.0005	0.0003	0.0090	-87.31	98.45	-39.06	0.750	-5.099	3.759
17	HCl	100	240	11	0.0008	0.0005	-0.0084	34.61	-160.65	-45.36	0.750	1.534	-9.665
18	HBr	62	135	7	0.0000	0.0003	-0.0053	76.92	-105.73	-31.38	0.833	15.984	-3.839
19	H_3PO_4	100	30	14	0.0000	-0.0011	-0.0070	62.54	32.37	-53.44	0.875	1.357	16.531
20	H_3PO_4	62	135	9	0.0074	0.0004	0.0047	-62.55	-0.51	-19.83	1.000	0.690	-25.111
21	HCl	62	310	9	0.0002	0.0001	0.0022	-47.12	-197.03	-43.21	1.000	-16.146	9.976
22	H_3PO_4	62	135	15	0.0003	-0.0013	-0.0022	-193.00	-1.53	-44.64	1.000	-3.672	-12.354
23	HCl	19	240	1	0.0000	0.0002	0.0010	-95.61	-191.65	-71.02	1.000	-2.183	-3.057
24	HBr	19	240	4	-0.0002	0.0001	0.0051	-22.22	-213.65	-83.07	1.078	41.485	85.618

	Etchant	Temp	Duration	Etchant	ETCH RATE (g/min)			SURFACE ROUGHNESS(nm)			ETCH RATIO		
		(^oC)	(minutes)	concentration	Experiment	RSM	ANN	Experiment	RSM	ANN	Experiment	RSM	ANN
25	H_3PO_4	62	0	12	-0.0039	-0.0006	-0.0042	-35.86	35.74	-26.09	1.100	0.662	37.303
26	HBr	19	240	8	0.0001	0.0004	0.0002	-251.28	-244.39	-236.02	1.333	35.003	93.907
27	HBr	62	135	4	-0.0001	0.0002	0.0007	12.02	-120.94	9.32	1.833	19.280	4.834
28	HCl	100	240	7	-0.0023	0.0000	0.0000	41.22	-85.22	-41.68	2.000	0.263	4.638
29	HBr	100	30	8	-0.0074	0.0006	-0.0171	3.72	19.99	-33.06	2.000	-11.702	-23.632
30	HCl	19	30	11	-0.0070	-0.0002	0.0083	3.72	71.42	-62.75	2.500	1.310	11.109
31	H_3PO_4	100	135	12	0.0000	-0.0004	-0.0001	-235.73	-6.02	-50.97	2.500	8.107	-20.428
32	H_3PO_4	0	135	12	-0.0009	-0.0004	0.0050	9.72	7.13	39.84	2.500	24.021	-21.580
33	HBr	62	135	7	0.0012	0.0003	-0.0053	-43.40	-105.73	-31.38	2.667	15.984	-3.839
34	HCl	62	135	9	0.0002	0.0002	0.0011	-348.52	-30.23	-41.27	3.000	0.830	2.657
35	HCl	100	135	11	0.0008	0.0005	-0.0108	3.08	-57.64	-45.75	3.500	3.560	6.004
36	HCl	19	30	7	0.0074	0.0001	0.0246	-22.22	112.16	-15.51	3.500	15.348	-12.941
37	HCl	19	240	7	-0.0009	0.0000	0.0124	-37.05	-85.66	-28.05	3.500	1.462	10.787
38	HCl	62	135	9	0.0007	0.0002	0.0011	-22.22	-30.23	-41.27	4.000	0.830	2.657
39	HCl	62	135	9	0.0004	0.0002	0.0011	-47.12	-30.23	-41.27	4.500	0.830	2.657
40	H_3PO_4	19	240	14	0.0000	-0.0005	0.0046	106.84	-63.84	-12.04	16.000	-0.216	16.135
41	HBr	62	310	7	0.0004	0.0003	0.0024	-47.12	-263.23	-40.84	5.000	2.956	3.000
42	H_3PO_4	19	30	10	-0.0010	0.0000	0.0021	99.84	40.47	45.74	0.387	19.527	22.964
43	H_3PO_4	19	240	10	0.0191	0.0004	0.0087	-36.22	-14.38	22.22	1.726	-0.207	6.247
44	HBr	19	30	6	-0.0002	0.0002	0.0057	-22.22	-26.99	-62.06	2.123	50.635	6.563
45	HBr	100	240	6	0.0008	0.0000	-0.0001	-22.22	-174.70	-21.49	1.301	0.574	88.117
46	HBr	100	30	6	-0.0001	0.0007	-0.0080	5.77	-45.09	-14.43	-1.245	0.258	-3.224
47	H_3PO_4	62	135	12	-0.0023	-0.0004	0.0022	-32.90	-1.02	-32.58	-0.352	2.831	-21.037
48	HBr	0	135	7	0.0001	0.0001	0.0009	-301.12	-125.41	-241.09	0.358	66.026	-0.333
49	HBr	62	0	7	0.0005	0.0004	-0.0076	-30.42	15.78	-22.61	1.608	7.010	2.750

	Etchant	Temp	Duration	Etchant	ETCH RATE (g/min)			SURFACE ROUGHNESS(nm)			ETCH RATIO		
		(^{o}C)	(minutes)	concentration	Experiment	RSM	ANN	Experiment	RSM	ANN	Experiment	RSM	ANN
50	HBr	62	0	7	0.0005	0.0004	-0.0076	-30.42	15.78	-22.61	1.608	7.010	2.750
51	HBr	62	135	7	0.0001	0.0003	-0.0053	-34.31	-105.73	-31.38	1.431	15.984	-3.839
52	HCl	0	135	9	0.0005	-0.0001	0.0136	-47.12	-20.43	-61.37	2.034	20.474	1.683
53	HCl	100	30	9	0.0006	0.0007	-0.0012	-68.02	50.46	-43.79	-0.038	1.655	6.262
54	HCl	62	135	12	0.0006	0.0003	-0.0089	-4.82	-78.23	-52.10	1.862	-8.726	7.538

Table 7-2 Data comparison between Experimental, Predictive model by RSM and ANN for MGC

	Etchant	Temp (°C)	Duration (minutes)	Etchant concentration	ETCH RATE (g/min)			SURFACE ROUGHNESS(nm)			ETCH RATIO		
					Experiment	RSM	ANN	Experiment	RSM	ANN	Experiment	RSM	ANN
1	H_3PO_4	62	135	9	0.00003	-.00011	-0.00006	89.400	119.48	90.239	1.833	2.829	1.140
2	HBr	62	135	4	0.00013	0.00026	0.00023	10.062	-19.54	13.424	4.000	2.735	2.912
3	HCl	62	135	6	0.00027	0.00029	0.00022	-24.629	-11.63	-20.187	3.000	2.197	1.083
4	H_3PO_4	19	30	10	-0.00059	-.00035	-0.00030	23.358	21.97	25.450	0.000	0.555	-0.580
5	H_3PO_4	19	240	10	0.00013	0.00003	0.00005	83.918	87.39	81.286	8.000	5.586	2.189
6	H_3PO_4	100	30	10	0.00024	0.00036	0.00026	61.352	63.57	68.893	3.963	1.400	3.963
7	H_3PO_4	100	240	10	0.00015	0.00022	0.00016	102.757	126.13	116.112	3.000	1.974	2.438
8	HBr	19	30	6	0.00003	-.00001	-0.00004	-18.688	-6.14	-33.569	0.514	1.439	0.514
9	HBr	19	240	6	0.00007	-.00003	0.00023	-14.458	-24.02	-10.586	9.000	7.602	7.867
10	HBr	100	30	6	0.00118	0.00112	0.00080	17.192	27.69	3.244	1.500	0.302	2.691
11	HBr	100	240	6	0.00051	0.00058	0.00053	29.473	6.93	33.667	0.010	2.008	0.369
12	HCl	19	240	7	0.00001	0.00010	0.00031	-30.975	-16.03	-22.786	1.268	5.703	1.268
13	HCl	19	30	7	0.00007	-.00004	0.00000	1.651	6.08	-18.941	1.200	-0.118	1.185
14	HCl	100	30	7	0.00124	0.00097	0.00058	28.417	33.03	18.784	1.000	0.769	1.371
15	HCl	100	240	7	0.00059	0.00058	0.00044	7.574	8.05	6.940	1.600	2.132	2.527
16	H_3PO_4	0	135	12	0.00000	-.00002	-0.00018	-3.883	-22.38	-14.623	0.000	1.220	-0.538
17	H_3PO_4	62	0	12	0.00000	-.00012	-0.00015	-25.939	-38.75	-34.858	0.000	0.670	-1.483
18	H_3PO_4	62	135	12	-0.00001	-.00014	-0.00012	32.197	12.07	25.783	1.000	1.611	1.442
19	H_3PO_4	62	135	12	0.00002	-.00014	-0.00012	32.197	12.07	25.783	2.000	1.611	1.442
20	H_3PO_4	62	310	12	-0.00005	0.00003	0.00007	81.188	77.95	86.500	1.000	2.831	1.389
21	H_3PO_4	62	135	12	-0.00015	-.00014	-0.00012	42.197	12.07	25.783	1.250	1.611	1.442
22	H_3PO_4	62	135	12	-0.00026	-.00014	-0.00012	42.197	12.07	25.783	3.000	1.611	1.442
23	H_3PO_4	100	135	12	0.00003	-.00011	-0.00006	89.400	119.48	90.239	4.511	1.851	4.511
24	HBr	0	135	7	0.00013	.00026	0.00023	10.062	-19.54	13.424	0.000	3.858	1.608

	Etchant	Temp	Duration	Etchant	ETCH RATE (g/min)			SURFACE ROUGHNESS(nm)			ETCH RATIO		
		(°C)	(minutes)	concentration	Experiment	RSM	ANN	Experiment	RSM	ANN	Experiment	RSM	ANN
25	HBr	62	0	7	0.00003	-0.0001	-0.0001	50.237	33.19	47.973	0.000	1.063	0.936
26	HBr	62	135	7	0.00013	0.00026	0.00023	-6.219	5.47	-5.087	2.593	2.732	2.593
27	HBr	62	135	7	0.00027	0.00029	0.00022	37.051	36.71	42.037	2.593	2.732	2.593
28	HBr	62	135	7	-0.00059	-0.0004	-0.0003	19.912	33.97	21.208	4.000	2.732	2.593
29	HBr	62	135	7	0.00013	0.00003	0.00005	19.912	33.97	21.208	1.667	2.732	2.593
30	HBr	62	310	7	0.00024	0.00036	0.00026	19.912	33.97	21.208	3.424	4.896	3.424
31	HBr	100	135	7	0.00015	0.00022	0.00016	19.912	33.97	21.208	1.000	2.042	1.581
32	HCl	0	135	9	0.00003	-0.00001	-.00004	19.897	30.43	10.488	0.000	1.486	-0.299
33	HCl	62	0	9	0.00007	-0.00003	0.00023	36.573	51.44	38.773	0.000	0.459	-0.186
34	HCl	62	310	9	0.00118	0.00112	0.00080	27.208	15.04	18.048	3.826	3.787	3.826
35	HCl	62	135	9	0.00051	0.00058	0.00053	52.024	43.72	53.586	-1.000	1.908	1.117
36	HCl	62	135	9	0.00001	0.00010	0.00031	27.759	31.21	29.567	2.000	1.908	1.117
37	HCl	62	135	9	0.00007	-0.00004	0.00000	48.339	38.27	48.523	1.117	1.908	1.117
38	HCl	62	135	9	0.00124	0.00097	0.00058	48.339	38.27	48.523	1.117	1.908	1.117
39	HCl	100	135	9	0.00059	0.00058	0.00044	48.339	38.27	48.523	3.000	2.167	3.348
40	H_3PO_4	19	30	14	0.00000	-0.00002	-0.0002	48.339	38.27	48.523	0.000	-1.706	0.080
41	H_3PO_4	19	240	14	0.00000	-0.00012	-0.0002	63.220	52.51	66.447	0.000	0.925	1.293
42	H_3PO_4	100	30	14	-0.00001	-0.00014	-0.0001	-164.405	-126.2	-132.70	2.500	2.928	3.591
43	H_3PO_4	100	240	14	0.00002	-0.00014	-0.0001	-41.548	-30.46	-36.696	1.500	1.101	3.666
44	HBr	19	30	8	-0.00005	0.00003	0.00007	-89.600	-74.91	-81.491	1.000	0.625	0.162
45	HBr	19	240	8	-0.00015	-0.00014	-0.0001	13.239	17.96	18.559	8.000	4.388	6.634
46	HBr	100	30	8	-0.00026	-0.00014	-.00012	62.711	37.28	69.444	5.500	3.276	3.594
47	HBr	100	240	8	0.00003	-0.00011	-.00006	55.880	49.70	51.653	2.000	2.582	0.689
48	HCl	19	240	11	0.00013	0.00026	0.00023	97.804	80.79	93.341	1.125	2.149	0.782
49	HCl	19	30	11	0.00027	0.00029	0.00022	50.237	33.19	47.973	1.250	-1.272	2.327

	Etchant	Temp	Duration	Etchant	ETCH RATE (g/min)			SURFACE ROUGHNESS(nm)			ETCH RATIO		
		(°C)	(minutes)	concentration	Experiment	RSM	ANN	Experiment	RSM	ANN	Experiment	RSM	ANN
50	HCl	100	30	11	0.00056	0.00045	0.00063	89.467	90.34	83.070	1.000	3.403	0.453
51	HCl	100	240	11	0.00005	0.00007	0.00018	56.840	53.39	63.514	5.000	2.367	3.440
52	H_3PO_4	62	135	15	0.00016	0.00001	-0.0001	41.875	45.18	33.759	0.667	0.393	1.545
53	HBr	62	135	9	0.00073	0.00078	0.00075	70.028	81.82	71.704	1.000	2.730	2.410
54	HCl	62	135	12	0.00044	0.00031	0.00047	91.408	87.15	99.145	2.000	1.620	1.137

Table 7-3 Data comparison between Experimental, Predictive model by RSM and ANN for SiC

	Etchant	Temp (°C)	Duration (minutes)	Etchant concentration	ETCH RATE (g/min)			SURFACE ROUGHNESS(nm)			ETCH RATIO		
					Experiment	RSM	ANN	Experiment	RSM	ANN	Experiment	RSM	ANN
1	H_3PO_4	62	135	9	0.104	0.180	0.083	14.867	13.824	14.442	5.059	2.889	5.059
2	HBr	62	135	4	0.000	0.000	0.061	-27.710	-19.223	-19.248	-11.328	-0.864	-11.328
3	HCl	62	135	6	0.000	0.000	0.139	-5.577	-5.166	-7.534	2.000	2.065	6.692
4	H_3PO_4	19	30	9	0.000	0.000	-0.012	-3.417	-4.040	-2.472	2.500	2.424	-0.513
5	H_3PO_4	19	240	9	-0.001	0.215	0.029	44.741	45.942	43.339	1.000	0.920	-2.928
6	H_3PO_4	100	30	9	0.000	0.000	0.029	-10.168	-10.365	-13.241	2.000	2.187	3.801
7	H_3PO_4	100	240	9	0.000	0.215	-0.003	36.792	38.755	39.776	2.000	1.938	0.587
8	HBr	19	30	4	0.000	0.000	-0.024	-41.075	-40.290	-40.378	-7.037	-4.945	-7.037
9	HBr	19	240	4	0.000	0.000	0.013	14.192	11.770	13.456	0.000	0.013	1.330
10	HBr	100	30	4	0.000	0.000	0.015	-20.338	-37.482	-30.889	0.000	0.000	-3.319
11	HBr	100	240	4	0.000	0.000	-0.007	15.051	13.717	12.898	6.000	6.213	4.285
12	HCl	19	30	7	1.000	0.000	0.586	-26.979	-22.892	-25.089	2.000	2.060	5.042
13	HCl	19	240	7	0.000	0.000	0.023	25.694	24.885	21.429	-6.365	0.300	-6.365
14	HCl	100	30	7	0.000	0.000	0.067	-28.588	-27.716	-31.352	3.000	1.893	9.012
15	HCl	100	240	7	0.000	0.000	-0.108	21.337	19.200	21.450	-2.000	1.389	-3.291
16	H_3PO_4	0	135	12	0.000	-0.022	0.006	27.588	29.461	28.005	0.000	0.136	-0.853
17	H_3PO_4	62	0	12	0.000	-0.015	0.008	-8.879	-9.734	-8.852	0.000	-0.168	1.158
18	H_3PO_4	62	135	12	0.003	0.001	-0.002	28.306	22.571	24.162	2.000	0.395	2.179
19	H_3PO_4	62	135	12	0.000	0.001	-0.002	21.429	22.571	24.162	1.667	0.395	2.179
20	H_3PO_4	62	135	12	0.000	0.001	-0.002	21.429	22.571	24.162	2.000	0.395	2.179
21	H_3PO_4	62	310	12	0.000	0.179	0.008	59.831	64.448	63.113	-3.941	1.124	-3.941
22	H_3PO_4	62	170	12	0.000	0.022	-0.012	39.214	30.946	32.461	0.333	0.540	0.637
23	H_3PO_4	100	135	12	-0.010	-0.010	-0.021	17.722	18.348	18.214	0.667	0.553	3.970
24	HBr	0	135	8	0.000	-0.022	0.004	-6.331	-3.944	-5.269	0.000	-1.739	1.001

	Etchant	Temp	Duration	Etchant	ETCH RATE (g/min)			SURFACE ROUGHNESS(nm)			ETCH RATIO		
		(^{o}C)	(minutes)	concentration	Experiment	RSM	ANN	Experiment	RSM	ANN	Experiment	RSM	ANN
25	HBr	62	0	7	0.000	0.122	0.007	-39.768	-37.483	-34.483	0.000	-2.231	-4.921
26	HBr	62	135	7	0.000	0.000	-0.007	-5.116	-3.843	-4.537	2.000	2.486	3.604
27	HBr	62	310	7	0.000	0.000	0.002	39.038	39.766	39.469	102.377	8.600	102.377
28	HBr	100	135	7	0.000	-0.010	-0.027	-5.323	-3.781	-2.555	5.500	5.076	5.166
29	HBr	62	135	7	0.000	0.000	-0.007	-5.116	-3.843	-4.537	2.000	2.486	3.604
30	HBr	62	135	7	0.000	0.000	-0.007	-5.116	-3.843	-4.537	3.000	2.486	3.604
31	HBr	62	135	7	0.000	0.000	-0.007	-5.116	-3.843	-4.537	3.604	2.486	3.604
32	HCl	0	135	9	0.000	-0.022	0.178	8.508	8.907	6.706	0.000	0.170	-1.608
33	HCl	62	0	9	0.000	0.122	0.156	-26.883	-27.721	-27.351	0.000	0.085	6.162
34	HCl	62	310	9	0.000	0.000	-0.042	45.472	43.207	45.756	1.000	0.999	-4.002
35	HCl	62	135	9	0.000	0.000	-0.065	5.283	3.167	5.560	1.079	0.483	1.079
36	HCl	62	135	9	0.000	0.000	-0.065	5.283	3.167	5.560	0.333	0.483	1.079
37	HCl	62	135	9	0.000	0.000	-0.065	5.283	3.167	5.560	0.690	0.483	1.079
38	HCl	62	135	9	0.000	0.000	-0.065	5.283	3.167	5.560	1.000	0.483	1.079
39	HCl	100	135	9	0.000	-0.010	-0.089	2.286	-0.352	1.098	0.500	0.675	2.664
40	H_3PO_4	19	30	14	0.000	0.000	0.032	8.470	8.029	10.245	0.027	-2.203	0.027
41	H_3PO_4	19	240	14	0.000	0.000	-0.008	55.095	59.466	54.087	-0.250	-0.281	1.085
42	H_3PO_4	100	30	14	0.000	0.000	0.007	-5.959	-2.787	-3.793	4.233	-2.544	4.233
43	H_3PO_4	100	240	14	0.001	0.001	0.007	50.141	47.789	48.658	4.040	0.633	4.598
44	HBr	19	30	8	0.000	0.214	0.043	-18.854	-20.324	-23.108	-0.214	-2.615	3.186
45	HBr	19	240	8	0.000	0.000	-0.015	33.965	33.191	31.845	114.702	5.769	114.702
46	HBr	100	30	8	0.001	0.214	0.002	-20.338	-22.006	-16.747	2.000	2.226	6.963
47	HBr	100	240	8	0.000	0.000	-0.007	29.682	30.648	27.311	117.226	11.865	117.226
48	HCl	19	30	11	0.000	0.214	0.119	-10.599	-11.317	-8.607	1.333	-1.482	2.241
49	HCl	19	240	11	0.000	0.000	-0.075	38.248	37.916	36.300	3.500	0.185	3.462

	Etchant	Temp	Duration	Etchant	ETCH RATE (g/min)			SURFACE ROUGHNESS(nm)			ETCH RATIO		
		(^{o}C)	(minutes)	concentration	Experiment	RSM	ANN	Experiment	RSM	ANN	Experiment	RSM	ANN
50	HCl	100	30	1	0.000	0.214	-0.079	-16.939	-20.631	-19.308	20.000	-1.752	6.030
51	HCl	100	240	1	0.000	0.000	0.166	30.204	27.740	32.944	1.000	1.170	6.638
52	H_3PO_4	62	135	1.68	0.000	0.000	-0.022	31.191	31.318	32.005	2.944	-2.099	2.944
53	HBr	62	135	1.68	0.000	0.179	-0.033	11.552	11.538	8.887	100.000	5.836	94.815
54	HCl	62	135	1.68	0.000	0.180	-0.022	12.716	11.499	15.990	3.353	-1.099	3.353

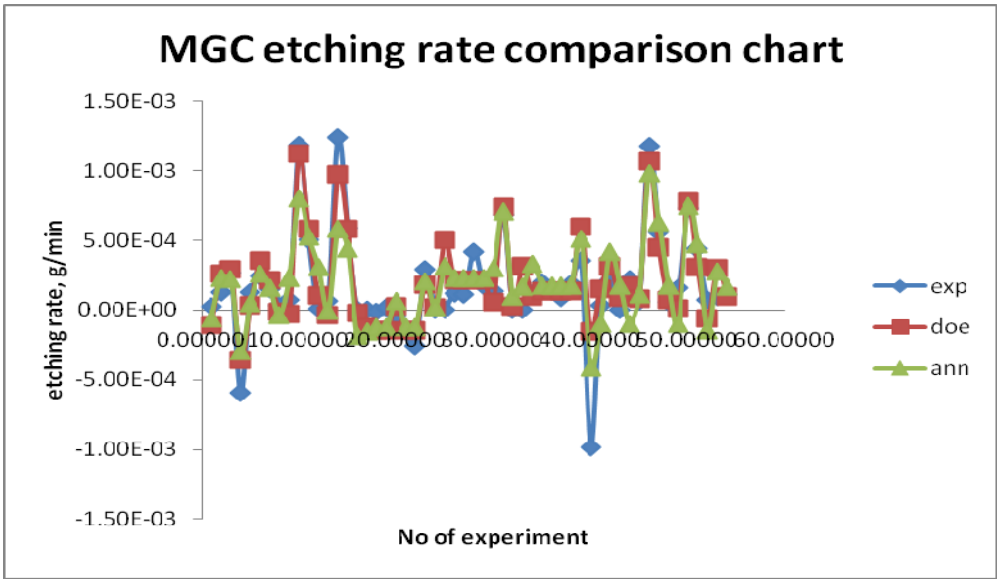

Figure 7-19 Predictive of MGC etch rate by RSM and ANN compared to experimental result

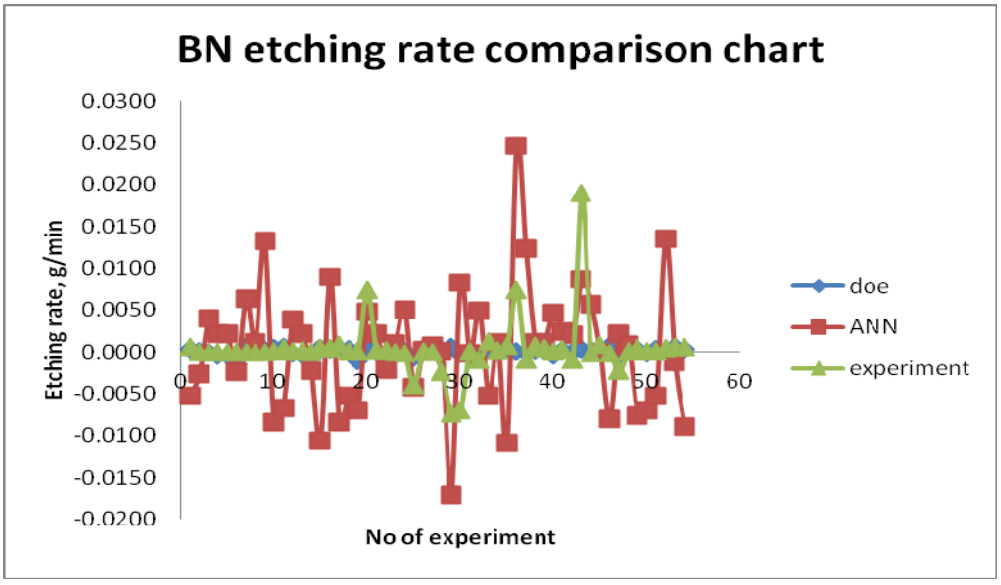

Figure 7-20 Predictive of BN etch rate by RSM and ANN compared to experimental result

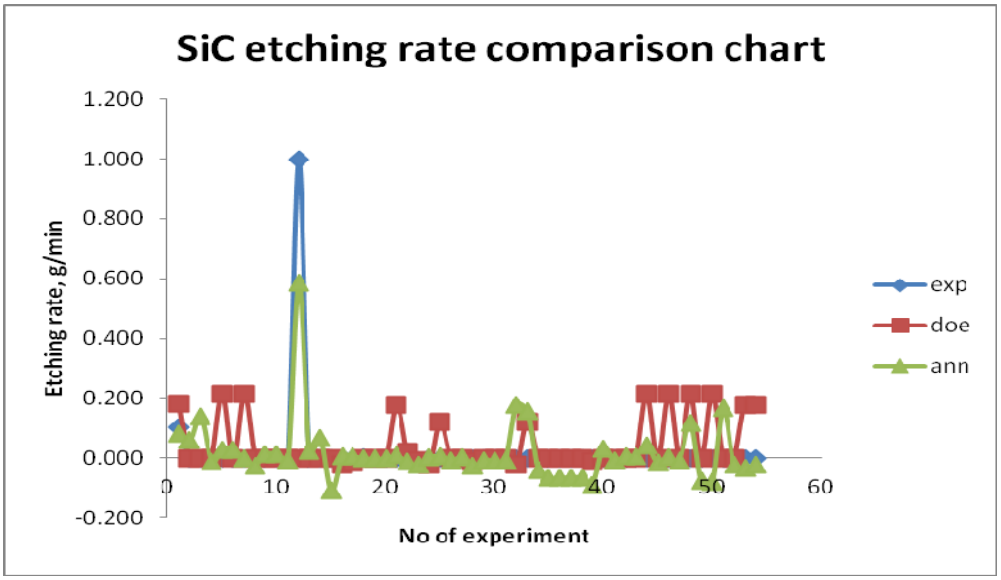

Figure 7-21 Predictive of MGC etch rate by RSM and ANN compared to experimental result

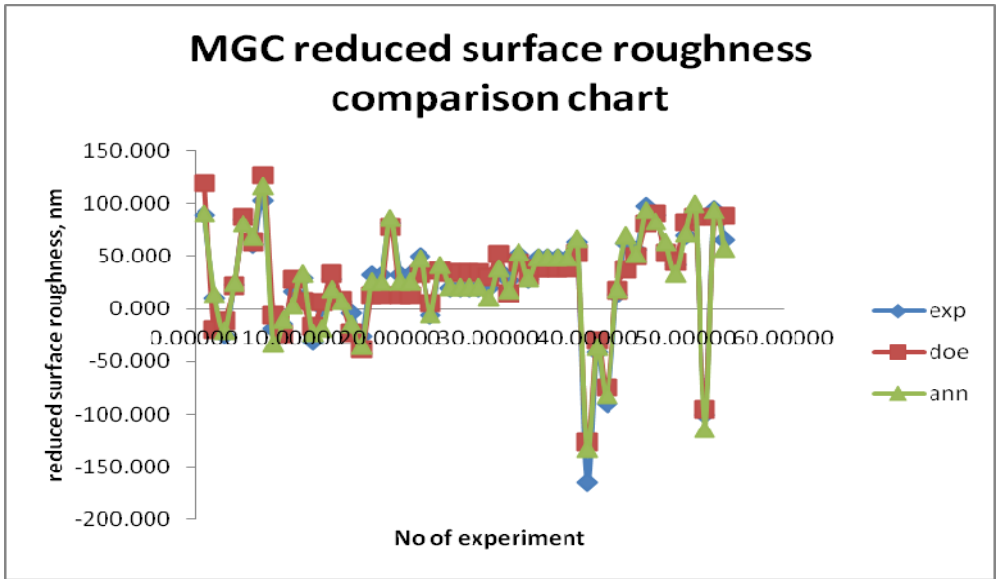

Figure 7-22 Predictive of MGC reduced surface roughness by RSM and ANN compared to experimental result

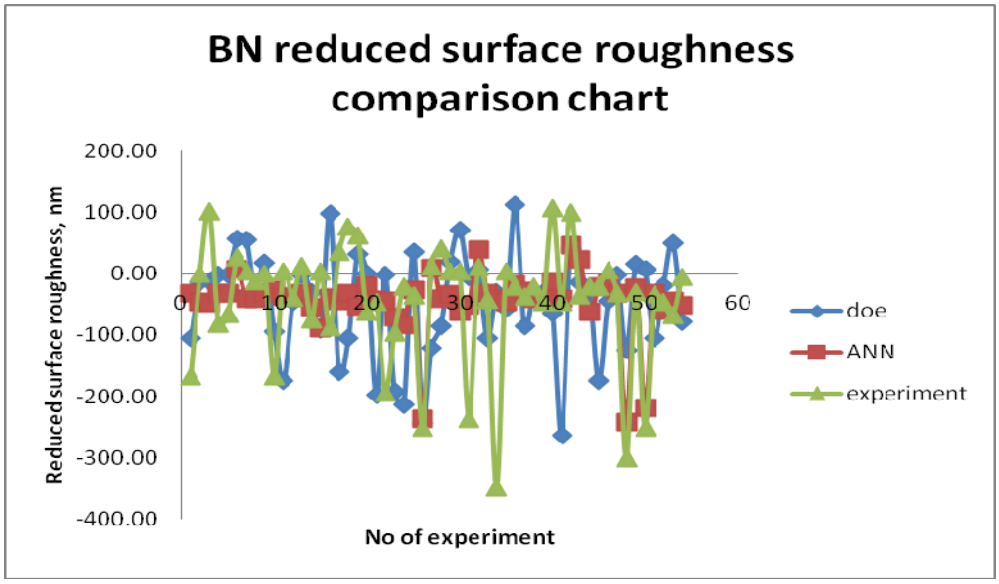

Figure 7-23 Predictive of BN reduced surface roughness by RSM and ANN compared to experimental result

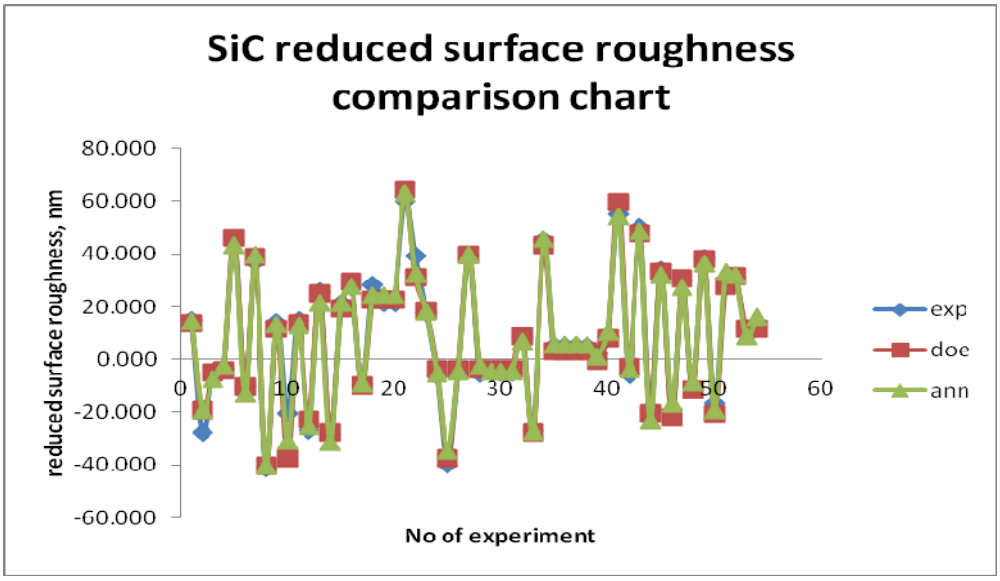

Figure 7-24 Predictive of SiC reduced surface roughness by RSM and ANN compared to experimental result

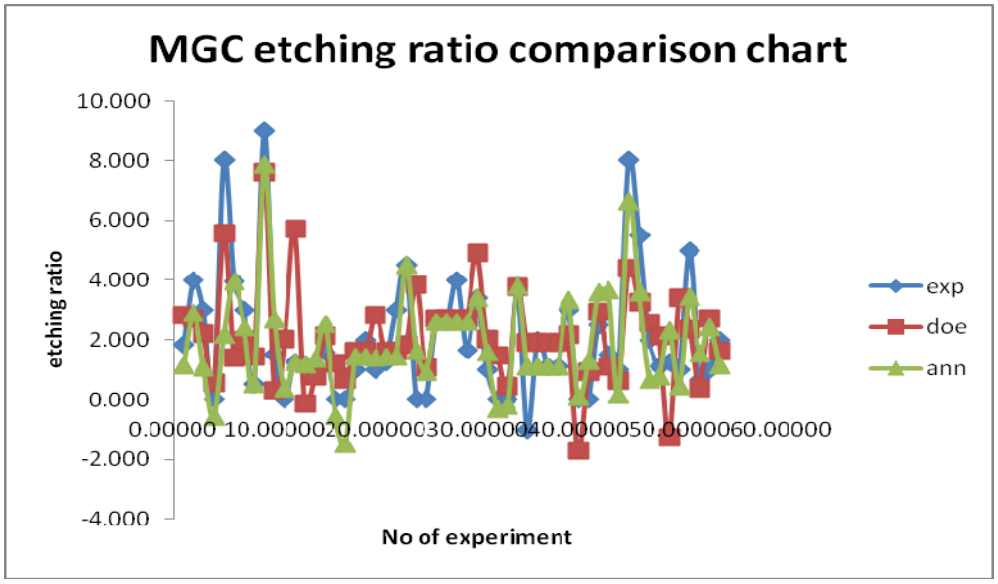

Figure 7-25 Predictive of MGC etch ratio by RSM and ANN compared to experimental result

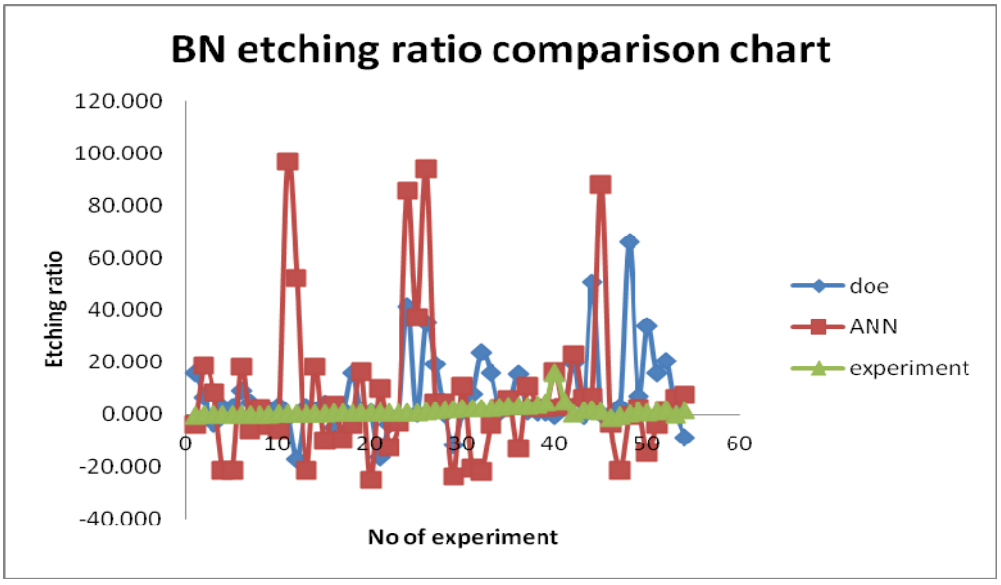

Figure 7-26 Predictive of BN etch ratio by RSM and ANN compared to experimental result

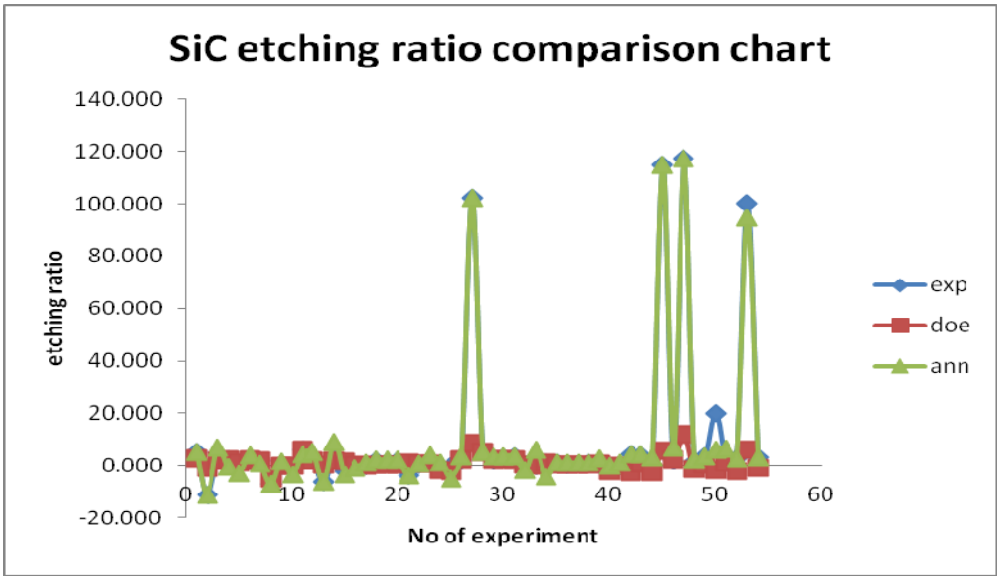

Figure 7-27 Predictive of SiC etch ratio by RSM and ANN compared to experimental result

7.3 OPTIMISATION

For optimisation of chemical machining performance, each variable has to be at its peak and achieve the highest etch rate with good surface roughness and dimensional accuracy. In the optimisation study using DE 7, priority has been set to all features with high etch rate, high reduced surface roughness and high etch ratio. Reduced surface roughness has been set to maximum because the higher the reduced surface roughness is, the lower the value of surface roughness obtained after etching. Similarly, for the best patterning with good dimensional accuracy, the etch rate at non-indented area has to be higher compared to etch rate at indented area. Thus, a maximum rate of etch ratio is desirable.

Results obtained by DE 7 are shown in Table 7-4. In optimisation, etching temperature, etching duration, etchant and etchant's concentration were set to the range as determined earlier in first-order model. Etchant is one of the main significant factors almost in all features. It is shown that chemical machining's optimum point for all substrates occurred with HBr as an etchant.

Chemical machining of MGC in HBr etched best compared to other etchants. With highest temperature (100^{o}C) and lowest etching duration (30 minutes) at 8.5 molarity, MGC can be etched at 0.0011g/min. At this point, etch ratio of 3.277 was the highest among other etching etchants with improvement of 80.879nm on the surface roughness. Next is HCl where it etched at 100^{o}C for 30 minutes in 8.5 molarity. This is the optimum point for HCl with etch rate of 0.0008g/min, 81.2nm reduced surface roughness and 1.617 etch ratio. With least desirability, optimum etching of MGC in H_3PO_4 is around 100^{o}C for 109 minutes in 9.5 molarity, etch rate is 0.0238g/min with reduced surface roughness of 0.0003nm and etch ratio of 1.617.

HBr etching showed its best result in chemical machining of BN followed by HCl and H_3PO_4. In 6 Molarity of HBr etching of BN, optimum variables occurred at 40^{o}C after a duration of 62 minutes in 6 molarity. Result for etch rate is 0.00025g/min, reduced surface roughness is 0.00001nm and etch ratio is 3.153. In 9.5 molarity of HCl etching of BN, optimum etch rate is approximately 0.0005g/min with reduced surface roughness of

0.000001nm and etch ratio of 0.5332. Extent of BN etching in 9.5M H_3PO_4 is lowest compared to HBr and HCl. At 25^oC and 137 minutes, the optimum of BN etching in H_3PO_4 occurred at 0.00017g/min with 0.000001nm improvement of surface roughness and 1.4497 etch ratio.

Chemical machining of SiC is the most difficult given that it is the hardest substrate among the others. Compared to optimisation of MGC chemical machining, SiC shows similar higher etch rate and reduced surface roughness. The only difference is etching of SiC in all etchants takes longer. Again, HBr etched the best compared to other etchants for etching of SiC. Results obtained for etching of SiC in 8.5M HBr at 75^oC for 240 minutes is 0.0009g/min with 128.71nm of reduced surface roughness and 10.004 etch ratio. In SiC, H_3PO_4 etching is better than HCl with etch rate of 0.0118g/min, reduced surface roughness of 34.17nm and etch ratio of 2.018.

In compliance to high desirability and features mentioned above, HBr etching displayed the best performance among all substrates. Overall, HBr etching of MGC and SiC showed the best result, in terms of etch rate, reduced surface roughness and etch ratio.

Table 7-4 Optimisation by DE 7

	MGC			BN			SiC		
Desirability	0.586	0.392	0.240	0.563	0.337	0.242	0.954	0.525	0.419
Etchant	HBr	HCl	H_3PO_4	HBr	HCl	H_3PO_4	HBr	H_3PO_4	HCl
Temperature, ^oC	100	100	100	40	100	25	75	100	74
Duration, minutes	30	30	109	62	128	137	240	172	240
Concentration, Molarity	8.5M	10.5M	9.5M	6M	9.5M	9.5M	8.5M	9.5M	10.5M
Etch rate, g/min	0.0011	0.0008	0.0003	0.00025	0.0005	0.00017	0.0009	0.0118	0.0003
Reduced surface roughness, nm	80.7	81.818	87.230	0.00001	0.000001	0.000001	128.71	34.169	62.786
Etch ratio	3.277	3.403	1.617	3.1530	0.5332	1.4497	10.004	2.018	0.858

Chapter 8 Conclusions and Recommendations

8.1 CONCLUSIONS

Although the development and studies of CHM have been established decades ago, the achievement on CHM of advanced ceramics has not been making significant inroads. CHM of advanced ceramics was seen as impractical because of their extreme hardness, high strength, and high resistance to corrosive material and to high temperature. Part of the reason is due to the lack of knowledge on the characteristics of the CHM process and as such the current study demands answers to three important questions: what etchant should be used, which variables need to be controlled and what are the levels of relationships and interactions between the machining variables? Despite the lack of knowledge, and challenges faced by the CHM process of advanced ceramics, its benefits including cost effectiveness and space saving have become the reason why CHM has recently been receiving a renewed boost. This positive trend is also attributable to the increasing demand of micro and nano-technology of advanced ceramics materials from the industries. Hence, the initiation of the research studies to explore and seek the answers to the above questions.

Before we draw this thesis to a close we would like to highlight and draw out the significance of some key findings that we believe have contributed to the new scientific knowledge on the CHM process and characteristics of advanced ceramics. A number of these findings have been published in some of the distinguished journals mentioned in the beginning.

8.1.1 Development of Etch Rate Models

- The past studies of CHM process of advanced ceramics by others were only able to establish the relationship between etch rate with not more than two variables at a time. Very few and limited studies had been conducted with the applications of statistical tools, and none of these studies had ever produced any predictive models for etch rate of CHM.
- DoE was applied in our studies and we were able to develop the first order model for CHM. The initial results showed that the etch rate for the selected materials was influenced by a number of variables tested. The second order model was successfully established and we were able to demonstrate the significance of the variables on etch rate and identify the specific relationship between each variables and the etch rate of CHM for BN, MGC and SiC.
- Further analyses of ANOVA indicated that the etch rate increased with increase in the etching temperature within the temperature ranged tested. Amongst the variables studied, the nature of the etchant was found to impact the etch rate.
- HBr etchant showed considerable impact on the etch rate compared to HCl and H_3PO_4. The result indicated that HBr etchant performed the best in all the substrates tested under the selected range of concentration or temperature.
- In this study the relationships between etchants and other variables, including etching temperature, etching duration and etchant's concentration have been clearly identified. This has led us to conclude that the choice of etchant is a critical factor in determining the quality and effectiveness of the CHM process.
- Predictive models were generated for the benefits of further research and the industry.

8.1.2 Development of Surface Roughness Models

- The quality of CHM determines the characteristic of the surface roughness. Good surface roughness is always desired in all kind of machining, especially in nano-machining. However, there are difficulties in controlling the surface roughness, especially for CHM, given the various variables involved in the chemical process.

- Most of the research studies were confined to examining the relationship of the surface roughness between one or two variables at a time. This is because longer period is required to study the effect of more variables without the application of statistical tool. None of the past surface roughness studies have produced any predictive models.
- We have successfully established the second order model for the surface roughness process and demonstrated that the surface roughness of different substrate responded invariably to different dependent variables. For MGC, temperature and relationship between etchant and its concentration are affecting surface roughness of the substrate. For BN, temperature and the types of etchant were found to influence the surface roughness. The relationship between temperature and etchant's concentration, and that of etchant and its concentration also showed significant influence on surface roughness**.** For SiC, etching duration and etchant are the main variables that influence surface roughness.
- Overall, the higher the temperature used, the better is the surface roughness obtained. Surface roughness is improved at the optimum etching temperature of approximately 75^{o}C, however a rougher surface was obtained after the optimum point.
- Etching duration appeared to exhibit similar effect as etching temperature does. Better surface roughness was obtained with longer etching process, however for BN and SiC, surface roughness only improved at a varied duration and decreased after the optimum duration.
- Predictive models were generated for the future use in research field and also the industry. These models could be applied directly in the future study.

8.1.3 Development of Etch Ratio Models

- In most cases, the final product is rejected due to the undercut, misalignment or defect on the desired pattern. Therefore, the method employed for patterning is crucial in ensuring a high level of dimensional accuracy.
- The old or commonly used method is mask patterning for CHM patterning. The disadvantages of mask patterning include the possibility of the adhesive mask peeling

off during CHM and undercut and moreover, the methods of applying the mask on the substrates are sometimes hazardous to the environment.

- We introduced, micro indentation, a new method using a simple innovative rolling tool that we designed and fabricated on our own. Although this was only an early stage of study on patterning by means of a mechanical mechanism, we have demonstrated the feasibility of using this new simple procedure for patterning studies.
- In fact we were able to produce patterning of good quality and although the patterning at the moment is simple, micro indentation does show its potential and capability as a method for CHM patterning.
- Etch ratio results obtained were similar to that of etch rate, where it is mainly influenced by the etching temperature and etchant. The higher the etching temperature, the better the etch ratio.
- Predictive models were generated and these models could be applied directly in the industry and also for further research purposes. One of the advantages is that it is able to reduce the pre-examining period with the given predictive models when similar variables are applied.

8.1.4 Predictive Models and Optimisation

- In our study, predictive models were successfully developed using RSM and ANN.
- We established that the RSM and ANN are capable of analysing the experimental data. The proposed predictive models generated by these analytical tools showed good agreement with the experimental data as shown in the Figures 7-19 – 7-27. These models can be potentially applied in the industry with the added advantage of reducing the process duration as no preliminary process is required with predictive models.
- The use of Neural Network (NN) in predicting chemical etching parameters was found to be effective. The results obtained by NN were in good agreement with that predicted by RSM and indicated that these methods have great potential to be employed in predicting optimum chemical etching parameters of MGC, BN and SiC without needing extensive iterative trials.

- The relationship between etching rate, surface roughness and etching ratio with etching temperature, etching duration and solution concentration were successfully established.
- To date no optimisation studies have been reported for CHM process. We have established that for chemical etching of advanced ceramics, the optimum conditions that are required to maximise the etching rate and etching ratio with lower surface roughness are as follows:-

a. Machinable glass ceramics: optimum etching rate of 0.0011g/min, with surface roughness enhancement of 80.789nm and 3.277 etching ratio at 100^{o}C etching temperature for 30 minutes in 8.5M HBr.
b. Boron nitride: optimum etching rate is 0.00025g/min, with surface roughness enhancement of 0.0001nm and 3.215 etching ratio at 40^{o}C etching temperature for 62 minutes in 6M HBr.
c. Silicon carbide: optimum etching rate is 0.0009g/min, with surface roughness enhancement of 128.71nm and 10.004 etching ratio at 75^{o}C etching temperature for 240 minutes in 8.5M HBr.

We believe, we have achieved the objectives of our research study that we set out in the beginning. In summary, our studies have provided some important scientific findings on CHM of advanced ceramics, namely MGC, BN and SiC with solution of HCl, HBr and H_3PO_4. We have discussed on various types of DoE and their application, identified material machinability, established the relationship between etching rates, surface roughness and dimensional accuracy and presented the predictive models by RSM and ANN. The results supported the feasibility of wet chemical micro-patterning of advanced ceramics for micro-devices applications. Direct patterning was successfully introduced to meet the increasingly local demand for multi-kind and small quantity production. In this leading-edge research involving the use of micro- and nanotechnology, more flexible patterning techniques are desired.

8.2 SUGGESTION FOR FURTHER WORKS

We suggest the following for further improvement and future research direction:

- Additional chemical reagent and process

At the current stage, CHM process is purely chemical in nature and does not involve additional process or chemical reagent. Research studies showed that the result of CHM can be improved by applying specific chemical additives. Similar study might be able to carry out using chemical reagents of different properties. Stirring process might help to improve the etch rate of CHM. Studies showed that the extent of chemical reaction tends to increase with the help of stirring process by avoiding static ion which might form as a protective layer on top of substrate layer and thus stopping the etching process from proceeding [10, 56].

- Micro-Indentation

Micro-indentation is new to the patterning in CHM and more study is required to fully understand the characteristics of this process. It has proven its capability in successfully patterning a simple micro type pattern. Further research should be carried out in more complex patterning. Given the surge of industry toward nano-technology, further study on the improvement of micro-indentation is warranted.

- Robustness

Currently, CHM was carried out in laboratory scale system, where only one substrate was examined each time. This is not practical in the real plant, especially in mass production. Different results might be obtained at the end of the process. Thus, further study on mass production of CHM should be carried out to reduce the noise of the process.

- Statistical approaches

For further work, it is suggested that a similar approach to be used to predict chemical etching parameters of other advanced ceramics using more variables. In addition, Fuzzy logic could be employed to analyse the results. A different kind of NN with different learning rule and transfer function could be incorporated. Further work could also be extended to the current order to 4^{th} order to find the 3^{rd} and 4^{th} level of interactions.

References

1. Kalpakjian, S., *Manufacturing engineering and technology*. 2001: Upper Saddler River, N. J : Prentice Hall, .
2. Upadhyaya, G.S., *Trends in Advanced Materials and Processes.* Materials and Design, 1990. **11**(4): p. 171-179.
3. *Macor Machinable Glass Ceramics*.
4. Iliescu, C., F.E.H. Tay, and J. Miao, *Strategies in deep wet etching of Pyrex glass.* Sensors and Actuators A, 2007. **133**: p. 395-400.
5. Liu, J., et al., *Etch rate and surface morphology of plasma etched glass and glass-ceramic substrates.* Journal of Non-Crystalline Solids, 2004. **342**: p. 110-115.
6. Williams, K.R., K. Gupta, and M. Wasilik, *Etch rates for micromachining processing-Part 2.* Journal of Microelectromech. Syst., 2003. **12**(6): p. 761-778.
7. Williams, K.R. and R.S. Muller, *Etch rates for micromachining processing.* Journal of Microelectromech. Syst., 1996. **5**(4): p. 256-269.
8. Tehrani, A.F. and E. Imanian, *A new etchant for the chemical machining of St304.* Journal of Materials Processing Technology, 2004. **149**: p. 404-8.
9. Sato, K., et al., *Characterization of orientation-dependent etching properties of single-crystal silicon: effects of KOH concentration.* Sensors and Actuators A, 1998. **64**: p. 87-93.
10. Steinert, M., et al., *Study on the mechanism of silicon etching in HNO_3-Rich HF/ HNO_3 mixtures.* Journal of Physical Chemistry C, 2007. **111**: p. 2133-40.
11. Saito, Y., et al., *Fabrication of micro-structure on glass surface using micro-indentation and wet etching process.* Applied Surface Science, 2008. **254**: p. 7243-49.
12. Rahaman, M.N., *Ceramic Processing*. Vol. 1. 2006, Florida: Taylor & Francis Group.
13. Harris, W.T., *Chemical Milling*. 1974, UK: Oxford University Press.
14. E. P. DeGarmo, J.T.B., R. A. Kohser, B. E. Klamecki, *Materials and Processes in manufacturing*. Vol. 9. 2003, United States of America: John Wiley & sons, Inc.
15. Ma, L.J. and A. Yu, *Influencing of technological parameter on tools wear during turning fluorophologopite glass-ceramics.* JOurnal of Rare Earths, 2007. **25**: p. 330-333.
16. Wang, Z.Y., K.P. Rajarkar, and M. Murugappan, *Cryogenic PCBN turning of ceramic (Si_3N_4).* Wear, 1996. **195**: p. 1-6.
17. Dabnun, M.A., M.S.J. Hashmi, and M.A. El-Baradie, *Surface roughness predictive model by design of experiments for turning machinable glass-ceramic*

(Macor). Journal of Materials Processing Technology, 2005. **164-165**: p. 1289-1293.
18. Yan, B.H., F.Y. Huang, and H.M. Chow, *Study on the turning characteristics of alumina-based ceramics.* Journal of Materials Processing Technology, 1995. **54**: p. 341-347.
19. Vermeulen, J.P.M.B., P.C.J.N. Rosielle, and P.H.J. Schellekens, *An advanced ceramics optical diamond turning machine design and prototype development.* Annals of the CIRP, 2000. **49**: p. 201-204.
20. Tuersley, I.P., A. Jawaid, and I.R. Pashby, *Review: Various methods of machining advanced ceramics materials.* Journal of Materials Processing Technology, 1994. **42**: p. 377-390.
21. Huang, H. and Y.C. Liu, *Experimental investigations of machining characteristics and removal mechanisms of advanced ceramics in high speed deep grinding.* International Journal of Machine Tools & Manufacture, 2003. **43**: p. 811-823.
22. Marinescu, M., et al., *Handbook of Machining with Grinding Wheels*, in *CRC Press*2006.
23. Tsutsumi, C., K. Okano, and T. Suto, *High quality machining of ceramics.* Journal of Materials Processing Technology, 1993. **37**: p. 639-654.
24. Zubel, I., *Silicon anisotropic etching in alkaline solution II on the influence of anisotropy on the smoothness of etched surfaces.* Sensors and Actuators A, 1998. **70**: p. 260-268.
25. Kim, H.W., et al., *Etching characteristics of photoresist and low-k dielectrics by Ar/O_2 ferrite-core inductively coupled plasma.* Microelectronic Engineering, 2008. **37**: p. 295-307.
26. Gi, S.C. and H.C. Gi, *Process analysis and monitoring in abrasive water jet machining of alumina ceramics.* International Journal of Machine Tools & Manufacture, 1997. **37**: p. 295-307.
27. Chen, L., E. Siores, and W.C.K. Wong, *Keft characteristics in abrasive water jet machining of alumina ceramics.* International Journal of Machine Tools & Manufacture, 1996. **36**(1201-1206).
28. Chen, L., E. Siores, and W.C.K. Wong, *Optimizing abrasive waterjet cutting of ceramic materials.* International Journal of Machine Tools & Manufacture, 1998. **74**: p. 251-254.
29. Siores, E., W.C.K. Wong, and J.G. Wager, *Enhancing abrasive waterjet cutting of ceramic by head oscillation technique.* CIRP Annals- Manufacturing Technology, 1996. **45**(1): p. 327-330.
30. Hu, C.F., Y.C. Zhou, and Y.W. Bao, *Material removal and surface damage in EDM of Ti_3SiC_2 ceramic.* Ceramics International, 2008. **24**: p. 537-541.
31. Liu, Y.H., et al., *Effect of machining fluid on the process performance of electric discharge milling of insulating Al_2O_3 ceramic.* Journal of Materials Processing Technology, 2008. **48**: p. 1030-1035.
32. Muttamara, A., et al., *Effect of electrode material on electrical discharge machining of alumina.* Journal of Materials Processing Technology, 2008. **28**: p. 1-8.

33. Puertas, I. and C.J. Luis, *A study on the electrical discharge machining of conductive ceramics.* Journal of Materials Processing Technology, 2004. **153-154**: p. 1033-1038.
34. Yong, L., et al., *Localized electrochemical micromachining with gap control.* Sensors and Actuators A, 2003. **108**: p. 144-148.
35. Lu, X. and Y. Leng, *Electrochemical micromachining of titanium surfaces for biomedical application.* Journal of Materials Processing Technology, 2005. **2005**(169).
36. Ashruf, C.M.A., *Electrochemical etch stop engineering for bulk micromachining.* Mechatronics, 1998. **8**: p. 595-612.
37. Landolt, D., R.-F. Chauvy, and O. Zinger, *Electrochemical micromachining, polishing and surface structuring of metals: fundamentals aspects and new developments* Electrochemica Acta, 2003. **48**: p. 3185-3201.
38. Bhattacharyya, B., B.B. Doloi, and S.K. Sorkhel, *Experimental investigations into electrochemcial discharge machining of non-conductive ceramic materials.* Journal of Materials Processing Technology, 1995. **95**: p. 145-154.
39. Datta, M. and D. Harris, *Electrochemical micromachining: an environmentally friendly, high speed processing technology.* Electrochemica Acta, 1997. **42**: p. 3007-3012.
40. Chang, C.-W. and C.-P. Kuo, *Evaluation of surface roughness in laser-assisted machining of aluminum oxide ceramics with Taguchi method.* International Journal of Machine Tools & Manufacture, 2007. **47**: p. 141-7.
41. Chang, C.-W. and C.-P. Kuo, *An investigation of laser-assisted machining of Al_2O_3 ceramics planning.* International Journal of Machine Tools & Manufacture, 2007. **47**: p. 452-461.
42. Tsai, C.-H. and H.-W. Chen, *Laser milling of cavity in ceramic substrate by fracture machining element technique.* Journal of Materials Processing Technology, 2003. **136**(158-165).
43. Tsai, C.-H. and C.-H. Ou, *Machining a smooth surface of ceramic material by laser fracture machining technique.* Journal of Materials Processing Technology, 2004. **155-156**: p. 1797-1804.
44. Black, I., S.A.J. Livingstone, and K.L. Chua, *A LBM database for cutting of ceramic tile.* Journal of Materials Processing Technology, 1998. **84**: p. 47-55.
45. Thoe, T.B., D.K. Aspinwall, and M.L.H. Wise, *Review on ultrasonic machining.* International Journal of Machine Tools & Manufacture, 1998. **38**: p. 239-255.
46. Li, Z.C., et al., *Edge-chipping reduction in rotary ultrasonic machining of ceramics: finite element analysis and experimental verification.* International Journal of Machine Tools & Manufacture, 2006. **46**(12-13): p. 1469-1477.
47. Prabhakar, D., et al., *A theoretical model for predicting material removal rates in rotary ultrasonic machining of ceramics.* Transactions of the North American Manufacturing Research Institution of SME, 1993. **21**: p. 167-172.
48. Zeng, W.M., et al., *Experimental observation of tool wear in rotary ultrasonic machining of advanced ceramics.* International Journal of Machine Tools & Manufacture, 2005. **45**: p. 1468-1473.
49. Bowker, R.R.C.S., *Scientific & Technical Books & Serials in Print*, ed. B. Staff. Vol. 16. 1989, michigan: R. R. Bowker LLC.

50. Lilien, O., *History of industrial gravure printing up to 1920*. 1972, California: Lund Humphries. 155.
51. Harris, W.T., *Chemical Milling: the Technology of Cutting Materials by Etching*. 1976, Michigan: Claredon Press.
52. Benedict, G.F., *nontraditional manufacturing processes*. Vol. 1. CRC. 402.
53. Jaeger, R.C., *Introduction to Microelectric Fabrication*. 2002, New York: Prentice Hall.
54. Ravi, K., *Imperfections and impurities in Semiconductor Silicon*. Vol. 1. 1986, New York: Wiley Publication. 130-154.
55. Kinder, B.M. and T.L. Tansley, *A comparative study of photoenhanced wet chemical etching and reactive ion etching of GaN epilayers grown on various substrates.* IEEE, 1999: p. 195-198.
56. Makino, E., T. Shibata, and Y. Yamada, *Micromachining of fine ceramics by photolithography.* Sensors and Actuators A, 1999. **75**: p. 278-288.
57. Peng, L.-H., et al., *Hydration effects in the photoassisted wet chemical etching of gallium nitride.* IEEE Journal of Selected Topics in Quantum Electronics, 1998. **4**(3): p. 564-9.
58. Yuan, F., et al., *Microfabrication of crystalline silicon by controlled alkali etching.* Journal of Materials Processing Technology, 2004. **149**: p. 567-572.
59. Piconi, C. and G. Maccauro, *Zirconia as ceramic biomaterial.* Biomaterial, 1999. **20**: p. 1-25.
60. Cakir, O., H. Temel, and M. Kiyak, *Chemical etching of Cu-ETP copper.* Journal of Materials Processing Technology, 2005. **162-163**: p. 275-279.
61. Cai, J., et al., *Effects on etching rates of copper in ferric chloride solutions* in *1998 IEMT/IMC Proceeding*1998.
62. Zubel, I. and I. Barycka, *Silicon anisotropic etching in alkaline I. The geometric description of figures developed under etching Si(100) in various solutions.* Sensors and Actuators A, 1996. **60**: p. 200-205.
63. Vartuli, C.B., et al., *Wet chemical etching survey of III-nitrides.* Solid-State Electronics, 1997. **41**(12): p. 1947-1954.
64. Liu, J., *Etch rate and surface morphology of plasma etched glass and glass-ceramic substrates* Journal of Non-Crystalline Solids, 2004. **342**: p. 110-115.
65. Niebuhr, D., *Cavitation erosion behavior of ceramics in aqueous solutions.* Wear, 2007. **263**: p. 295-300.
66. Fang, Q., P.S. Sidky, and M.G. Hocking, *The effect of corrosion and erosion on ceramic materials.* Corrosion science, 1997. **39**: p. 511-527.
67. Gelder, W.V. and V.E. Hauser, *The etching of silicon nitride in phosphoric acid with silicon dioxide as a mask.* Journal of The Electrochemical Society, 1967. **114**(8): p. 869-872.
68. Vladuta, C., *Ceramic interface properteis evaluation based on contact angle measurement.* Surface & Coatings Technology, 2008. **202**: p. 2442-2452.
69. Kuech, T.F., et al., *Effect of surface preparation on production of interfaces.* Journal of Crystal Growth, 1986. **77**: p. 539-545.
70. Baranova, G.K. and L.A. Dorosinskii, *Chemical polishing and etching of Bi-Sr-Ca-Cu-O high temperature superconduting system.* Physica C, 1992. **194**: p. 425-9.

71. Cook, S.G., J.A. Little, and J.E. King, *Etching and microstructure of engineering ceramics.* Materials Characterization, 1995. **34**(1): p. 1-8.
72. Bickermann, M., et al., *Wet KOH etching of freestanding AIN single crystals.* Journal of Crystal Growth, 2007. **200**: p. 299-307.
73. Youtsey, C., et al., *Smooth n-type GaN surfaces by photoenhaced wet chemical etching.* Appl. Phys. Lett, 1998. **72**: p. 560-562.
74. Jardiel, T., et al., *Domain structure of $Bi_4Ti_3O_{12}$ ceramics revealed by chemical etching.* Journal of European Ceramic Society, 2006. **26**: p. 2823-26.
75. Saito, Y., et al., *Mechanism of etching rate change of aluminosilicate glass in HF acid with micro-indentation.* Applied Surface Science, 2008. **255**: p. 2290-4.
76. saito, Y., et al., *Micro-fabrication techniques applied to aluminosilicate glass surfaces: Micro-indentation and wet etching process.* Thin Solid Films, 2008.
77. S.W. Youn, C.G.K., *Maskless pattern fabrication on Pyrex 7740 glass surface by using nano-scratch with HF wet etching* Scripta Materialia, 2005. **52**: p. 117-122.
78. J. Kurachi, K.M., H. Inomata, Y. Saito. *Micro-fabrication techniques with HF wet etching*. in *10th International Conference on the Physics of Non-Crystalline Solids Parma*. 2003. Italy.
79. W. H. Cubberly, R.B., *Desk Edition: Tool and Manufacturing Engineers*. 4 ed. 1989, New York: CRC.
80. Jacques, M., *The chemistry of failure analysis.* IRPS, 1979. **1**: p. 197-200.
81. Chu, T. and R.J. Keim, *Secco etch of ceramics.* Journal of Electrochemical Society, 1975. **95**: p. 122-132.
82. Hua, Y. *Studies of a new chemical etching method-152 Secco etch in failure analysis of wafer fabrication*. in *IEEE conference*. 1998. KL: IEEE.
83. Cook, S.G., J.A. Little, and J.E. King, *Etching and microstructure of engineering ceramics.* Materials Characterization, 1995. **34**: p. 1-8.
84. Elliot, D., *Integrated Circuit Fabrication Technology*. 1982: McGraw Hill.
85. Hua, Y., *Studies of a new chemical etching method - 152 Secco etch in failure analysis of wafer fabrication.* Proceeding in ICSE, 1998: p. 20-26.
86. James, P.F., *Glass Ceramics: new compositions and uses.* Journal of Non-Crystalline Solids, 1995. **181**: p. 1-15.
87. Hou, Z., et al., *Study on crystallization and microstructure of Li_2O-Al_2O_3-SiO_2 glass ceramics.* Journal of University of Science and Technology Beijing, 2006. **13**(6): p. 564-9.
88. Lynch, C.T., *CRC Handbook of Materials Science*, ed. C.T. Lynch. 1975: CRC Press.
89. Richerson, D.W., *Modern ceramic engineering: properties, processing, and use in design*. 3 ed. 2006: CRC Press.
90. Rosen, C.Z., B.V. Hiremath, and R.E. Newnham, *Piezoelectricity*. 1992: Springer.
91. Cekli, C. and G. Goller, *The crystallisation behaviour and machinability of sodium-porassium mica and fluorapatite containing glass ceramics.* Journal of Aust. Ceram. Society, 2007. **43**(1): p. 9-17.
92. Bach, H. and D. Krause, *Low thermal expansion glass ceramics*. 2 ed. 2005: Springer.
93. Wise, D.L., *Encyclopedic handbook of biomaterials and bioengineering*. Vol. 2. 1995: Marcel Dekker.

94. Radonjic, L. and L. Nikolic, *The effect of fluorine source and concentration on the crystallization of machinable glass-ceramics.* Journal of the European Ceramic Society, 1991. **7**: p. 11-16.
95. Alizadeh, P., B.E. Yekta, and T. javadi, *Sintering behavior and mechanical properties of the mica-diopside machinable glass-ceramisc.* Journal of European Ceramic Society, 2008. **28**: p. 1569-1573.
96. Li, X., T. Abe, and M. Esashi, *Fabrication of high-density electrical feed-throughs by deep-reactive-ion etching of Pyrex glass.* Journal of Microelectromech. Syst., 2002. **1-6**: p. 625-630.
97. Watanabe, T., *Mass production of quartz high-speed chemical etching applied to at-cut wafers.* 2001 IEEE International Frequency Control Symposium and PDA Exhibition, 2001: p. 368-375.
98. Gaiseanu, F., et al., *Chemical etching control during the self-limitation process by boron diffusion in silicon: analytical results.* Proceeding of 1997 IEEE Semiconductor Conference, 1997. **1**: p. 247-250.
99. Minhao, Y., M.J. Henderson, and A. Gibaud, *On the etching of silica and mesoporous silica films determined by X-ray reflectivity and atomic force microscopy.* Thin Solid Films, 2009. **514**: p. 3028-3035.
100. Olsen, M.E., et al., *Effect of varying etching times on the bond strength of ceramic brackets.* American Journal of Orthodontics and Dentofacial Orthopedics, 1996. **109**(4): p. 403-409.
101. *boron nitride*. 2009 Encyclopædia Britannica Online]. Available from: http://www.britannica.com/EBchecked/topic/74404/boron-nitride.
102. Lavrenko, V.A. and A.F. Alexeev, *High Temperature Oxidation of Boron Nitride.* Ceramics International, 1986. **12**: p. 25-31.
103. Acheson, E.G., *Production of artificial crystalline carbonaceous material*, in *492*, U.S. Patent, Editor 1983: US. p. 767.
104. Dunwoody, H.C., *Wireless telegraph system (silicon carbide detector)*, U.S. Patent, Editor 1906: US. p. 616.
105. Davidge, R.W., *Mechanical behaviour of ceramics*. 1979, USA: CUP Archive.
106. Evans, R.S., et al., *REACTION BONDED SILICON CARBIDE:*
SFF, PROCESS REFINEMENT AND APPLICATIONS, 2008, Department of Mechanical Engineering, University of Texas: Austin.
107. Jahanmir, S., *Friction and wear of ceramics*, ed. S. Jahanmir. 1994: CRC Press.
108. Pope, J.E., *Rules of thumb for mechanical engineers: a manual of quick, accurate solutions to everyday mechanical engineering problems*. 1997: Gulf Professional Publishing.
109. Rahaman, M.N., *Ceramic processing and sintering*. 2 ed. Vol. 23 of Materials engineering. 2003: CRC Press.
110. Mortensen, A., *Concise encyclopedia of composite materials*. 2 ed. 2007: Elsevier.
111. Grogan, A.F. and D.F. Smart, *Ceramic surfaces for tribological components.* Materials and Design, 1981. **2**: p. 197-201.
112. B. Kim and B.T. Lee, *Relationships between etch rate and roughness of plasma etched surface.* IEEE Transactions of Plasma Science, 2002. **30**(5): p. 2074-2077.

113. Scharnholtz, S., et al., *Depnedence of channel mobility on the surface step orientation in planar 6H-SiC MOSFETS.* Materials Science Forum, 1998. **264-268**: p. 1001-1004.
114. B.Casady, J., et al., *Surface roughness of reactive ion etched 4H-SiC in SF_6/O_2 and $CHF_3/H_2/O_2$ plasmas.* Journal of Electrochemical Society, 1998. **145**(4): p. L58-60.
115. Kim, B., H.J. Choi, and B.T. Lee, *Surface roughness of silicon carbide etched in a C_2F_6/O_2 inductively coupled plasmas.* Journal of Vac. Sci. Technology A, 2002. **20**(2): p. 424-429.
116. Wang, J.J., et al., *ICP Etching of SiC.* Solid-State Electronics, 1998. **42**(12): p. 2283-2288.
117. Trutna, L., et al., *Engineering Statistics Handbook*, C. Croarkin and P. Tobias, Editors. 2003, NIST.
118. Fantozzi, G., et al., *Advanced Ceramics Materials: Summary of Possible Applications.* Materials: Science and Engineering, 2001: p. 32-36.
119. Bezerra, M.A., et al., *Response surface methodology (RSM) as a tool for optimization in analytical chemistry.* Talanta, 2008. **76**: p. 665-677.
120. Montgomerty, D.C., *Design and Analysis of Experiment*. 5 ed. 2001: John Wiley & Sons, Inc.
121. Baldassari, S., et al., *DOE analyses on aqueous suspensions of TiO_2 nanoparticles.* Journal of European Ceramic Society, 2008. **28**: p. 2665-2671.
122. Pierlot, C., et al., *Design of experiments in thermal spraying: A review.* Surface & Coatings Technology, 2008. **202**: p. 4483-4490.
123. Montevechi, J.A.B., et al. *Application of design of experiment on the simulation of a process in an automotive industry*. in *2007 Winter Simulation Conference*. 2007.
124. Anderson, M.J. and P.J. Whitcomb, *RSM simplified: optimizing processes using response surface methods for design of experiments*. 2 ed. 2005.
125. Anderson, M.J. and P.J. Whitcomb, *DOE Simplified: practical tools for effective experimentation*. 2 ed. 2007, New YOrk: Productivity Press.
126. Hung, C.C., H.C. Lin, and H.C. Shih, *Response surface methodology applied to silicon trench etching in $Cl_2/HBr/O_2$ using transformer coupled plasma technique.* Solid-State Electronics, 2002. **46**: p. 791-5.
127. Mead, R. and D.J. Pike, *A review of response surface methodology from a biometric viewpoint.* Biometrics, 1975. **31**: p. 803-851.
128. Hill, W.J. and W.G. Hunter, *A review of response surface methodolgy: a literature survery.* Technometrics, 1966. **8**(571-590).
129. Desai, K.M., et al., *Comparison of artificial neural network (ANN) and response surface methodology (RSM) in fermentation media optimization: Case study of fermentative production of scleglucan.* Journal of Biochemical Engineering, 2008. **41**: p. 266-273.
130. Benardos, P.G. and G.C. Vosniakos, *Predicting surface roughness in machining: a review.* International Journal of Machine Tools & Manufacture, 2003. **43**: p. 833-844.
131. Stergiou, C. and D. Siganos, *Neural networks.* SURPRISE 96 Journal, 1996. **4**(11).
132. The Mathworks, I. *What is neural networks?* 2005.

133. Gurney, K., *An Introduction to Neural Networks*. Vol. 1. CRC press.
134. Haykin, S., *Neural Networks and Learning Machines*. 3 ed. 2008, New Jersey: Prentice Hall.
135. Bishop, C.M., *Neural Networks for Pattern Recognition*. Vol. 1. Oxford University Press.
136. Smith, M., *Neural Networks for statistic modeling*. 1993, New York: Van Nostrand Reinhold.
137. Mathew, M.D., D.W. Kim, and W.-S. Ryu, *A neural network model to predict low cycle fatigue life of nitrogen-alloyed 316L stainless steel.* materials science and Engineering A, 2008. **474**: p. 247-253.
138. Shahin, M. and M. Elchalakani, *Neural networks for modelling ultimate pure bending of steel circular tubes.* JOurnal of Construction Steel Research, 2007.
139. Benardos, P.G. and G.-C. Vosniakos, *Predicting surface roughness in machining: a review.* International Journal of Machine Tools Manufacture, 2003. **43**: p. 833-844.
140. Trippi, R.R. and E. Turban, *Neural Networks Finance and Investment: Using Artificial Intelligence to Improve Real-World Performance* 1996: Irwin Professional Pub.
141. Serajzadeh, S., *Prediction of thermo-mechanical behaviour duringhot upsetting using neural networks.* Materials Science and Engineering A, 2008. **472**: p. 140-147.
142. Liao, T.W., *Modelling process mean and variation with MLP neural networks.* International Journal of Machine Tools Manufacture, 1996. **36**(12): p. 1307-19.
143. Aydinalp-Koksal, M. and V.I. Ugursal, *Comparison of neural netwok, conditional demand analysis, and engineering approaches for modelling end-use energy consumption in the residential sector.* Applied Energy, 2008. **85**: p. 271-296.
144. Hornik, K., M. Stinchcombe, and H. White, *Multilayer feedforward networks* Neural networks, 1989. **2**: p. 359-366.
145. Funahashi, K., *On the approximate realization of continuous mappings by neural networks.* Neural networks, 1989. **2**: p. 183-192.
146. Bryson, A.E. and Y.C. Ho, *Applied optimal control: optimization, estimation, and control*. revised ed. 1975, UK: Taylor & Francis.
147. Russell, S., *Artificial Intelligence: a Modern Approach*. 2004: Pearson plc.
148. Wilamowski, B.M., Y. Chen, and A. Malinowski. *Efficient algorithm for training neural networks with one hidden layer*. in *International Joint Conference on Neural Networks*. 1999. Washitong, D. C.
149. Pearlmutter, B.A., *Fast exact multiplication by the Hessian*, in *Neural Computation*. 1994, MIT Press: Cambridge, MA.
150. Lourakis, M.I.A. *A Brief Description of the Levenberg-Marquardt Algorithm Implemented by levmar*. 2005; Available from: http://www.ics.forth.gr/~lourakis/levmar/levmar.pdf.
151. Fredj, N.B., R. Amamou, and M.A. Rezgui, *Surface roughness prediction based upon experimental design and neural network models.* IEEE SMC, 2002. **2**.
152. Ko, Y.-D., et al., *Modeling and optimization of the growth rate for ZnO thin films using neural networks and genetic algorithms.* Expert Systems with Application 2009. **36**: p. 4061-6.

153. Ozerdem, M.S. and S. Kolukisa, *Artificial neural network approach to predict mechanical properties of hot rolled, nonresulfurized, AISI 10xx series carbon steel bars.* Journal of Materials Processing Technology, 2008. **199**: p. 437-439.
154. balestrassi, P.P., et al., *Design of experiments on neural network's training for nonlinear time series forecasting.* Neurocomputing, 2008.
155. Paliwal, M. and U.A. Kumar, *Neural networks and statistical techniques: A review of applications.* Expert Systems with Application, 2009. **36**: p. 2-17.
156. Suresh, P.V.S., P.V. Rao, and S.G. Deshmukh, *A genetic algorithmic approach for optimization of surface roughness prediction model.* International Journal of Machine Tools Manufacture, 2002. **42**: p. 675-680.
157. Jensen, K. and P. Paralkar, *Analysis of design of experiments used as a tool to implemetn environmentally safe cleaning process in manufacturing*, in *IEEE*1995, Bourns Inc. Integrated Technologies Division: Utah.
158. Thompson, J.Y., S.C. Bayne, and H.O. Heymann, *Mechanical properties of a new mica-based machinable glass ceramic for CAD/CAM restorations.* The Journal of Prosthetic Dentistry, 1996. **76**(6): p. 619-623.
159. Guedes, A., et al., *Multilayered interface in Ti/Macor machinable glass-ceramics joints.* Materials Science and Engineering A, 2001. **301**: p. 118-124.
160. Carpick, R.W. and M. Salmeron, *Scratching the surface: Fundamental investigations of tribology with atomic force microscopy.* Chemical Reviews, 2007. **97**(4): p. 1163-1194.
161. Humphris, A.D.L., M.J. Miles, and J.K. Hobbs, *A mechanical microscope: high-speed atomic force microscopy.* Applied Physics Letters, 2005. **88**: p. 034106-1-3.
162. Morita, S., R. Wiesendanger, and E. Meyer, *Noncontact atomic force microscopy*. 2002: Springer. 439.
163. Muller, D.J., U. Aebi, and A. Engel. *Imaging, measuring and manipulating native biomolecular systems with the atomic force microscope*. 1995; Available from: http://www.mih.unibas.ch/Booklet/Booklet96/Chapter3/Chapter3.html.
164. instruments, n. *Atomic Force Microscopy*. Available from: http://www.nanoscience.com/education/AFM.html.
165. Gao, F., et al., *Changing the size and shape of Ge island by chemical etching.* Journal of Crystal Growth, 2001. **231**(1-2): p. 17-21.
166. Saxena, A. and K.K. Dwivedi, *Chemical etching characteristics of glass detectors.* International Journal of Radiation Applications and Instrumentation. Part D. Nuclear Tracks and Radiation Measurements, 1986. **12**(1-6): p. 161-164.
167. O. Cakir, A.Y., T. Ozben, *Chemical machining.* Archives of Materials Science and Engineering, 2007. **28**(8): p. 499-502.
168. Maki, H., et al., *Control of surface morphology of ZnO image by hydrochloric acid etching.* Thin Solid Films, 2002. **411**(1): p. 91-95.
169. Somogyi, G., *Current problems in chemical track etching.* Nuclear Tracks and Measurements, 1984. **8**(4): p. 27-35.
170. Geldger, W.V. and V.E. Hauser, *The etching of silicon nitride in phosphoric acid with silicon dioxide as a mask.* Journal of Electrochemical Society, 1967. **114**(8): p. 869-872.
171. Virginia Semiconductor, I., *Wet-Chemical etching and cleaning of Silicon*, 2003, Virginia Semicondcutor, Inc: Fredericksburg.

172. Peng, J., et al., *Micro-patterning of 0.70Pb($Mg_{1/3}Nb_{2/3}$)O_3-0.30$PbTiO_3$ single crystals by ultrasonic wet chemical etching.* Materials letters, 2008. **62**(17-18): p. 3127-3130.
173. Houston, P.L., *Chemical kinetics and reaction dynamics*. Vol. 1. 2001: McGraw-Hill. 48-51.
174. Sundararaman, C.S., A. Mouton, and J.F. Currie, *Chemical etching of InP.* Indium Phosphide and Related Materials, 1990, 2nd International Conference, 1990: p. 224-227.
175. Hirota, K., Y. Tsukiyama, and T. Yassumi, *Precision blanking of thin sheet metals with the help of chemical etching.* Journal of Materials Processing Technology, 2008. **201**: p. 209-213.
176. Bittner, A. and U. Schmid, *The porosification of fired LTCC substrates by applying a wet chemical etching procedure.* Journal of European Ceramic Society, 2009. **29**: p. 99-104.
177. Noor, M.M., B. bais, and B.Y. Majlis, *The effets of temperature and KOH concentration silicon etching rate and membrane surface roughness.* Proceeding in ICSE 2002, 2002(524-528): p. 524.
178. Don L. Kendall, C.B.F., Kevin J. Malloy, *Chapter 7 Critical Technologies for the Micromachining of Silicon.* Semiconductors and Semimetals, 1992. **37**: p. 293-337.
179. Choi, H.-J., et al., *Sliding wear of silicon carbide modified by etching with chlorine at various temperatures.* Wear, 2009. **266**: p. 214-219.
180. Cakir, O., *Chemical etching of aluminium.* Journal of Materials Processing Technology, 2008. **199**: p. 337-340.
181. Prudhomme, N., et al., *Design of high frequency $GaPO_4$ BAW resonators by chemical etching.* Sensors and Actuators B, 2008. **131**: p. 270-278.
182. Prudhomme, N., et al., *Gallium orthophoshate device manufacturing by chemical etching.* Proceeding of 2003 IEEE International Frequency Control Symposium and PDA Exhibition 2003: p. 688-693.
183. Wang, G.X., N. Li, and D. Li, *Effect of Pd ions in the chemical etching solution.* Journal of University of Science and Technology Beijing, 2007. **14**(3): p. 286-289.
184. Saito, Y., et al., *Fabrication of micro-structure on glass surface using micro-indentation and wet etching process.* Applied Surface Science, 2008. **254**: p. 7243-7.
185. Nagai, T., A. Imanishi, and Y. Nakato, *Scratch induced nano-wires acting as a macro-pattern fro formation of well-ordered step structures on H-terminated Si (111) by chemical etching.* Applied Surface Science, 2004. **237**(1-4): p. 533-537.